Gesellschaft für Mikroelektronik

The Society for Microelectronics

Annual Report

2001

Vienna, October 2002

Gesellschaft für Mikroelektronik

The Society for Microelectronics

Annual Report

2001

Gesellschaft für Mikroelektronik
c/o Technische Universität Wien
Institut für Industrielle Elektronik und Materialwissenschaften
Gußhausstraße 27-29/366, A-1040 Wien

Vienna, October 2002

Editor: Karl Riedling

Layout: Claudia Benedela
Karl Riedling

ISBN: 3-901578-09-9

© 2002 Gesellschaft für Mikroelektronik (GMe)
c/o Technische Universität Wien
Institut für Industrielle Elektronik und Materialwissenschaften
Gußhausstraße 27-29/366, A-1040 Wien

The Society for Microelectronics (GMe — Gesellschaft für Mikroelektronik)

E. Gornik, K. Riedling

Gesellschaft für Mikroelektronik,
c/o Institut für Industrielle Elektronik und Materialwissenschaften,
TU Wien
Gußhausstraße 27 – 29, A-1040 Wien

1. Goals of the Society for Microelectronics

The Society for Microelectronics (GMe) was founded in 1985 with the aim to "*support microelectronics technology and its applications*" in Austria. The GMe defines its tasks as follows:

- Support of university-based "high-tech" research in the areas of microelectronics, semiconductor technology, sensors, and opto-electronics;
- Operation of research facilities;
- Support and consulting for industry, in particular, for small and medium enterprises, within the area of microelectronics.

The central task of the GMe is to provide an internationally competitive *infra-structure* in the area of microelectronics technology. The GMe allocates funds to maintain research projects in the fields of semiconductor technology, sensors, opto-electronics, and ASIC design. Thus the infra-structure support generates a base for research projects that are funded by other funding agencies.

2. Activities of the Society

Due to funding constraints, the present focal point activity of the GMe is the operation of university-based laboratories for microelectronics technology. Nevertheless, the GMe tries to support the other activities mentioned above in their submission and administration of certain projects.

The main task of the GMe in the area of microelectronics technology is the operation of the cleanroom laboratories in Vienna and Linz. The GMe has coordinated the construction of the Microstructure Center (MISZ — Mikrostrukturzentrum) in Vienna; the funds were supplied by the Austrian Federal Ministry of Science and Research. The GMe now finances a significant part of the operation costs for the cleanroom laboratories in Vienna and Linz.

2.1 Microelectronics Technology — Cleanroom Vienna

The following university institutes receive support within this focal point activity:

- TU Wien:
  - Institut für Festkörperelektronik
  - Institut für Industrielle Elektronik und Materialwissenschaften

2.2 Microelectronics Technology — Cleanroom Linz

The following university institutes receive support within this focal point activity:

- Johannes Kepler Universität Linz:
  - Institut für Halbleiter- und Festkörperphysik
  - Institut für Mikroelektronik

3. Other Activities of the Society

In 2001, the biennial GMe seminar took place at the Vienna University of Technology on April 5 and 6, 2001 under the title "*GMe Forum 2001*". The seminar presented twelve invited lectures given by international experts, and 37 oral and poster contributions which resulted from work supported by the GMe. Great emphasis was put into making the seminar more attractive to an industrial audience, thus contributing to an improved knowledge transfer between universities and industry.

One of the declared tasks of the GMe is to provide information on current Austrian academic activities in the field of microelectronics to industry, in particular to Austrian small- and medium enterprises (SMEs). To enhance the distribution of the results of the research work done with GMe support, the GMe has put the contents of its annual reports — 1995 through 2001 — and the proceedings of the latest seminars organized by the GMe in 1999 and 2001 on its Web server. In late 2000, a new GMe Web server has been introduced. This server now provides a variety of search facilities into the reports, thus acting as a Microelectronics Knowledge Base. The server has apparently been fairly well accepted by the international community. Access statistics show an average of 77 requests per day, with peaks of more than 100; an amazingly large percentage of the accesses to the GMe server — about two thirds — originates from net domains outside Austria. The GMe Web server is available under the address:

http://gme.tuwien.ac.at/

4. Changes to the Society's Managing Committee

Günther BAUER, who has been the Society's president for the past two years, stepped down by the end of 2001. His successor is Erich GORNIK, head of the Institute of Solid State Electronics (*Institut für Festkörperelektronik*) at the Vienna University of Technology, and in charge of the cleanroom laboratories at his university. Gerhard KRAINZ who represented the Wirtschaftskammer Österreich has retired in late 2001; Heinz LASEK who is affiliated to the same organization took his place. Arnold SCHMIDT who has been a long-standing member of the board stepped down from his position in the board, and Rainer URANSCHEK who has been the representative of the Forschungs- und

Prüfzentrum Arsenal in Vienna left this institution in 2000 and therefore also the GMe's board. Ernst HAMMEL and Humbert NOLL newly joined the board as representatives of Electrovac GmbH and AMS Austria Mikrosystems AG, respectively.

We also have the sad duty to announce that Wolfgang ATTWENGER has died in the Winter of 2002. He was formerly with ÖFZ Seibersdorf and has been a member of the GMe's board from the time of the Society's foundation, and only retired from the board by the end of 1999. We will remember him as a person who untiringly promoted the issues of microelectronics during his lifetime.

5. The Annual Report for 2001 of the Society for Microelectronics

The GMe is currently supporting the microelectronics technology activities of the clean-room laboratories in Vienna and Linz. All projects described in this report were carried out in the cleanrooms in Vienna and Linz, respectively. They are *not* specific projects of the GMe but were funded by a variety of other sources. They all have in common that they use the infra-structure provided by the GMe. It would therefore not have been possible to carry out these projects without the support by the GMe.

Contents

Microelectronics Technology — Cleanroom Vienna

Cleanroom Vienna

G. Strasser

**Mikrostrukturzentrum der Technischen Universität Wien,
Floragasse 7, A-1040 Vienna, Austria**

In this report a summary of the main activities in the MISZ TU Wien (Mikrostrukturzentrum der Technischen Universität Wien) during the year 2001 will be given. We will focus on projects taking intensive use of the cleanroom and the available technologies within. Part of the mission of the MISZ is the development and production of optoelectronic and microelectronic prototype devices. This includes state of the art growth of III-V nanostructures and silicon processing, structuring techniques utilizing standard contact lithography, the production of patterned masks, ion milling as well as dry etching and plasma enhanced chemical vapor deposition, electron beam writing, focused ion beam etching and depositing, and different metallization techniques. A variety of device characterization techniques like transport measurements, spectroscopic techniques for optoelectronic devices and surface probing like scanning tunneling microscopy and atomic force microscopy are available.

1. Introduction

An overview of the main research efforts with a high need of technological input are presented within this scientific report. This summary includes the majority of experimental projects of the solid state electronics institute (Festkörperelektronik TU Wien) during the last twelve months. All the projects described below like transport studies in low dimensional semiconductor nanostructures, scanning probe spectroscopy, realization of new and improved optoelectronic devices, quantum cascade lasers, THz sources, and the characterization of microelectronic devices take full advantage of the technologies installed in the cleanroom of the MISZ (Reinraum Mikrostrukturzentrum der TU Wien).

To structure this yearly increasing number of various activities four research areas are introduced, namely:

- Optoelectronics
- Transport in III-V Semiconductors
- Silicon Device Testing
- Focused Ion Beam Developments

To satisfy this variety of topics and demonstrate e.g. optoelectronic devices as well as basic research and the development of new tools for semiconductor industries, various technologies have to be kept at state of the art performance.

This includes growth of semiconductor nanostructures (molecular beam epitaxy), as well as a complete process line including structure definition (lithography), structure transfer (reactive ion etching, focussed ion beam etching, ion milling, wet chemical etching techniques) and coating with metals and/or dielectrics (plasma-enhanced chemical vapor deposition, sputtering, electron gun evaporation, focussed ion beam deposi-

tion). Surface morphology as well as local carrier concentrations probing is done with a conventional Atomic Force Microscope (AFM) in combination with a Scanning Capacitance Microscopy (SCM) extension.

All the equipment necessary for the above mentioned technologies needs the cleanroom environment (cooling, filtered air, constant temperature and humidity, high quality water, different inert gases) as well as periodic maintenance of the equipment and the cleanroom itself, e.g. pumping systems (rotary pumps, turbo pumps), exhaust filtering, liquid nitrogen, and cleaning and repair. Testing of the cleanroom quality and adjustment (laminar airflow, filters, cooling, humidity, and temperature) is done periodically.

For a more general overview the listed projects and the attached publication list may give more insides on the broad range of activities in our facility.

2. Research Activities

The research activities are described in detail in the subsequent part of this report:

2.1 Optoelectronics

E. Gornik. G. Strasser, R. Zobl, M. Kast, C. Pacher:
Search for Plasma Instability Driven THz Radiation Sources

J. Darmo, G. Strasser, T. Müller, K. Unterrainer:
THz Plasmon Emission from an LT-GaAs/GaAs Homojunction

J. Darmo, G. Strasser, T. Müller, K. Unterrainer, Tuan Le, A. Stingl:
Voltage Controlled Intracavity Emitter of Terahertz Radiation

T. Müller, R. Bratschitsch, G. Strasser, K. Unterrainer:
Direct Measurement of Intersubband Population Dynamics

J. Ulrich, J. Kreuter, W. Schrenk, G. Strasser, K. Unterrainer:
Long Wavelength (15 and 23 µm) GaAs/AlGaAs Quantum Cascade Lasers

W. Schrenk, S. Anders, E. Gornik, G. Strasser:
Room Temperature Operation of Distributed Feedback GaAs/AlGaAs Quantum-Cascade Lasers

S. Anders, W. Schrenk, G. Strasser:
Room Temperature Lasing of Electrically Pumped Quantum Cascade Micro-Cylinders

R. Zobl, E. Gornik, I.V. Altukhov, M.S. Kagan:
Spectrum of Low-Voltage THz Emission of Strained p-Ge Resonant-State Laser

2.2 Transport in III-V Semiconductors

M. Coquelin, C. Pacher, M. Kast, G. Strasser, E. Gornik:
Transport Studies on Double Period Superlattices Utilizing Hot Electron Spectroscopy

M. Kast, C. Pacher, G. Strasser, E. Gornik:
Transport Through Wannier-Stark States in Biased Finite Superlattices

C. Pacher, G. Fasching, M. Kast, G. Strasser, E. Gornik:
Study of Electron-LO Phonon Scattering in Wide GaAs Quantum Wells Utilizing Hot Electron Spectroscopy

J. Smoliner, D. Racoszy, G. Strasser:
Electron Transport in Kinetic Heterostructures

2.3 Silicon Device Testing

W.Brezna, S.Harasek, H.Enichlmair, E.Bertagnolli, E.Gornik, J.Smoliner:
Scanning Capacitance Microscopy with Zirconium Oxide as High-k Dielectric Material

M. Litzenberger, D.Pogany, E.Gornik, K. Esmark:
Effect of Pulse Risetime on Trigger Homogeneity in Grounded Gate nMOSFET Electrostatic Discharge Protection Devices

M. Blaho, D. Pogany, E. Gornik, W. Wilkening, J. Hieber:
Backside Interferometric Investigations of a DMOS Clamp Under ESD Stress

D. Pogany, C. Fürböck, M. Litzenberger, P. Kamvar, S. Bychikhin, E. Gornik:
Study of Trigger Instabilities in ESD Protection Devices Using Backside Laser Interferometry

S. Bychikhin, M. Litzenberger, P. Kamvar, D. Pogany, E. Gornik, G. Groos, M. Stecher:
Laser Interferometric Mapping of Smart Power ESD Protection Devices with Different Blocking Capabilities

V. Dubec, S. Bychikhin, M. Litzenberger, D. Pogany, E. Gornik, K. Esmark, W. Stadler:
An Optical Setup for Investigation of Internal Device Behavior Under CDM-Like ESD Stress

S. Harasek, B. Basnar, J. Smoliner, E. Bertagnolli:
Ultrathin Zirconium Dioxide for future MOS Technology

G. Otto, G.Hobler:
Molecular Dynamic Simulations of Ion Induced Damage in Silicon

2.4 Focused Ion Beam Developments

H.D. Wanzenboeck:
Fabrication Technology for Sub-100 nm Semiconductor Devices

H. Langfischer:
Evolution of Tungsten Film Deposition Induced by Focused Ion Beam

A. Lugstein. E. Bertagnolli, C. Krantz, B. Mizaikoff:
Integrating Micro- and Nanoelectrodes into Atomic Force Microscopy Cantilevers using Focused Ion Beam Techniques

A. Lugstein. W. Brezna, E. Bertagnolli:
Impact of Focused Ion Beam Assisted Front End Processing on n-MOSFET Degradation

Project Information

Project Manager

Reinraum MISZ TU Wien, G. Strasser

Floragasse 7, A-1040 Wien

Project Group

Last Name	First Name	Status	Remarks
Anders	Solveig	postdoc	
Bertagnolli	Emmerich	o. prof.	
Blaho	Matej	dissertation	
Boxleitner	Winfried	postdoc	
Bychikhin	Sergey	postdoc	
Bratschitsch	Rudolf	dissertation	
Coquelin	Michael	student	
Darmo	juraj	postdoc	
Dzigal	Elvira	technician	
Fasching	Gernot	student	
Fehlmann	Gerhard	student	
Fürböck	Christoph	dissertation	
Gornik	Erich	o. prof.	
Harasek	Stefan	dissertation	
Hobler	Gerhard	ao. prof.	
Kamvar	Parvis	student	
Kast	Michael	dissertation	
Kellermann	Peer	dissertation	
Kröll	Peter	technician	
Langfischer	Helmut	dissertation	GMe
Litzenberger	Martin	dissertation	
Lugstein	Alois	univ. ass.	
Maier	Harald	student	
Müller	Thomas	dissertation	
Otto	Gustav	dissertation	
Pacher	Christoph	dissertation	
Pogany	Dionyz	univ. ass.	

Last Name	First Name	Status	Remarks
Prinzinger	Johannes	technician	
Rakoczy	Doris	dissertation	
Riegler	Erich	technician	
Schinnerl	Markus	technician	
Schenold	Helmut	technician	
Schrenk	Werner	dissertation	
Smoliner	Jürgen	ao. prof.	
Strasser	Gottfried	univ. ass.	
Ulrich	Jochen	dissertation	
Unterrainer	Karl	ao. prof.	
Wanzenböck	Heinz	univ. ass.	
Zobl	Reinhard	dissertation	

Books and Contributions to Books

1. E.Gornik, R.Kersting, "*Coherent THz Emission in Semiconductors*", Semiconductors and Semimetals, 67, 389, Academic Press (2001)
2. R. Bratschitsch and K. Unterrainer, "*Terahertz physics of semiconductor heterostructures*"; Encyclopedia of Modern Optics, Academic Press, to be published February 2002.

Publications in Reviewed Journals

1. K. Unterrainer, R. Kersting, R. Bratschitsch, T. Müller, G. Strasser, J.N. Heyman; "*Few-cycle THz spectroscopy of semiconductor quantum structures*"; Physica **E9**, 76 (2001)
2. K. Kempa, E. Gornik, K. Unterrainer, M. Kast and G. Strasser, "*Resonant Tunneling mediated by resonant emission of inter-subband plasmons*"; Phys. Rev. Lett. **86**, 2850 (2001)
3. J. Smoliner, R. Heer, G. Strasser, C.Strahberger, "*Magnetic field effects and $k_{//}$-filtering in BEEM on GaAs-AlGaAs resonant tunneling structures*", Applied Physics **A72**, 233, (2001)
4. G. Strasser; "*Monomodige GaAs/AlAs Quantenkaskadenlaser im Dauerstrichbetrieb – Continuous wave operation of single mode GaAs/AlAs quantum cascade lasers*"; LaserOpto **33**, 30 (2001)
5. H. Bachhofer, H. Reisinger, E. Bertagnolli, H. von Philipsborn, "*Transient conduction in multidielectric silicon-oxide-nitride-oxide-semiconductor structures*", J. Appl. Phys **89**, 2791 (2001).
6. C. Strahberger, J. Smoliner, R. Heer, G. Strasser, "*Enhanced $k_{//}$filtering effects in ballistic electron emission experiments*", Phys. Rev. **B63**, 205306 (2001)

7. C. Kranz, G. Friedbacher, B. Mizaikoff, A. Lugstein, J. Smoliner, E. Bertagnolli, "*Integrating an Ultramicroelectrode in an AFM Cantilever*", Combined Power for Enhanced Information, Anal. Chem. **73**, 2491, (2001)

8. G. Strasser, S. Gianordoli, W. Schrenk, E. Gornik, A. Mücklich, M. Helm; "*MBE-grown GaAs/AlGaAs and strained InGaAs/AlGaAs/GaAs quantum cascade lasers*"; Journal of Crystal Growth **227-228**, 197 (2001)

9. M. Kast, C. Pacher, G. Strasser, E. Gornik, "*Narrow electron injector for ballistic electron spectroscopy*", Appl. Phys. Lett. **78**, 3639 (2001).

10. D. Pogany, J.A. Chroboczek, G. Ghibaudo, "*Random telegraph signal noise mechanisms in reverse base current of hot carrier degraded submicron bipolar transistors: Effect of carrier trapping during stress on noise characteristics*", J. Appl. Phys., **89**, 4049 (2001).

11. B.Basnar, S.Golka, E.Gornik, S.Harasek, E.Bertagnolli, M.Schatzmayer, and J.Smoliner, "*Quantitative scanning capacitance microscopy investigations on p-doped Si-Multilayers*", J. Vac. Sci. Technol. **19**, 1808 (2001)

12. B. Goebel, D. Schumann, and E. Bertagniolli, "*Vertical MOSFETs for Extremelely High Density Memories: The Impact of Interface Orientation on Device Performance*", IEEE Trans. El. Devices **48**, 897 (2001).

13. J.N. Heyman, P. Neocleous, D. Herbert, P.A. Crowell, T. Müller, K. Unterrainer, "*Terahertz emission from GaAs and InAs in a magnetic field*", Phys. Rev. B **64**, 085202 (2001).

14. C. Pacher, C. Rauch, G. Strasser, E. Gornik, F. Elsholz, G. Kießlich, A. Wacker, and E. Schöll, "*Antireflection coatings for miniband transport and Fabry-Pérot resonances in GaAs/AlGaAs superlattices*", Appl. Phys. Lett. **79**, 1486 (2001).

15. T. Müller, R. Bratschitsch, G. Strasser, K. Unterrainer, "*Intersubband absorption dynamics in coupled quantum wells*", Appl. Phys. Lett. **79**, 2755 (2001).

16. R. Bratschitsch, T. Müller, N. Finger, G. Strasser, K. Unterrainer, C. Sirtori: "*Monitoring the ultrafast electric field change at a mid-infrared plasma Bragg mirror*"; Opt. Lett., **26**, 1618 (2001).

17. J. Smoliner, B. Basnar, S.Golka, E. Gornik, B.Löffler, M.Schatzmayer, H.Enichlmair, "*Mechanism of bias dependent contrast in Scanning Capacitance Microscopy images*", Appl. Phys. Lett. **79**, 3182 (2001)

18. M. Leicht, G. Fritzer, B. Basnar, S. Golka, J. Smoliner, "*A reliable course of Scanning Capacitance Microscopy analysis applied for 2D-Dopant Profilings of Power MOSFET Devices*", Microelectronics Reliabilitiy **41**, 1535 (2001)

19. A. Edelmann, C. Ruzicka, J. Frank, B. Lendl, W. Schrenk, E. Gornik, G. Strasser; "*Towards functional group specific detection in high-performance liquid chromatography using mid infrared quantum cascade lasers*"; J. Chromatogr. A **934**, 123 (2001)

20. L. Palmetshofer, M. Gritsch, and G. Hobler, "*Range of ion-implanted rare earth elements in Si and SiO_2*", Mater. Sci. Eng. B **81**, 83 (2001).

21. W. Boxleitner, G. Hobler, V. Klüppel, and H. Cerva, "*Dynamic simulation of topography evolution and damage formation in TEM sample preparation using focused ion beams*", Nucl. Instr. Meth. B **175-177**, 102 (20019.

22. W. Boxleitner and G. Hobler, "*FIBSIM -- Dynamic Monte Carlo simulation of compositional and topography changes caused by focused ion beam milling*", Nucl. Instr. Meth. B **180**, 125 (2001).

23. G. Hobler and G. Betz, "*On the useful range of application of molecular dynamics simulations in the recoil interaction approximation*", Nucl. Instr. Meth. B **180**, 203 (2001).

24. F. Elsholz, A. Wacker, E. Schöll, M. Kast, G. Strasser, E. Gornik: "*Magnetotransport through semiconductor superlattices*"; Phys. Rev. B **63**, 33312 (2001)

25. C. Messner, H. Kostner, R.A. Höpfel, K. Unterrainer, "*Time-resolved THz-Spectroscopy of Proton Bombarded InP*", JOSA B **18**, 1369 (2001).

26. S. Bychikhin, M. Litzenberger, R. Pichler, D. Pogany, E. Gornik, G. Groos and M. Stecher, "*Thermal and free carrier laser interferometric mapping and failure analysis an "anti"-serially connected npn transistor ESD protection structures of smart power technology*", *Microel. Reliab.*, **41** (2001), pp.1501-1506.

27. M. Litzenberger, R. Pichler, S. Bychikhin, D. Pogany, K. Esmark, H. Gossner and E. Gornik, "*Effect of pulse risetime on trigger homogeneity in single finger grounded gate nMOSFET electrostatic discharge protection devices*", *Microel. Reliab.,* **41** (2001), pp. 1385-1390.

28. K. Unterrainer, R. Bratschitsch, T. Müller, R. Kersting, J.N. Heyman, G. Strasser; "*Few-cycle THz Spectroscopy of Semiconductor Quantum Structures*"; in *Proc. 25th Int. Conf. Phys. Semicond.*, Editors: N. Miura, T. Ando, Springer proceedings in physics **87**, 579 (2001)

29. T. Schwarzl, W. Heiss, G. Springholz, S. Gianordoli, G. Strasser, M. Aigle, H. Pascher; "*Strongly detunded IV-VI microcavity and microdisk resonances: mode splitting and lasing*"; in *Proc. 25th Int. Conf. Phys. Semicond.*, Editors: N. Miura, T. Ando, Springer proceedings in physics **87**, 677 (2001)

30. M. Helm, G. Strasser; "*Correlation of vertical transport and infrared absorption in GaAs/AlGaAs superlattices*"; in *Proc. 25th Int. Conf. Phys. Semicond.*, Editors: N. Miura, T. Ando, Springer proceedings in physics **87**, 715 (2001)

31. C. Pacher, G. Strasser, E. Gornik, F. Elsholz, A. Wacker, E. Schöll, "*Optics with Ballistic Electrons: Anti-Reflection Coatings for GaAs/AlGaAs Superlattices*", in Proc. 25th Int. Conf. Phys. Semicond., Editors: N. Miura, T. Ando, Springer proceedings in physics **87**, 743 (2001)

32. J. Ulrich, R. Zobl, G. Strasser, K. Unterrainer, "*Terahertz emission from semiconductor nanostructures*" in Terahertz Sources and Systems, NATO Science series, II. Mathematics, Physics and Chemistry – Vol. 27

33. S. Bychikhin, M. Litzenberger, R. Pichler, D. Pogany, E. Gornik, G. Groos and M. Stecher, "*Thermal and free carrier laser interferometric mapping and failure analysis an "anti"-serially connected npn transistor ESD protection structures of smart power technology*", ESREF 2001, 1.-5.Oct. 2001, Bordeaux, France

34. M. Litzenberger, R. Pichler, D. Pogany, E. Gornik, K. Esmark and H. Gossner "*Influence of Layout parameters on Triggering Behaviour in 0.35µm and 0.18µm Process gg-nMOS ESD Protection Devices*", *Proc. ESSDERC 2001*, Sept. 11.-13. 2001, Nürnberg, Germany, pp. 335-338.

35. S. Bychikhin, M. Litzenberger, P. Kamvar, D. Pogany and E. Gornik G. Groos and M. Stecher, "*Laser Interferometric Mapping of Smart Power ESD Protection Devices with Different Blocking Capabilities*", *Proc. ESSDERC 2001*, Sept. 11.-13. 2001, Nürnberg, Germany, pp. 232-234.

36. D. Pogany, C. Fürböck, M. Litzenberger, G. Groos, K. Esmark, P. Kamvar, H. Gossner, M. Stecher and E. Gornik, "*Study of trigger instabilities in smart power technology ESD protection devices using a laser interferometric thermal mapping technique*", Proc. EOS/ESD Symposium, Sept 9-13, Portland, USA, p.216-227.

37. D. Pogany, E. Gornik, K. Esmark, and H. Gossner, "*RTS noise due to electrostatic discharge (ESD) stress-induced localized damage in the channel of grounded-gate nMOS ESD protection devices*", accepted to Int. Conf. on Noise in Physical Systems and 1/f Fluctuations (ICNF'2001), Gainsville, 22-25 Oct. USA.

38. M. Litzenberger, R. Pichler, C. Fürböck, S. Bychikhin, D. Pogany, E. Gornik, K. Esmark, G. Groos, H. Gossner, and M. Stecher, "*Laser-interferometric investigation of triggering behavior in CMOS and smart power technology electrostatic discharge (ESD) protection structures*", GME Days, 5.-6. April 2001.

39. W. Schrenk, N. Finger, S. Gianordoli, L. Hvozdara, E. Gornik, G. Strasser; "*Infrared Quantum Cascade Laser*", ISBN: 3-901578-07-2, Proceedings GMe Forum 2001, 67 (2001)

40. R. Bratschitsch, T. Müller, G. Strasser, K. Unterrainer; "*Coherent Terahertz Emission from Optically Pumped Parabolic Quantum Wells*", ISBN: 3-901578-07-2, Proceedings GMe Forum 2001, 107 (2001)

41. C. Pacher, M. Kast, C. Coquelin, G. Fasching, G. Strasser, E. Gornik; "*Ballistic Electron Spectroscopy of Quantum Mechanical Anti-reflection Coatings for GaAs/AlGaAs Superlattices*", ISBN: 3-901578-07-2, Proceedings GMe Forum 2001, 137 (2001)

42. D. Rakoczy, G. Strasser, J. Smoliner; "*Ballistic Electron Emission Spectroscopy on Biased GaAs-AlGaAs Superlattices in Transverse Magnetic Fields*", ISBN: 3-901578-07-2, Proceedings GMe Forum 2001, 143 (2001)

43. J. Ulrich, R. Zobl, W. Schrenk, G. Strasser, K. Unterrainer, E. Gornik; "*Band Structure Engineering for Terahertz Quantum Cascade Lasers*", ISBN: 3-901578-07-2, Proceedings GMe Forum 2001, 151 (2001).

44. T. Berer, G. Pillwein, G. Brunthaler, G. Strasser; "*Fabrication of AlGaAs Nanostructures*", ISBN: 3-901578-07-2, Proceedings GMe Forum 2001, 159 (2001)

45. T. Schwarzl, W. Heiss, G. Springholz, S. Gianordoli, G. Strasser, M. Aigle, H. Pascher; "*Mode Splitting and Lasing in Detuned Lead Salt Microcavity and Microdisk Resonances*", ISBN: 3-901578-07-2, Proceedings GMe Forum 2001, 197 (2001)

46. M. Litzenberger, R. Pichler, S. Bychikhin, D. Pogany, K. Esmark, H. Gossner and E. Gornik, "*Effect of pulse risetime on trigger homogeneity in single finger grounded*

gate nMOSFET electrostatic discharge protection devices", ESREF 2001, 1.-5.Oct. 2001, Bordeaux, France

47. M. Litzenberger, C. Fürböck, D.Pogany, E. Gornik, K. Esmark, G. Groos, H. Gossner, M. Stecher: "*Study of trigger homogeneity in ESD protection devices using backside laser interferometry*", To be published in Proc. ITE'2001, Informationstagung Mikroelektronik 2001, Vienna, pp.xx-yy.
48. G. Strasser; "*Light emitter based on intersubband transitions*"; Proc. of the Optoelectronics & Photonics Winter School, 4-11.3.2001 Trento, Italy, to be published in "quaderni di ottica e fotonica"
49. Heinz D.Wanzenboeck, Emmerich Bertagnolli,Josef Brenner, Herbert Störi; "*Effects of Gas Phase Composition on Focused Ion Beam Induced Surface Deposition*"; to be published in Proceedings of the Electrochemical Society, ECS Spring 2001 Meeting, Washington D.C.
50. Heinz D.Wanzenboeck, Emmerich Bertagnolli, Bernhard Basnar, Juergen Smoliner, Martin Gritsch, Herbert Hutter, Josef Brenner, C. Tomastik, Herbert Störi; "*Surface and Interface Study of Ion Beam Deposited Silicon Oxide Thin Films*", to be published in Proceedings of the Electrochemical Society, ECS Spring 2001 Meeting, Washington D.C.
51. H.D. Wanzenböck, E. Bertagnolli, U. Grabner, G. Hammer, P. Pongratz , "*Structure investigationof FIB-prepared microchips using transmission electron microscopy (TEM)*", to be published in Proc. ITE'2001, Informationstagung Mikroelektronik 2001, Vienna
52. H.D. Wanzenboeck, S.G. Gergov, W. Brezna, E. Bertagnolli, "*Local Deposition of Silicon Oxide for phase shift photomasks*", to be published in Proc. ITE'2001, Informationstagung Mikroelektronik 2001, Vienna
53. J. Ulrich, R. Zobl, W. Schrenk, G. Strasser, K. Unterrainer, "*Terahertz quantum cascade emitters*" to published in Proceedings of the Workshop on Electronic Material Nanostructures, Warsaw, Poland (2001).
54. D.Rakoczy, G.Strasser, J.Smoliner, "*Band offsets of InAs Self-assembled Dots on GaAs studied by Ballistic Electron Emission Microscopy*", STM01 Conference, Vancouver (15-20.07.2001)
55. H. Wanzenboeck, A. Lugstein, H. Langfischer, S. Harasek, E. Bertagnolli; U. Grabner, P. Pongratz, B. Basnar, J. Smoliner, E. Gornik; "*Effects of Ga-ion irradiation on chemical and electrical properties of materials processed by a Focused Ion Beam (FIB)*", MRS Proceedings Volume 647, O6.6 (2001)
56. W. Schrenk, S. Gianordoli, N. Finger, E. Gornik, G. Strasser, "*Continuous-wave operation of distributed feedback AlAs/GaAs quantum cascade lasers*", CLEO2001, Technical Digest, 54 (2001)
57. T. Müller, R. Bratschitsch, N. Finger, G. Strasser, K. Unterrainer, and C. Sirtori, "*Ultrafast response of a plasma Bragg mirror*"; CLEO/QELS '01 OSA Technical Digest, ISBN 1-55752-676-1, p. 315 (2001).
58. J. Ulrich, R. Zobl, G. Strasser, K. Unterrainer, "*Terahertz emission from semiconductor nanostructures*"; in "Terahertz Sources and Systems", 115-124, Eds. R. E. Miles et al., Kluwer, Dordrecht (2001)

59. G. Hobler and C. S. Murthy, "*Towards a comprehensive model of electronic stopping in amorphous and crystalline silicon*", Ion Implantation Technology 2000, pp. 209-212, IEEE, 2001.

60. G. Hobler and V. Moroz, "*Initial conditions for transient enhanced diffusion: Beyond the plus-factor approach*", Proc. SISPAD 2001, pp. 34-37, Springer, Wien, 2001.

61. M. Litzenberger, D. Pogany, E. Gornik , K. Esmark and H. Gossner "*Influence of stress current and pulse risetime on triggering behavior of submicron gg-NMOSFET protection devices investigated by a thermal mapping technique*", Tagungsband 7 ESD-Forum 2001, 11 –12.12.2001, Berlin, BRD p. 105

62. R. Bratschitsch, T. Müller, G. Strasser, K. Unterrainer; "*Intersubband relaxation dynamics in semiconductor quantum structures*"; accepted for publication in Physica E

63. J. Ulrich, G. Strasser, K. Unterrainer; "*Terahertz quantum cascade emitters based on AlAs/GaAs*"; accepted for publication in Physica E

64. W. Schrenk, E. Gornik, H. Page, C. Sirtori, V. Ortiz, G. Strasser; "*High performance single mode GaAs quantum cascade lasers*"; accepted for publication in Physica E

65. M. Kast, C. Pacher, M. Coquelin, G. Fasching, G. Strasser, E. Gornik; "*Narrow electron injector for hot electron spectroscopy*"; accepted for publication in Physica E.

66. S. Hofer, H. Hirner, R. Bratschitsch, G. Strasser, K. Unterrainer; "*Photoconductive Response of InAs/GaAs quantum dot stacks*"; accepted for publication in Physica E

67. M. Kast, C. Pacher, M. Coquelin, G. Fasching, G. Strasser, E. Gornik; "*LO-phonon assisted hot electron transport in biased superlattices*"; accepted for publication in Physica B.

68. C. Pacher, G. Strasser, E. Gornik, F. Elsholz, G. Kießlich, A. Wacker, and E. Schöll, "*Optics with ballistic electrons: antireflection coatings for GaAs/AlGaAs superlattices*", accepted for publication in Physica E.

69. D. Rakoczy, G. Strasser, J. Smoliner, "*Ballistic Electron Emission Microscopy for Local Measurement of Band Offsets on InAs Self-assembled Quantum Dots on GaAs*", accepted for publication in Physica B

70. T. Müller, R. Bratschitsch, G. Strasser, K. Unterrainer, "*Direct measurement of intersubband dynamics*", accepted for publication in Physica B

71. D. Rakoczy, G.Strasser, J.Smoliner; "*Ballistic Electron Emission Microscopy of "on-surface" Self Assembled InAs Dots and Wetting Layers*"; accepted for publication in J. Vac. Sci. Technol. B

72. A. Lugstein, E. Bertagnolli, C. Kranz, B. Mizaikoff, "*Fabrication of a Ring-Nanoelectrode Integrated in an AFM-Tip: A Novel Approach Towards Simultaneous Electochemical and opographical Imaging*", Surface and Interface Analysis, accepted for publication

73. G. Strasser, W. Schrenk, S. Anders, E. Gornik; "*Single mode GaAs Quantum Cascade Laser*"; accepted for publication in Microelectronic Engineering (NPMS-5)

74. S. Anders, W. Schrenk, E. Gornik, G. Strasser, "*Room temperature emission of GaAs/AlGaAs superlattice quantum cascade lasers at 12.6 μm*", accepted for publication in Appl. Phys. Lett.
75. J. Ulrich, J. Kreuter, W. Schrenk, G. Strasser, K. Unterrainer, "*Long wavelength (15 and 23 μm) GaAs/AlGaAs quantum cascade lasers*", acepted for publication in Appl. Phys. Lett.
76. J.Smoliner, R. Heer, G.Strasser, "*BEEM/S on GaAs-AlGaAs resonant tunneling structures and quantum wires*", submitted to Surface and Interface Analysis
77. D.Rakoczy, G.Strasser, J.Smoliner, "*L-Valley Electron Transport in GaAs-AlAs Double Barrier Resonant Tunneling Structures Studied by Ballistic Electron Emission Microscopy*", submitted to Phys. Rev. Lett.
78. B.Basnar, S.Golka, E.Gornik, J.Smoliner, H.Enichlmair, "*Calibrated Scanning Capacitance Microscopy for Two-Dimensional Carrier Mapping of n-type Implants in p-doped Si–Wafers*", submitted to Semicond. Sci. Technol.
79. K. Kempa, Y. Zhou, J. R. Engelbrecht, P. Bakshi, H. I. Ha, J. Moser, M.J. Naughton, J. Ulrich, G. Strasser, E. Gornik, K. Unterrainer; "*Transport signatures of intersubband electron-electron scattering in quantum wells in strong magnetic fields*"; submitted to Phys. Rev. Lett.
80. F. Eickemeyer, R. Reimann, M. Woerner, T. Elsaesser, S. Barbieri, C. Sirtori, G. Strasser, T. Müller, R. Bratschitsch, K. Unterrainer; "*Ultrafast coherent electron transport in semiconductor quantum cascade structures*"; submitted to Phys. Rev. Lett.
81. J. Darmo, G. Strasser, T. Müller, R. Bratschitsch, and K. Unterrainer, "*Surface-modified GaAs terahertz plasmon emitter*", submitted to Appl. Phys. Lett.
82. S. Harasek, H.D. Wanzenboeck, B. Basnar, J. Smoliner, J. Brenner, H. Stoeri, E. Gornik, and E. Bertagnolli, "*MOCVD Growth and Nanoscale Characterization of Zirconium Oxide Thin Films*", submitted to Thin Solid Films

Presentations

1. E. Gornik, S. Gianordoli, L. Hvozdara, W. Schrenk, A. Lugstein, N. Finger, J. Faist, G. Strasser; (invited) "*Long-wavelength GaAs-AlGaAs quantum-cascade microlasers*", Photonics West, San Jose, California, USA, 20-26.1.2001
2. K. Unterrainer (invited), "*THz emission from semiconductor quantum structures*", Workshop on Quantum Heterostructures and THz Electronics, Regensburg, Germany, 1.2.2001.
3. G. Strasser (invited); "*Nanostructures in Photonics*"; Optoelectronics & Photonics Winter School, Trento, Italy, 4-11.3.2001
4. G. Strasser (invited); "*Single mode continous wave GaAs quantum cascade lasers*"; APS March Meeting, 12-16.3.01, Seattle, USA
5. R. Bratschitsch, T. Müller, N. Finger, G. Strasser, K. Unterrainer, C. Sirtori; "*Non-instantaneous response of a plasma Bragg mirror*"; APS March Meeting, 12-16.3.01, Seattle, USA

6. J.Smoliner, "*Rasterkapazitätsmikroskopie and Halbleiterbauelementen*", GME-Forum, Wien 06.04.2001
7. W. Schrenk, N. Finger, S. Gianordoli, L. Hvozdara, E. Gornik, G. Strasser, "*Infrarot-Quantenkaskadenlaser*", GMe-Forum 2001, Wien, 5.-6.4.2001
8. R. Bratschitsch, T. Müller, G. Strasser, K. Unterrainer; "*Coherent Terahertz Emission from Optically Pumped Parabolic Quantum Wells*"; GMe-Forum 2001, Wien, Austria, 5.-6.4.2001
9. C. Pacher, M. Kast, C. Coquelin, G. Fasching, G. Strasser, E. Gornik; "*Ballistic Electron Spectroscopy of Quantum Mechanical Anti-reflection Coatings for GaAs/AlGaAs Superlattices*"; GMe-Forum 2001, Wien, Austria, 5.-6.4.2001
10. D. Rakoczy, G. Strasser, J. Smoliner; "*Ballistic Electron Emission Spectroscopy on Biased GaAs-AlGaAs Superlattices in Transverse Magnetic Fields*"; GMe-Forum 2001, Wien, Austria, 5.-6.4.2001
11. J. Ulrich, R. Zobl, W. Schrenk, G. Strasser, K. Unterrainer, E. Gornik; "*Band Structure Engineering for Terahertz Quantum Cascade Lasers*"; GMe-Forum 2001, Wien, Austria, April 5-6 2001.
12. G. Strasser und W. Schrenk; "*Epitaktisches Wachstum von gitterangepassten und verspannten III-V Verbindungen*"; GMe-Forum 2001, Wien, Austria, 5.-6.4.2001
13. T. Berer, G. Pillwein, G. Brunthaler, G. Strasser; "*Fabrication of AlGaAs Nanostructures*"; GMe-Forum 2001, Wien, Austria, 5.-6.4.2001
14. T. Schwarzl, W. Heiss, G. Springholz, S. Gianordoli, G. Strasser, M. Aigle, H. Pascher; "*Mode Splitting and Lasing in Detuned Lead Salt Microcavity and Microdisk Resonances*"; GMe-Forum 2001, Wien, Austria, 5.-6.4.2001
15. H. Langfischer, B. Basnar, E. Bertagnolli, H. Hutter, "*Focused ion beam induced local tungsten deposition*", GMe-Forum 2001, Wien, 5.-6. April 2001
16. M. Litzenberger, R. Pichler, C. Fürböck, S. Bychikhin, D. Pogany, E. Gornik, K. Esmark, G. Groos, H. Gossner, and M. Stecher, "*Laser-interferometric investigation of triggering behavior in CMOS and smart power technology electrostatic discharge (ESD) protection structures*", Proceedings GMe Forum 2001, 5.-6. April 2001, ISBN 3-901578-07-2, p.129-132.
17. S. Harasek, S. Golka, J. Smoliner, E. Bertagnolli; "*Ultrathin Silicon Dioxide: Growth and Characterization*", GMe-Forum 2001, Wien, 5.-6. April 2001
18. W. Schrenk, S. Gianordoli, N. Finger, E. Gornik, and G. Strasser, "*Continuous-wave operation of distributed feedback quantum cascade lasers*", CLEO2001, Baltimore, USA, May 6-8 2001
19. T. Müller, R. Bratschitsch, N. Finger, G. Strasser, K. Unterrainer, C. Sirtori; "*Ultrafast response of a plasma Bragg mirror*", CLEO2001, Baltimore, USA, May 6-8 2001
20. J. Ulrich, R. Zobl, W. Schrenk, G. Strasser, and K. Unterrainer; "*Terahertz-quantum cascade emitters*", Middle Infrared Coherent Sources (MICS'2001), St. Petersburg, Russia, June 25-29 2001.
21. C. Kranz, E. L. Huang, B. Mizaikoff, A. Lugstein, E. Bertagnolli, "*Integration of an Ultramicroelectrode in an AFM Cantilever - A Novel Approach for Combining AFM*

and SECM", 2nd International Workshop on Scanning Electrochemical Microscopy, Southamptom, UK, June 29 - July 2, 2001.

22. D.Rakoczy, G.Strasser, J.Smoliner, "*Band offsets of InAs Self-assembled Dots on GaAs studied by Ballistic Electron Emission Microscopy*", STM01 Conference, Vancouver (15-20.07.2001)
23. J.Smoliner, B.Basnar, S.Golka, E.Gornik, S. Harasek, E. Bertagnolli, B.Löffler, M.Schatzmayer, H.Enichlmair: "*Quantitative scanning capacitance microscopy on p-doped Si-Multilayers*", STM01 Conference, Vancouver (15-20.07.2001)
24. B.Basnar, S.Golka, E.Gornik, S. Harasek, E. Bertagnolli, B.Löffler, M.Schatzmayer, H.Enichlmair, J.Smoliner, "*Bias dependent contrast in Scanning Capacitance Microscopy images*", STM01 Conference, Vancouver (15-20.07.2001)
25. C. Pacher, G. Strasser, E. Gornik, F. Elsholz, A. Wacker, G. Kießlich, E. Schöll; "*Optics with Electrons: Fabry-Pérot Resonances and Anti-Reflection Coating for Ballistic Electrons in Finite Superlattices*"; 10th Int. Conf. on Modulated Semiconductor Structures MSS10, Linz, Austria, 23.-27.7.2001
26. W. Schrenk, E. Gornik, H. Page, C. Sirtori, V. Ortiz, G. Strasser; "*High performance single mode GaAs quantum cascade lasers*"; 10th Int. Conf. On Modulated Semiconductor Structures MSS10, Linz, Austria, 23.-27.7.2001
27. J. Ulrich, R. Zobl, W. Schrenk, G. Strasser, K. Unterrainer; "*Terahertz-Quantum Cascade Emitters*"; 10th Int. Conf. on Modulated Semiconductor Structures (MSS10), Linz, Austria, July 23-27 2001.
28. M. Kast, C. Pacher, M. Coquelin, G. Fasching, G. Strasser, E. Gornik, "*An Ultra-narrow Electron Injector for Ballistic Electron Spectroscopy*", 10th International Conference on Modulated Semiconductor Structures (MSS10), Linz, Austria, July 23-27 2001.
29. R. Bratschitsch, T. Müller, G. Strasser, K. Unterrainer, "*Intersubband relaxation dynamics in semiconductor quantum structures*", 10th International Conference on Modulated Semiconductor Structures (MSS10), Linz, Austria, July 23-27 2001.
30. D.Rakoczy, G.Strasser, J.Smoliner, "*Band offset of InAs Self-assembled Dots on GaAs*", 10th International Conference on Modulated Semiconductor Structures (MSS10), Linz, Austria, July 23-27 2001.
31. S. Hofer, H. Hirner, R. Bratschitsch, G.Strasser, K. Unterrainer; "*Photoconductive response of InAs/GaAs quantum dot stacks*"; 10th Int. Conf. on Modulated Semiconductor Structures (MSS10), Linz, Austria, 23.-27.7.2001
32. C. Brink, D. Schneider, G. Ploner, G. Strasser, E. Gornik, "*Magnetophonon resonance in the confinement of an n-GaAs/AlGaAs-heterojunction tuned to a quasi-one-dimensional quantum wire*"; 14th Int. Conf. On the Electronic Properties of Two-dimensional Systems, Prague, Czech Republic, 30.7.-3.8.2001
33. C. Pacher, G. Strasser, E. Gornik, F. Elsholz, G. Kießlich, A. Wacker, E. Schöll, "*Optics with ballistic electrons: antireflection coatings for GaAs/AlGaAs superlattices*", 14th Int. Conf. On the Electronic Properties of Two-dimensional Systems, Prague, Czech Republic, 30.7.-3.8.2001.

34. M. Kast, C. Pacher, M. Coquelin, G. Fasching, G. Strasser, E. Gornik, "*LO-phonon assisted hot electron transport in biased superlattices*", 12th International Conference on Nonequilibrium Carrier Dynamics in Semiconductors (HCIS12), Santa Fe (New Mexico), USA, August 27-31 2001
35. T. Müller, R. Bratschitsch, G. Strasser, K. Unterrainer, "*Direct measurement of intersubband dynamics*", 12th International Conference on Nonequilibrium Carrier Dynamics in Semiconductors (HCIS12), Santa Fe (New Mexico), USA, August 27-31 2001
36. J. Ulrich, R. Zobl, W. Schrenk, G. Strasser, K. Unterrainer, "*Terahertz quantum cascade emission and detection*", 12th International Conference on Nonequilibrium Carrier Dynamics in Semiconductors (HCIS12), Santa Fe (New Mexico), USA, August 27-31 2001.
37. D.Rakoczy, G.Strasser, J.Smoliner, "*Ballistic electron emission microscopy for local measurement of band offsets on InAs self-assembled quantum dots on GaAs*", 12th International Conference on Nonequilibrium Carrier Dynamics in Semiconductors (HCIS12), Santa Fe (New Mexico), USA, August 27-31 2001
38. G. Hobler, V. Moroz, "*Initial conditions for transient enhanced diffusion: Beyond the plus-factor approach*", International Conference on Simulation of Semiconductor Processes and Devices (SISPAD 2001), Athens, Greece, 5.-7.9.2001.
39. D. Pogany, C. Fürböck, M. Litzenberger, G. Groos, K. Esmark, P. Kamvar, H. Gossner, M. Stecher and E. Gornik, "*Study of trigger instabilities in smart power technology ESD protection devices using a laser interferometric thermal mapping technique*", EOS/ESD Symposium, Sept 9-13, Portland, USA, in: Proc. EOS/ESD Symp.'2001, pp.216-227.
40. G. Strasser, W. Schrenk, S. Gianordoli, E. Gornik, H. Page, C. Sirtori, V. Ortiz (invited); "*Room temperature & continuous wave GaAs quantum cascade lasers*"; 6th Int. Conf. on Intersubband Transitions in QuantumWells (ITQW), Asilomar, USA, 10.-14.9.2001
41. R. Bratschitsch, T. Müller, G. Strasser, and K. Unterrainer: "*Ultrafast intersubband probing in the mid-infrared*", 6th International Conference on Intersubband Transitions in Quantum Wells, ITQW '01, Asilomar, USA, 10.-14. 9. 2001.
42. J. Ulrich, R. Zobl, W. Schrenk, G. Strasser, K. Unterrainer (invited); "*Terahertz quantum cascade emitters: the role of intersubband scattering*", 6th International Conference on Intersubband Transitions in Quantum Wells (ITQW '01), Asilomar, USA, September 10-14 2001.
43. W. Schrenk, S. Gianordoli, L. Hvozdara, N. Finger, E. Gornik, and G. Strasser, "*Single mode AlGaAs based quantum cascade lasers*", ITQW´01, Asilomar, USA, 10-14.9.2001
44. J. Darmo, R. Bratschitsch, T. Müller, G. Strasser, K. Unterrainer; "*Coherent THz emission from semiconductor heterostructures*"; Int. Conf. on infrared and millimeter waves (IRMMW), Toulouse, France 10.-14.9.2001
45. M. Litzenberger, R. Pichler, D. Pogany, E. Gornik, K. Esmark and H. Gossner "*Influence of Layout parameters on Triggering Behaviour in 0.35µm and 0.18µm*

Process gg-nMOS ESD Protection Devices", POSTER ESSDERC 2001, Sept. 11.-13. 2001, Nürnberg, Germany, p. 335-338

46. S. Bychikhin, M. Litzenberger, P. Kamvar, D. Pogany and E. Gornik G. Groos and M. Stecher, "*Laser Interferometric Mapping of Smart Power ESD Protection Devices with Different Blocking Capabilities*", ESSDERC 2001, Sept. 11.-13. 2001, Nürnberg, Germay, p.231-234
47. A. Lugstein (invited), W. Brezna, E. Bertagnolli, "*Nonuniform Channel MOS Device*", Symposium Ion Beam Processing of Semiconductor Devices, (ESSDERC 2001 Short Course 1), Sept. 11, Erlangen, Germany
48. C. Kranz, E. L. Huang, B. Mizaikoff, H.-S. Noh, P. Hesketh, A. Lugstein, E. Bertagnolli, "*Electrochemical Imaging with Submicro- and Nanoelectrodes Integrated in AFM-Tips*", 2nd Georgia Tech Conference on Nanoscience and Nanotechnology, Atlanta, U.S.A., Sept. 19-21, 2001.
49. J. Ulrich, R. Zobl, W. Schrenk, G. Strasser, K. Unterrainer (invited); "*Terahertz quantum cascade emitters*", Workshop on Electronic Material Nanostructures: Fabrication and Characterisation, Warsaw, Poland, September 20-23 2001.
50. E. Bertagnolli, "*Focused Ion Beam Technology; A Route to Silicon Nanofabrication*" (invited), CELDIS Workshop on Electronic Material Nanostructures: Fabrication and Characterisation, Warsaw, Poland, Sept. 20-23, 2001
51. D. Piester, M. Ursu, A.A. Ivanov, A.S. Bakin, H.-H. Wehmann, A. Schlachetzki, T. Klaffs, B. Güttler, G. Strasser, E. Gornik; "*InGaAs/InP-Nanostrukturen für Quantenkaskadenlaser*"; Volkswagen-Stiftung Photonik-Symposium 2001, Baden, Austria, 23.-25.9.2001
52. H. Maier, P.O. Kellermann, N. Finger and E. Gornik, R. Winterhoff and F. Scholz, "*Visible red surface-emitting distributed-feedback lasers with a surface grating*", Volkswagen Stiftung Photonik-Symposium 2001, Baden, Austria, 23-25.9.2001.
53. P.O. Kellermann, N. Finger, H.Maier, E. Gornik, M. Ost, F. Scholz, H. Schweitzer, "*Laser diodes with contradirectional surface mode coupling*", Volkswagen Stiftung Photonik-Symposium 2001, Baden, Austria, 23-25.9.2001.
54. C. Kranz, B. Mizaikoff, G. Friedbacher, A. Lugstein, J. Smoliner, E. Bertagnolli, "*Combining SECM and AFM - Integration of an Ultramicroeelctrode in an AFM-Tip*", 4th International Conference on the Development and Technological Application of Scanning Probe Methods (SXM4), Münster, Germany, Sept. 25-27, 2000.
55. M. Litzenberger, R. Pichler, S. Bychikhin, D. Pogany, K. Esmark, H. Gossner and E. Gornik, "*Effect of pulse risetime on trigger homogeneity in single finger grounded gate nMOSFET electrostatic discharge protection devices*", ESREF 2001, 1.-5.Oct. 2001, Bordeaux, France
56. S. Bychikhin, M. Litzenberger, R. Pichler, D. Pogany, E. Gornik, G. Groos and M. Stecher, "*Thermal and free carrier laser interferometric mapping and failure analysis of anti-serial smart power ESD protection structures*", (POSTER) ESREF 2001, 1.-5.Oct. 2001, Bordeaux, France

57. M. Leicht, G. Fritzer, B. Basnar, S. Golka, J. Smoliner, "*A reliable course of Scanning Capacitance Microscopy analysis applied for 2D-Dopant Profilings of Power MOSFET Devices*", Proc. 12th European Symposium on the Reliability of Electron Devices Failure Physics and Analysis (ESREF), 1.-5.Oct. 2001, Bordeaux, France
58. M. Litzenberger, C. Fürböck, D. Pogany, E. Gornik, K. Esmark, G. Groos, H. Gossner, M. Stecher: "*Study of trigger homogeneity in ESD protection devices using backside laser interferometry*", Proc. ITE'2001, Informationstagung Mikroelektronik 2001, Vienna, p.-.
59. D. Pogany, E. Gornik, K. Esmark, and H. Gossner, "*RTS noise due to electrostatic discharge (ESD) stress - induced localized damage in the channel of grounded-gate nMOS ESD protection devices*", accepted to Int. Conf. on Noise in Physical Systems and 1/f Fluctuations (ICNF'2001), Gainsville, 22-25 Oct. USA.
60. C. Kranz, E. L. Huang, B. Mizaikoff, A. Lugstein, E. Bertagnolli, "*Towards Electrochemical Imaging on a Nanometer Scale with Submicro- and Nanoelectrodes Integrated in AFM-Tips*", IEEE-NANO 2001, Maui, Hawaii, Oct. 28-30, 2001.
61. G. Strasser (invited); "*Single mode GaAs quantum cascade lasers*"; 5th Int. Symp. on New Phenomena in Mesoscopic Structures, Waikoloa, USA, 25.-30.11.2001
62. K.Unterrainer, (invited) "*Ultrabroadband THz Generation and Spectroscopy*", 1st Int. Conf. on Biomedical Imaging&Sensing Applications of Terahertz Tevhnology, Leeds, England, 30.11.-1.12.2001.
63. M. Litzenberger , D. Pogany, E. Gornik , K. Esmark and H. Gossner "*Influence of stress current and pulse risetime on triggering behavior of submicron gg-NMOSFET protection devices investigated by a thermal mapping technique*", 7th ESD-Forum, Dec. 11th -12th 2001, Berlin, BRD

Habilitations

1. Gottfried Strasser, "*Quantum Cascade Semiconductor Laser*", January 2001.

Doctor's Theses

1. Christoph Fürböck, "*Characterization of Semiconductor Power Devices: Laser Interferometry and Failure Analysis*", February 2001
2. Bernd Goebel, "*Vertical n-channel MOSFETs for extremely high density integration*", June 2001
3. P.O. Kellermann, "*Entwicklung von Halbleiterlasers mit postepitaktischer Adjustierung der Wellenlänge*", June 2001
4. Rudolf Bratschitsch, "*Time-resolved THz-Spectroscopy of Semiconductor Nanostructures*", November 2001
5. Werner Schrenk, "*Distributed Feedback Quantum Cascade Lasers*", November 2001

Cooperations

1. Universität Linz, W. Heiss, F. Schäffler, H. Thiem, L. Palmetshofer, W. Jantsch
2. Universität Wien, H. Kauffmann
3. Universität für Bodenkultur Wien, U.Sleytr, D. Pum
4. AMS-Unterbremstätten, H.Enichlmair, K. Tschernay, F. Unterleitner
5. Philips Consumer Electronics, E. Kaun
6. Siemens AG, E. Wolfgang, G. Sölkner, W. Maurer
7. Infineon, M. Stoisiek, D. Schuhmann, J. Willer, R. Zelsacher
8. Femtolasers, Wien, A. Stingl
9. Plansee AG, Reutte, Dr. P. Willhartitz
10. High Q Laser, Hohenems, Dr. D. Kopf
11. TU-München, G. Abstreiter, P. Vogl, C. Strahberger, Deutschland
12. Universität Regensburg, W. Wegscheider, Deutschland
13. LMU München, N. Hecker, Deutschland
14. TU Braunschweig, D. Schneider, A. Schlachetzki
15. Technische Universität Berlin, A. Wacker, Deutschland
16. Heinrich Hertz Institut, Berlin, H. Künzel, Deutschland
17. Paul Drude Institut, Berlin, H. Grahn, Deutschland
18. Universität Bremen, D. Hommel, Deutschland
19. Universität Stuttgart, M.H. Pilkuhn, Deutschland
20. Forschungszentrum Rossendorf, Dresden, M. Helm, Deutschland
21. Mütek Infrared Laser Systems, H. Wachernig, Deutschland
22. Centre National de la Recherche Scientific, Laboratoire de Microstructures et de Microelectronique, B. Etienne, Cedex, Frankreich
23. Thales-CSF LCR, Orsay , C. Sirtori, D. Corbin, Frankreich
24. Universite Paris Sud, F. Julien, Frankreich
25. Institute National des Sciences Appliques de Lyon, VilleUrbanne, Frankreich
26. Interuniversity Microelectronics Center (IMEC), Leuven, Belgien
27. Ioffe Physico-Technical Institute, St. Petersburg, Y. Ivanov, Rußland
28. Sub-Micron Center, Weizmann Institute, Rehovot, M. Heiblum, Israel
29. Univ. of California, Lawrence Berkeley Laboratories, E. E. Haller , USA
30. Univ. of California, Santa Barbara, J. Allen, A. Gossard, USA
31. Columbia University, New York, H. Störmer, USA
32. Princeton University, S. Lyon, USA
33. IBM Fishkill, C.S. Murthy, USA

34. Lucent Technologies, C. Gmachl, USA
35. Boston College, Boston, MA, K. Kempa, P. Bakshi, USA
36. EPI MBE Components, St. Paul, Minnesota, USA
37. Univ. Osaka, C. Hamaguchi, Japan
38. Univ. Nagoya, N. Sawaki, Japan
39. Herriot Watt University, Edinburgh, C. Pidgeon, Schottland
40. Univ. Glasgow, C. Ironside, Schottland
41. Univ. Nottingham, M. Chamberlain, England
42. University of Sheffield, M. Skolnick, J. Coburn, England
43. University of Surrey, B.N. Murdin, England
44. INFM-SNS Pisa, F. Beltram, Italien
45. Technische Universität Delft, Wenckebach, Holland
46. University Neuchatel, J. Faist, Schweiz
47. EPFL Lausanne, M. Ilegems, Schweiz
48. ETH Zürich, W. Fichtner, Schweiz
49. Orbisphere Semiconductor Lasers, Schweiz
50. Alpes Lasers, Neuchatel, A. Müller, Schweiz
51. Slovak Academy of Sciences, Bratislava, Slowakei

Search for Plasma Instability Driven THz Radiation Sources

E. Gornik, G. Strasser, R. Zobl, M. Kast, C. Pacher

GaAs/AlGaAs as a model material is a promising candidate for realizing coherent emission at long wavelengths. Utilizing quantum cascade emitters based on intersubband and interminiband transitions in the conduction band of a semiconductor, electroluminescence was demonstrated in the wavelength range from 3.3 to 85 THz. To our knowledge, the longest wavelength for electrically pumped lasing in a GaAs device is ≈ 23 THz [1]. All attempts to move beyond this value did not succeed so far. The performance of long wavelength devices is strongly decreased due to free carrier absorption. This is evident from an emission intensity dependence on the square root of the device current [2], which is a clear indication that electron-electron scattering in the upper excited level limits the nonradiative lifetime. That means that as long as this mechanism is dominant an increase in injection current does not lead to an increased emission. The emission intensity saturates and gain cannot be achieved as long as electron-electron scattering is the dominant nonradiative relaxation mechanism.

To circumvent this problem a collective excitation scheme is used to induce a plasma instability. The main difficulty with this kind of approach is that the starting bandstructure is changed significantly by the applied bias. Only at a given situation the mechanism of injection and extraction together with the proper energy level splitting will give a plasma instability.

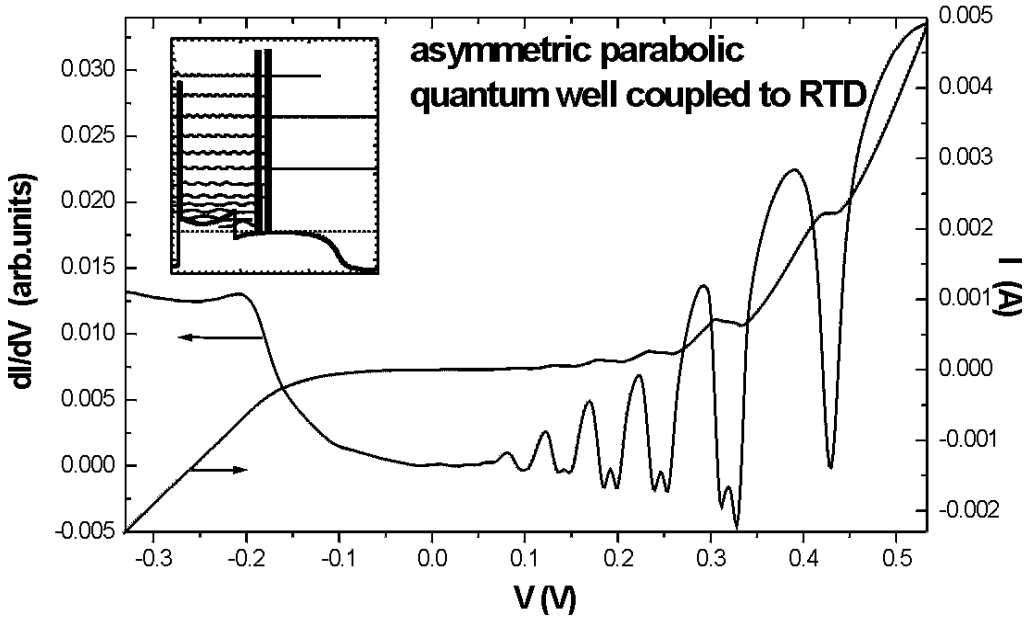

Fig. 1: Current and conductivity-voltage characteristic for sample G428. The sample is nominally undoped in the active region. The inset shows the band diagram.

We have done a first step in this direction by growing a new sample, without doping in the active region but compensating the doping by a parabolic potential (sample G428). The result is shown in Fig. 1, where the current and the derivative of the current are plotted as a function of the bias voltage. In the positive bias direction a spectroscopy of the levels above the Fermi level is performed. Each peak in the current represents the passing through a resonant level. For negative bias (forward direction) the levels below the Fermi level are scanned. This bias provides the situation for the extraction through the levels in the RTD and the pocket. The resonances in the derivative have become larger than in a previously grown sample G301 [3], but are still not visible clearly in the current. The extraction through the RTD is evident in the derivative at a bias of 0.2 V. This is the position to look for an instability.

This structure has also shown first emission results, however with a rather weak emission intensity [3]. An increase in emission is expected from cascaded structures. To cascade parabolic quantum wells similar to the situation in the QCL structures, a vertical injection scheme is favorable as has been reported recently by Maranowski et al. [4]. This cascading can be introduced by using bridging regions to combine different wells and offering extraction and blocking of carriers. A significant increase in the emission intensity was achieved with an experimental curve for a 30 μm mesa (sample G428) in forward bias.

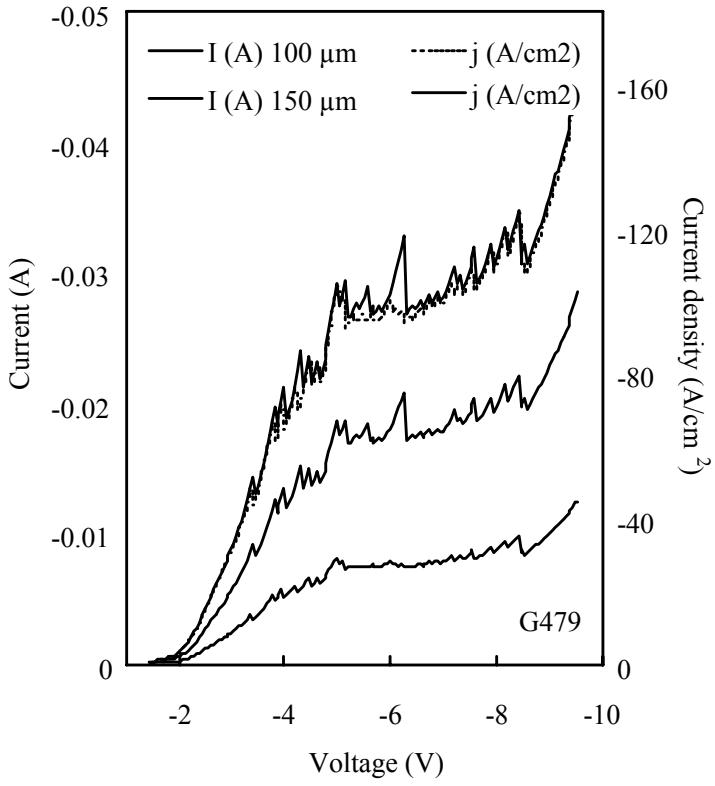

Fig. 2: Current-voltage characteristics and current density vs. external bias for two circular mesa structures processed into sample G479. The mesa diameters are 100 and 150 microns, respectively. The measurement are performed at liquid Helium temperatures.

We have previously demonstrated THz emission from parabolic quantum wells up to lattice temperatures of 200 K, where electrons are injected laterally in the parabolic well of carriers depending on the carrier energy [5]. In contrast to square wells, an extraction at low energies is specially critical, because the tunneling barrier gets thicker for lower energies, a direct consequence of the shape of the wells.

A cascaded parabolic quantum well structure (G479) consisting of 35 stages was MBE-grown on highly n-doped material to realize a homogeneous electron injection. A top layer with a carrier concentration of about 1-2x10^{18} cm^{-3} is to ensure a defined carrier injection. The well material is doped homogeneously to achieve an overall doping concentration in the active region of about 1x10^{16} cm^{-3} electrons per cubic centimeter, the barrier material is not doped intentionally.

For current-voltage measurements the samples are processed into small cylindrical mesas to probe the electrical behavior of the structure.

Figure 2 shows the current versus voltage and current density versus voltage behavior at low temperatures for two different mesa sizes to demonstrate the homogeneous injection of the electrons into the structure. The current densities are literally identical, the only detectable differences are in the regime where the structures breaks up into high and low field domains. This well known behavior reproduces a variety of peaks. The exact number of peaks has to be 35, so each well should be resolvable. The different mesa sizes are given in Fig. 2. The IV measurements are performed at cryogenic temperatures.

First emission experiments were performed with the cascaded plasmon structure sample G479 to repeat the experimental results of Maranowski et al [4]. We have processed the sample into stripes of 25 µm width and 1000 µm length. The emission sample consisted of 8 stripes giving a total emission area of about 0.228 mm^2.

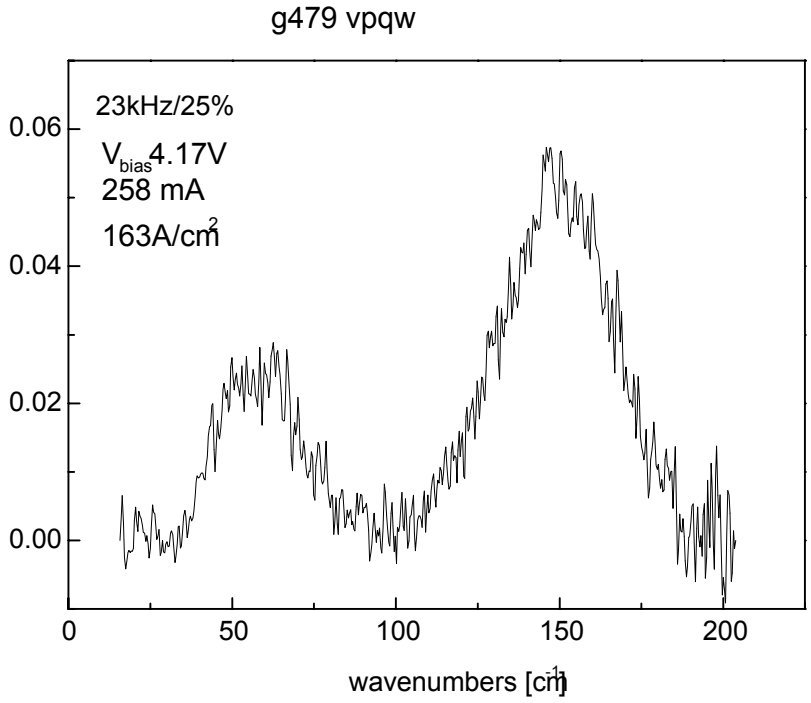

Fig. 3: Emission spectrum measured with a InSb detector as a function of the frequency (in wavenumbers).

The emission spectrum is measured with a InSb detector with a resolution of 10 wavenumbers. The spectrum consists of a main peak at 150 cm^{-1} corresponding to the plasmon energy of the parabolic bandstructure. This result is in agreement with the results of Maranowski et al. [4]. However we find an additional emission line at 60 cm^{-1}. The origin of this emission is not clear yet, it could be due to transitions between impurity states as it corresponds to the impurity ionization energy of close to 5 meV. Further investigations are under way.

References

[1] G. Strasser et.al., Appl. Phys.Lett. 75, 1345 (1999).

[2] J. Ulrich et.al., Appl. Phys.Lett.76, 19 (2000).

[3] P.Bakshi et.al., Appl. Phys.Lett.75, 1685 (1999).

[4] K.D. Maranowski and A.C. Gossard, Journal of Appl. Physics 88, 172 (2000).

[5] Ulrich et.al., Appl. Phys. Lett. 74, 3158 (1999).

THz Plasmon Emission From an LT-GaAs/GaAs Homojunction

J. Darmo, G. Strasser, T. Müller, K. Unterrainer

Few-cycle THz radiation can be generated from semiconductor epilayers by coherent plasma oscillations [1], [2]. Emitters relying on those principles have found wide applications in spectroscopy of semiconductor structures, chemistry, and medical imaging in the frequency range of 0.1 – 10 THz. Output power and long term stability of these emitters are key parameters in such applications.

We have addressed the issue of the terahertz (THz) output power and stability. The standard model of the plasmon emitter relies on the build-in electric field at the surface of the structure. A stronger field leads to a larger emitted power. For the standard emitter the surface states are used to pin the Fermi level which gives rise to the surface field. The surface states arise from the surface imperfection, impurities and the oxide surface layer, hence their concentration and charge state can be modified by the laboratory ambient. To take full control over the built-in electric field we can pin the Fermi level position by deep level defects. Low-temperature grown (LT) GaAs [3] can serve as an efficient pinning medium. Such material possesses a high density of defect states with the energy level close to the GaAs mid-gap [3], hence it firmly pins the Fermi level. A presence of the LT-GaAs in the emitter structure leads to a replacement of the surface field of the emitter with the field at the junction LT-GaAs/GaAs where the THz radiation is now generated.

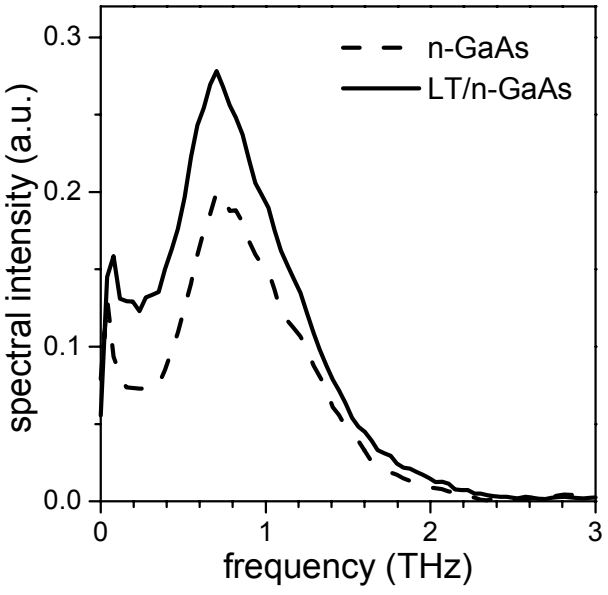

Fig. 1: Power spectra (right panel) of the THz emission from the n-doped GaAs plasmon emitter and from the n-doped GaAs plasmon emitter with LT-GaAs surface layer.

We have grown two structures with an identical n-doped GaAs layer on semi-insulating GaAs substrates, but one with an additional low-temperature grown GaAs surface layer. A mode locked Ti:sapphire laser (12fs pulse width) was used to excite the plasma oscillation and the emitted THz radiation was measured by an autocorrelation technique with a liquid helium cooled silicon bolometer. The autocorrelation technique allows to measure the spectrum of the signal as well as the average power of the radiation. The emission spectra of both samples show the same spectral dependence. However, the emitter with the LT-GaAs surface layer has 1.4x larger output THz power than the emitter without LT-GaAs layer which proves that the improved effective pinning of the Fermi level leads to an increase of the THz generation.

Additionally, we have tested the resistance of the emitters against oxidation. The emitters were oxidized in hot wet air. The LT-GaAs layer revealed an enhanced performance stability since the surface field does not rely on the surface states.

References

[1] X.-C. Zhang et al. *Appl. Phys. Lett.* 56, 1011 (1990).

[2] R. Kersting et al., *Phys. Rev. Lett.* 79, 3038 (1997).

[3] D.C. Look, *Thin Solid Films* 231, 61 (1994).

Voltage Controlled Intracavity Emitter of Terahertz Radiation

J. Darmo, G. Strasser, T. Müller, K. Unterrainer, Tuan Le, A. Stingl

Generation of THz radiation within a femtosecond mode-locked laser cavity was recently demonstrated [1], [2]. A saturable Bragg reflector (SBR) with a single quantum well (SQW) was employed, but the performance of the SQW based emitter is restricted in terms of radiation intensity, frequency, as well as efficiency. A low-temperature molecular beam epitaxy grown (LT) GaAs layer is an alternative to the SQW for both as a saturable absorber and as a THz emitter. Here we present a new type of THz emitters capable to operate in a femtosecond mode-locked Ti:sapphire laser cavity. A new degree of freedom is added to the THz emitter as the emitted THz power can be modulated pseudo-independently from the laser operation.

The voltage controlled intracavity THz emitter comprises a Bragg mirror stack made of AlGaAs/AlAs layers and the LT GaAs layer grown at 220 °C and annealed at 600 °C. The electrical contacts to the LT GaAs layer were formed photolithographically by Ti/Au metals and had a form of parallel metallic stripes 20 μm width and separated by 50 μm. The processed emitter structure was mounted onto a high resistive silicon substrate with a hemispherical lens attached to it to form an emitter unit. The emitter unit was placed into a cavity of a standard mode-locked 12 fs femtosecond laser head as the end mirror. The laser is in this configuration self-starting regardless of the emitter biasing.

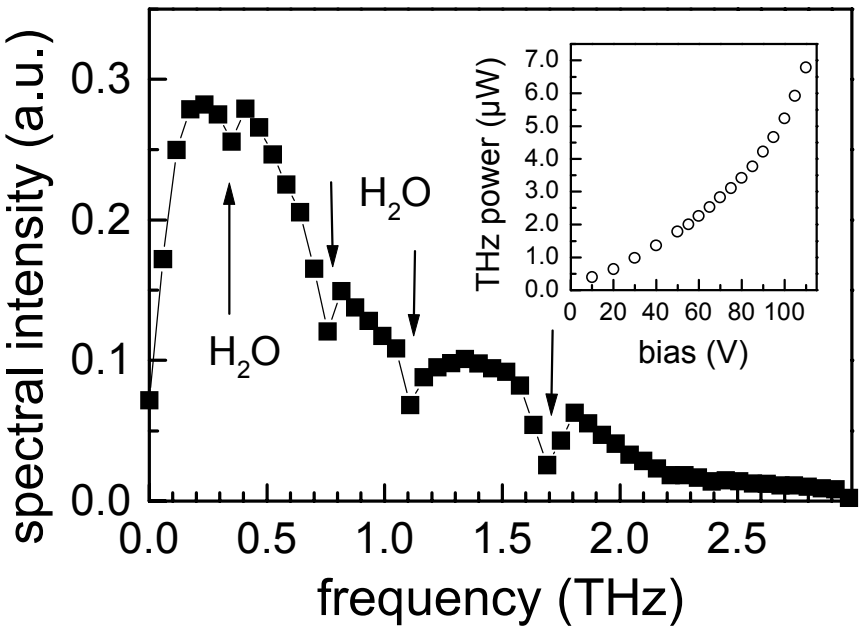

Fig. 1: Fast Fourier spectrum of the THz radiation from the LT/SBR emitter. The inset shows the output THz power as a function of the emitter bias.

The generated THz radiation was detected by a free space electro-optic detection technique using a 1 mm thick ZnTe crystal. Figure 1 presents a typical intensity spectrum of the terahertz transient measured for the emitter element biased at 80 V and at an average intracavity optical power of 900 mW. The experimental set-up was not purged with dry nitrogen, therefore, absorption lines of water vapor are visible in the spectrum. The THz emission spectrum has maximum at about 0.3 THz with frequencies extending beyond 2 THz.

The average THz power measured by a 4.2 K cooled silicon bolometer increases quadratically with bias without any tendency to saturate. The maximum THz power generated from the intracavity emitter was about 6.7 μW at a intracavity optical power of 900 mW.

References

[1] N. Sarakura et al., Jpn. J. Appl. Phys. 36, L560-L562 (1997).

[2] N. Sarukura et. al., Jpn. J. Appl. Phys. 37, L125-L126 (1998).

Direct Measurement of Intersubband Population Dynamics

T. Müller, R. Bratschitsch, G. Strasser, K. Unterrainer

We have studied the time-resolved photo-induced intersubband absorption in an undoped GaAs/AlGaAs coupled-well. We apply a novel interband pump/intersubband probe technique that directly allows us to measure the temporal evolution of the intersubband absorption spectrum after optical excitation.

In the experiment an interband pump pulse injects electrons into the first and second subband of an asymmetric double quantum well with a level spacing smaller than the optical phonon energy. The time evolution of the electron population in these two subbands is monitored by probing the mid-infrared (MIR) transition to the empty subbands 3 and 4. Ultrashort MIR pulses are generated by phase-matched difference-frequency mixing in GaSe, and the spectrum of the transmitted MIR pulses through the sample (T = 5 K) is recorded by performing an interferometric correlation technique.

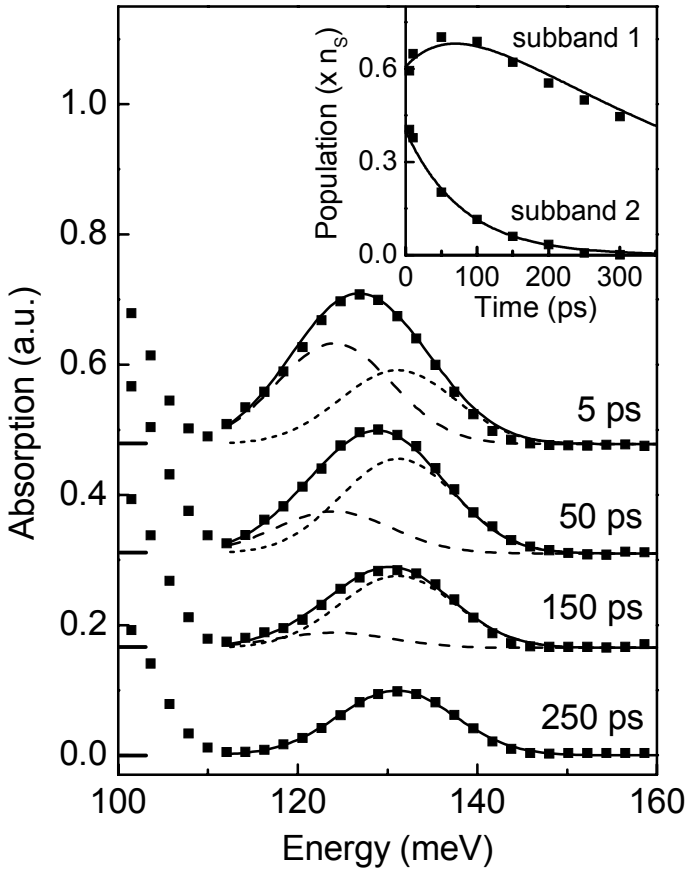

Fig. 1: Intersubband absorption at different time delays with Gaussian fits. Inset: Subband population of level 1 and 2.

Figure 1 shows the intersubband absorption spectrum recorded at different time-delays after the pump pulse. We observe an absorption peak, corresponding to the transitions 1-4 and 2-4, that clearly shifts to higher energies over time.

In addition we observe the onset of a second peak at lower energies, which we attribute to the transitions 1-3 and 2-3, that cannot be resolved due to the cut-off of our detector. We explain the blue shift of the absorption by relaxation of carriers from the second to the first subband. In Fig. 1 we have fitted two Gaussian peaks to the measured data: one at 124 meV, corresponding to the transition 2-4, and another one at 131 meV, corresponding to the transition 1-4. Since the area under the peak (i-4) (i = 1, 2) is directly proportional to the subband population $n_i(t)$, we are able to determine the population dynamics in the quantum well on the basis of the time-resolved absorption spectra. The inset of Fig. 1 shows the electron population of the first and second subband as a function of time delay after optical excitation (symbols). About 40% of the photo-excited carriers are injected into the second subband, while the remaining 60% are injected into the first subband at higher k-value. The population in the second subband (squares) shows an exponential decay. The carriers relaxing down from the second subband add to the population in the ground level. Subsequently, the population in the ground level drops due to carrier recombination. The lines are the results obtained from a simple rate equation model.

Long Wavelength (15 and 23 µm) GaAs/AlGaAs Quantum Cascade Lasers

J. Ulrich, J. Kreuter, W. Schrenk, G. Strasser, K. Unterrainer

Quantum cascade lasers based on GaAs/AlGaAs chirped superlattice active regions have been achieved at wavelengths of 15 (sample A) and 23 µm (sample B). In pulsed mode they operate up to temperatures of 220 K and 100 K, respectively. Sample A employs a standard waveguide with n+-doped cladding, sample B was made with a metallic surface plasmon waveguide. The threshold current densities at cryogenic temperatures of 2.2 kA/cm^2 (A) and 10.2 kA/cm^2 (B) reflect the differences in intersubband lifetimes and waveguide losses close to the reststrahlenband.

The lasers have been grown by molecular beam epitaxy on n^+-doped substrates. The active zone consists of 60 periods, each of them containing four quantum wells of the laser transition superlattice plus five injector wells. The Al content of the barriers of $x = 45\%$ for sample A yields the maximum Γ-Γ band offset of 390 meV without introducing indirect barrier states. For sample B, where carrier leakage into the continuum plays a minor role, we considered $x = 35\%$ to be appropriate in order to avoid ultra-thin barriers. The standard waveguide of sample A is a sandwich composed of the active zone embedded in two lightly doped GaAs spacer layers between two n^+-doped confinement layers, see Fig. 1(a) for details. We calculate a waveguide loss coefficient of $\alpha_w = 26$ cm^{-1} and a confinement factor of $\Gamma = 58\%$. The calculated values are for the surface plasmon waveguide of sample B are $\alpha_w = 86$ cm^{-1} and $\Gamma = 80\%$. Notice that the surface plasmon waveguide of sample B is still 22% thinner than the standard waveguide of the shorter wavelength sample A.

The 50 µm wide laser ridges of sample A and B are defined by reactive ion etching. An insulation layer is deposited on the entire surface and later etched away on top of the ridge. After that, a TiAu contact metallization is sputtered onto the top of the structure and onto the backside of the substrate. In case of sample B, a wide window on top of the ridges is left open for subsequent evaporative deposition of the Au plasmon carrying layer. The samples were cleaved to produce Fabry-Pérot resonators of lengths ($L_A = 1330$ µm, $L_B = 1005$ µm).

As illustrated in Fig. 2, lasing occurs on multiple longitudinal modes. The light versus current density characteristics of sample A, displayed in Fig. 3(a), reveal the high performance of this laser: A low threshold current density of $j_{th} = 2.2$ kA/cm^2 and the broad operation current range up to ~4×j_{th} at cryogenic temperatures and a functionality up to a temperature of 220 K. Sample B is characterized by an approximately 5 times higher threshold current density of $j_{th} = 10.2$ kA/cm^2. Consequently the maximal current density is only about ~1.5×j_{th}, and the temperature range is limited to 100 K.

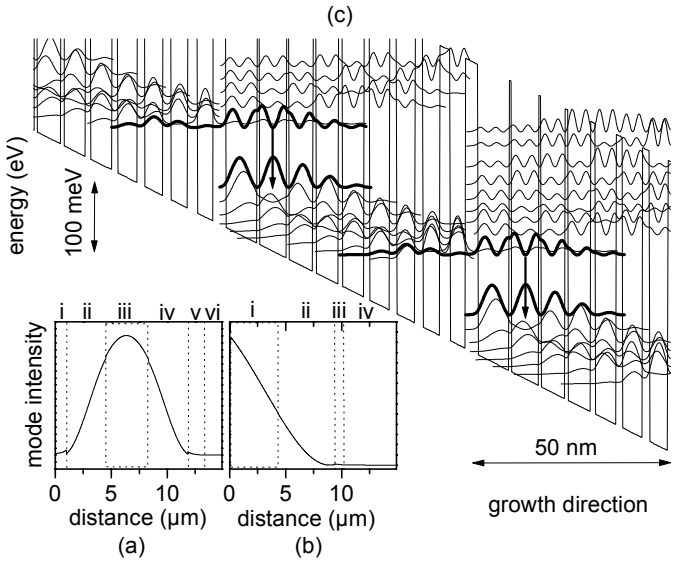

Fig. 1: The calculated optical mode profile (a) for the n^+-confinement waveguide of sample A. The distance is measured from the metal semiconductor interface. The thicknesses [μm] and doping levels [cm^{-3}] of the waveguide layers are: n^+-layer *i* 1.0, 2×10^{18}; spacer *ii* 3.5, 2×10^{16}, active zone *iii* 3.84, 6.5×10^{16}, spacer *iv* 3.5, 2×10^{16}, n^+-layer *v* 0.1, 2×10^{18}, substrate *vi* ~200, ~2×10^{18}. The optical mode profile (b) for the surface plasmon waveguide of sample B with the layers: active zone *i* 4.23, 5.8×10^{16}, spacer *ii* 5.0, 2×10^{16}, n^+-layer *iii* 0.1, 2×10^{18}, substrate *iv* ~200, ~2×10^{18}. The conduction band structure (c) of three periods of sample A at an electric field of 27 kV/cm. The moduli squared of the wavefunction are displayed at their corresponding eigenenergies. The layer thicknesses [nm] of one period, beginning with the injection barrier from left to right, are: **3.2**, 7.8, **0.65**, 6.8, **0.65**, 6.0, **0.8**, 5.5, **1.2**, 5.3, **1.5**, 5.0, **1.8**, 4.6, **2.0**, 4.2, **2.5**, 3.9. $Al_{0.45}Ga_{0.55}As$ barrier thicknesses are typed bold face, GaAs quantum wells normal. The wells corresponding to the underlined thicknesses are Si-doped to $n = 2.3\times10^{17}$ cm^{-3}. The band structure of sample B (not shown) is very similar. The layer thicknesses [nm] are: **3.0**, 9.4, **0.5**, 8.3, **0.55**, 6.8, **1.3**, 5.8, **1.4**, 5.6, **1.5**, 5.4, **1.7**, 5.1, **2.0**, 4.8, **2.3**, 4.5. The barriers are $Al_{0.35}Ga_{0.65}As$ (bold), the wells GaAs. Underlined wells are doped to $n = 2.1\times10^{17}$ cm^{-3}.

The higher threshold current density of sample B originates mainly from two causes to be discussed in the following: 1. the shorter lifetime of carriers in the initial subband of the laser transition, limited by longitudinal optical (LO) phonon emission, and 2. the increased waveguide loss from free carrier and multiphonon absorption. We estimate the threshold current density. The calculation reveals 0.7 kA/cm^2 (A) and 2.9 kA/cm^2 (B) and it underestimates the threshold current densities for both samples by a factor of about three. Even though the calculation cannot account for the absolute values of j_{th}, it can successfully explain the difference between sample A and B. The relaxation time of the initial subband τ_i and the waveguide losses α_w deviate essentially. These are the parameters in which the proximity to the reststrahlenband of 23 μm manifests itself most clearly.

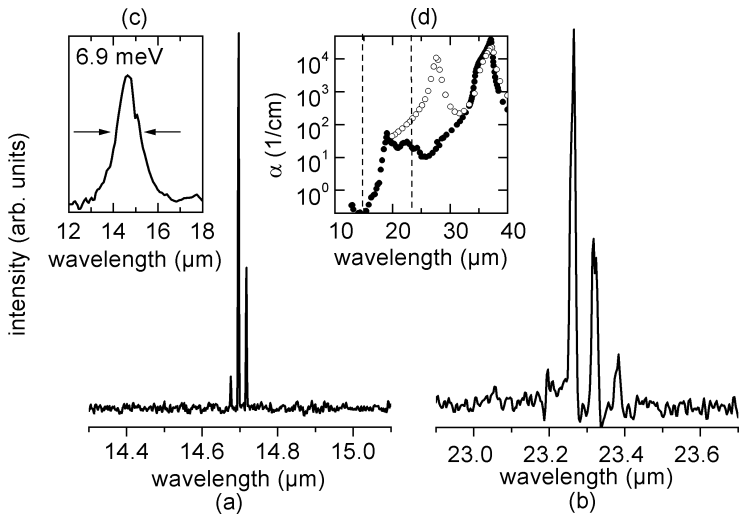

Fig. 2: Laser spectra at a temperature of 5 K (a) of sample A at a current density of 5.1 kA/cm^2 and (b) of sample B at a current density of 11.9 kA/cm^2. The spectra were recorded with a Fourier-transform spectrometer at a resolution of 0.125 cm^{-1} and a liquid N_2-cooled HgCdTe detector. The lasers were operated with 100 ns long pulses at 5 kHz repetition rate. (c) The spontaneous emission spectrum of sample A was measured with the same set up with 2 μm pulses at 50 kHz. (d) The intrinsic absorption coefficient α of undoped bulk GaAs (full symbols) and $Al_{0.14}Ga_{0.86}As$ (open symbols). The emission wavelengths of the two samples are marked with dashed lines.

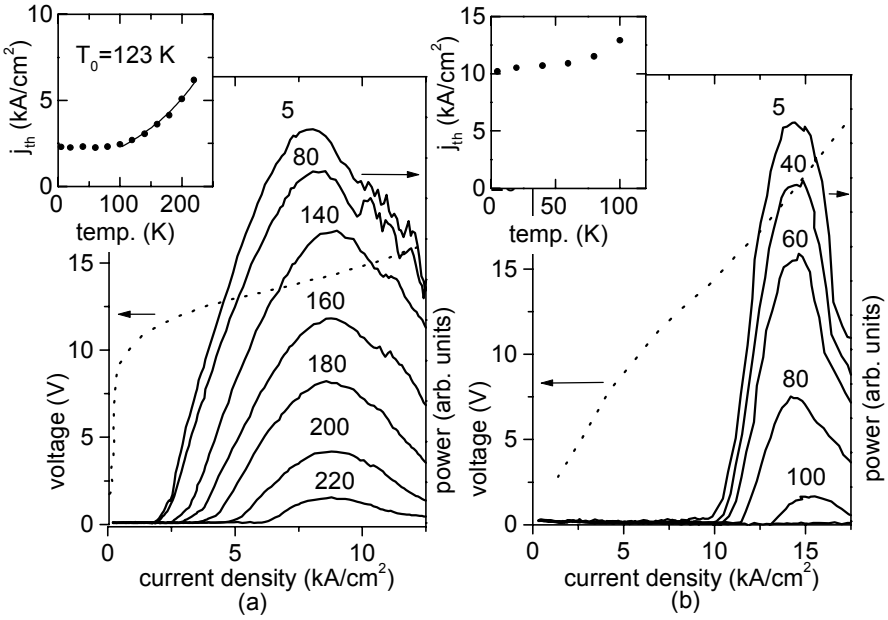

Fig. 3: Light output power (right axis) and voltage (left axis) vs. current density (a) of sample A and (b) of sample B for various temperatures given next to the curves in Kelvin. Pulse conditions and detection technique were the same as for the spectral measurements. The insets show the derived threshold current densities j_{th} vs. the heat sink temperature.

Room Temperature Operation of Distributed Feedback GaAs/AlGaAs Quantum-Cascade Lasers

W. Schrenk, S. Anders, E. Gornik, G. Strasser

Quantum cascade lasers (QCL) are mid infrared light sources. So far, QCLs have been demonstrated only in two material systems, InGaAs/InAlAs on InP and AlGaAs/GaAs grown on GaAs, though spontaneous emission from quantum cascade structures has been achieved in some other materials. Recently, room temperature operation of GaAs/AlGaAs based QCL has been demonstrated, which before was a privilege for QCL grown on InP. This is an important step for commercial applications. However, single mode lasers are favored for gas sensing via infrared spectroscopy (single- or multiple pass absorption).

We achieved pulsed room temperature operation of first order distributed feedback (DFB) quantum cascade lasers in the GaAs/AlGaAs material system. Two different designs were used for the active material. Sample A is a design where the active cell is formed by three coupled quantum wells and sample B is a chirped superlattice. For both samples, an Al content of 45% was chosen. The emission wavelength of the sample A is around 9.5 μm and around sample B emits at an wavelength of 12.5 μm. The larger band discontinuity of the $Al_{0.45}Ga_{0.55}As$ barriers compared to the previously used $Al_{0.33}Ga_{0.67}As$ has been shown to be singularly responsible for the higher operating temperature of these devices.

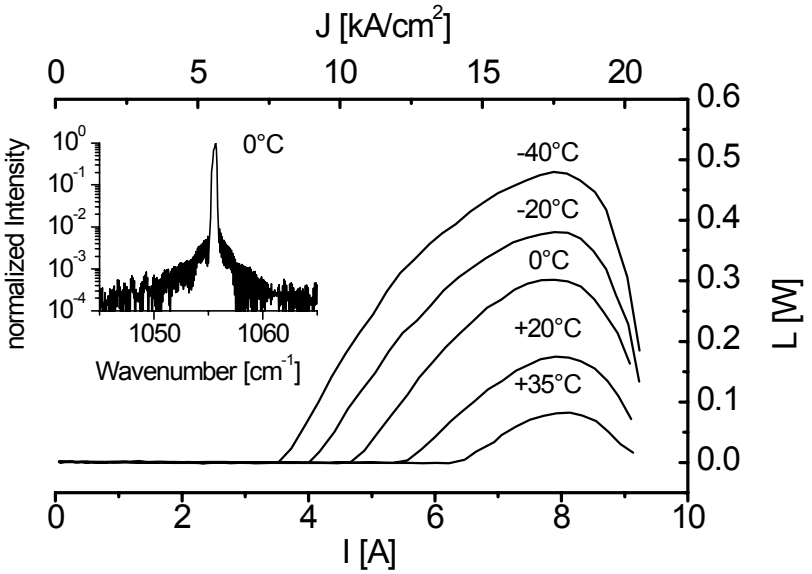

Fig. 1: Light output power versus current of an L = 1.5 mm long and w = 30 μm wide DFB laser in pulsed operation for several heat sink temperatures (Peltier cooler) between –40 °C and +35 °C. The inset shows the emission spectrum at 0 °C.

We fabricated first-order distributed feedback lasers with a metallized surface relief grating. The calculated coupling coefficients are $\kappa = (-19.6 - i0.3)$ cm^{-1} for sample A (grating period $\Lambda = 1.48$ µm, grating depth 850 nm) and $\kappa = (65 + i5.8)$ cm^{-1} for sample B (grating period $\Lambda = 2.00$ µm, grating depth 1200 nm). The large coupling coefficient allows the realization of short devices with reasonable low threshold current densities. The advantages of shorter devices are the reduced currents and lower heat dissipation.

Both types of lasers show room temperature operation in pulsed mode. The highest working temperature of sample A was measured to be 335 K for a 2 mm long device. Figure 1 shows the light output power versus current for several heat sink temperatures for a three well design laser mounted on a Peltier cooler. The 1.5 mm long and 30 µm wide DFB laser is operated in pulsed mode with 50 ns pulses at 10 kHz. The maximum peak power of the single mode emission is 0.5 W at –40°C, and still 80 mW at +35°C. The slope efficiency is 172 mW/A (-40°C), and 64 mW/A (+35°C).

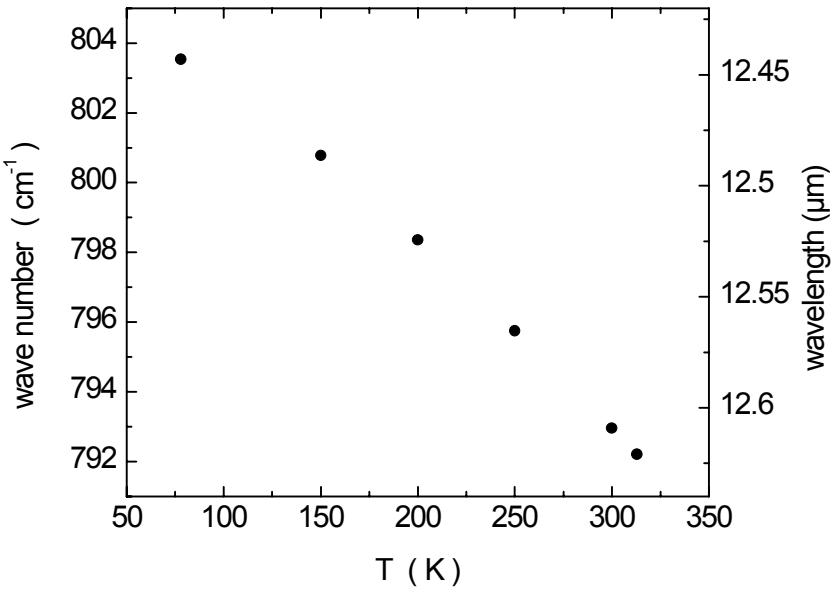

Fig. 2: Emission wavelength as a function of the heat sink temperature. The laser is operated in pulsed mode with 100 ns long pulses at 5 kHz repetition rate.

The emission wavelength of DFB lasers is continuously tunable with the temperature. Figure 2 shows the emission wavelength of sample B as a function of the heat sink temperature.

Room Temperature Lasing of Electrically Pumped Quantum Cascade Micro-Cylinders

S. Anders, W. Schrenk, G. Strasser

We investigated the lasing properties of micro-cylinders that were processed into a quantum cascade heterostructure. For close-to-circular micro-cavities, mirror losses are small because the light travels by total internal reflection close to the perimeter of the disk. Compared to ridge geometries, the reduced optical losses result in a decreased lasing threshold. Quantum cascade lasers (QCLs) – semiconductor heterostructure devices with several tens of photon-emitting cascades – are particularly suited for the microresonator geometry. Non-radiative surface recombination of electrons and holes does not occur in the unipolar QCLs, and small-scale surface roughness affects the QCLs with their relatively long emission wavelength of about 10 μm very little.

We compare the lasing performance of micro-cylinders with conventional Fabry-Perot (FP) resonators as well as with distributed feedback (DFB) lasers, all processed from the same GaAs/AlGaAs superlattice structure. We find that the threshold at low temperatures for both micro-cylinder and DFB lasers is decreased by a factor of about 2 below that of the FP laser (Fig. 1). The reason for this is that the emission losses of the FP laser are higher and therefore the threshold is higher. The maximum operating temperatures of the micro-cylinder and the DFB lasers exceeds the maximum operating temperature of the FP laser by at least 50 °C, again a benefit from the reduced threshold.

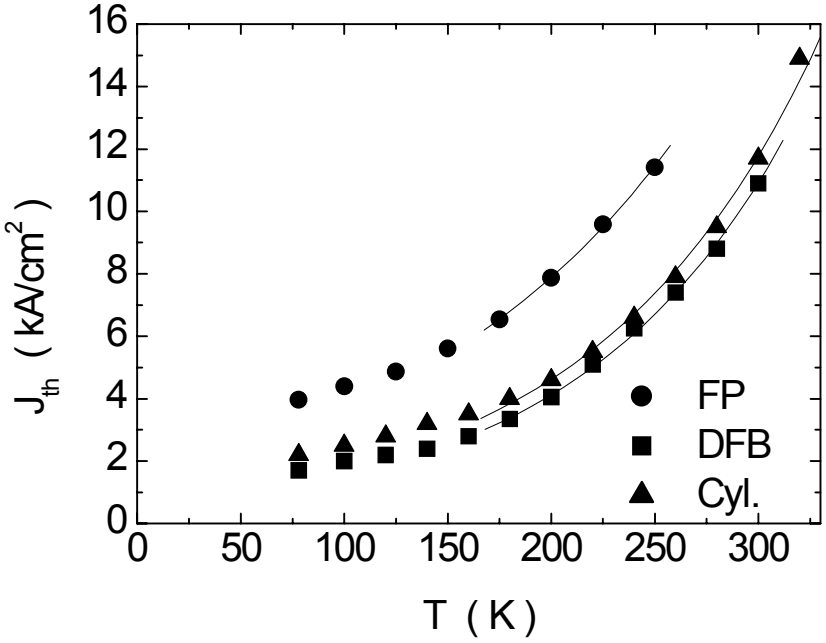

Fig. 1: Threshold current density as a function of temperature for different laser cavities (FP: Fabry Perot, DFB: distributed feedback, Cyl.: micro-cylinder) in pulsed mode operation.

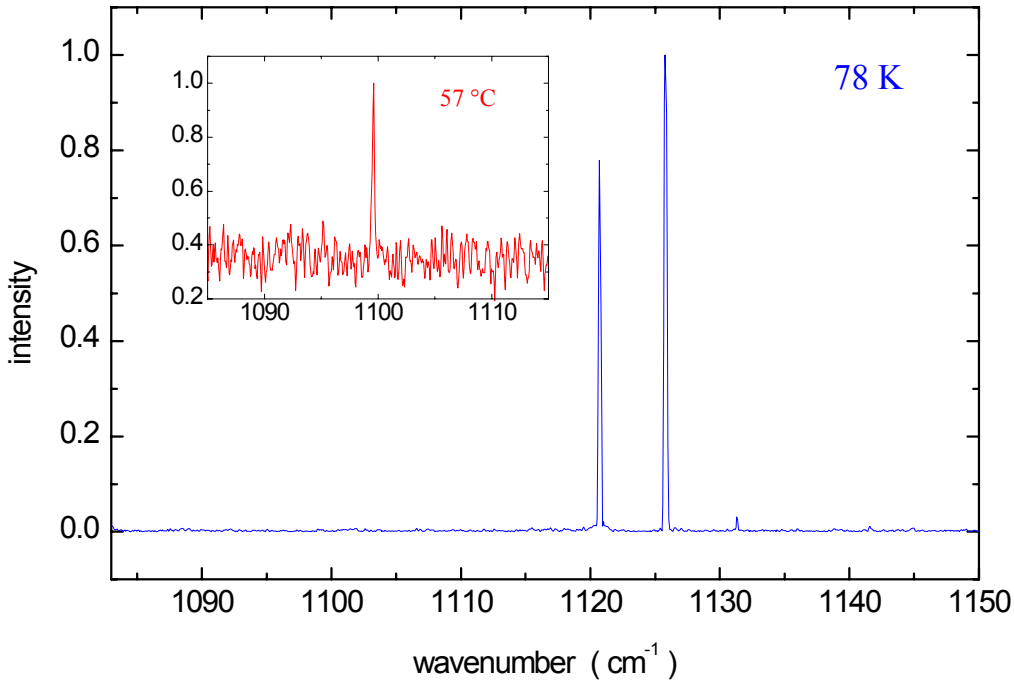

Fig. 2: Emission spectra of a micro-cylinder laser at cryogenic temperature (78 K) and at the highest working temperature (57 °C).

The maximum operating temperature of around 50 °C for micro-cylinder lasers significantly exceeds the previously reported maximum operating temperature for a micro-cylinder, –3 °C, which was obtained for an InP based quantum cascade laser.

Figure 2 shows the emission spectra of micro-cylinder lasers in pulsed mode operation. The spectra were measured with a Fourier transform infrared spectrometer.

Spectrum of Low-Voltage THz Emission of Strained p-Ge Resonant-State Laser

R. Zobl, E. Gornik, I.V. Altukhov, M.S. Kagan

The spectrum of stimulated THz emission of a uniaxially stressed p-Ge resonant-state laser (RSL) is measured at low electric fields at which the continuous-wave operation of RSL is possible. The lines observed show that the mechanism of lasing in diffusive regime of electric field heating carriers is the same as at high voltages when the carriers accomplish the streaming motion. It is due to an inverted population of resonant states of acceptors induced by strain. A new line caused by optical transitions between continuum and resonant states is found.

Gallium-doped Ge crystals with Ga concentration of $2*10^{14}$ cm^{-3} were used in the experiment at liquid helium temperature. The samples of a square cross section of $0.7*0.9$ mm^2 and 10 mm long were cut in the [111] crystallographic direction. Uniaxial pressure *P* and electric field *E* were applied along the samples. Voltage pulses of 1 msec duration were applied to contacts positioned on the long (lateral) plane of the sample on a distance 7 mm one from another. The resonator formed in our case by well-parallel lateral sample planes (plane parallelism was better than 5 arcsec) was necessary to obtain the low-voltage stimulated THz emission. The spectrum of THz radiation was registered by a cooled InSb detector tuned by a magnetic field.

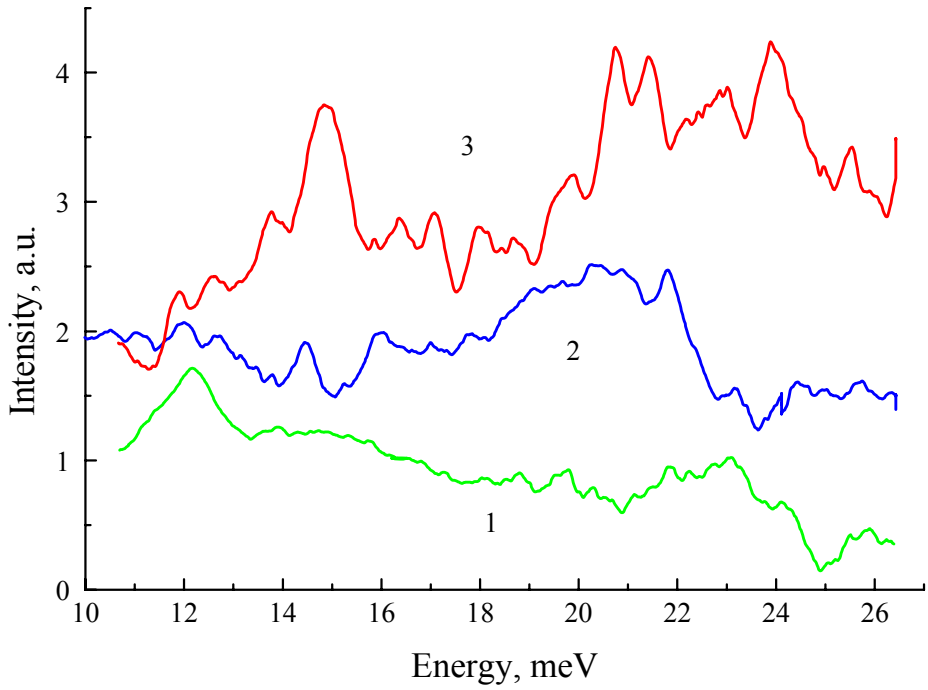

Fig. 1: Radiation spectrum at different electric fields.

The spectrum of THz radiation from compressed p-Ge at different voltages just above the voltage of impurity breakdown is shown in Fig.1. The upper curve shows that the low-voltage stimulated emission spectrum contains several peaks corresponding to direct optical transitions between different resonant and localized acceptor states. At the pressure of 7.15 kbar, the peak energies are 20.5, 21.5, 23, 24 and 25.5 meV (Fig. 2). The peak positions are shifted approximately by 1 meV to higher energies as compared with those observed at the pressure of 6.85 kbar under excitation with short (0.5 μsec) pulses of high voltage (up to 3 kV/cm); the high-voltage spectrum is shown, for comparison, in Fig. 2, too. This shift corresponds to the difference in pressure.

There are different regimes of heating carriers by high and low electric field applied. If the electric field is high enough for carriers to reach the optical phonon energy, the distribution function is stretched along the field direction. It is so called *streaming motion* regime. It begins at electric fields above approximately 20 V/cm for p-Ge. At low fields, the distribution function is due to *diffusive* heating regime and is nearly of Boltzmann type with electron temperature. Nevertheless, as it clearly seen from the existence of peaks in the emission spectrum (Figs. 1 and 2), the mechanism of low-voltage lasing in case of diffusive heating carriers is the same as for high electric fields when carriers accomplish the streaming motion. The lasing is due to stimulated optical transitions between strain-split acceptor states caused by an inversion of population of resonant acceptor states relative to that of localized states.

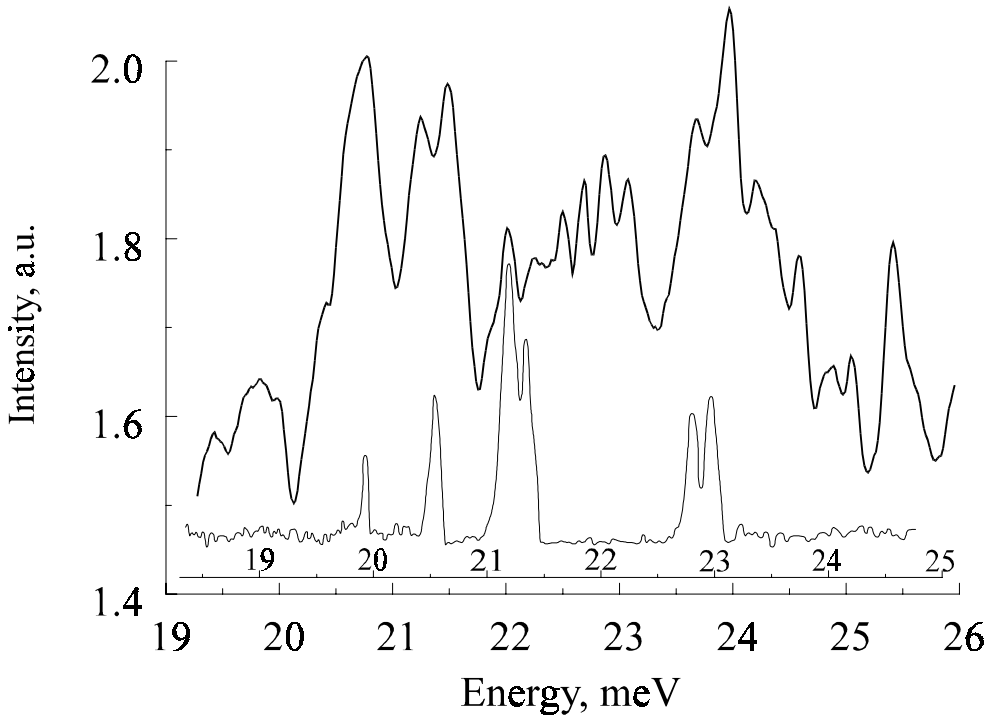

Fig. 2: Stimulated emission spectra at 14 V/cm (upper curve) and 3 kV/cm pulsed (0.5 μsec) electric field.

Transport Studies on Double Period Superlattices Utilizing Hot Electron Spectroscopy

M. Coquelin, C. Pacher, M. Kast, G. Strasser, E. Gornik

The transmission properties of double period superlattices were studied using hot electron spectroscopy. In superlattices with two different alternating well widths each miniband splits into two subminibands [1]. Figure 1 shows the conduction band of the two investigated superlattice structures. The barrier width (b) and well widths (w_1, w_2) are identical in both structures, the only difference is the sequence of the wells. The coherent transmission of these structures was calculated using a transfer matrix method taking nonparabolicity into account.

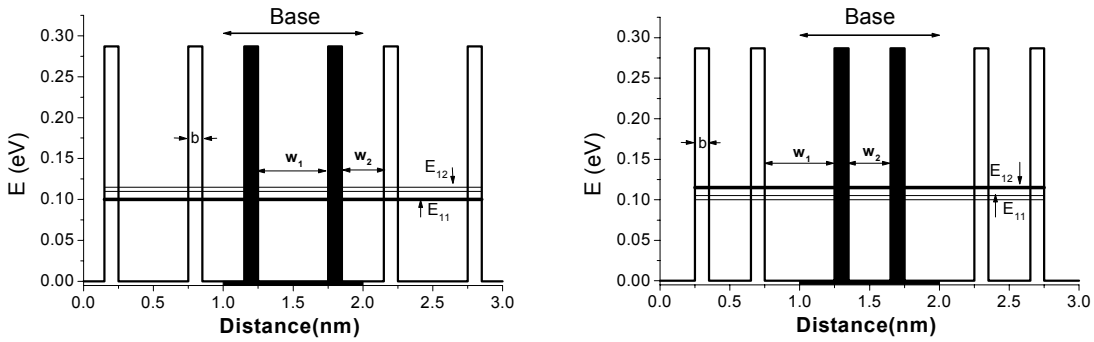

Fig. 1: Conduction band of the investigated double period superlattices.

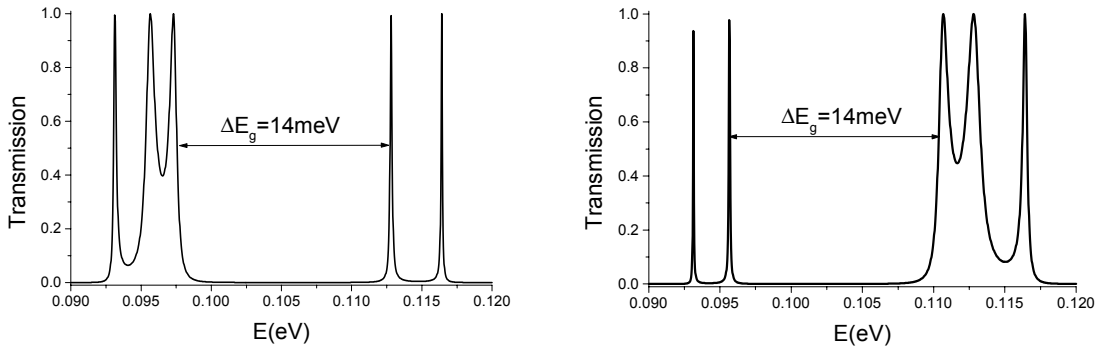

(a) (b)

Fig. 2: Transmission functions of the investigated double period superlattices.

The structure where narrow wells (w_2) encapsulate the superlattice show two narrow resonances at lower energies and broad resonances at higher energies (Fig. 2 (b)). The superlattice encapsulated by broad wells (w_1) shows an exciting difference in the transmission: the narrow energy resonances are formed at higher energies, and the broad resonances build up at lower energies. This leads to a long lifetime of the resonant electrons at higher energies while the lower resonances provide a channel where electrons can effectively be extracted (Fig. 2 (a)). Thus this system is ideally suited to achieve inversion.

The chosen width of the barriers (b = 4.3 nm) and the wells (w_1 = 4.3nm, w_2 = 3.8nm) shall lead to two clearly separated subminibands with an energy gap $\Delta E_{gap} < 36$ meV, to exclude energy relaxation by LO-phonons in the superlattice. The experiments have been performed with a three terminal device (3TD, Fig. 3) at a temperature T = 4.2 K. In a 3TD hot electrons are injected through a tunnel barrier between two contacts (emitter and base) into a drift region. The energy of these hot electrons is tunable by the applied voltage between the emitter contact and the base contact. After traversing the drift region, the hot electrons reach the double period superlattice structure. In a third contact the electrons, which have been transmitted through the superlattice, are detected as collector current. From the ratio $\alpha = I_C/I_E$ of the measured currents the transmission function is obtained energy-resolved. The high resolution (ΔE = 10meV) [2] of the spectrometer allows it to resolve the two subminibands and to obtain the transmission amplitudes.

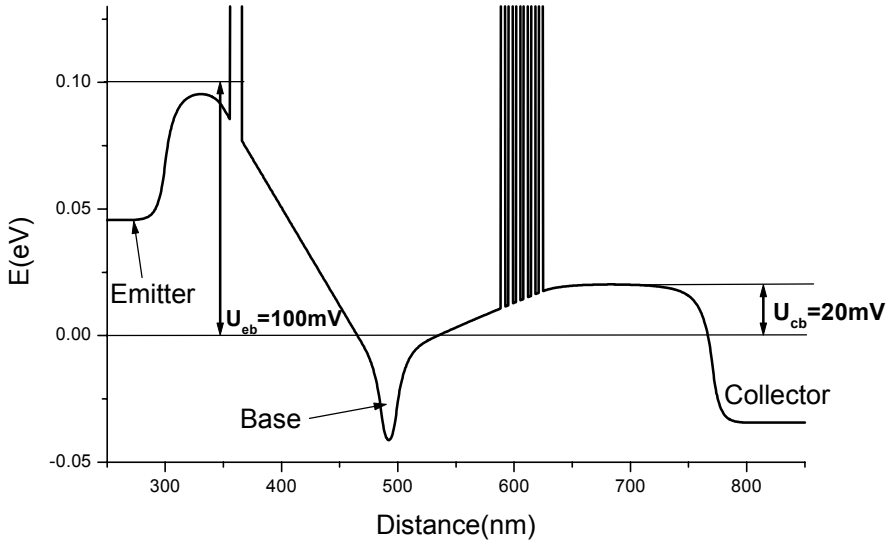

Fig. 3: Conduction band structure of the 3 terminal device.

The experimental results are shown in Fig. 4. The transfer ratio is plotted versus the voltage between emitter and base (U_{be}). The two peaks of both subminibands are indicated by E_{11} and E_{12}. Due to scattering at LO-phonons the transfer ratio stays finite. The peak positions obtained from the transfer ratio show good agreement with the calculated energies of the transmission resonances. Deconvoluting the transfer ratio with the injected energy distribution [2] gives the amplitudes of the low and high energy transmission channels, also in very good agreement with our calculations.

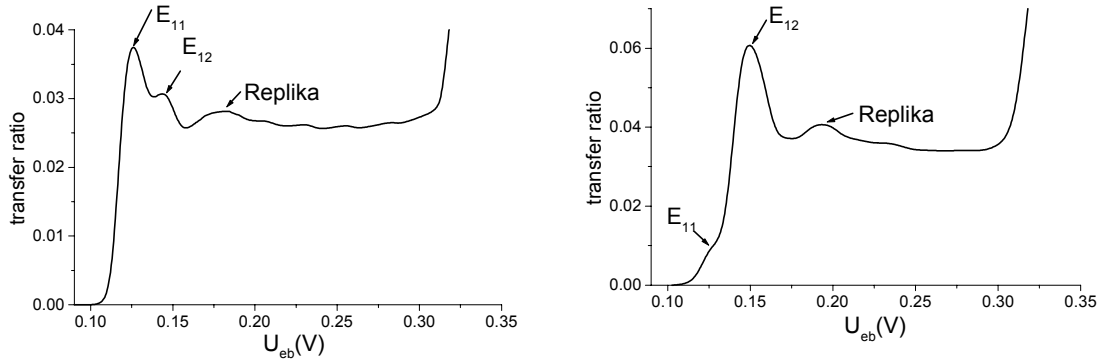

(a) (b)

Fig. 4: Measured transfer ratio of the investigated double period superlattices.

In summary we have shown that double period superlattices can be constructed in a manner that they are perfect systems to achieve inversion.

References

[1] E. H. Boudouti et al., *Phys. Rev. B*, 56, 9603 (1997).

[2] M. Kast, C. Pacher, G. Strasser, and E. Gornik, *Appl. Phys. Lett.* 78, 3639 (2001).

Transport Through Wannier-Stark States in Biased Finite Superlattices

M. Kast, C. Pacher, G. Strasser, E. Gornik

In semiconductor superlattices, the strong coupling of the electronic eigenstates of adjacent wells leads to the formation of minibands which are separated by minigaps. In superlattices with a finite number N of periods, each single miniband is formed by N eigenstates which are delocalized over the whole superlattice length. Applying an external electric field perpendicular to the layer planes alters the quantum mechanical confinement between the neighboring wells and leads to a splitting and a localization of the states which are then given by the Wannier-Stark states. Due to this localization phenomena the transmission channels for resonant tunneling through the miniband of the superlattice are quenched, and as a consequence, electron transport through the miniband vanishes. Therefore investigations on Wannier-Stark states in semiconductor superlattices were mainly done using optical measurement techniques [1], [2].

Studying transport in biased finite superlattices requires to overcome the electric field induced decrease of resonant tunneling through the Wannier-Stark states. In this work this is achieved by the use of LO phonon scattering which can induce transitions between localized weakly overlapping states. For this purpose two different superlattices has been designed. The first superlattice consists of 5 periods of 3.5 nm $Al_{0.3}Ga_{0.7}As$ barriers and 3 nm GaAs wells, the second superlattice consists of 4 periods of 4 nm $Al_{0.3}Ga_{0.7}As$ barriers and 3.2 nm GaAs wells. The miniband width of the 5 period SL equals the optical phonon energy (36 meV) whereas the miniband width of the 4 period SL (23 meV) is well below the optical phonon energy. For this superlattice LO-phonon assisted transport through the miniband sets in at electric fields where the Wannier-Stark splitting tunes into the optical phonon energy.

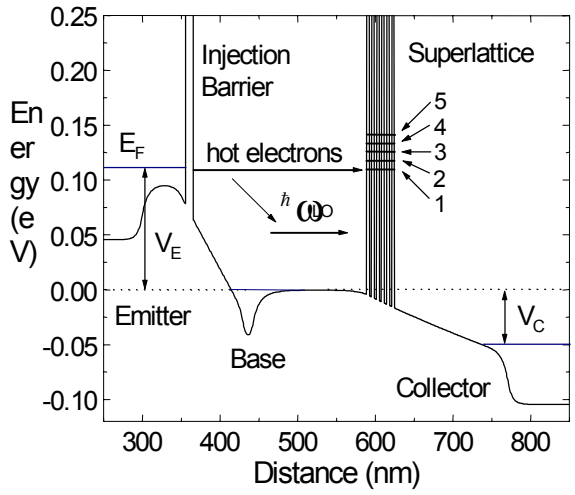

Fig. 1: Calculated conduction band diagram of a 3TD with positive bias applied to a 5 period superlattice.

A hot electron transistor [3], [4] is used to investigate electron transport through the first minibands of the superlattices. The band structure of the device is shown in Fig.1. The transmittance of the superlattice can be measured directly at given superlattice bias Vc by tuning the energy of the injected electron beam generated at the tunneling emitter barrier. The main characteristic thereby is the static transfer ratio $\alpha=I_c/I_e$ which directly reflects the probability of a hot electron to be transmitted through the superlattice. Due to the high resolution [4] of the spectrometer we are able to observe the energy splitting (Fig. 2) and the transmission behavior (Fig. 3) of the individual Wannier-Stark states separately in transport for both superlattices.

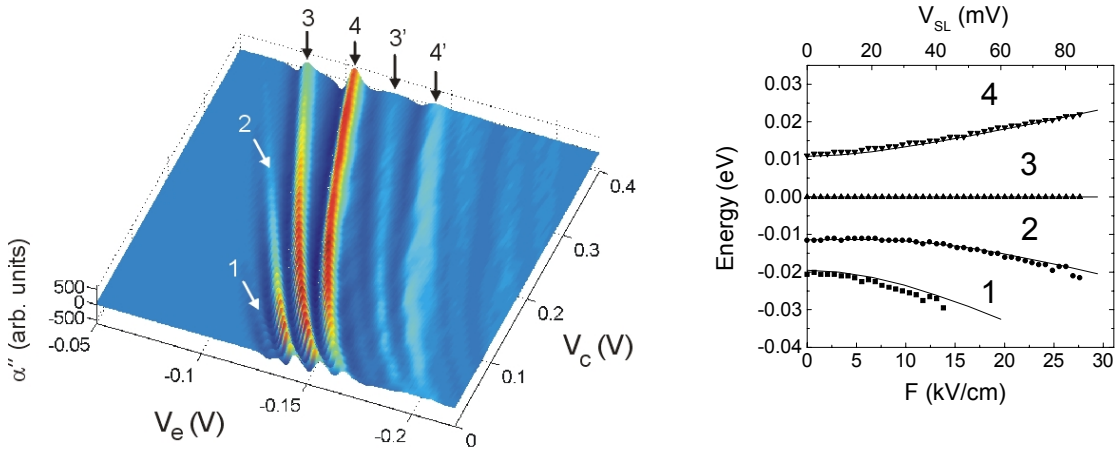

(a) (b)

Fig. 2: (a) Second derivatives of the transfer ratio vs. emitter bias at different collector biases for the 5 period superlattice; (b) Wannier-Stark states (symbols) of the 4 period superlattice compared to calculations (solid lines).

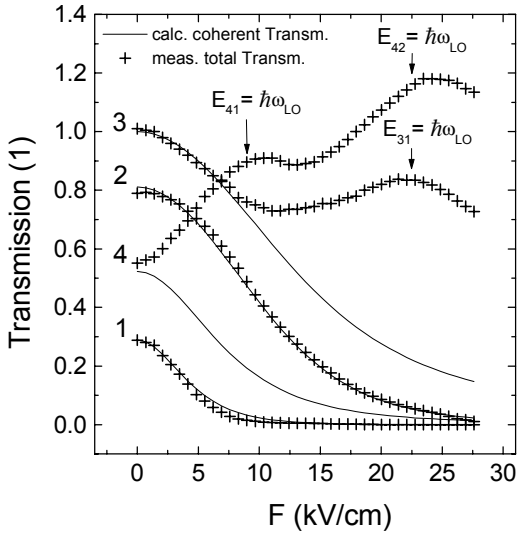

Fig. 3: Measured total transmission per states as a function of the electric field (crosses) compared to the calculated coherent transmissions of the individual Wannier-Stark states for the 4 period superlattice (solid lines).

The basic transport through Wannier-Stark states is identified to be coherent, the amplitudes of the quantum mechanical transmission are directly observed. Individual transport channels induced by LO-phonon scattering are observed when the Wannier-Stark states spacing tunes into the optical phonon energy as shown in Fig. 3.

References

[1] E. E. Mendez et al., *Phys.Rev.Lett.* 60, 2426 (1988).

[2] P. Voisin and J. Bleuse, *Phys. Rev. Lett.* 61, 1639 (1988)

[3] C. Rauch et al., *Phys. Rev. Lett.* 81, 3495 (1998)

[4] M. Kast, C. Pacher, G. Strasser, and E. Gornik, *Appl. Phys. Lett.* 78, 3639 (2001)

Study of Electron-LO Phonon Scattering in Wide GaAs Quantum Wells Utilizing Hot Electron Spectroscopy

C. Pacher, G. Fasching, M. Kast, G. Strasser, E. Gornik

Electron-LO phonon scattering in wide GaAs quantum wells is experimentally studied. New results from a hot electron spectroscopy study utilizing a three terminal device (3TD) are reported. In the past we have used 3TDs to study different transport phenomena, like the onset of diffusive miniband transport in superlattices [1], quantum mechanical anti reflection coatings for miniband transport [2], and increased the energy resolution of this spectroscopy technique to approx. 10 meV [3]. A further decrease of the FWHM of the injected electron distribution compared to Ref. [3] gave us the possibility to study different scattering mechanisms in GaAs energy resolved by simple current measurements.

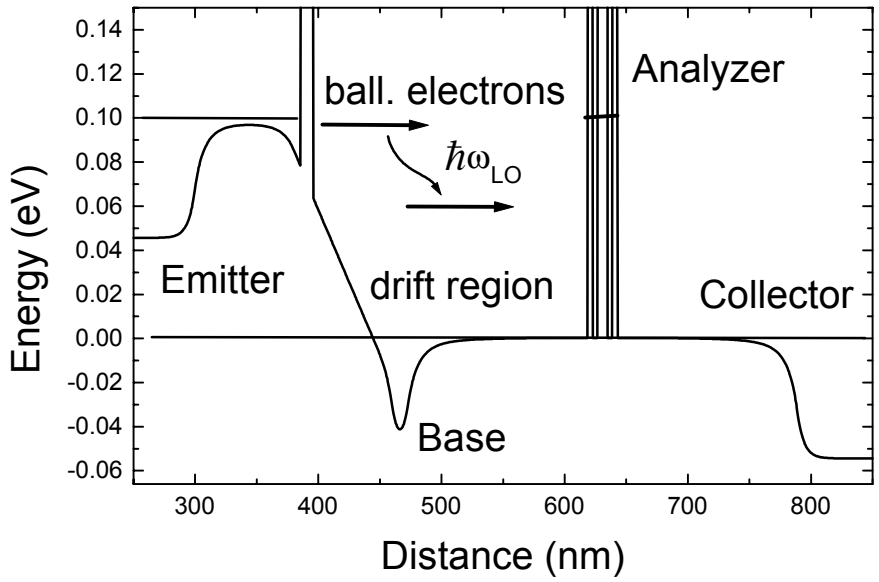

Fig. 1: Calculated conduction band diagram of a three terminal device.

In a 3TD, hot electrons are injected through a $Al_{0.3}Ga_{0.7}As$ tunnel barrier into a GaAs drift region. These hot electrons are tunable in their energy by the applied voltage between the emitter contact (E) and the base contact. After traversing the drift region, where they undergo various scattering mechanisms, the hot electrons hit an energy filter with a FWHM of 1 meV. In a third contact, the collector (C), the electrons which have been transmitted through the filter are detected as collector current. From the ratio $\alpha = I_C/I_E$ of the measured currents at T = 4.2 K an energy-resolved spectrum of the electron distribution is obtained.

In our experiments we observed resonances in the emitter current which are due to electron injection into bound states in the drift region. Due to scattering these resonances persist in the calculated transfer ratio $\alpha=I_C/I_E$ and gave us the possibility to directly measure elastic scattering in the highly doped base layer and LO phonon scattering in the drift region energy resolved. Since the LO phonon scattering takes mainly place between different bound states we also get information on the q-dependence of the LO phonon scattering. In the experiments we used three different lengths (150 nm, 250 nm, 400 nm) for the drift region to study the LO phonon scattering in more detail. The mentioned resonances in the emitter current are most pronounced for the shortest sample (150 nm), less pronounced for the 250 nm sample and vanish for the longest sample (400 nm). The reason is the different energy spacing of the bound states, which is 9.7meV, 5.8meV and 3.6meV, respectively. In the latter case, the energy separation is smaller than the energy distribution leading to smooth transfer ratio. A first estimate, considering only the amplitudes of the ballistic peaks, leads to a LO phonon scattering time of 324 fs in wells with a width between 150 and 250 nm, and to 161 fs for wells with a width between 250 and 400 nm. This is a clear evidence for the confinement dependence of the LO-phonon scattering rate.

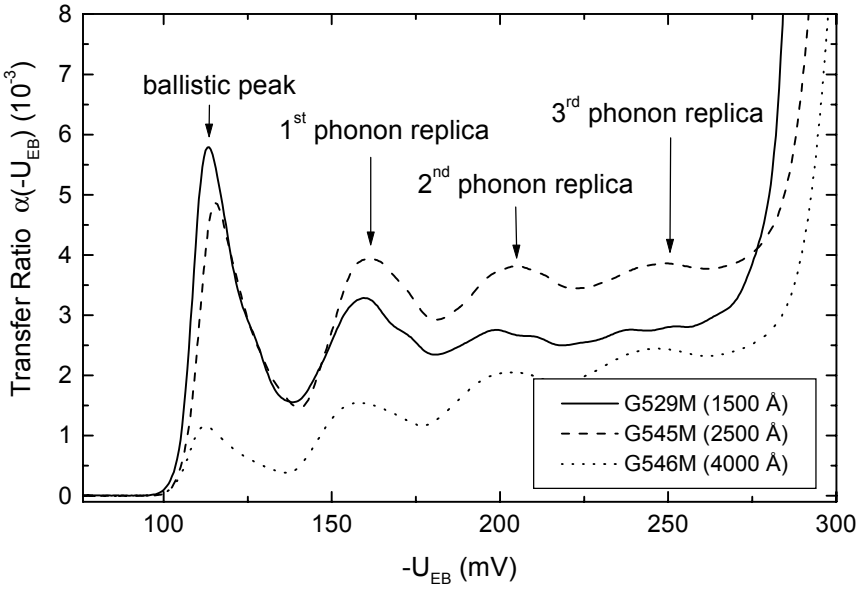

Fig. 2: Transfer ratios vs. emitter bias of the analyzer for three different drift region lengths.

References

[1] C. Rauch et al., *Phys. Rev. Lett.* **81**, 3495 (1998).

[2] C. Pacher, *et. al.*, *Appl. Phys. Lett.* **79**, 1486 (2001).

[3] M. Kast, C. Pacher, G. Strasser, and E. Gornik, *Appl. Phys. Lett.* **78**, 3639 (2001).

Electron Transport in Kinetic Heterostructures

J. Smoliner, D. Racoszy, G. Strasser

The scope of this project is the investigation of heterostructures with large differences between the effective masses in the corresponding semiconductor materials. In 2001, mainly samples based on the InAs-GaAs material system were investigated, since our MBE for Sb based heterostructures was not yet operational. The masses in InAs and GaAs differ by a factor of three. The first samples we investigated were InAs self assembled dots and wetting layers since these sample are also interesting for various other applications in our institute. For our investigations, we employ Ballistic Electron Emission Microscopy (BEEM), a method which provides spectroscopic information on ballistic electron transport with nm spatial resolution.

Figure 1 (a) shows a sketch of the experimental setup and the cross-section view of the sample. The corresponding conduction band profile is shown in Fig. 1 (b). If the bias between the tip and the Au-base layer is large enough, ballistic electrons penetrating into the semiconductor can overcome the barrier at the InAs/GaAs interface and are collected at the collector contact. The corresponding current I_c as a function of bias V_t is called BEEM spectrum. The barrier height V_b is directly determined from the bias position of the current onset.

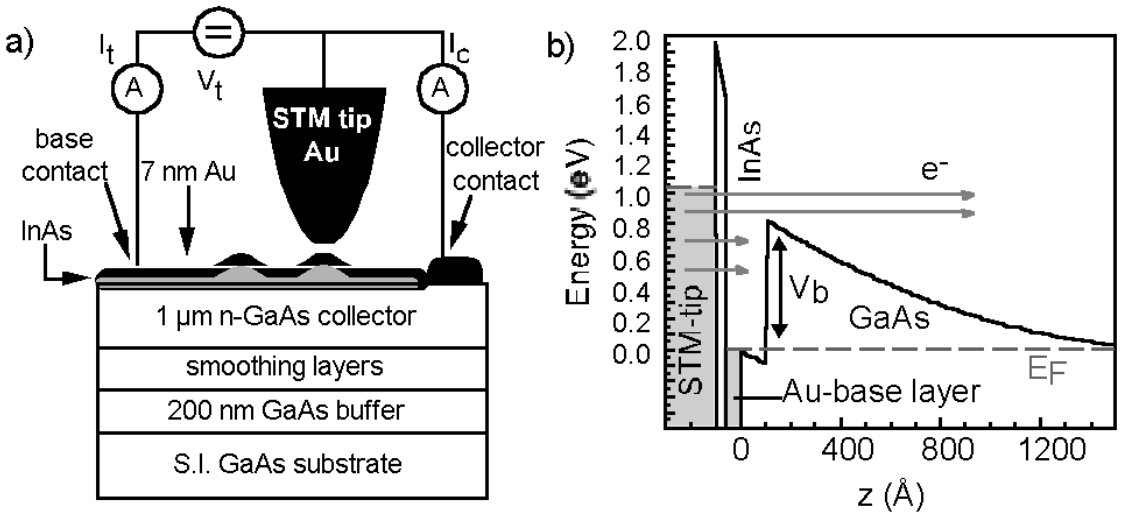

Fig. 1: Principle of BEEM operation. a) experimental setup, b) corresponding conduction band profile of our sample. V_t is the tunneling voltage, I_t the tunneling current, I_c the collector current (BEE current), E_F the Fermi energy, and V_b is the barrier height at the InAs-GaAs interface.

Figure 2 (a) shows a topographic STM (scanning tunneling microscope) image of our quantum dot sample. One small and three big dots are clearly visible. The granular

structure in this image is due to the Au film covering the sample. Figure 2 (b) shows the corresponding BEEM image. Here the dots are visible as brighter spots indicating areas of enhanced electron transmission. Due to the influence of the wetting layer, the contrast between the on-dot and off-dot regions is rather weak.

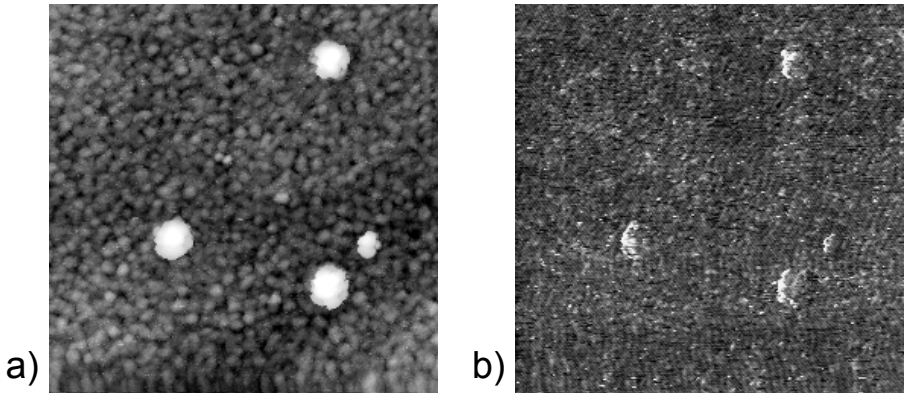

Fig. 2: a) STM topographic image of our sample, (scan size: 500 nm x 500 nm, V_t = 1.3 V, I_t = 2 nA). One small and three big dots are clearly visible. The granular structure in this image is due to the Au film covering the sample. b) corresponding BEEM image. The weak contrast is due to the wetting layer.

To investigate the contrast mechanism in more detail, BEEM spectra were measured on the dots and also at off-dot positions. Figure 3 shows a typical example of two BEEM spectra at T = 300 K, one measured on a dot and the other one measured in some distance from the dot. Already from the raw data one can clearly see that the onset voltage on the dot is strongly reduced compared to the off-dot onset voltage, which in turn is smaller than the value expected for a Au/GaAs Schottky contact (0.9 V). The barrier height gained from the power law fit is 0.69 eV and 0.80 eV for the on-dot and the off-dot position respectively. Further measurements at other positions on the sample show that at 300 K the barrier height on the dots is in general between 0.61 eV and 0.74 eV (mean value 0.69 eV), while for off-dot locations it varies from 0.73 eV to 0.87 eV (mean value 0.80 eV).

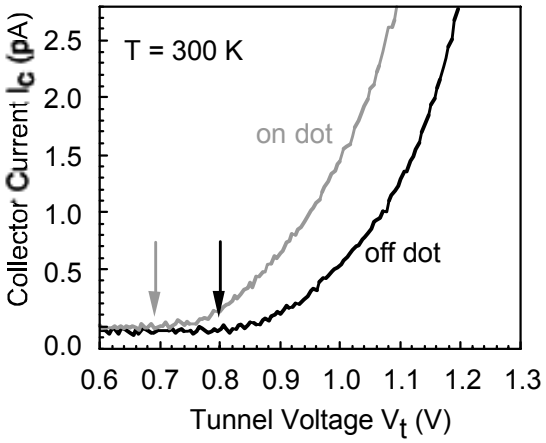

Fig. 3: Typical BEEM spectra measured on an InAs dot and in an off-dot region (I_t = 2 nA, T = 300 K).

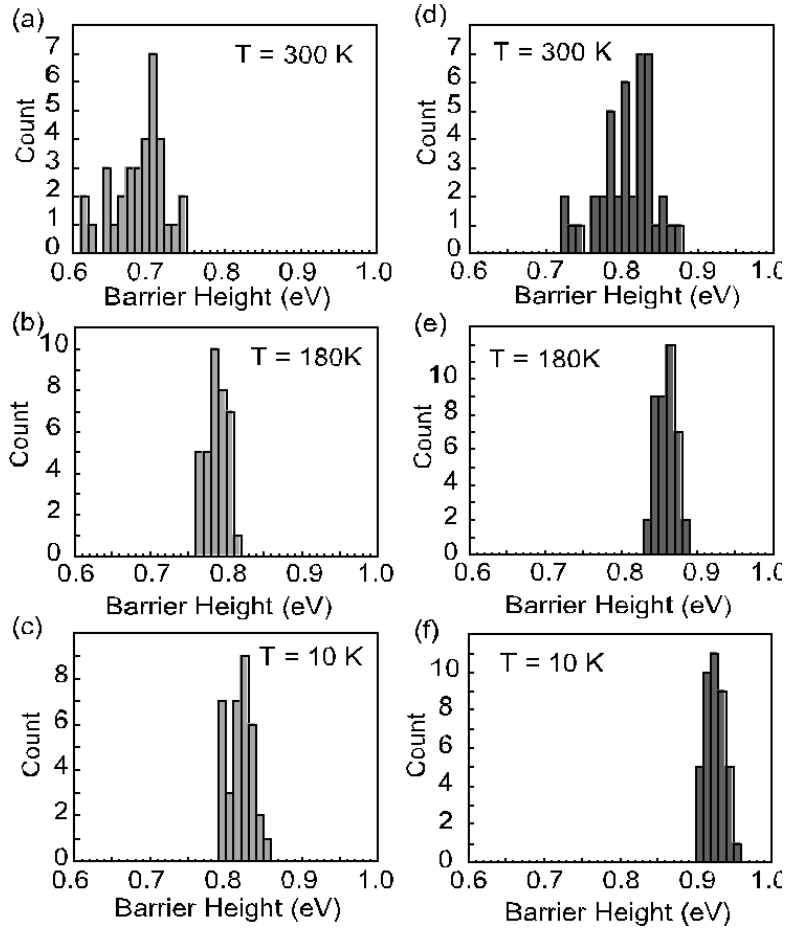

Fig. 4: (a – c) Histograms of the InAs/GaAs barrier heights measured on quantum dots at temperatures of 300 K, 180 K and 10 K, respectively. (d – f) Histograms of the barrier heights between the InAs wetting layer and the GaAs measured in off-dot regions at temperatures of 300 K, 180 K and 10 K, respectively.

To investigate the InAs/GaAs barrier height in dependence of the temperature we also sampled BEEM curves on various on-dot and off-dot positions at 180 K and 10 K, respectively. As can be seen from Fig. 4, the measurements show an increase in barrier height with decreasing temperature both for the on-dot positions and the wetting layer. On the dots (a – c), the mean value of the barrier height rises from 0.69 eV (standard deviation 34 meV) to 0.79 eV (standard deviation 13 meV) between T = 300 K and T = 180 K. A further lowering of the temperature down to 10 K results just in a slightly higher mean barrier height of 0.82 eV (standard deviation 16 meV). Note that the distribution of the barrier height becomes significantly narrower between T = 300 K and T = 180 K but approximately maintains its width when the temperature is further reduced. In our opinion this behavior is mainly due to the reduction of drift problems with decreasing temperature. On the wetting layer (Fig. 4 (d – f)) the mean value of the barrier height rises from 0.80 eV (standard deviation 35 meV) at T = 300 K to 0.86 eV (standard deviation 12 meV) at T = 180 K and to 0.93 eV (standard deviation 13 meV) at T = 10 K.

It is quite instructive to compare our results with BEEM measurements on an Au-InAs-GaAs system with homogeneous InAs interlayers of various thickness, carried out by Mao-Long Ke et al. [1].

They report that, at T = 300 K, a single monolayer of InAs lowers the barrier height rapidly from 0.9 eV to 0.8 eV, while an increase of the nominal InAs layer thickness to 3 monolayers yields a further decrease to approximately 0.74 eV. For thicker layers the barrier height remains almost constant up to 27 monolayers, where it drops again and finally reaches ≈0.63 eV for a thickness of 33 monolayers (≈11 nm) and beyond. These data indicate that the average thickness of our wetting layer is about one monolayer, while our dots are on average approximately 30 monolayers thick and the large dots appear to have a thickness of more than 33 monolayers. This result agrees very well with the dot height gained from AFM measurements. Of course one must bear in mind that the data from Ke et al. were obtained on homogeneous InAs layers rather than on InAs dots. In contrast to a partially strain-relaxed system of SAQDs on a wetting layer, thin homogeneous InAs layers are fully strained and thick homogeneous InAs layers are strain-relaxed via dislocations. The different strain conditions for the two systems most probably influence the barrier height.

In summary, we have used BEEM/S to study InAs self assembled quantum dots on a GaAs substrate. It is found that in first approximation the barrier height between the quantum dots and the GaAs behaves similar to that of homogeneous InAs layers on GaAs reported in the literature. On the basis of these results, our data suggest a thickness of one monolayer for the wetting layer and a thickness of 30 monolayers and more for the dots, which is in excellent agreement with results from AFM measurements. Furthermore, a significant increase of the barrier height for lower temperatures is observed. The complex influence of both geometry factors and temperature on the InAs-GaAs barrier height and, therefore, on the energy levels inside of InAs quantum dots will make bandstructure engineering for quantum dot applications a quite difficult task.

Reference

[1] Mao-Long Ke, D.I. Westwood, C.C. Matthai, B.E. Richardson, and R.H. Williams, J. Vac. Sci. Technol. B **14(4)**, 2786 (1996).

Scanning Capacitance Microscopy with Zirconium Oxide as High-k Dielectric Material

W. Brezna, S. Harasek, H. Enichlmair, E. Bertagnolli, E. Gornik, J. Smoliner

Scanning Capacitance Microscopy (SCM) is an extension of conventional Atomic Force Microscopy (AFM) and a promising tool for semiconductor device characterization. The main application of this method is two-dimensional carrier profiling for failure analysis and process control. Unfortunately, SCM is not an easy and straightforward technique to use. Quantitative reproducible measurements are a serious problem, since the preparation of the insulator required on the sample surface (up to now exclusively SiO_2) has a dramatic influence on the results, especially in cross sectional measurements. As main problem, standard high temperature industrial oxidation techniques cannot be used because on processed devices, the high temperature broadens all doping profiles or destroys the samples completely. Thus, low temperature oxidation processes have to be used, which usually yield a much lower oxide quality and moreover, are not extremely reproducible.

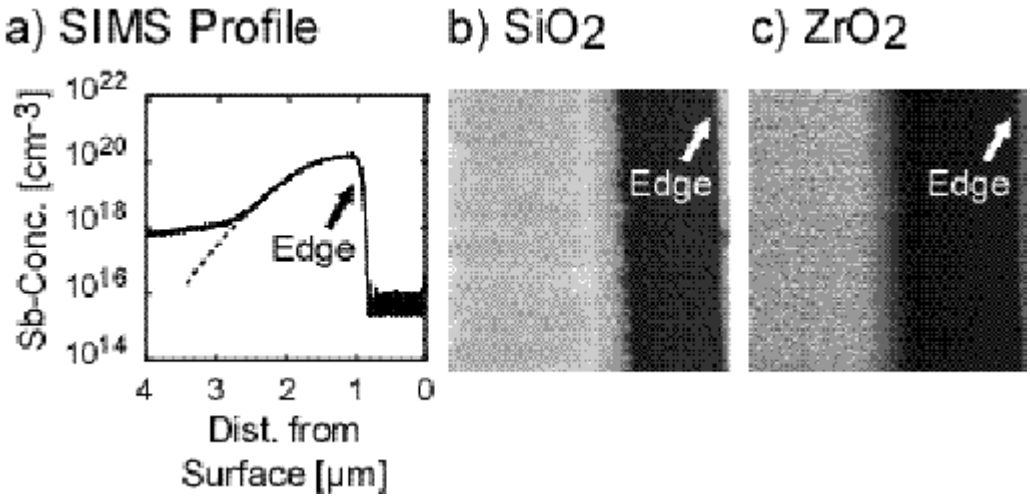

Fig. 1: The dopant profile of the n-type (Sb) region of the investigated pn-junction is plotted in picture a). SCM-images of a SiO_2 coated and ZrO_2 coated junction are shown in b) and c), respectively.

For this reason, we tried to replace the SiO_2 with high quality, low temperature CVD grown ZrO_2, which recently attracted much attention as a possible high-k gate dielectric in microelectronic metal-oxide-semiconductor (MOS) devices, because it is promising to overcome the tunneling limits of SiO_2. The effective dielectric constant of thin and ultra thin films in the range of k = 18, the wide band-gap of more than 5 eV, favorable band-mismatch to silicon and finally high thermodynamic stability on silicon make ZrO_2

a promising dielectric for scanning capacitance microscopy. To gain comparable results, the dielectric thicknesses were adjusted to get the same capacitance for both SiO_2 and ZrO_2 samples, which means that the SiO_2 layers were 4 nm and the ZrO_2 layers were approximately 20 nm thick. The greater thicknesses of the ZrO_2 layers should compensate for the material's bigger dielectric constant. To demonstrate the utilization of ZrO_2 as a dielectric material for SCM measurements, we first compare the SCM images of a pn-junction which were obtained with industrial quality SiO_2 and with ZrO_2 layers grown by CVD (Fig. 1). The pn-junctions were manufactured at Austria Mikro Systeme International AG (AMS) by implanting a highly doped buried layer (Sb) into a low boron (p-type) doped silicon wafer. The dopant profile obtained via SIMS is shown in Fig. 1 a). As one can see in Fig. 1 b), very good contrast was obtained between the p- and n-type regions on a sample with SiO_2 as dielectric. If we compare these data with the results obtained on the ZrO_2 layer, we see in Fig. 1 c) that ZrO_2 can compete easily in terms of contrast generation.

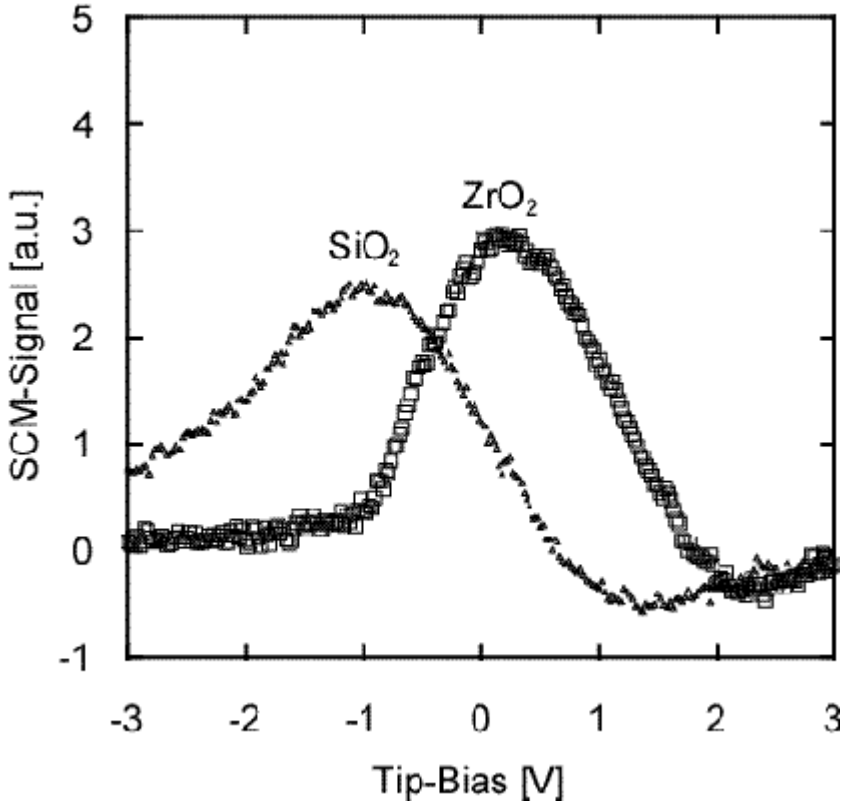

Fig. 2: dC/dV plots of p^--doped samples with different dielectric layers.

One of the most important parameters describing the oxide quality both for SCM analysis and gate dielectrics in MOS transistors is the amount of fixed oxide charges and interface trapped charges. Figure 2 compares the dC/dV plots obtained by SCM measurements both for SiO_2 and ZrO_2. According to MOS theory textbooks the different parasitic charges found in real oxides influence the formation of depletion and inversion zones and therefore influence the shape of signal versus voltage plots. Large amounts of either positive or negative fixed oxide charges move the plots vertically from their spe-

cial flatband condition to negative or positive tip bias values, respectively, because the fixed charges have to be compensated. The shapes of the curves remain unchanged. The nearer the peaks are to zero voltage position, the higher is the oxide quality. As one can see, the peak's position is +0.18 V for ZrO_2 and –1 V for high temperature SiO_2 respectively, which demonstrates the excellent electrical properties of the zirconium oxide layer. On the other hand, a large amount of interface trapped charges does not alter the peak's voltage-axis position, but broadens the plot.

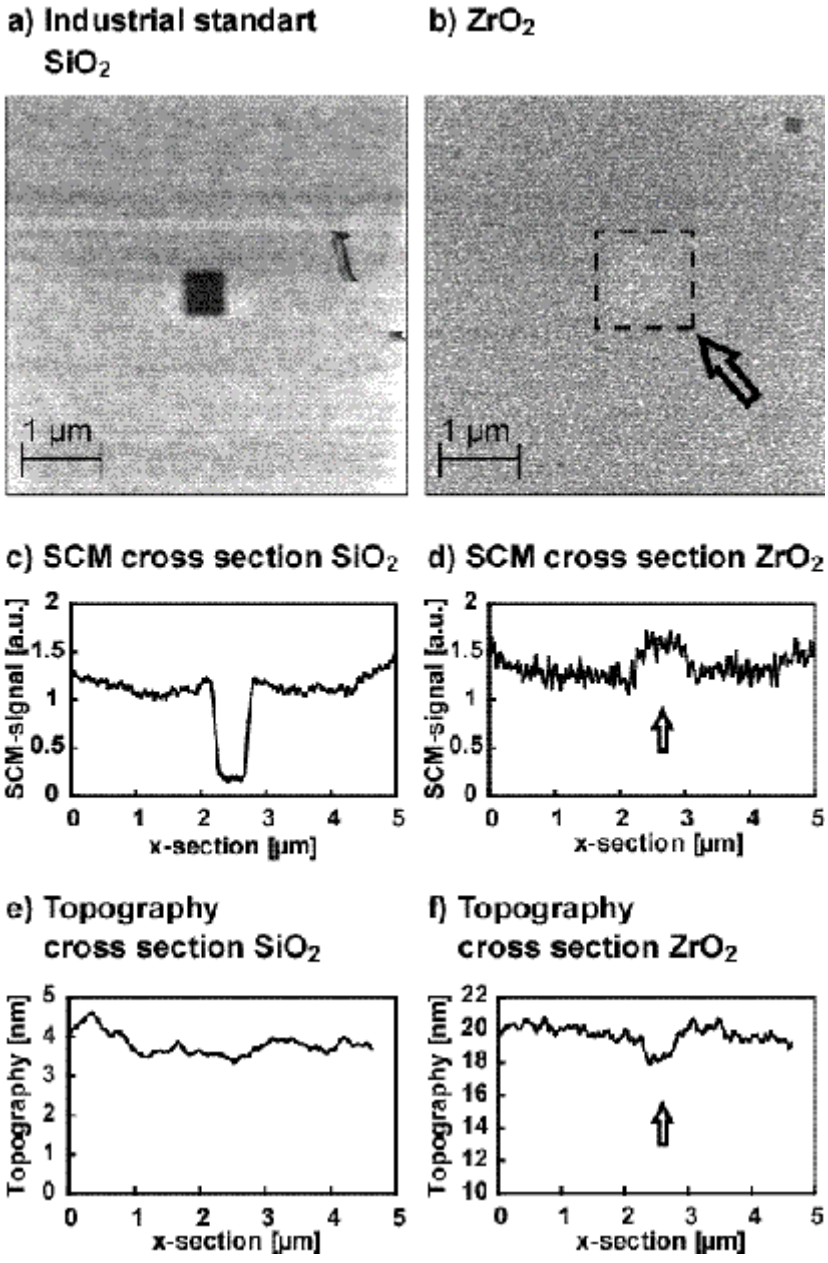

Fig. 3: Impact of dielectric layer degradation on SCM contrast. Degradation on a) SiO_2 leads to SCM signal lowering, on b) ZrO_2 the signal is higher in the stressed region. c) and d) show a signal cross section of the stressed areas for SiO_2 and ZrO_2, respectively. The topography of e) the SiO_2 layer remains unaltered, whereas f) the ZrO_2 layer was thinned due to scratching effects.

The broader peak of the SiO_2 sample is assumed to be due to anodic oxide growth and diffusion of contaminants which is more likely in thin (4 nm) SiO_2 than in the quite thick (20 nm) ZrO_2 layer. This shows the superior behavior of ZrO_2 in contrast to SiO_2. On the other hand, the reduction of oxide quality during SCM measurement can lead to contrast degradation, which is shown in Figs. 3 a) and b). Cross sections of both samples are shown in Figs. 3 c) and 3 d). In this experiment, a silicon oxide (Fig. 3 a)) and a zirconium oxide sample (Fig. 3 b)) were stressed by SCM scanning at a tip voltage of -3 V in a small area of about 500 x 500 nm. After 8 scans the resulting degradation was investigated by taking a 5 x 5 µm picture in capacitance mode with a tip bias adjusted to get the maximal signal. In the case of silicon oxide, the result is shown in Figs. 3 a) and 3 c), respectively. In the untreated region the normal signal for the investigated doping type was obtained whereas inside the stressed area the SCM signal was approximately zero. This indicates a severe degradation of the quality of the thin silicon oxide due to continuos SCM measurement. On the other hand, using zirconium oxide can prevent such problems concerning reproducibility as it is shown in Figs. 3 b) and 3 d), respectively. Only a slight signal increase occurs in the treated region, which is qualitatively different from the lowering in silicon oxide. Our interpretation concerning this fact is that material is scratched away by the tip which leads to a thinner dielectric. Subsequently the SCM signal is increased. Topographic investigations of the stressed region show an average lowering of 2 nm in Fig. 3 f).

Effect of Pulse Risetime on Trigger Homogeneity in Grounded Gate nMOSFET Electrostatic Discharge Protection Devices

M. Litzenberger, D.Pogany, E.Gornik, K. Esmark

The inhomogeneities in the triggering of the parasitic bipolar transistor in grounded gate (gg) nMOS protection devices (PD) are known to reduce the ESD failure threshold. As well the risetime of the ESD pulse is known to have an influence on the triggering behavior of the CMOS ESD PD's. Short pulse risetime has been found to lead to a more homogeneous current flow along the device width and consequently to a higher ESD failure threshold. This has mainly been attributed to the contribution of the displacement current (depending on the device capacitance and the pulse risetime) to the total base trigger current. This effect is known as dU/dt-triggering. We have studied triggering behavior in submicron gg-nMOS ESD PD's by a backside laser interferometric method to investigate the current flow homogeneity in CMOS gg-nMOS ESD PD's of different technology as a function of pulse risetime.

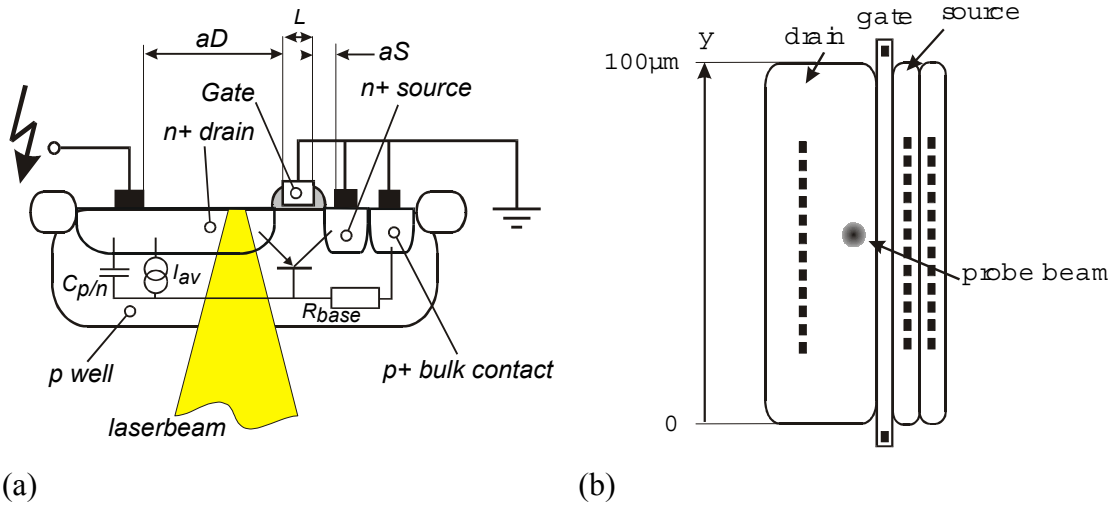

(a) (b)

Fig. 1: (a) Cross-section of the gg-nMOS with equivalent circuit and the position of the probing laser beam indicated. The layout parameters a_S, a_D and L, as used in the paper are also indicated. (b) Top view of the gg-nMOS with the indication of the probing beam and the y-axis of the coordinate system used.

We have investigated single finger gg-nMOS ESD PD's of 0.35 and 0.18 µm technology with a variation of the drain contact to gate spacing a_D, source contact to gate spacing a_S, and gate length L. The source, gate, and the bulk contacts of the devices are connected to ground. Figure 1 shows the simplified cross section (a) and the layout (b) of the investigated devices. In Fig. 1 (a) the equivalent circuit of the gg-nMOS is also indicated.

To measure the current flow homogeneity we have used a scanning backside laser interferometric method. The temperature induced change in the Si refractive index (thermooptic effect) during current stress pulses of 100 ns and 150 ns length and different risetimes of 1 ns and 20 ns, respectively, is probed by measuring the phase shift of an infrared (IR) laser beam (wavelength $\lambda = 1.3$ µm). The phase shift of the probing laser beam is detected by a heterodyne interferometer setup and is in a first approximation a measure of the current density.

Figure 2 (a) shows a typical result for a measurement of the current flow homogeneity in a 0.35 µm technology gg-nMOS during ESD pulses of 1 ns risetime, for different stress currents. It can be seen that the MOSFET first triggers in the middle of the gate width at low stress currents, resulting in a current flow there. At higher stress currents the width of the triggered region increases and the current flow spreads towards the device corners. With a further increase of the stress current the device triggers over the whole width resulting in a homogenous current flow. Figure 2 (b) shows the current density distribution in the same device, when stressed with pulses of 20 ns risetime. For low stress currents the device first triggers at the gate corners.

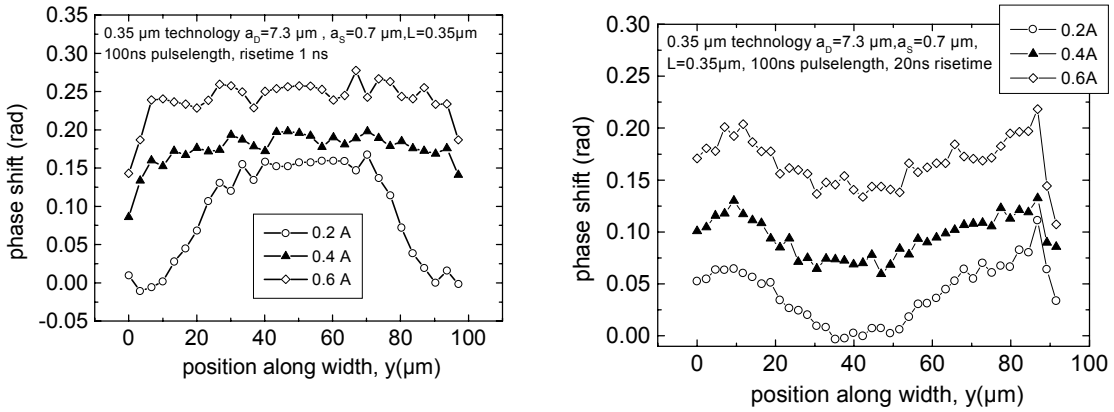

(a) (b)

Fig. 2: Phase shift distribution along the device width at the end of a 100 ns long pulse with 1 ns (a) and 20 ns (b) risetime in the 0.35 µm gg-nMOS device for three different current pulse amplitudes.

With increasing stress current the current flow spreads to the middle of the device, leading to a homogenization of the current flow. However, the phase shift (so the current density) still exhibits two maxima at the two device corners, even at a stress current of 0.6 A. For the 0.18 µm technology devices, the current distribution does not show any qualitative difference between the stress with 1 ns and 20 ns risetime, and it is similar to that shown in Fig. 2 (a).

The difference in the triggering behavior for shorter and longer pulse risetime in the 0.35 µm technology devices indicates that the displacement current $I_{dU/dt}$ ($=C_{p/n}.dU/dt$) ($C_{p/n}$ is the substrate/drain capacitance, see equivalent circuit in Fig. 1 (a)) plays a crucial role in the device triggering. At 20 ns risetime, $I_{dU/dt}$ contribution to the substrate current I_{SUB} is negligible compared to that from the avalanche generation I_{AV} ($I_{SUB} = I_{dU/dt} + I_{AV}$). I_{AV} is dominant at the structure corners, due to a higher electrical field caused by the spherical shape of the drain diffusion at the corners. Therefore the device

triggers preferentially at the corners, independently on the stress current. At 1 ns risetime, the $I_{dU/dt}$ contribution is supposed to be comparable to I_{AV}. We have recently suggested that the triggering of the devices in the middle is due to a combined effect of the conductivity modulation in the drain/base region and a lower base resistance in the device middle. Our present results therefore imply that in order to "activate" the conductivity modulation in the 0.35 μm devices, a certain current density level has to exist in the device at the first moment of the triggering. This is reached by high value of $I_{dU/dt}$. The reason why the triggering in the middle (so also the conductivity modulation) in the 0.18 μm devices occurs also under long pulse risetime stress ($I_{dU/dt}$ is expected to be negligible here) is not yet understood. The effect of risetime on trigger homogeneity is therefore supposed to be technology dependent, at least for low stress currents.

Backside Interferometric Investigations of a DMOS Clamp Under ESD Stress

M. Blaho, D. Pogany, E. Gornik, W. Wilkening, J. Hieber

Power DMOS transistors are building blocks of output drivers and switches in automotive applications. Their protection against electrostatic discharge (ESD) events can be obtained by self-protection or by appropriate gate-biasing active clamping. Such a clamp represents a circuit which may exhibit a complex behavior during an ESD event. The monitoring of a discharge paths in such circuit is important for understanding of the circuit behavior. Scanning backside interferometry is a useful tool for investigation of internal device behavior in semiconductor devices. In this work we have optically investigated thermal and free-carrier signals related to a discharge path in the active gate-biasing clamp circuit.

The gate-biasing active clamp circuit consist of a LDMOS transistor connected in series with a diode D added to block negative polarity stress; another diode that is in a parallel branch to the previous one to clamp the negative polarity stress; and the gate-biasing sub-circuit. Additionally, monitoring devices are used to monitor internal device voltages under the ESD event. Gate-biasing active clamp circuits with three different LDMOS areas (50%, 100% and 400% of a reference size) were investigated. The circuits were stressed by positive 100 ns and 300 ns long current pulses (up to 3.5 A) using a transmission line pulser (TLP). The optical mapping is performed using the backside laser scanning technique. A focused infrared laser beam (λ = 1.3 μm) scans the device, and the temperature induced (positive sign) and free-carrier induced (negative sign) contributions to the phase signal are interferometrically detected. For a dominant thermal contribution, the phase shift represents directly the 2D energy density in the device.

The differential resistance R_{diff} obtained from the pulsed IV measurements of the circuit is nearly stress current independent below the device failure threshold. $1/R_{diff}$ scales nearly linearly with the DMOS area, indicating that the current flow in the LDMOS device under ESD stress is homogeneous. This is confirmed by the thermal mapping across the fingers of the LDMOS (Fig. 1). It can be concluded that the gate-bias subcircuit effectively opens the channel of the LDMOS and supports the homogeneous current flow in the device.

During the positive ESD stress the diode D connected in series with the LDMOS transistor is forward biased. The optical mapping of the diode area exhibits a large negative signal during the stress pulse (Fig. 2), indicating a large free carrier injection. A linearly increasing thermal phase shift component is superimposed on the free-carrier signal. After the pulse end it becomes positive and reaches its maximum 400 ns after the end of the stress pulse. The effect of this delayed maximum cannot be explained by a lateral heat transfer from some different hot area of a circuit, because the maximum heat dissipating region is in the middle of the diode area. The closer analysis of the data suggests that the phase dynamics after the pulse is caused by an existence of a tail in the free-carrier evolution. The decay in the free-carrier signal is determined by the carrier recombination dynamics inside the diode region.

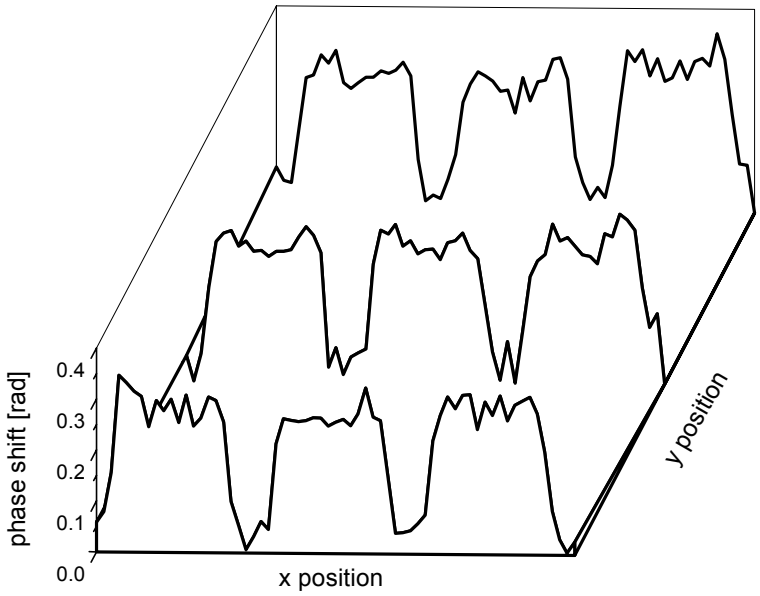

Fig. 1: The phase shift distribution in the 100% LDMOS at the end of the stress TLP pulse of 1.4A @ 300ns. Three fingers of the LDMOS are easy to distinguish. As the phase shift reaches the same values in all fingers in all scan lines, it can be concluded that the heat distribution in the LDMOS area is homogeneous.

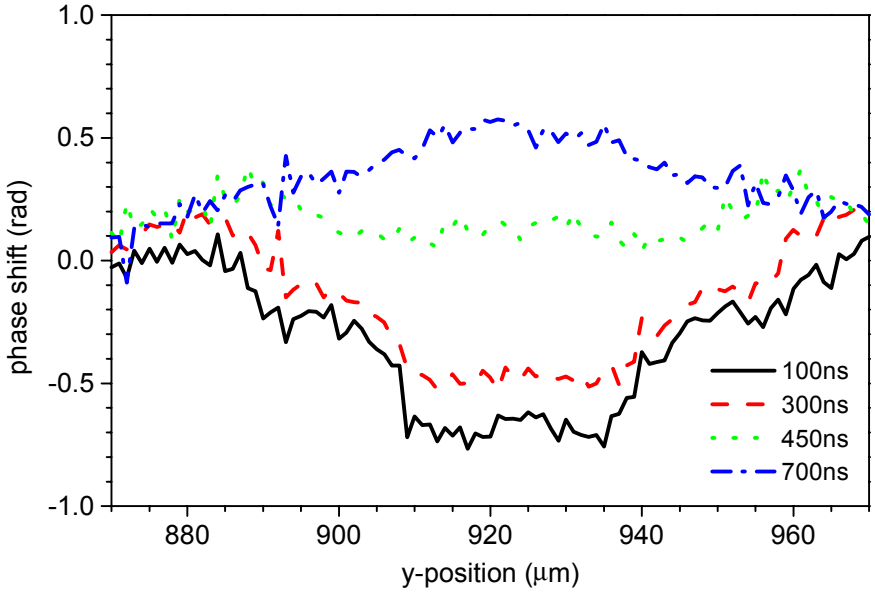

Fig. 2: The phase shift distribution in the diode D at the end of the stress TLP pulse of 1.4A @ 300ns. The time is a parameter (the stress starts at time 0 ns).

No other discharge paths were found in the gate-biasing active clamp circuit. Finally it was found that the circuit fails in the monitor sub-circuit.

Study of Trigger Instabilities in ESD Protection Devices Using Backside Laser Interferometry

D. Pogany, C. Fürböck, M. Litzenberger, P. Kamvar, S. Bychikhin, E. Gornik

The self-heating effect is the main failure cause in electrostatic discharge protection devices (ESD PDs). Inhomogeneous current flow, non-destructive current filaments of larger size, are often found in ESD PDs. The current filamentation is related to a negative differential resistance (NDR) region in the device IV characteristics. Another temperature effect, plausible for ESD protection, is the homogenization of the current flow during the ESD pulse. We have studied the trigger dynamics and instabilities causing pulse-to-pulse (PTP) variations in the triggering place along the width of different types of ESD protection devices fabricated by a smart power technology. Backside laser interferometry was used allowing the investigation of thermal dynamics during a single ESD event with a ns time scale resolution.

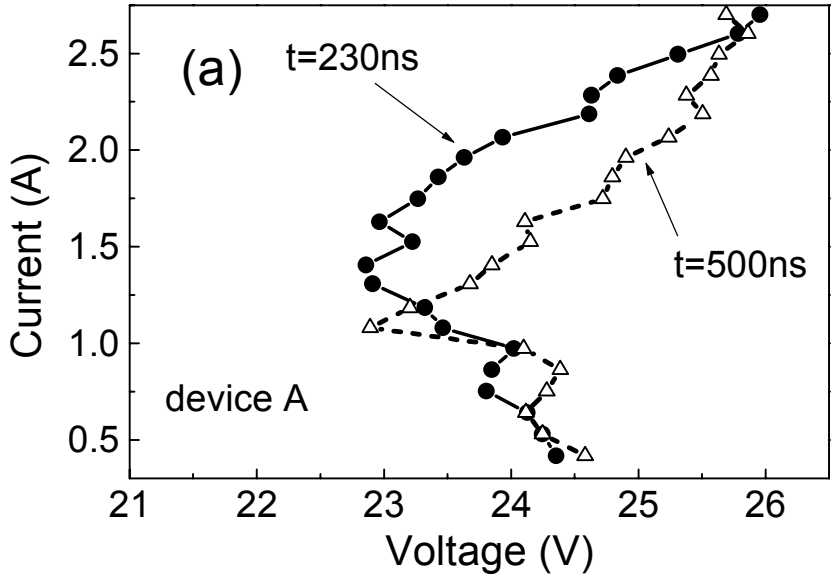

Fig. 1: IV characteristics of the ESD protection device recorded at two time instants. The NDR can be seen up to the stress current of 1.5A.

The studied protection devices are npn transistors with breakdown and sustaining voltages of 44 V and 24 V, respectively. The measured phase shift represents, in the first approximation, the 2D-lateral density of thermal energy in the silicon. The devices were stressed by rectangular current pulses using a DMOS switch (duration 170 – 500 ns). In order to study the PTP variation in the phase shift dynamics, ten to fifty ESD pulses were applied at each position of the device during a scanning procedure.

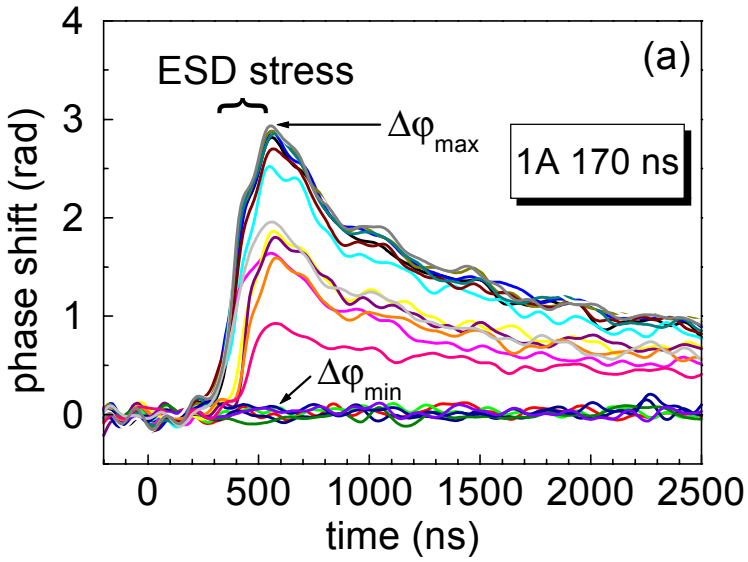

Fig. 2: Typical pulse to pulse variations in the phase evolution demonstrating the instabilities in the current flow from pulse to pulse.

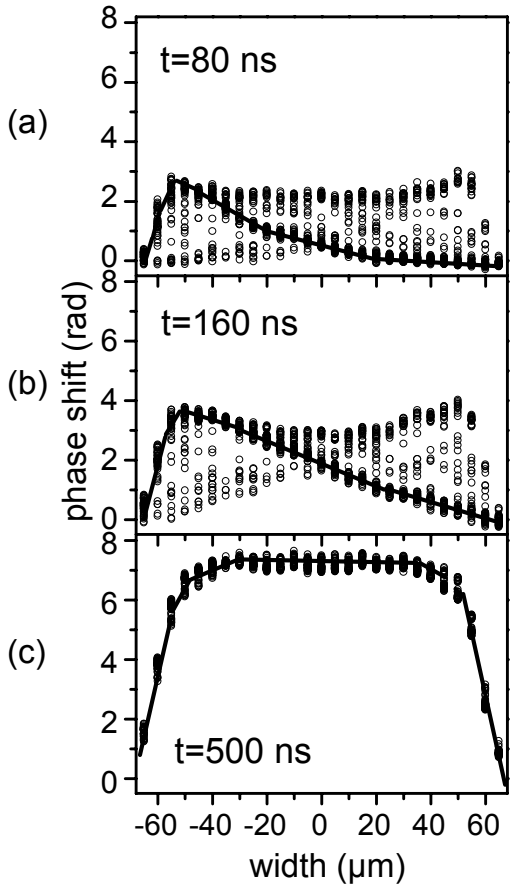

Fig. 3: Phase shift distribution along the device width at three time instants during the stress pulse of $I = 2$ A. At each position 50 phase shift values are given. The envelopes (solid lines) indicate the heat energy for the case when the device triggers in the left part.

Large PTP variations in the local phase shift value have been observed in the studied devices (see Fig. 1). They occur only in devices exhibiting a NDR region in the IV characteristics (see Fig. 2). The scattered data of phase shift along the device width can be grouped into two distributions forming envelopes, which are symmetrical to each other around the middle of the device (see Fig. 3). These envelopes represent two different possible thermal energy distributions (heated regions) during a stress pulse. It means that, from pulse to pulse, the device triggers either in one or another half of its width, forming thus a large current filament. The origin of the current filamentation is attributed to the NDR in the IV curves. The heated region increases with progressing time during the pulse. This indicates a spreading of the current distribution with time. The increase in the stress current magnitude has the same effect on the current spreading, leading to a current flow homogenization. The spreading effect is attributed to a negative feedback from the local temperature increase due to the self-heating effect. The increasing temperature causes a decrease in the impact ionization coefficient. In a result the current flow tends to move to a cooler region, leading to the current flow homogenization. The observed increase of the holding voltage with time (see. Fig. 1) supports this hypothesis. The current homogenization with time and stress current explains the high ESD robustness of this device (>8 kV Human Body model stress type).

Laser Interferometric Mapping of Smart Power ESD Protection Devices with Different Blocking Capabilities

S. Bychikhin, M. Litzenberger, P. Kamvar, D. Pogany, E. Gornik, G. Groos, M. Stecher

Protection against electrostatic discharge (ESD) in smart power technology devices has to take into account multiple bias source requirements. Consequently devices with different blocking capability, breakdown, and snapback voltages must be produced by simple layout variations. To optimize the design, physical failure analysis methods are usually used to get information on position of dominant hot spots causing the damage. The interferometric thermal and free carrier mapping techniques have a good potential to extract such information. In this contribution we investigate by this method the position of hot spots in two types of smart power ESD protection devices which block in one or in both polarities.

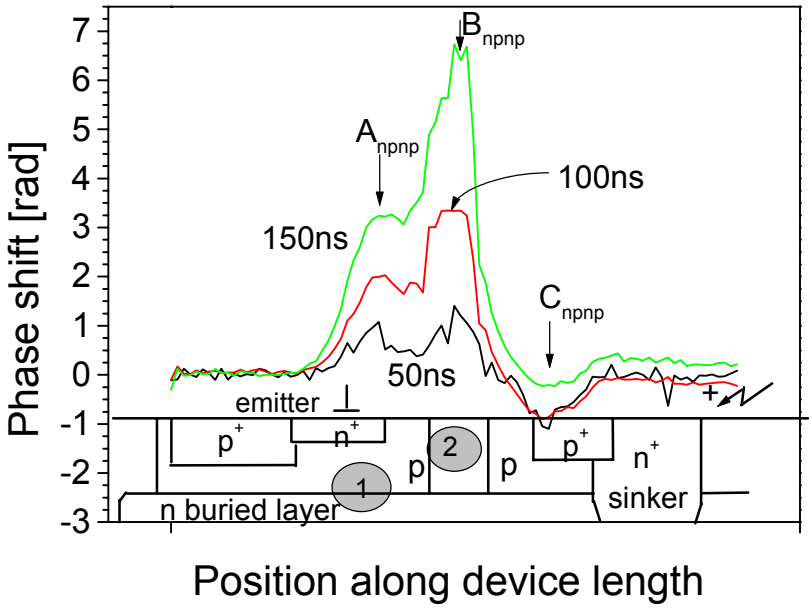

Fig. 1: Phase shift distributions along the length of the npnp structure at stress conditions 3.8 A, 150 ns and anti-serial device.

The thermal energy and free carrier distribution is studied using the measurements of temperature- and free carrier-induced optical phase shift. The phase shift distribution measurements in both devices exhibits two maxima (see Figs.1 and 2). The A peaks are related with heat source in the vertical npn that is marked as gray regions 1 in Fig.1 and 1, 3 in Fig. 2. The B peaks are due to a lateral current flow in the lateral pnp transistor

(marked as a gray region 2 in Figs.1 and 2). The negative phase shift C is attributed to plasma-optical effect due to carrier injection.

A failure analysis has been performed on the devices. An ESD damage in the npnp structure could not be observed for stress currents lower than 10 A (150 ns duration). The threshold for the defect creation in the anti-serial devices is in the 5 – 8 A range (for 150 ns pulses), depending on the stress polarity. This damage was established as a degradation of the contact metallization in the emitter region.

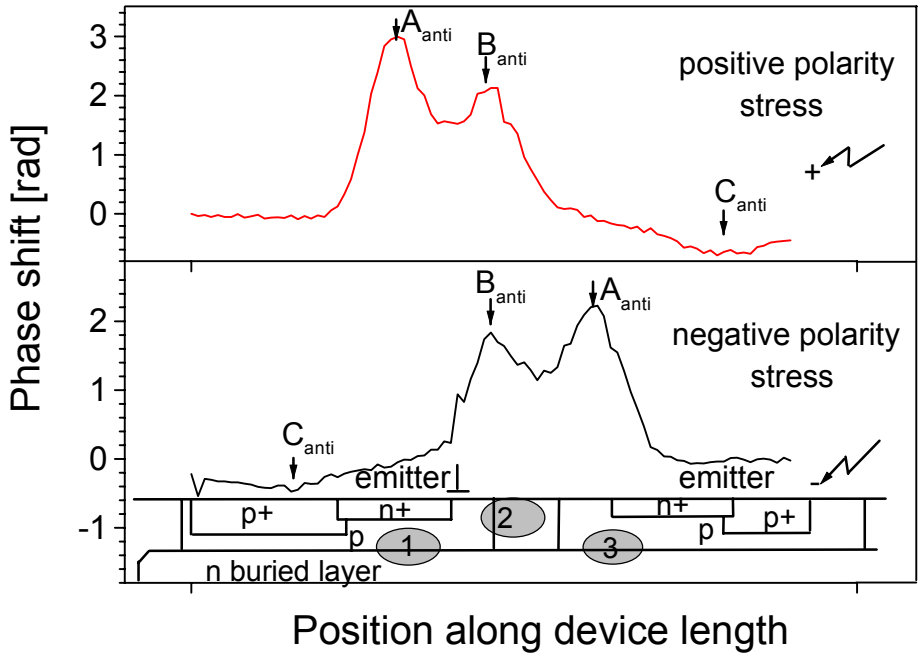

Fig. 2: Phase shift distributions along the length of the npnp structure at stress ±2 A, 150 ns.

The different ESD ruggedness of the two structures is attributed to different positions of the dominant hot spot. In the npnp device, the dominant hot spot is located under the LOCOS insulation. SiO_2 oxide or the Si/SiO_2 interface is known not to be very sensitive to thermal stress. In the anti-serial device, the dominant hot spot is located under the emitter, close to the contact metallization which is vulnerable to thermal damage.

An Optical Setup for Investigation of Internal Device Behavior Under CDM-Like ESD Stress

V. Dubec, S. Bychikhin, M. Litzenberger, D. Pogany, E. Gornik, K. Esmark, W. Stadler

Due to the increasing degree of automation in the integrated circuit production, electrostatic discharge (ESD) protection against the charge device model (CDM) stress becomes more and more important compared to the standard human body (HBM) stress. Backside laser interferometry is a unique and powerful tool to investigate internal device behavior under ESD stress. In the previous studies using the heterodyne setup, the duration of the high current stress was 100 ns or more. The time resolution of the heterodyne setup (about 3 ns) cannot be improved due to complicated optics. Therefore for investigation of CDM-like events occurring in the 1 – 10 ns scale a new Michelson-like interferometer was built.

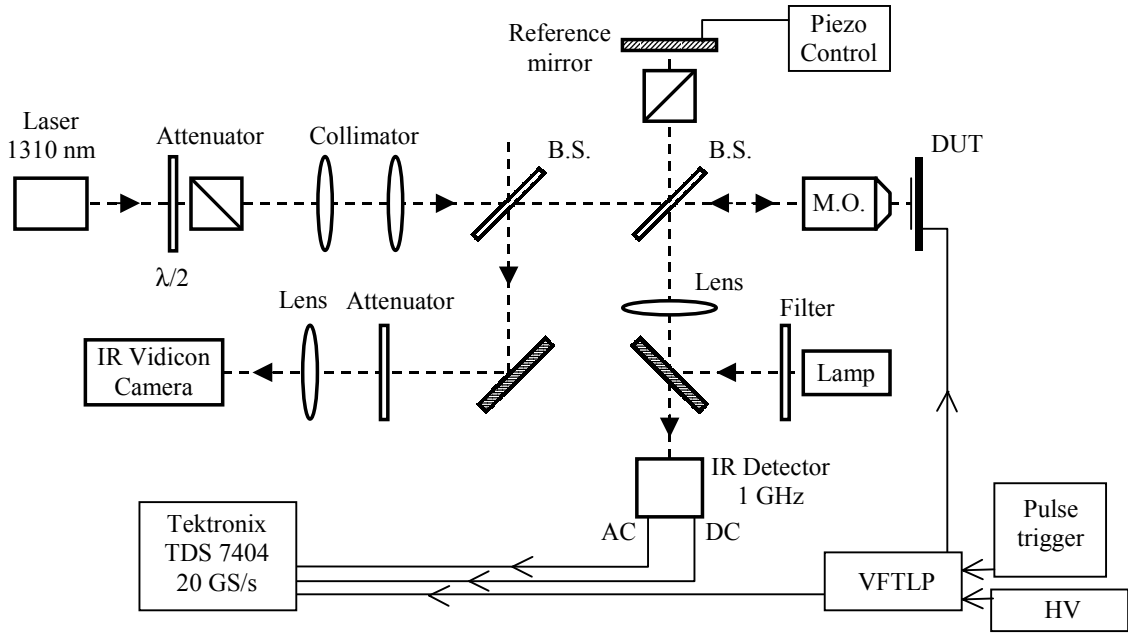

Fig. 1: Simplified scheme of the setup.

The scheme of the optical setup is depicted in Fig. 1. A DFB laser diode with the wavelength $\lambda = 1.3$ μm is used as a source of coherent light. The beam is collimated and then split by a beamsplitter into the probe and reference beams. The probe beam is focused by a microscope objective (M.O.) to the backside of the investigated device (DUT). The laser spot size of approx. 2 μm defines the space resolution. The beam is then reflected from the device surface, passes the same way back and reflects from the beamsplitter to the detector. The reference beam is reflected from a mirror mounted on a piezo mirror-

shifter. The intensity of the reference and probe beams can be controlled independently. Both beams are focused to the detector to get an interference signal. The signal from the detector (400 ps risetime) is recorded by a high sample rate oscilloscope (Tektronix TDS 7404). For the positioning of the beam on the device an IR vidicon camera is used. The stress was performed by a very fast transmission line pulser (VF-TLP) providing a CDM-like stress. The current and voltage on the device were calculated from the calibrated incident and reflected stress voltage waveform. The measurements are performed in an RF-shielded environment to reduce the pick-up of radiated noise from the fast-rising high-current pulses. The optical response was carefully time-aligned with the electrical stress pulse, taking into account all electrical and optical delays.

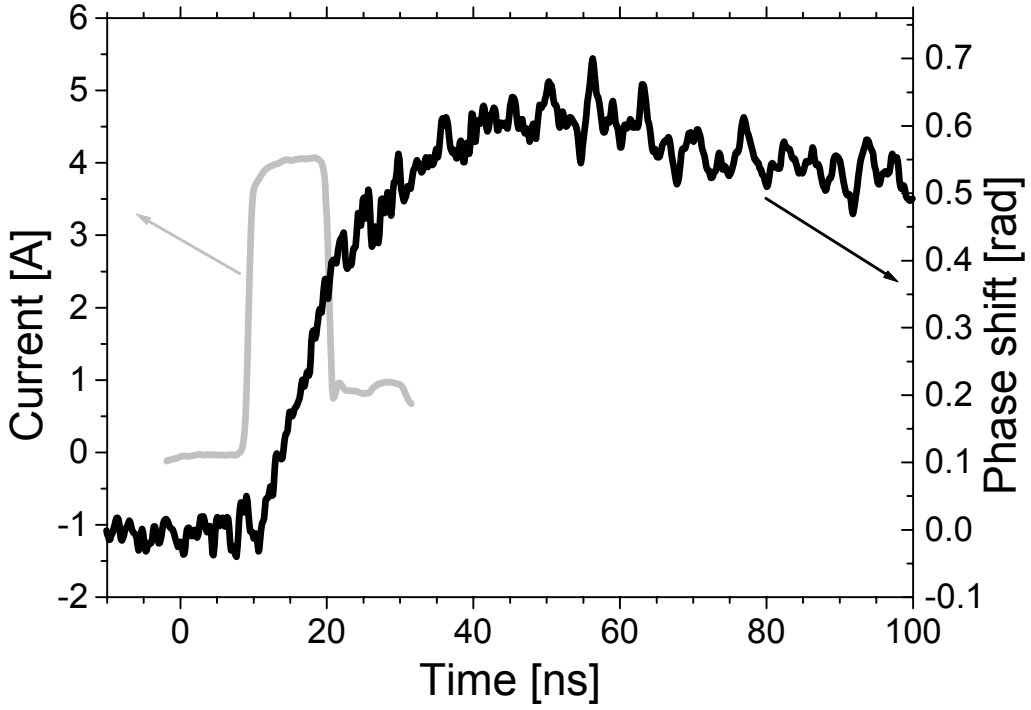

Fig. 2: Phase shift at a single point in the CMOS structure and corresponding current pulse. The curves are 20-times averaged.

The studied CMOS ESD protection devices are grounded gate (gg) NFETs of 0.35 µm technology with different gate to drain contact and gate to source contact spacings. Current pulses of 10 ns length and 4 A amplitude were applied, see Fig. 2. The current through the device causes a heating in the drain region. The optical signal shows a fast rise with a delayed maximum after the end of the pulse. The dynamics of the signal during the stress pulse reflects well the thermal energy dynamics. The delay is caused by the heat transfer effect as the probe laser beam is laterally shifted some 2 µm away from the position of the maximal heat dissipation. The setup is sufficiently sensitive to record phase shift related to a single stress event. This is important for the investigation of possible trigger instabilities. The method is useful for the verification of the results of device and circuit simulation models in the CDM time domain.

Ultrathin Zirconium Dioxide for Future MOS Technology

S. Harasek, B. Basnar, J. Smoliner, E. Bertagnolli

Recently ZrO_2 attracted much attention as a possible high-k gate dielectric in micro-electronic metal-oxide-semiconductor (MOS) devices, promising to overcome the tunneling limits of SiO_2 and thus allowing further reduction of device dimensions [1]. An effective dielectric constant of thin and ultrathin films in the range of k = 18, a wide band-gap of more than 5 eV, favorable band mismatch to silicon and finally high thermodynamic stability on silicon led to increasing interest in the growth and electrical characterization of ZrO_2 thin films. We focus our research activities in the high-k field on the deposition and integration of ZrO_2 in MOS technology using low-temperature processes. This takes the inevitable need for continual reduction of the thermal budget during processing into consideration. The deposition process utilizes MOCVD (Metal Organic Chemical Vapor Deposition) from tetrakistrifluoro-acetylacetonate zirconium as precursor followed by a post-deposition annealing step. Overall goal is to avoid temperatures above 650 °C in the gate insulator preparation while taking full advantage of the favorable properties of ZrO_2.

The outlined approach interlinks the two promising research topics high-k materials and MOCVD in the field of semiconductor technology, opening up an entirely new area of application.

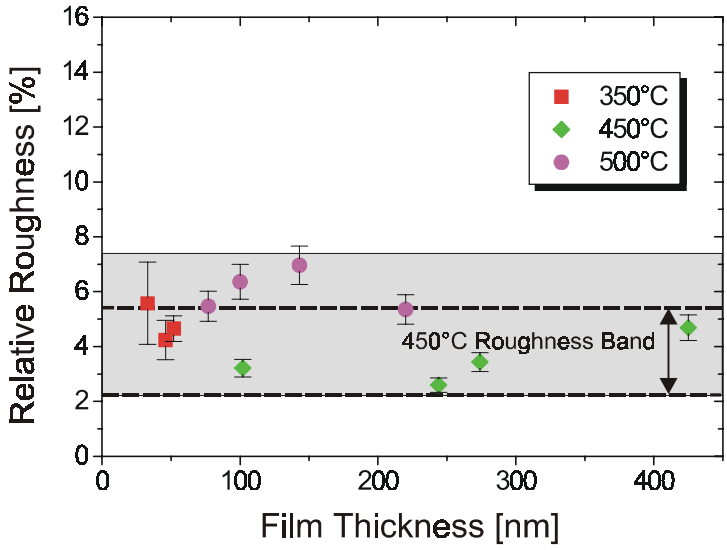

Fig. 1: Relative surface roughness of ZrO_2 thin films.

Morphological analysis using AFM and REM showed the deposited films to be polycrystalline with a relative roughness between 2 and 5% (Fig. 1). Moreover it was shown that the relative roughness is largely independent of the absolute film thickness [2]. The

chemical composition of the deposited layers was examined by Auger-electron spectroscopy (Fig. 2). Besides the elements zirconium and oxygen also the presence of carbon is unveiled, while no fluorine contamination is observed. The carbon content can be reduced to the limit of detection by spike-annealing to temperatures between 650 and 850 °C. This thermal treatment results in an almost stoichiometric composition of the thin film.

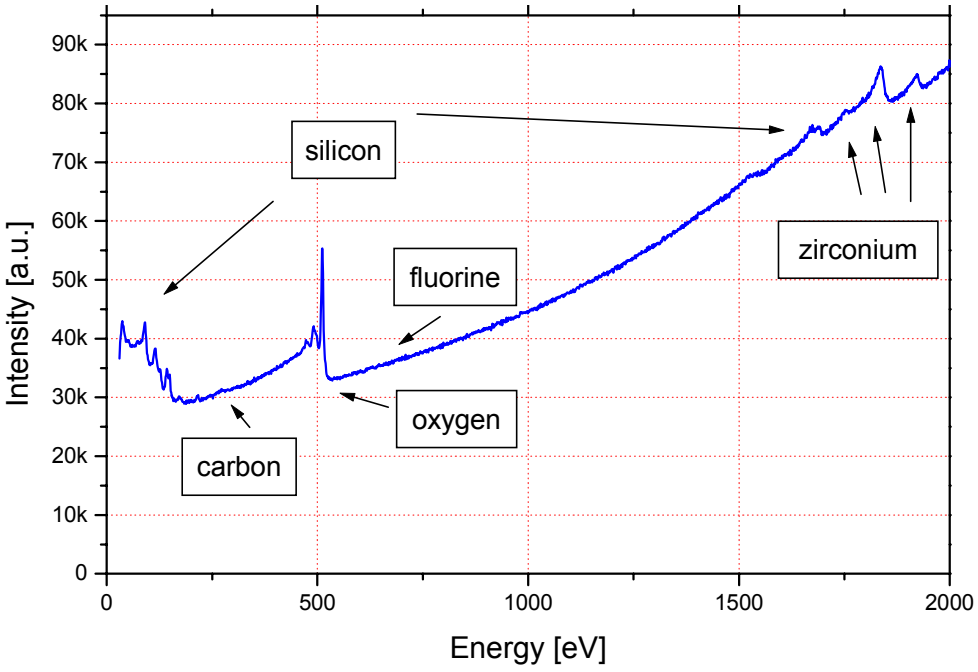

Fig. 2: Auger spectrum of a MOCVD ZrO_2 thin film.

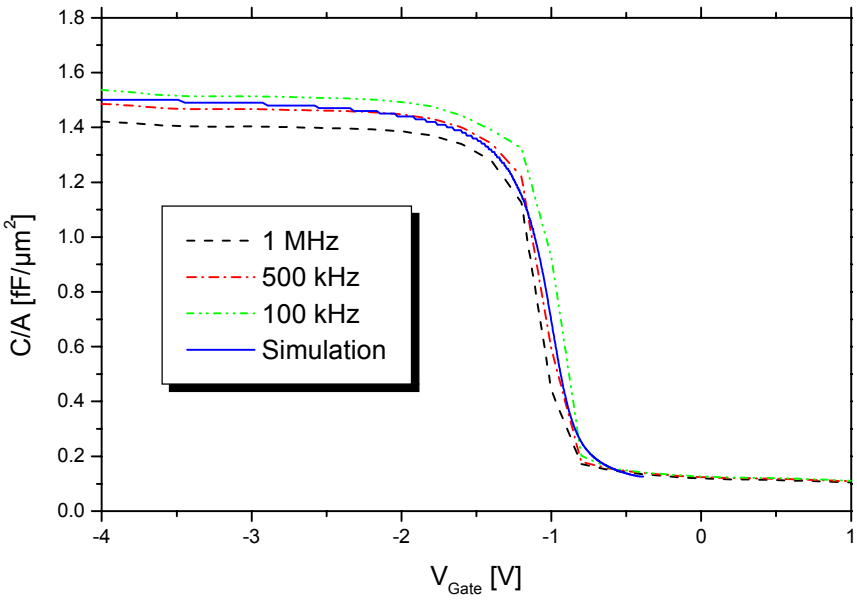

Fig. 3: Capacitance-voltage curve of a ZrO2 MOSCAP.

Electrical characterization of the layers is accomplished employing capacitance-voltage and current-voltage measurements on MOSCAP structures. EOT of the examined films reached down to about 3 nm. Fig. 3 gives an example of the achieved capacitance-voltage curves. The striking agreement between simulation and experimental results indicates a low interface trap density as well as low volume charges. The promising characteristics described are obtained by low-temperature processing not exceeding 650 °C.

References

[1] "*International Technology Roadmap for Semiconductors*", SIA, San Jose 1999

[2] S. Harasek, H.D. Wanzenboeck, B. Basnar, J. Smoliner, J. Brenner, H. Stoeri, E. Gornik, and E. Bertagnolli; "*MOCVD Growth and Nanoscale Characterization of Zirconium Oxide Thin Films*", submitted to *Thin Solid Films*

Molecular Dynamic Simulations of Ion Induced Damage in Silicon

G. Otto, G. Hobler

Molecular dynamic simulations are performed by us to aid binary collisions model development of both simple defects and amorphous pockets and for a quantitative comparison with RBS/C measurements.

The molecular dynamics simulations are done with the program MDSWV, which has been provided by Konrad Gärtner from the University of Jena. It is based on the Stillinger-Weber potential and uses the Verlet algorithm for time integration with an adaptive step. An atom in the center of the MD cell has been kicked in a random direction with an energy from 5 to 80 eV. The final state of the MD cell has been compared with the ideal lattice and the displaced atoms have been examined.

The molecular dynamic cell consists of $10 \times 10 \times 10$ unit cells (8000 atoms). Periodic boundary conditions in x and y directions and a fixed bottom and top layer in z-direction have been chosen. The temperature was set to 300 K. The simulations lasted approximately 2.5 ps. After about 1 ps there was no significant change in the final configuration of the displaced atoms

To identify a displaced atom the following criterion has been applied: An atom is considered to be displaced if the probability that its deviation is caused by the lattice vibration is under 10^{-6} (assuming a Gaussian distribution around the ideal lattice site). Calculations yield that for a temperature of 300 K an atom is displaced if it has a distance above 0.44 Å from the ideal lattice site.

To separate interstitials, vacancies, bond, and other defects from atoms which are displaced from their lattice site by the forces of the neighboring defect, another criterion has been applied. It is based on spheres centered on ideal lattice sites defined by the undisturbed lattice. If the sphere contains no atoms, the lattice position is labeled a vacancy. An atom that has no free lattice site in the sphere centered at the atom position (i.e. there are no lattice sites in the sphere or only lattice sites that are occupied by nearer atoms) is labeled an interstitial. The radius of the sphere is set equal to half the next neighbor distance.

In the observed energy range mainly Frenkel pairs, bond defects and di-interstials could be found, also several clusters with three interstitials (about 3% of the number of the Frenkel pairs). Greater amorphous pockets could not be created in this energy range (see Fig. 1). Clusters with more than two interstitials are very seldom and therefore are not included into the statistics. Additionally it can be seen that the defect distribution is much less than those of the Kinchin-Pease approach.

The interstitials have been investigated with respect to their structure. 90% of the generated Frenkel pairs are split-interstitials. The rest are tetrahedral interstitials.

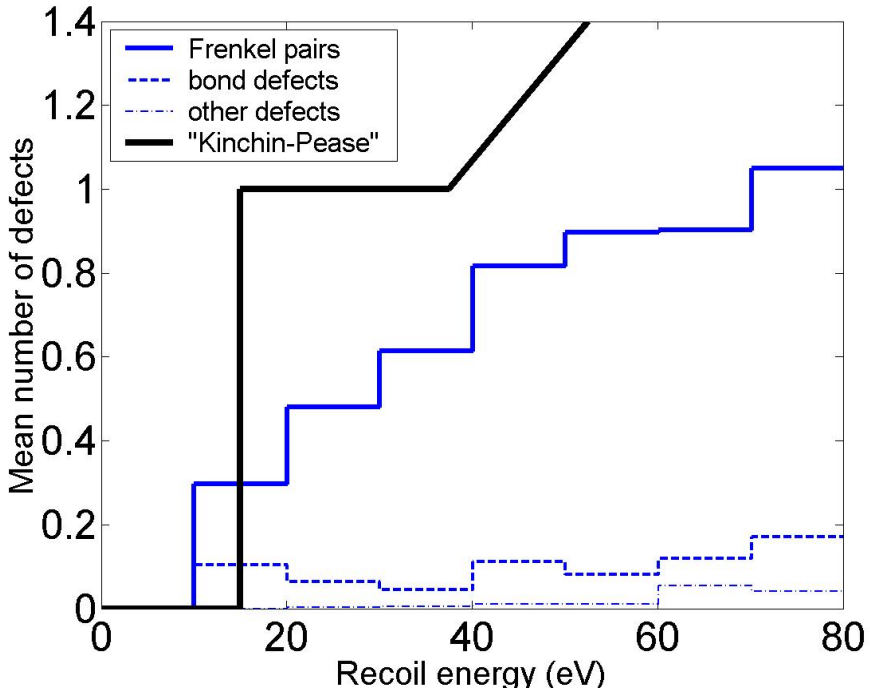

Fig. 1: Mean number of Frenkel pairs and other effects per recoil event and “the modified Kinchin-Pease” model.

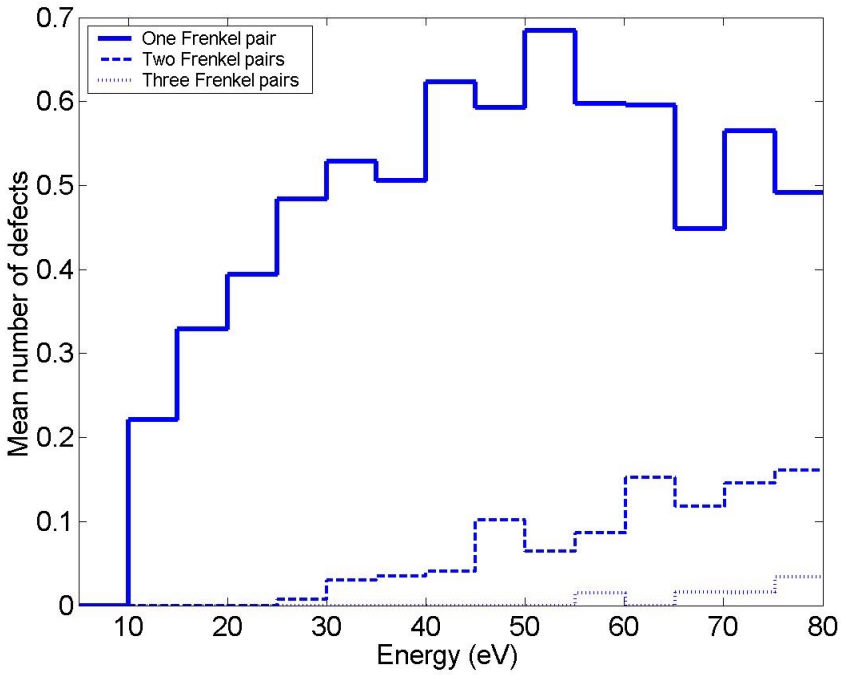

Fig. 2: Probability that 1, 2, or 3 Frenkel pairs are generated in a recoil event.

Figure 2 shows that in most cases exactly one Frenkel pair is generated. But at higher energies the proportion of the cases in which more than one Frenkel pair is generated

increases. That in this energy range most Frenkel pairs have an I-V separation below 9.2 Å is shown in Fig. 3.

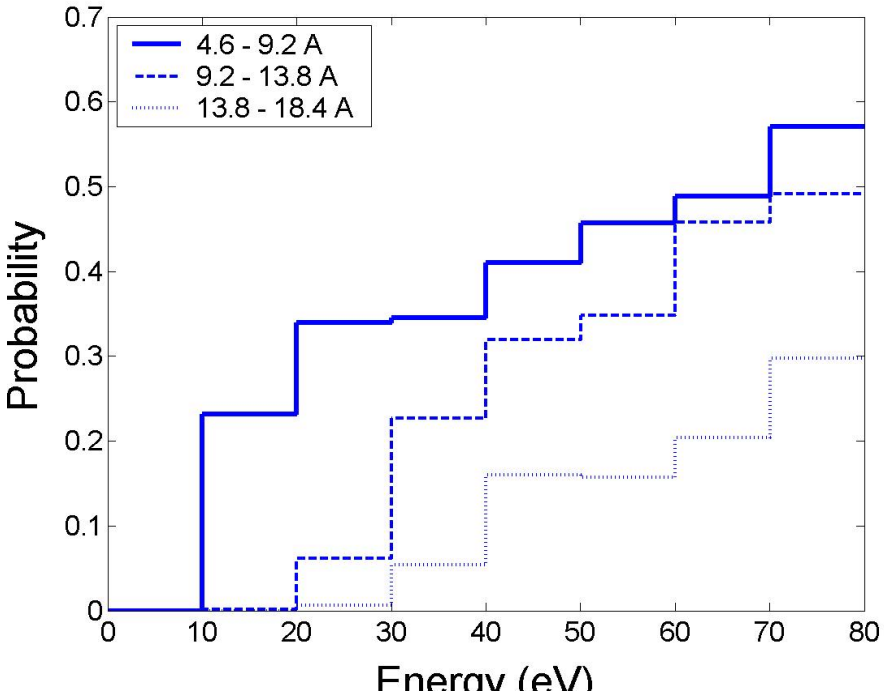

Fig. 3: Probability that a Frenkel pair with distances between I and V in the given ranges is generated in a recoil event.

Fabrication Technology for Sub-100 nm Semiconductor Devices

H.D. Wanzenboeck

For rapid prototyping of modern sub-100 nm devices a method for the direct deposition of nanostructures of material was developed This direct-write lithography is a maskless technology and requires only a single process step. By local deposition of silicon oxide and tungsten rewiring of chips and reverse engineering becomes feasible. This position-controlled local fabrication of sub-µm dielectric structures opens a versatile alternative for backend processing. Chemical vapor deposition of silicon dioxide induced by a focused ion beam was used to obtain material deposition confined to µm and sub-µm dimensions. Using metal-insulator-metal test vehicles the deposition rate and insulating properties of obtained materials were investigated. Dielectric breakdown of thin layers is correlated to impurities in the deposited material. Material properties appear to respond sensitively towards a change of process parameters such as the composition of the precursor gas. With an appropriate process control this method can provide interconnect and interline dielectrics for advanced rapid prototyping and multilevel rewiring of integrated circuits.

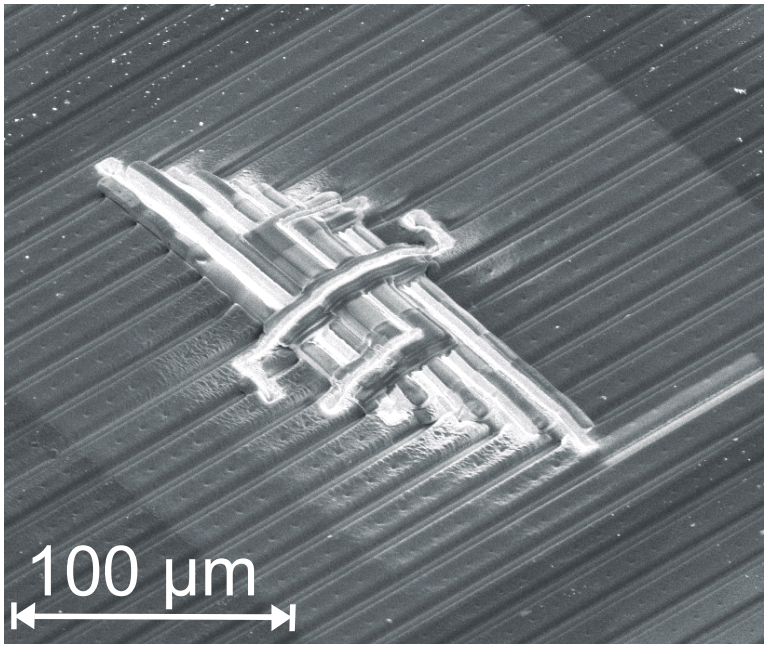

Fig. 1: Typical lines of an interconnect layer with FIB processed multilevel rewiring.

A research topic focusing on industrial fabrication technology of semiconductor devices is the development of a repair method for photomasks. Phase shift masks (PSM) are an enabling technology in lithographic fabrication of modern integrated circuits (IC) with a feature size below 250 nm. Phase shift technology allows to obtain a small structure size

remaining under the wavelength of the light source used for the lithographic exposure. Alternating aperture phase shift masks consist of a flat reflective chromium mask and a 3-dimensional structured quartz substrate. The production of phase shift masks is cost intensive and the yield is low due to defects in the quartz substrate or the chromium layer. Focused Ion Beam (FIB) technology offers a versatile repair method allowing a locally confined deposition of material utilizing chemical vapor deposition (CVD) initiated within the scanned area.

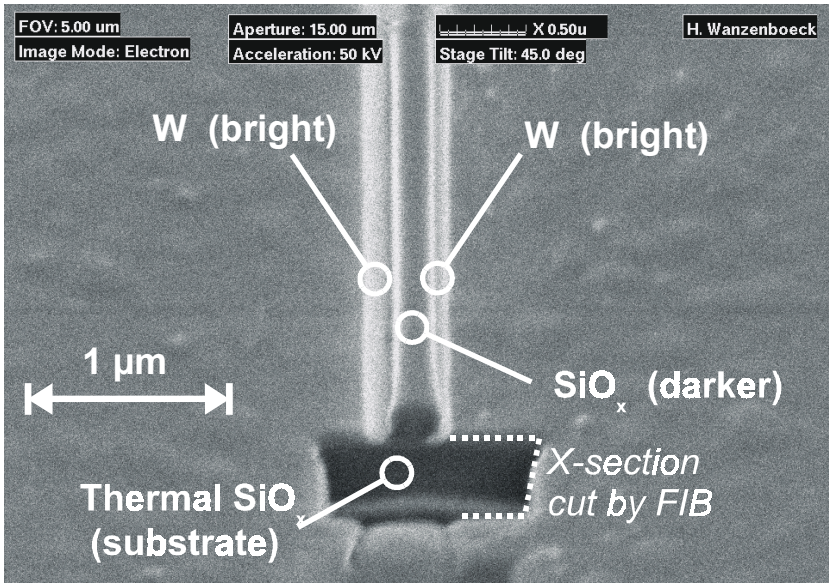

Fig. 2: FIB deposited structure showing two bright W wires (120 nm width) and a darker silicon oxide line (200 nm wide) in the middle. The sample is 45° tilted for this image. A hole is milled into the substrate displaying the cross-section of the deposited structures.

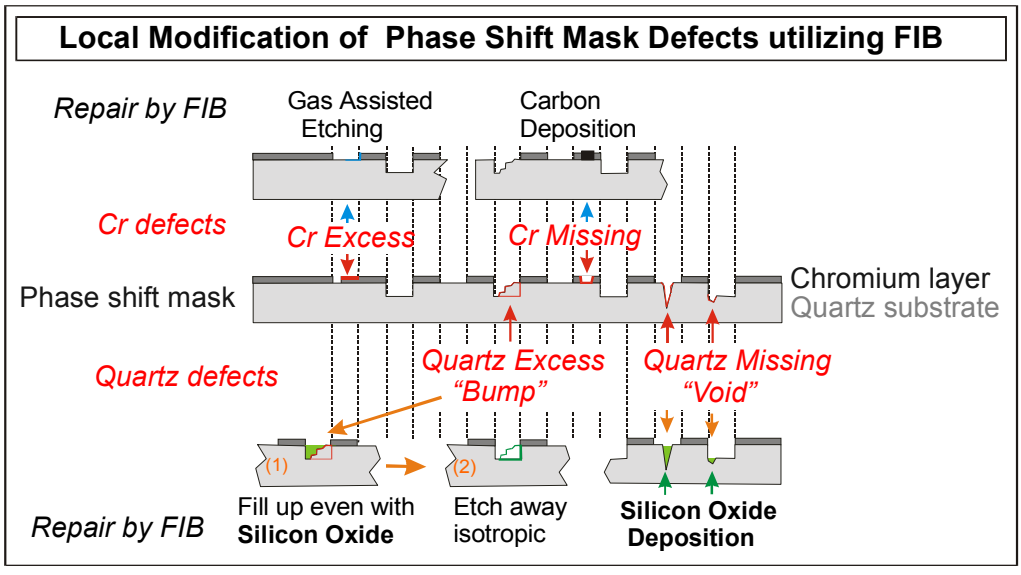

Fig. 3: Schematic illustration of different defect types of alternating aperture phase shift masks and corresponding repair strategies.

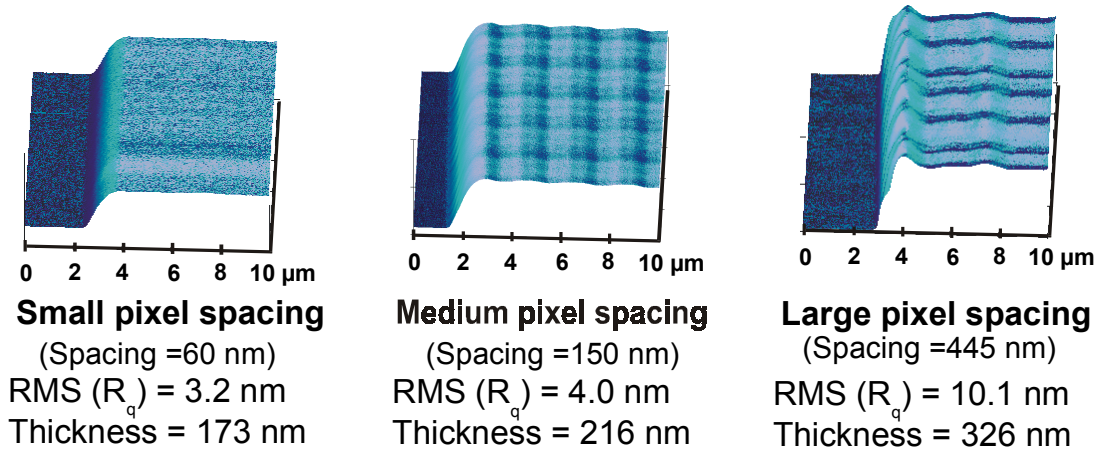

Fig. 4: Surface topology of silicon oxide deposited by FIB was imaged by AFM. The same total ion dose and the same gas composition was used. The varying pixel spacing resulted in a different surface roughness and geometry (image 10 x 10 µm).

The proposed repair strategy for quartz defects utilizes the local deposition of CVD silicon oxide as this material is most similar to the quartz of the original photomask. Silicon oxide structures down to 200 nm can be deposited with this method. The chemical composition of the deposited material was found to vary with the process parameters. The surface roughness and the potential of this process for phase shift mask repair was investigated.

Evolution of Tungsten Film Deposition Induced by Focused Ion Beam

H. Langfischer

Direct write metallization is an important approach for circuit modification and prototyping. We investigate the evolution of the chemical vapor deposition of tungsten induced by a 50 keV focused Ga^+ ion beam. Time resolved imaging in combination with atomic force microscopy reveals that chemical vapor deposition of tungsten by focused ion beam proceeds via two clearly distinguishable regimes of layer growth. Deposition starts with the nucleation of nanoscale tungsten deposits scattered over the substrate surface. Despite the local impact of the ion beam no correlation of the nucleation sites with the scan path of the beam can be found. The nanoscale tungsten particles preserve their positions and typical shapes during further deposition. Only after merging the particles to a contiguous tungsten layer, the second regime of growth characterized by deposition of tungsten on a tungsten surface sets on. In this regime the deposition process is determined by the total ion dose and the average current density the sample was subjected to. Deposition yields up to 3.5 atoms per incident gallium ion are achieved. The layer quality is determined by Auger analysis, showing the fractions of Ga and C in the W layer.

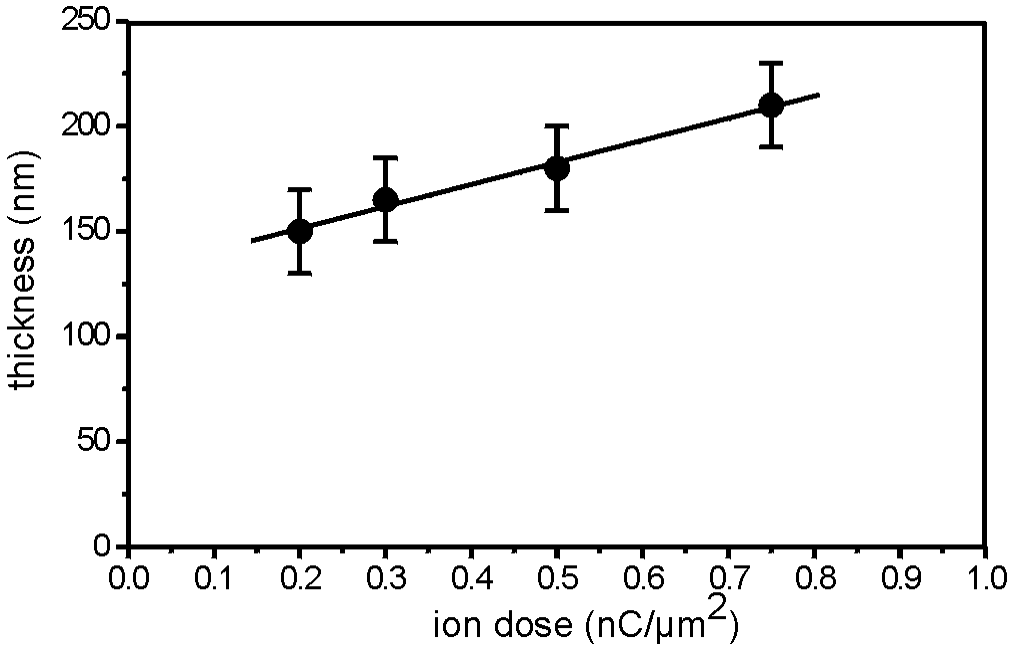

Fig. 1: Tungsten layer thickness versus total ion dose. The solid line represents a linear fit to the data.

Depth profiling by secondary ion mass spectra showed the depth profiles of these constituents and confirmed the existence of a 50 – 100 nm thick transition zone between the tungsten layer and the substrate. Electrical sheet resistances of the metal layer of

200 μΩcm and current densities up to 3.5×10^6 A/cm^2 are measured by means of van der Pauw test structures. In order to give a concise description of the experimental findings the data were interpreted utilizing an analytic model mainly incorporating precursor gas coverage, precursor gas transformation cross section, and ion induced sputtering. The critical ion current density where ion sputtering exceeds deposition was identified by the model. Because the model shows excellent agreement with the measurement it should be suitable for further survey concerning focused ion beam process development.

Ion beam induced deposition occurs if the adsorbed hexacarbonyl molecules are decomposed during ion beam exposure. After a contiguous tungsten layer formation, the deposition process is characterized by homological growth of tungsten on tungsten and the thickness of deposited metal correlates with the total ion dose like shown in Fig. 1. The analytic model used to describe the deposition kinetics is based on differential rate equations describing the precursor gas kinetics and its coverage of the sample surface. This equations rely on the following parameters: molecular precursor gas flux Φ (cm^{-2} s^{-1}), density of surface sites for precursor gas adsorption n_0 (cm^{-2}), precursor transformation cross section σ (cm^2), the atomic sputter yield Y_S, and average ion current density J (cm^{-2} s^{-1}). In this case the average ion current density J is defined as the number of impinging ions per cm^2 per second and related to j simply by $J = j/e$, with e being the unit charge. For the steady state condition the resulting expression for the atomic deposition yield is

$$Y_A = \frac{\sigma n_0 \left(\Phi/J - Y_S\right)}{\sigma n_0 + \Phi/J}. \qquad (1)$$

In Fig. 2 the atomic deposition yield Y_A determined by experiments is plotted versus the average ion current density. The negative yield values correspond to conditions where the sputter effect of the ions exceeds the ion induced deposition.

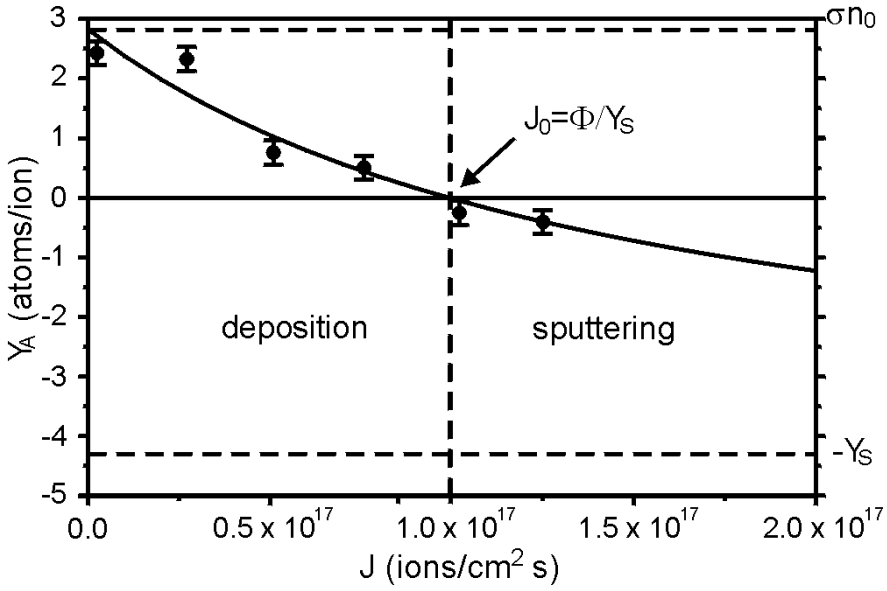

Fig. 2: Atomic deposition yield of tungsten hexacarbonyl under ion exposure as a function of the average ion current density. The solid line represents a fit due to the analytic model.

The solid line represents a fit of eq. (1) to the data. This expression contains three independent parameters: Φ, σn_0, and Y_S. The first two where extracted from a least square fit to the data. Y_S was determined by an independent sputter experiment without any gas contribution. $-Y_S$ is the limit of Y_A for very high ion current densities. The value obtained for the molecular precursor gas flux Φ is in the order of magnitude of values found by Melngailis and coworkers from their FIB experiments. The extracted value for the dimensionless parameter σn_0 is the limit of eq. (1) when J reaches zero and can be interpreted as the asymptotic deposition yield at very low ion current densities. When J is increasing the yield is decreasing because of the depletion of precursor gas molecules due to an accelerated precursor conversion.

In addition, the model allows to calculate the critical value for the current density J_0, from where on sputtering exceeds deposition resulting in a negative atomic yield. Exactly at J_0 deposition and sputtering are in dynamic equilibrium.

Integrating Micro- and Nanoelectrodes Into Atomic Force Microscopy Cantilevers Using Focused Ion Beam Techniques

A. Lugstein, E. Bertagnolli, C. Krantz, B. Mizaikoff

The investigation and manipulation of surfaces at an atomic scale has been revolutionized by the introduction scanning probe microscopic (SPM) techniques. Complex analytical problems in material and life sciences demand complementary information on physical and chemical properties at the molecular level. Hence, combination of SPM techniques is the logical consequence.

Scanning electrochemical microscopy (SECM) uniquely provides *in-situ* electrochemical, chemical, and biochemical information on surfaces and interfaces. An ultramicroelectrode is scanned in the nearfield across the sample surface (solid or liquid). The surface properties of the substrate influence the electrochemical response of the ultramicroelectrode, providing information on the nature of the substrate. Due to the difficulty in positioning electrodes at the nanometer range, SECM offers limited lateral resolution compared to scanning tunneling (STM) and atomic force microscopy (AFM). In particular, the trend towards nanoelectrodes for enhanced spatial resolution and the use of micro/nanosensors as SECM tips demands innovative approaches for manufacturing and positioning the SECM probe.

The recent development of micro- and nanoelectrodes integrated into AFM cantilevers demonstrates a novel approach combining micro- and nanoelectrochemistry with AFM measurements. Frame- or ring-microelectrodes are integrated into standard AFM cantilevers by microfabrication techniques. Consequently, electrochemical processes can be imaged or induced at a nanoscale during simultaneous AFM measurements.

Chemical modification of the electrode surface with bioreceptors (e.g. enzymes) integrates (bio)sensing devices for enhanced molecular recognition and specificity.

This concept can be extended towards multifunctional scanning probes/sensors, combining e.g. SECM with AFM and scanning nearfield optical microscopy (SNOM) into a single tri-functional tip or integrating multiple electrode/sensor systems.

The production of SECM/AFM tips is entirely based on microfabrication processes. The main processing steps include deposition of the electrode material (60 – 100 nm) onto the cantilever surface by sputtering. In case of a conducting tip prior deposition of an insulation layer is required. Commonly used electrode materials include gold, platinum, and modified carbon. Subsequent insulation is achieved by chemical vapor deposition of silicon nitride, mixed silicon nitride/oxide or parylene.

Exposing the micro-/nanoelectrode in the required working distance to the sample surface is achieved by a 3-step focused ion beam (FIB) cutting/milling process. FIB is used to expose and shape the integrated electrode, and to control the working distance by remodeling of an insulating AFM tip.

In order to demonstrate full functionality, the featured integrated SECM-AFM tip was mounted in a standard atomic force microscope (Nanoscope III, Digital Instruments), equipped with a fluid cell. The whole instrument was located in a faraday cage and the electrochemical signal was detected by a bi-potentiostat (CH Instruments 832A). All images were obtained in the contact mode of the AFM.

As a model surface a porous poly-carbonate membrane with a thickness of 11 µm and an average pore size of 1 µm was coated with a layer of 50 nm gold on the bottom side.

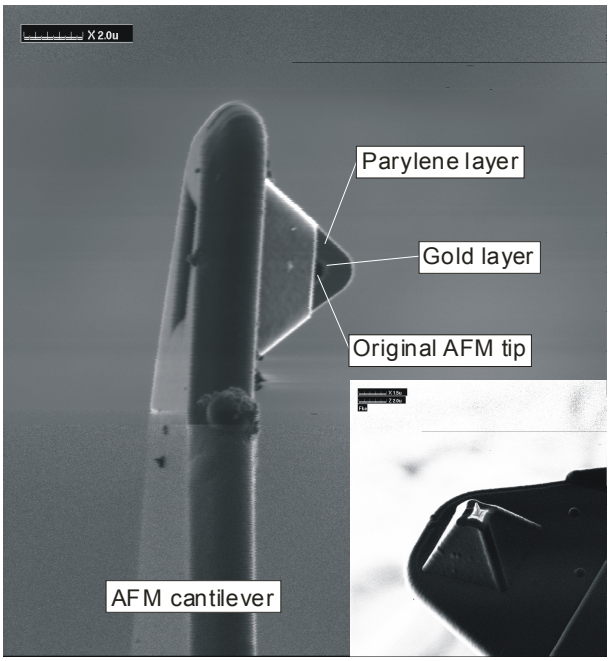

Fig. 1: FIB-image of an integrated SECM/AFM tip after first FIB cutting. Inset shows an integrated frame-nanoelectrode (bright square) with concentric re-shaped AFM-tip.

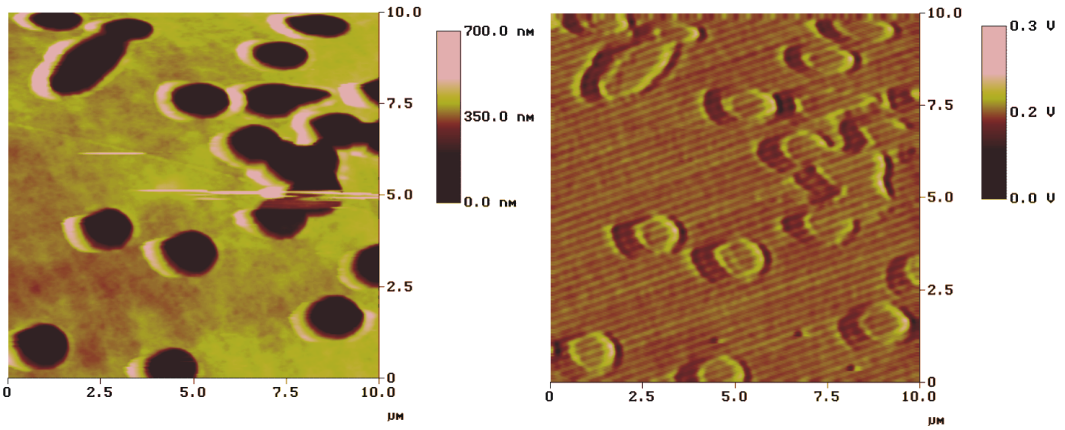

Fig. 2: Simultaneously recorded height and current images of a porous polymer membrane. (a) Top view of the AFM image and (b) top view of the simultaneously recorded current image. Redox mediator: 30 mM $Fe[CN]_6^{4-}$ in 0.5 M KCl electrolyte solution. Scan parameters: 2 Hz. Electrode edge length: 1 µm.

Impact of Focused Ion Beam Assisted Front End Processing on n-MOSFET Degradation

A. Lugstein, W. Brezna, E. Bertagnolli

Focused ion beam (FIB) systems are widely used for device modifications during the design debugging phase of integrated circuits (IC´s) development. Nevertheless, it appears necessary to further understand the interaction between the finely focused ion beam and IC´s to assure that these modifications do neither induce electrostatic discharge of the devices nor degradation due to FIB irradiation induced damage. We have investigated the focused ion beam interaction with n-MOSFET devices addressing irradiation damage related device degradation apart from charging effects.

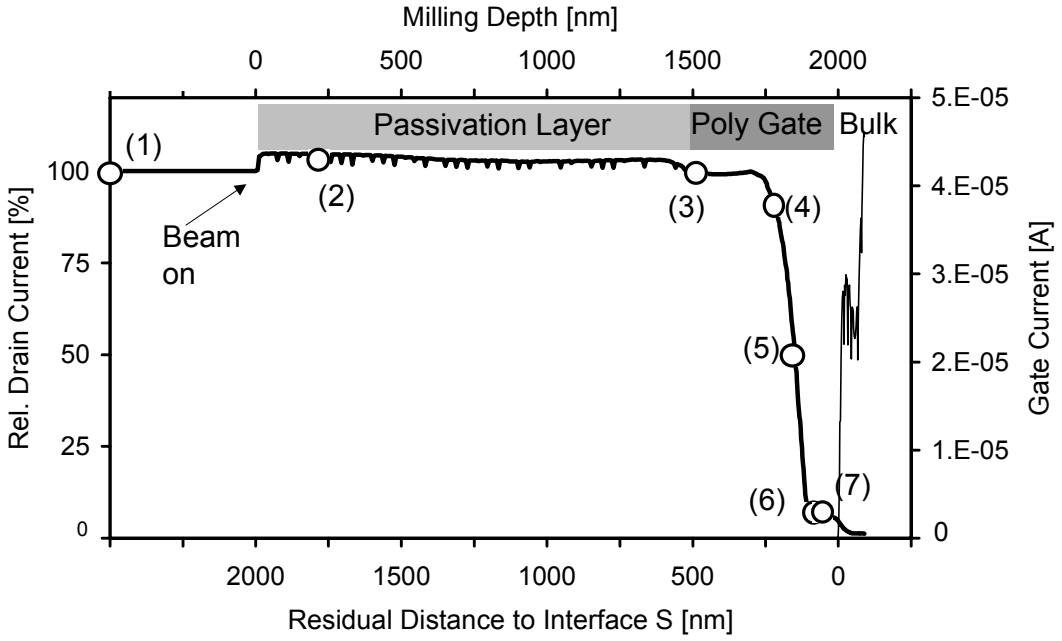

Fig. 1: Output and gate current of the n-MOS transistor vs. milling depth; bias conditions: $V_G = V_D = 3$ V; $V_S = V_{bulk} = 0$ V.

For the first time, monitoring of device parameters during ion beam exposure enables us to quantify the progressive nature of device degradation. By in-situ electrical sensing of the devices during focused ion beam milling, the impact on device parameters (I_{Dsat}, I_{Off}, and mobility) is studied. The FIB exposed MOSFET exhibits no damage related degradation as long as the milling is out of the reach of the active channel. Progressive degradation starts when long-range damage cascades extend into the channel region. The related damage can be attributed to mobility decrease in the channel region and has been quantified by a semi-empirical mobility model.

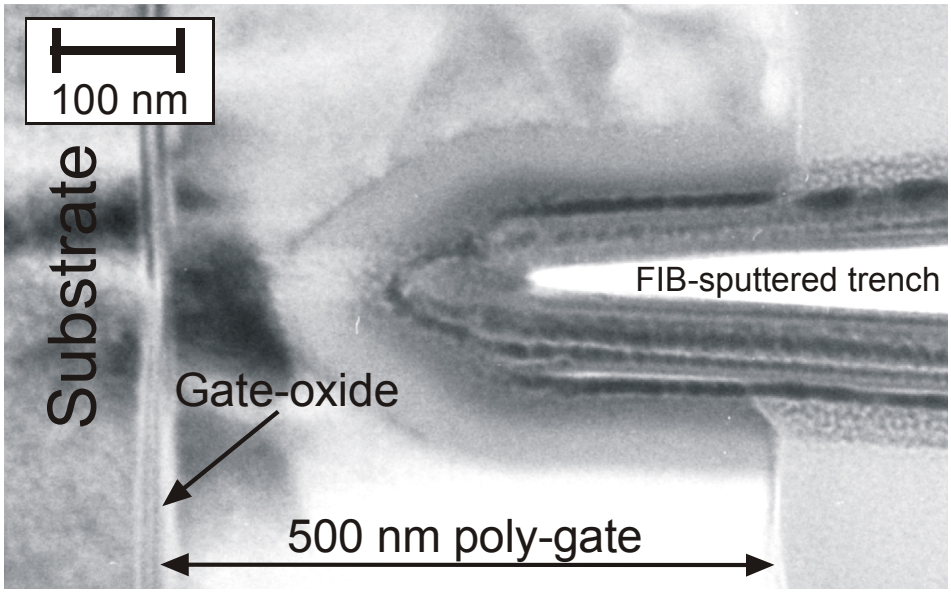

Fig. 2: Transmission electron microscope image of a transistor with a FIB milled trench reaching into the gate stack.

Microelectronics Technology — Cleanroom Linz

Micro- and Nanostructure Research: Cleanroom Linz

G. Bauer, H. Heinrich, H. Thim, G. Brunthaler

Institut für Halbleiter- und Festkörperphysik and Institut für Mikroelektronik,

Johannes Kepler Universität Linz, A-4040 Linz, Austria

The micro- and nanostructure research in the cleanrooms of the Institut für Halbleiter- und Festkörperphysik and the Institut für Mikroelektronik is supported by the Society for Microelectronics (GMe). In the field of Si/SiGe heterobipolar transistors, the incorporation of carbon was investigated in order to optimize the doping profiles. The material transport during process temperatures in nano-structured Si substrates was investigated as a relevant mechanism for future commercial devices. In the AlGaAs system, 'Hot electron injection field effect transistors' were modified and quantum point contacts were fabricated. In the field of optoelectronics, Er doped silicon light emitting diodes showed emission at 1.54 μm at room temperature. In the IV-VI system self-organized PbSe quantum dot superlattices were fabricated by molecular beam epitaxy. In the same material system, vertical cavities containing PbSe/PbEuTe superlattices with self-organized PbSe quantum dots, were investigated by transmission spectroscopy. A GaN MOCVD system was installed for the deposition of thin films and the in-situ optical characterization by ellipsometry. Si/SiGe cascade structures were characterized by x-ray reflectivity in order to assess their interface roughness and self-assembled SiGe nano-structures have been investigated by infra-red absorption and photoluminescence spectroscopy.

The funding of the activities in the two cleanrooms at the University of Linz which are jointly used by three groups is of vital importance for our micro- and nanostructure research activities. This basic funding allows for investigations which are made possible through additional funding coming from the FWF, the FFF, the European Commission, as well as through cooperation with industrial groups as listed in the report.

A short overview is given in the following on the achievements made in the year 2001 in the cleanrooms in Linz. The basic equipment which is available in these clean rooms allows for MBE growth of Si-based heterostructures, of II-VI and IV-VI heterostructures, for the deposition of ferromagnetic layers like Fe on II-VI compounds, as well as for MOCVD growth of III-V compounds like GaAs/GaAlAs and GaAs/GaInAs. The latest extension to that material systems happened with a European Project on the in-situ control of GaN deposition by MOCVD. Apart from in-situ and ex-situ structural characterization, lateral patterning is made possible through equipment like optical, holographic and electron beam lithography. Processing includes also facilities for the deposition on insulating as well as contact layers. A plasma deposition system for silicon nitrides was just installed in the last year. The transmission electron microscope, purchased one year earlier, is intensively used for the characterization of thin SiGeC layers.

The research efforts were concentrated on high frequency electronic and optoelectronic devices as described in the following.

Si-SiGe heterobipolar transistors are now widely introduced in the production for high speed bipolar and BiCMOS circuits, offering a great speed advantage over standard silicon technologies. In Linz steps towards the optimization of the doping and composition profiles for the SiGeC HBT technology were continued in collaboration with Austria Microsystems, Unterpremstätten. While it is well known that co-doping of the p-type SiGe base layer of an HBT with carbon can completely suppress transient enhanced diffusion of the boron dopants, little is known about the behavior of carbon. Because of the small solid solubility of C in Si and SiGe, its propensity to form complexes, and its diffusion behavior, which follows the same mechanism as boron, C contaminations are usually avoided in standard Si technology. We therefore studied the behavior of 0.2 - 1 at.% of substitutional C in Si and SiGe under annealing conditions. Fourier-transform infrared spectroscopy (FTIR) was employed to measure the intensity of the local vibration modes of substitutional C and of cubic SiC precipitates. We could follow SiC precipitate formation as a function of annealing temperature and time. We found that, as expected, C in Si forms cubic SiC precipitates in thermal equilibrium. However, this process is kinetically impeded and requires long annealing times at elevated temperatures.

With minimum device dimensions of commercial processes already below 100 nm, and with progress being made regarding self-organized growth schemes selective epitaxy and processing of nano-structured substrates at elevated temperatures become critical issues. During the in-situ thermal cleaning step of nano-structured Si substrates before MBE deposition we found a substantial amount of material transport on the surface. For example, wire structures of rectangular cross section are transformed into trapezoids with {311} facets after 5 min of annealing at 950 °C in vacuum. The same mechanism leads to the development of negative slopes on the flanks of SiO_2 wires, which are wetted by mobile surface Si atoms, and desorb after reacting to SiO. By systematically varying the annealing conditions and by cross-sectional transmission electron microscopy (TEM) we studied the kinetics of this phenomena. Especially the shape transformation of SiO_2 structures should allow the fabrication of self-aligned nano shadow masks.

A modified version of a GaAlAs ‘Hot Electron Injection Field Effect Transistor’ (HEIFET), utilizing the Gunn effect to enhance microwave performance, was developed. In the modified structure the ohmic source and drain contacts of a MESFET are both replaced by a combination of an ohmic contact and a Schottky contact. Due to improvements in the electron beam lithography system it was possible to reduce the length of the MESFET gate to values around 0.4 µm and the separation to values around 0.3 µm. The device operates up to a frequency of 45 GHz.

From two-dimensional AlGaAs structures quantum point contacts were fabricated by electron beam lithography in different techniques. Best electrical characteristics were achieved in split gate geometry. The resistance steps due to lateral quantization of the electron gas were observed. In addition conductance peaks in the high ohmic region due to Coulomb blockade of a random quantum dot appeared in the same samples.

Si:(Er,O) based light emitting diodes were developed and fabricated, emitting at room temperature in the breakdown regime at a wavelength of 1.54 µm. By adjusting the diode design we were able to increase the electroluminescence (EL) intensity by one order of magnitude. We also investigated codoping with hydrogen in order to increase the

luminescence. With this we achieved an increase of the luminescence intensity at temperatures below 150 K by a factor of five.

Self-organized PbSe quantum dot superlattices were fabricated by molecular beam epitaxy. Atomic force microscopy and high resolution x-ray diffraction studies of the ordering processes due to the dot interactions during epitaxial growth showed that well ordered dot superstructures with hexagonal as well as face centered cubic dot arrangements can be obtained. Also, the dot sizes and lateral spacings are found to be tunable by changes in the preset vertical superlattice periods. By inserting such superlattices into the cavity region of high finesse EuTe/PbEuTe microcavity structures optically stimulated mid-infrared vertical laser emission is obtained at wavelengths around 4 μm. Doped quantum dot superlattice structures were also fabricated for photocurrent measurements. These allow the characterization of the quantum dot energy levels. Furthermore, a new research project was started on the investigation of magnetic EuSe layers and superlattices. After optimization of the growth conditions several sample series were fabricated for magnetization and x-ray diffraction measurements. Another activity was centered around the investigation of strain relaxation mechanisms and dislocation formation in lattice-mismatched IV-VI heterostructures using in situ scanning tunneling microscopy. For the PbTe/PbSe (100) system, the formation of regular quasiperiodic nanoscale dislocation patterns were observed with periods down to 8 nm. These patterns could open new possibilities of fabricating novel types of self-organized nanostructures on the periodic strain fields induced by the dislocation grating.

The vertical cavities containing PbSe/PbEuTe superlattices with self-organized PbSe quantum dots, ordered in lateral as well as in vertical direction, were investigated also by transmission experiments. This allows to determine the absorption spectrum of the quantum dot superlattice by deducing it from the width of the resonator modes. The absorption from the quantum dots can be clearly distinguished from that of the wetting layer and the buffer layers. The absorption peak due to the quantum dots is only 8.7 meV broad, which clearly reflects the very high size homogeneity of the dot ensemble in our samples.

An MOCVD system was installed for the deposition of GaN. Additional sources for Al and In are also available for the fabrication of ternary nitrogen based compounds. As dopand sources we have Si for n-type and Mg for p-type. So we are able to grow single and multilayers of group III-nitrides together with the necessary doping profiles to fabricate blue light emitting diodes. However, the main task was to set up an in situ growth control. Therefore the growth reactor was specially designed to allow the attachment of an ellipsometer. The reactor chamber has three optical windows, which allow to measure reflectivity and spectral ellipsometry at an angle of 65°. With this attachment we can measure the growth rate and the layer composition during growth, which occurs at about 1000 °C in very pure hydrogen atmosphere. Post growth analysis of the GaAlN layers by SIMS and AES showed that the composition can be determined during growth with a precision of one percent.

Si/SiGe cascade structures, which show electroluminescence at about 10 μm were characterized by x-ray reflectivity in order to assess their interface roughness. This is of consequence for quantum well fluctuations and consequently for a broadening of the emission. By growing such structures at temperatures as low as 350 °C, the r.m.s. interface roughness can be kept below 0.3 nm, despite Ge contents as high as 45% in the wells.

However, such structures are highly metastable, annealing above 500 °C induces strain relaxation via misfit dislocation formation.

Optical characterization of self-assembled Si/SiGe quantum dots and wires by mid-infrared absorption and photocurrent spectroscopy and near-infrared photoluminescence have been performed. A comparison of the results of these experiments with calculations modeling the dependence of the optical response on the structural parameters of the nanostructures allows to estimate the alloy concentration and dimension of the nanostructures. The results show that the Ge concentration in the nanostructures is significantly lower than in the alloy indicating that significant alloying occurs during the overgrowth of the nanostructures even at moderate growth temperatures.

Project Information

Project Manager

ao.Prof. Dr. Gerhard Brunthaler

Institut für Halbleiter-und Festkörperphysik, Johannes Kepler Universität Linz, A-4040 Linz, Austria

Project Group

Last Name	First Name	Status	Remarks
Bauer	Günther	University professor	
Heinrich	Helmuth	University professor	
Jantsch	Wolfgang	University professor	
Schäffler	Friedrich	University professor	
Thim	Hartwig	University professor	
Brunthaler	Gerhard	Associate professor	
Diskus	Christian	Associate professor	
Helm	Manfred	Associate professor	
Krenn	Heinz	Associate professor	until January 31st
Palmetshofer	Leopold	Associate professor	
Springholz	Gunther	Associate professor	
Sitter	Helmut	Associate professor	
Bonanni	Alberta	Assistant professor	
Fromherz	Thomas	Assistant professor	
Heiss	Wolfgang	Assistant professor	
Kolmhofer	Erich	Assistant professor	
Lübke	Kurt	Assistant professor	
Stangl	Julian	Assistant professor	since March 1st
Binder	Fritz	Technician	
Bräuer	Stephan	Technician	since June 5th
Fuchs	Othmar	Technician	
Halilovic	Alma	Technician	since January 2nd
Haslgrübler	Klaus	Technician	since November 1st
Hinterreiter	Marion	Technician	until September 30th
Katzenmayer	Hans	Technician	
Rabeder	Klaus	Technician	until April 30 2001

Last Name	First Name	Status	Remarks
Wirtl	Elisabeth	Technician	½ paid by GME, until Oct. 31st
Hingerl	Kurt	Guest researcher	Austrian Academy of Sciences + Company Profactor, until June 30
Stepikhova	Margarita	Guest researcher	
Stifter	David	Guest researcher	Company Profactor
Zhong	Zhenyang	Post Doc	
Achleitner	Joachim	Ph.D. student	
Beyer	Harald	Ph.D. student	finished in 2001
Hesse	Anke	Ph.D. student	
Kocher	Gudrun	Ph.D. student	
Montaigne-R.	Alberto	Ph.D. student	
Mühlberger	Michael	Ph.D. student	
Prinz	Adrian	Ph.D. student	
Raab	Anneliese	Ph.D. student	
Roch	Tomas	Ph.D. student	
Sandersfeld	Nils	Ph.D. student	until May 31
Schmidegg	Klaus	Ph.D. student	
Schwarzl	Thomas	Ph.D. student	
Stangl	Julian	Ph.D. student	
Wiesauer	Karin	Ph.D. student	
Berer	Thomas	Diploma student	
Böberl	Michaela	Diploma student	
Griesser	Stefan	Diploma student	
Gruber	Daniel	Diploma student	
Lichtenberger	Herbert	Diploma student	
Pargfrieder	Stefan	Diploma student	
Pillwein	Georg	Diploma student	
Roither	Jürgen	Diploma student	
Schwinger	Wolfgang	Diploma student	
Simma	Matthias	Diploma student	

Publications in Reviewed Journals

Published:

1. A.Daniel, V. Holy, Y. Zhuang, T. Roch, J. Grenzer, Z. Bochnicek, G. Bauer: "*GID study of strains in Si due to patterned SiO_2*", J. Phys. D: Applied Physics 34, A197-A202 (2001).
2. A.Raab, G. Springholz: "*Oswald Ripening of Facetted Self-Assembled PbSe Quantum Dots during Annealing*", Phys. stat. sol. (b) 224, 509-513 (2001).

3. Andreev, H. Sitter, C.J. Brabec, P. Hinterdorfer, G. Springholz, N.S. Sariciftci: "*Self-assembled growth of highly ordered para-sexiphenyl thin films*", Synthetic Metals 121, 1379-1380 (2001).

4. C. Schelling, M. Mühlberger, G. Springholz, F. Schäffler: "*SiGe growth instabilities on vicinal Si(001) substrates: Kinetic vs. strain-induces effects*", Phys. Rev. B 64, 041301 (2001).

5. D. De Salvador, M. Tormen, M. Berti, A. V. Drigo, F. Romanato, F. Boscherini, J. Stangl, S. Zerlauth, G. Bauer, L. Colombo, S. Mobilio: "*Local lattice distortion in $Si_{1-x-y}Ge_xC_y$ epitaxial layers from x-ray absorption fine structure*", Phys. Rev. B 63, 045314 (2001).

6. D. Gruber, M. Mühlberger, F. Schäffler: "*Characterization of Si/$Si_{1-x-y}Ge_xC_y$ heterostructures for device applications*", In: Proceedings of the Seminar "GMe Forum 2001" , Vienna April 5-6, 2001, edited by K. Riedling, Gesellschaft für Mikroelektronik, Vienna 2001, p. 171.

7. D. Gruber, T. Fromherz, M. Mühlberger, C. Schelling, L. Palmetshofer, F. Schäffler: "*Characterization of Si/SiGeC heterostructures for device applications*", In: Proceedings of the Seminar "GMe Forum 2001" , Vienna April 5-6, 2001, edited by K. Riedling, Gesellschaft für Mikroelektronik, Vienna 2001, p. 79-82.

8. E. Thor, M. Mühlberger, L. Palmetshofer, and F. Schäffler: "*Deep-level transient spectroscopy of dislocation-related defects in epitaxial multilayer structures*", J. Appl.Phys. 90, 2252-2256 (2001).

9. F. Schäffler: "*Silicon-Germanium*", In: Properties of Advanced Semiconductor Materials, eds. M.E. Levinshtein, S.L. Rumyantsev, M.S. Shur, John Wiley & Sons, New York 2001, pp. 149-185.

10. G. Brunthaler, A. Prinz, G. Bauer, V.M. Pudalov: "*Exclusion of Quantum Coherence as the Origin of the 2D Metallic State in High-Mobility Silicon Inversion Layers*", Phys. Rev. Lett. 87, 096802 (2001).

11. G. Brunthaler, A. Prinz, G. Pillwein, G. Bauer, K. Brunner, G. Abstreiter, T. Dietl, V.M. Pudalov: "*Semiclassical origin of the 2D metallic state in high mobility Si-MOS and Si/SiGe structures*", Proc. 25th International Conference on the Physics of Semiconductors, Sept. 2000, Osaka, Japan, edited by N. Miura, T. Ando, Berlin Heidelberg New York, Springer 2001, p. 785-786.

12. G. Springholz, M. Pinczolits, G. Bauer, H.H. Kang, L. Salamanaca-Riba: "*Phase diagram of lateral and vertical ordering in self-organized PbSe quantum dot superlattice grown MBE*", J. Crystal Growth 227-228, 1126-1131 (2001).

13. G. Springholz, M. Pinczolits, V. Holy, P. Mayer, G. Bauer, H. Kang, L. Salamanca-Riba: "*Self-assembled molecular beam epitaxy of PbSe quantum dots*", Proceedings of the 6th International Symposium on Advanced Physical Fields: "Growth of Well-defined Nanostructures", Tsukuba, Japan, 6-9 March, 2001, edited by Nobuyuki Koguchi, National Research Institute for Metals, 2001, p. 97-102.

14. G. Springholz, M. Pinczolits, V. Holy, P. Mayer, G. Bauer, H.H. Kang, L. Salamanca-Riba: "*Controlling of lateral and vertical order in self-organized PbSe quantum dot superlattices*", Proc. 25th International Conference on the Physics of

Semiconductors, Sept. 2000, Osaka, Japan, edited by N. Miura, T. Ando, Berlin Heidelberg New York, Springer 2001, p. 355-358.

15. G. Springholz, M. Pinczolits, V. Holy, S. Zerlauth, I. Vavra, G. Bauer: "*Vertical and lateral ordering in self-organized quantum dot superlattices*", Physica E 9, 149-163 (2001).
16. G. Springholz, T. Schwarzl, W. Heiss, G. Bauer, M. Aigle, H. Pascher, I. Vavra: "*Midinfrared surface-emitting PbSe/PbEuTe quantum-dot lasers*", Appl. Phys. Lett. 79, 1225-1227 (2001).
17. G. Springholz, T. Schwarzl, W. Heiss, M. Aigle, H. Pascher: "*Molecular beam epitaxy of lead-salt-based vertical cavity surface emitting lasers for the 4-6 μm spectral region*", Journal of Crystal Growth 227-228, 722-728 (2001).
18. H. H. Kang, L. Salamanca-Riba, M. Pinczolits, G. Springholz, V. Holy, G. Bauer: "*TEM investigation of self-organized PbSe quantum dots as a function of space layer thickness and growth temperature*", Materials Science and Engineering B (Solid State Materials for Advanced Technology) B80, no.1-3, p.104-107 (2001).
19. J. Stangl, A. Daniel, V. Holy, T. Roch, G. Bauer, I. Kegel, T.H. Metzger, T. Wiebach, O.G. Schmidt, K. Eberl: "*Strain and composition distribution in free-standing SiGe islands from x-ray diffraction*", Appl. Phys. Lett. 79, 1474-1476 (2001).
20. J. Stangl, V. Holy, A. Daniel, T. Roch, G. Bauer, T. H. Metzger, J. Zhu, K. Brunner, G. Abstreiter: "*Shape and size of buried SiGe islands*", Proc. 25th International Conference on the Physics of Semiconductors, Sept. 2000, Osaka, Japan, edited by N. Miura, T. Ando, Berlin Heidelberg New York, Springer 2001, p. 363-364.
21. K. Himmelbauer, H. Sitter, H. Krenn: "*Magnetic properties of thin iron films*", In: Proceedings of the Seminar "GMe Forum 2001" , Vienna April 5-6, 2001, edited by K. Riedling, Gesellschaft für Mikroelektronik, Vienna 2001, p. 173-177.
22. K. Wiesauer, G. Springholz: "*Nano-scale dislocation patterning in PbTe on PbSe (100) heteroepitaxy studied by Scanning Tunneling Microscopy*", In: Proceedings of the Seminar "GMe Forum 2001" , Vienna April 5-6, 2001, edited by K. Riedling, Gesellschaft für Mikroelektronik, Vienna 2001, p. 209-212.
23. M. Aigle, H. Pascher, H. Kim, E. Tarhan, A.J. Mayur, M. Dean Sciacca, A.K. Ramdas, G. Springholz, G. Bauer: "*Optical phonons in PbEuTe epilayers and PbTe/EuTe superlattices: Berreman effect*", Phys. Rev. B 64, 035316 (2001).
24. M. Aigle, H. Pascher, M. Pinczolits, G. Springholz, T. Schwarzl, W. Heiss, G. Bauer: "*Optical Characterization of Self-Organized PbSe/$Pb_{1-x}Eu_xTe$ Quantum Dot Superlattices*", phys. stat. sol. (b) 224, 223-227 (2001).
25. M.S. Carroll, J.C. Sturm, E. Napolitani, D. De Salvador, M. Berti, J. Stangl, G. Bauer, D.J. Tweet: "*Diffusion enhanced carbon loss from SiGeC layers due to oxidation*", Phys. Rev. B 64, 3308-3311 (2001).
26. N. Sandersfeld, W. Jantsch, Z. Wilamowski, F. Schäffler: "*Modulation doped $Si/Si_{1-x}Ge_x$ -field-effect transistors*", In: Proceedings of the Seminar "GMe Forum 2001" , Vienna April 5-6, 2001, edited by K. Riedling, Gesellschaft für Mikroelektronik, Vienna 2001, p. 195.

27. N.Sandersfeld, W.Jantsch, Z.Wilamowski, F.Schäffler: "*Conduction Electron Spin Resonance in MBE-Grown Si/SiGe Quantum Wells*", In: Proceedings of the Seminar "GMe Forum 2001" , Vienna April 5-6, 2001, edited by K. Riedling, Gesellschaft für Mikroelektronik, Vienna 2001, p. 193.

28. R. Rupprecht, H. Pascher, H. Krenn, W. Faschinger, G. Bauer: "*Coherent Raman spectroscopy of CdTe/MnTe short period superlattices*", Phys. Rev. B 63, 115325 (2001).

29. R.T. Lechner, A. Raab, G. Springholz, M. Pinczolits, V. Holy, P. Mayer, G. Bauer, H.H. Kang, L. Salamanca-Riba: "*Molecular beam epitaxy of self-organized PbSe quantum dot superlattices*", In: Proceedings of the Seminar "GMe Forum 2001" , Vienna April 5-6, 2001, edited by K. Riedling, Gesellschaft für Mikroelektronik, Vienna 2001, p. 189-190.

30. T. Berer, G. Pillwein, G. Brunthaler, G. Strasser: "*Fabrication of AlGaAs nanostructures*", In: Proceedings of the Seminar "GMe Forum 2001" , Vienna April 5-6, 2001, edited by K. Riedling, Gesellschaft für Mikroelektronik, Vienna 2001, p. 159-164.

31. T. Ikaida, N. Miura, G. Springholz, M. Pinczolits, G. Bauer: "*Cyclotrone resonance in PbSe/PbEuTe quantum dot crystals*", Proc. 25th International Conference on the Physics of Semiconductors, Sept. 2000, Osaka, Japan, edited by N. Miura, T. Ando, Berlin Heidelberg New York, Springer 2001, p. 1057-1058.

32. T. Roch, V. Holy, A. Daniel, E. Höflinger, M. Meduna, T.H. Metzger, G. Bauer, J. Zhu, K. Brunner, G. Abstreiter: "*X-ray studies on self-organized wires in SiGe/Si multilayers*", Journal of Physics D: Appl. Phys. 34, A6-A10 (2001)

33. T. Roch, V. Holy, J. Stangl, E. Höflinger, A. Daniel, G. Bauer, I. Kegel, H. Metzger, J. Zhu, K. Brunner, G. Abstreiter: "*Structural investigations on self-organized Si/SiGe islands by grazing incidence small angle x-ray scattering*", Phys. stat. sol. (b) 224, 241-245 (2001).

34. T. Schwarzl, W. Heiss, G. Springholz, M. Aigle, H. Pascher, K. Biermann, K. Reimann: "*Lead salt based VCSELs for the 3 - 6 micron range*", SPIE Proceedings Vol. 4286 , p. 172 (2001).

35. T. Schwarzl, W. Heiss, G. Springholz, S. Gianordoli, G. Strasser, M. Aigle, H. Pascher: "*Strongly detuned IV-VI microcavity and microdisk resonances: mode splitting and lasing*", Proc. 25th International Conference on the Physics of Semiconductors, Sept. 2000, Osaka, Japan, edited by N. Miura, T. Ando, Berlin Heidelberg New York, Springer 2001, p. 677-678.

36. T. Schwarzl, W. Heiss, G. Springholz, S. Gianordoli, G. Strasser, M. Aigle, H. Pascher: "*Mode Splitting and Lasing in detuned lead salt microcavity and microdisk resonances*", In: Proceedings of the Seminar "GMe Forum 2001" , Vienna April 5-6, 2001, edited by K. Riedling, Gesellschaft für Mikroelektronik, Vienna 2001, p. 197-200.

37. V. Holy, J. Stangl, G. Springholz, M. Pinczolits, G. Bauer: "*High resolution x-ray diffraction from self-organized PbSe/PbEuTe quantum dot superlattices*", J. Phys. D: Appl. Phys. 34, A1-A5 (2001).

38. V. Holy, J. Stangl, G. Springholz, M. Pinczolits, G. Bauer: "*Lateral and vertical ordering of PbSe self-assembled quantum dots in PbSe/PbEuTe superlattices*", In: Morphological and compositional evolution of heteroepitaxial semiconductor thin films, eds. J. Mirecki Millunchick, A. L. Barabasi, N. A. Modine and E. D. Jones, Symposium Proceedings of Material Research Society, vol. 618, pp. 161-172 (2001).

39. V. Holy, T. Roch, J. Stangl, A. Daniel, G. Bauer, T.H. Metzger, Y. H. Zhu, K. Brunner, G. Abstreiter: "*Grazing incidence small-angle x-ray scattering study of self-organized SiGe wires*", Phys. Rev. B. 63, 205318 (2001).

40. W. Heiss, G. Prechtl, G. Springholz: "*Giant tunability of exciton photoluminescence emission in antiferromagnetic EuTe*", Phys. Rev. B 63, 165323 (2001).

41. W. Heiss, G. Prechtl, G. Springholz: "*Giant tunability of excitonic photoluminescence transitions in antiferromagnetic EuTe epilayers*", Proc. 25th International Conference on the Physics of Semiconductors, Sept. 2000, Osaka, Japan, edited by N. Miura, T. Ando, Berlin Heidelberg New York, Springer 2001, p. 240-241.

42. W. Heiss, G. Prechtl, G. Springholz: "*Giant tunability of excitonic photoluminescence transitions in antiferromagnetic EuTe epilayers induced by magnetic polarons*", Physica E 10, 419-423 (2001).

43. W. Heiss, G. Prechtl, G. Springholz: "*Magnetic field tunable excitonic photoluminescence transitions in antiferromagnetic EuTe epitaxial layers with an effective g factor in excess of 1000*", Appl. Phys. Lett. 78, 3484-3486 (2001).

44. W. Heiss, T. Schwarzl, G. Springholz: "*Spectroscopy on vertical microcavities for the mid-infrared*", phys. stat. sol. (a) 188, 929-935 (2001).

45. W. Heiss, T. Schwarzl, G. Springholz, K. Biermann, K. Reimann: "*Above-room temperature mid-infrared lasing from vertical cavity surface emitting PbTe quantum-well lasers*", Appl. Phys. Lett. 78, 862-864 (2001).

46. W. Heiss, T. Schwarzl, G. Springholz, T. Fromherz, G. Bauer, M. Aigle, H. Pascher, K. Biermann, K. Reimann: "*Lead-salt microcavities for the mid-infrared*", In: Proceedings of the Seminar "GMe Forum 2001" , Vienna April 5-6, 2001, edited by K. Riedling, Gesellschaft für Mikroelektronik, Vienna 2001, p. 73-77.

47. W. Heiss, T. Schwarzl, J. Roither, G. Springholz, M. Aigle, H. Pascher, K. Biermann, K. Reimann: "*Epitaxial bragg mirrors for the mid-infrared and their applications*", Progress in Quantum Electronics 25, p. 193 (2002).

48. W. Jantsch, Z. Wilamowski, N. Sandersfeld, F. Schäffler: "*Evidence for screening breakdown near the metal-to-insulator transition in two dimensions*", Proc. 25th International Conference on the Physics of Semiconductors, Sept. 2000, Osaka, Japan, edited by N. Miura, T. Ando, Berlin Heidelberg New York, Springer 2001, p. 859-860.

49. W. Märzinger, H. Krenn: "*In-line Prozesskontrolle mit einem kompakten Echtzeit-FTIR-Spektrometer*", In: Proceedings of the Seminar "GMe Forum 2001" , Vienna April 5-6, 2001, edited by K. Riedling, Gesellschaft für Mikroelektronik, Vienna 2001, p. 191.

50. Z. Wilamowski, N. Sandersfeld, W. Jantsch, D. Többen, F. Schäffler: "*Screening Breakdown on the Route toward the Metal-Insulator Transition in Modulation Doped Si/SiGe Quantum Wells*", Phys. Rev. Lett. 87, 026401 (2001).

51. Z. Wilamowski, W. Jantsch: "*Spin Resonance Properties of the Two-Dimensional Electron Gas*", Physica E **10**, 17-21 (2001)

52. W. Jantsch, G. Kocher, L. Palmetshofer, H. Przybylinska, M. Stepikhova, H. Preier: "*Optimisation of Er Centers in Si for Reverse Biased Light Emitting Diodes*", Mat. Sci. & Eng. B **81**, 86-90 (2001)

53. K. Himmelbauer, H. Sitter, H. Krenn: "*Magnetic Properties of Thin Iron Films",* Proc. GMe-Tagung Wien, 2001

54. E. Thor, M. Mühlberger, L. Palmetshofer, F. Schäffler: "*Deep-Level Transient Spectroscopy of Dislocation-Related Defects in Epitaxial Multilayer Structures*", J. Appl. Phys. **90**, 5, 2252-2256 (2001)

55. T. Schwarzl, W. Heiss, G. Springholz, S. Gianordoli, G. Strasser: "*Mode splitting and lasing in detuned lead salt microcavity and microdisk resonances*", Proc. GMe Forum 2001, Vienna 2001, ed. by K. Riedling (ISBN: 3-901578-07-2)

56. W. Heiss, T. Schwarzl, G. Springholz, T. Fromherz, G. Bauer, M. Aigle, H. Pascher, K. Biermann, K. Reimann: "*Lead-salt microcavities for the mid-infrared*", Proc. GMe Forum 2001, Vienna 2001, ed. by K. Riedling (ISBN: 3-901578-07-2)

57. W. Heiss, G. Prechtl, G. Springholz: "*Giant tunability of exciton photoluminescence emission in antiferromagnetic EuTe*", Phys. Rev. B **63**, 1653 (2001)

58. M. Aigle, H. Pascher, M. Pinczolits, G. Springholz, T. Schwarzl, W. Heiss, G. Bauer: "*Optical characterization of self-organized PbSe/Pb1-xEuxTe quantum dot superlattices*", phys. stat. sol. (b) **224**, 223 (2001)

59. W. Heiss, G. Prechtl, G. Springholz: "*Giant tunability of excitonic photoluminescence transitions in antiferromagnetic EuTe epilayers induced by magnetic polarons*", Physica E **10**, 419 (2001)

60. T. Schwarzl, W. Heiss, G. Springholz, S. Gianordoly, G. Strasser, M. Aigle, H. Pascher: "*Strongly detuned IV-VI microcavity and microdisk resonances: mod splitting and lasing*", Proc. 25th Int. Conf. Physics of Semiconductors, M. Miura, T. Ando (Eds.), Springer, Berlin, 2001, p 677

61. W. Heiss, G. Prechtl, G. Springholz: "*Giant tunability of excitonic photoluminescence transitions in antiferromagnetic EuTe epilayers*", Proc. 25th Int. Conf. Physics of Semiconductors, M. Miura, T. Ando (Eds.), Springer, Berlin, 2001, p 240

62. W. Heiss, T. Schwarzl, G. Springholz, K. Biermann, K. Reimann: "*Above-room-temperature mid-infrared lasing from vertical cavity surface emitting PbTe quantum-well lasers*", Appl. Phys. Lett**. 78**, 862 (2001)

63. W. Heiss, G. Prechtl, G. Springholz: "*Magnetic-field-tunable photoluminescence transitions in antiferromagnetic EuTe epilayers with an effective g factor of 1140*", Appl. Phys. Lett. **78**, 3484 (2001)

64. T. Schwarzl, W. Heiss, G. Springholz, M. Aigle, H. Pascher, K. Biermann, K. Reimann: "*Lead salt based VCSELS for the 3 -6 micron range*", Proc. SPIE, Vol. 4286, p 172 (2001) K.D. Choquette, C. Leit (Eds.)

65. W. Heiss, T. Schwarzl, G. Springholz: "*Spectroscopy on vertical microcavities for the mid-infrared*", phys. stat. sol. (a) **188**, No. 3, 929-935 (2001)

66. V.G. Shengurov, S.P. Svetlov, V.Yu. Chalkov, G.A. Maksimov, Z.F. Krasil'nik, B.A. Andreev, M.V. Stepikhova, L. Palmetshofer, H. Ellmer: "*Influence of the Growth Condition on Building-Up Processes of Rare Earth Dopants in Silicon Layers During Molecular Beam Epitaxy*", Proc. Russ. Acad. Sciences, Ser. Phys. **65**, 289 (2001) (in Russian)

67. R.E. Balderas-Navarro, K. Hingerl, A. Bonanni, H. Sitter, D. Stifter: "*In situ observation of stress relaxation in CdTe/ZnTe heterostructures by reflectance difference spectroscopy*", Appl. Phys. Lett. **78**, 3515 (2001)

68. K. Hingerl, R.E. Balderas-Navarro, A. Bonanni, D. Stifter: "*Influence of anisotropic inplane strain on critical point resonances in reflectance difference spectroscopy*", J. Vac. Sci.&Techn. B **19**, 1650 (2001)

69. G. Kocher, H. Przybylinska, M. Stepikhova, L. Palmetshofer, W. Jantsch: "*Erbium in SiO_2 environment: ways to improve the 1.54 μm emission*", Physica B **308-310**, 344-347 (2001)

70. H. Przybylinska, W. Jantsch, A. Kozanecki, D.J. As, K. Lischka: "*Photoluminescence properties of Er-doped GaN*", Physica B **308-310**, (2001)

71. Kozanecki, H. Przybylinska, D. Kuritsyn, W. Jantsch: "*Site selective excitation of Er^{3+} ions in oxygen-rich silicon*", Physica B **308-310**, (2001)

72. G. Kocher, W. Jantsch, N. Abrosimov, S. Egorov, A. Zabrodskii, B. Andreev, H.G. Grimmeiss: "*Alloy fluctuations in $Si_{1-x}Ge_x$ crystals*", Physica B **308-310**, 558-560 (2001)

Submitted / in print:

1. A. A. Darhuber, G. Bauer, P. Schittenhelm, G. Abstreiter: "*Structural Characterization of Self-organized Ge Islands*", In: "Self-organized Quantum Dots", ed. T.P. Pearsall, Gordon & Breach 2000, in print.

2. A. Andreev, H. Sitter, C. Brabec, P. Hinterdorfer, G. Springholz, N.S. Sariciftci, R. Resel, H. Plank: "*Self-assembled growth of highly oriented para-sexiphenyl thin films controlled by elastic strain*", Materials Research Society Symposium Proceedings, in print

3. A. Andreev, H. Sitter, N. S. Sariciftci, C. J. Brabec, G. Springholz, P. Hinterdorfer, H. Plank, R. Resel, A. Thierry, and B. Lotz: "*Highly ordered anisotropic nano-needles in para-sexiphenyl films*", Thin Solid Films 403 – 404, 444 – 448 (2002).

4. A.G. Touryanski, I.V. Pirshin, M.M. Rzaev, M. Mühlberger, F. Schäffler: "*Two wave X-ray optical diagnostics of Ge_xSi_{1-x}/Si modulation doped heterostructures*", Physica E, in print

5. A. Raab, G. Springholz, R. Lechner, I. Vavra, H. H. Kang, and L. Salamanca-Riba: "*Atomic Force Microscopy and Transmission Electron Microscopy Study of Self-*

Organized Ordering", in "Vertically Aligned PbSe Quantum Dot Superlattices", Materials Research Society Symposium Proceedings, in print

6. G. Dehlinger, L. Diehl, U. Gennser, H. Sigg, E. Müller, S. Stutz, J. Faist, J. Stangl, T. Roch, G. Bauer, D. Grützmacher: "*Si/SiGe quantum cascade structures emitting in the 10μm range*", Materials Science and Engineering C736 (2001), in print.
7. G. Grabecki, J. Wrobel, T. Dietl, E. Papis, E. Kaminska, A. Piotrowska, G. Springholz, G. Bauer: "*Spin alignment of electrons in PbTe/(Pb,Eu)Te nanostructures*", Proceedings 10th International Conference on Modulated Semiconductor Structures (MSS10), Physica E, submitted.
8. G. Springholz: "*Molecular Beam Epitaxy of IV-VI Heterostructures and Superlattices*", In: "Lead Chalcogenides: Physics and Applications", eds. D. Khoklov, Gordon and Breach, in print.
9. G. Springholz and K. Wiesauer: "*Nanoscale dislocation patterning in PbTePbSe (001) heteroepitaxy*", Physical Review Letters 88, 015507-1/4 (2002).
10. G. Springholz, M. Pinczolits, P. Mayer, A. Raab, R. Lechner, V. Holy, G. Bauer, T. Schwarzl, W. Heiss, M. Aigle, H. Pascher, H. Kang, L. Salamanca-Riba: "*Self-assembled PbSe quantum dot superlattices: ordering and device applications*", Proc. 10th Int. Conf. NGSC 2001, 161-164 (2002).
11. G. Springholz, T. Schwarzl, W. Heiss, M. Aigle, H. Pascher, K. Biermann, K. Reimann: "*Fabrication of mid-infrared vertical cavity surface emitting PbTe quantum well lasers for the 3-5 μm spectral region*", Proc. 10th Int. Conf. NGSC 2001, 142-144 (2002).
12. G. Springholz, T. Schwarzl, W. Heiss, T. Fromherz, G. Bauer, M. Aigle, H. Pascher, I. Vavra: "*Fabrication of 3.9-4.2μm mid-infrared surface emitting PbSe/PbEuTe quantum dot lasers using molecular beam epitaxy*", Physica E, in print.
13. G. Springholz, V. Holy, P. Mayer, M. Pinczolits, A. Raab, R.T. Lechner, G. Bauer, H. Kang, L. Salamanca-Riba: "*Self-organized ordering in self-assembled quantum dot superlattices*", Material Science and Engeneering B88, 143-152 (2002).
14. H. Kepa, J. Blinowski, P. Kacman, G. Springholz, G. Bauer, C.F. Majkrzak, K.I. Goldman, T.M. Giebultowicz: "*Interlayer exchange in antiferromagnetic-nonmagnetic semiconductor superlattices*", Proc. ICPS Jerusalem 2000, in print.
15. Hesse, J. Stangl, V. Holy, T. Roch, G. Bauer, O.G. Schmidt, U. Denker, B. Struth: "*Effect of overgrowth on shape, composition and strain of SiGe islands on Si(001)*", Phys. Rev. B, submitted.
16. J. Myslivecek, C. Schelling, F. Schäffler, B. Voigtländer, P. Smilauer, J. Krug: "*Step bunching during Si(001) homoepitaxy caused by the surface diffusion anisotropy*", Phys. Rev. Lett., submitted.
17. J. Mysliveçek, C. Schelling, G. Springholz, F. Schäffler, B. Voigtländer and P. Šmilauer: "*On the origin of the kinetic growth instability of homoepitaxy on Si(001)*", Mat. Sci. Eng. B 89, 1-3, 410 - 414 (2002)
18. J. Stangl, V. Holy, G. Springholz, G. Bauer, I. Kegel, T.H. Metzger: "*Self-organized semiconductor nanostructures: shape, strain and composition*", Materials Science and Engineering C19, 349-358 (2002).

19. K. Wiesauer, G. Springholz: "*Observation of misfit dislocation formation in PbTe/PbSe (001) lattice-mismatched heteroepitaxy by in situ RHEED and scanning tunneling microscopy*", IAP Conf. Proc. 2, 45-47(2002).

20. K. Wiesauer and G. Springholz: "*Strain relaxation and dislocation pattening in PbTePbSe (001) lattice-mismtached heteroepitaxy*", Applied Surface Science, in print.

21. K. Wiesauer and G. Springholz: "*Nano-scale dislocation patterning in PbTe on PbSe (100) heteroepitaxy studied by UHV scanning tunneling microscopy*", Physica E, in print.

22. L .Diehl, H. Sigg, G. Dehlinger, D. Grützmacher, E. Müller, U. Gennser, I. Sagnes, T. Fromherz, Y. Campidelli, O. Kermarrec, D. Bensahel, J. Faist: "*Intersubband absorption performed on p-type modulation doped $Si_{0.2}Ge_{0.8}$/Si quantum wells grown on $Si_{0.5}Ge_{0.5}$ pseudo-substrate*", Appl. Phys. Lett., submitted.

23. M. Meduna, V. Holy, T. Roch, G. Bauer, O. G. Schmidt, K. Eberl: "*Diffuse x-ray reflectivity from self-assembled ripples with superimposed roughness in Si/Ge superlattices*", Semicond. Sci. Technol., in print.

24. M. Mühlberger, C. Schelling, G. Springholz and F. Schäffler: "*Step bunching and strain effects in $Si_{1-x}Ge_x$ layers and superlattices on vicinal Si(001)*", Physica E, in print

25. M. Mühlberger, C. Schelling, G. Springholz and F. Schäffler: "*Step-bunching and strain-effects in $Si_{1-x}Ge_x$ layers and superlattices grown on vicinal Si(001)*", Mat. Sci. Eng. B 89, 1-3, 257 - 262 (2002)

26. M.S. Carroll, J.C. Sturm, E. Napolitani, D. De Salvador, M. Berti, J. Stangl, G. Bauer, D.J. Tweet: "*Silicon interstitial driven loss of substitutional carbon from SiGeC structures*", Proc. Symp. Mat. Res. Soc. 669, in print (2001). (presented Symp. MRS, San Francisco, CA, April, 2001, page numbers not avail. yet)

27. N. Sandersfeld, M. Mühlberger, W. Jantsch, Z. Wilamowski, F. Schäffler : "*Spin lifetimes and g-factor tuning in Si/SiGe quantum well*", Physica E, in print

28. A. Raab, R. T. Lechner, G. Springholz: "*Self-organized lateral ordering for vertically aligned PbSe/PbEuTe quantum dot superlattices*", Appl. Phys. Lett. 80, 1273-1275 (2002).

29. T. Fromherz, W. Mac, A. Hesse, G. Bauer, C. Miesner, K. Brunner, G. Abstreiter: "*Intraband absorption and photocurrent spectroscopy of self-assembled p-type Si/SiGe quantum dots*", Appl. Phys. Lett., in print.

30. T. Fromherz, W. Mac, C. Miesner, K. Brunner, G. Bauer, G. Abstreiter: "*Intersubband transitions of boron doped self-assembled Ge quantum dots*", Physica E (2002), in print.

31. T. Ikaida, N. Miura, S. Tsujino, S.J. Allen, G. Springholz, M. Pinczolits, G. Bauer: "*Study of electronic states in PbSe/PbEuTe quantum dot crystals by cyclotron resonance at very high magnetic fields*", IAP Conf. Proc. 2, 48-50 (2002)..

32. T. Roch, M. Meduna, J. Stangl, A. Hesse, R. Lechner, G. Bauer, G. Dehlinger, L. Diehl, U. Gennser, E. Müller, D. Grützmacher: "*Interface roughness in SiGe*

quantum-cascade structures from x-ray reflectivity studies", J. Appl. Phys., submitted.

33. T. Roch, V. Holy, A. Hesse, J. Stangl, T. Fromherz, G. Bauer, T.H. Metzger, S. Ferrer: "*Strain in buried self-assembled SiGe wires studied by grazing-incidence x-ray diffraction*", Phys. Rev. B, submitted.
34. T. Schwarzl, W. Heiss, G. Springholz, K. Biermann, K. Reimann: "*Above-room temperature operation of IV-VI microcavity lasers*", Physica E, in print.
35. V.M. Pudalov, G. Brunthaler, A. Prinz, G. Bauer: "*Weak anisotropy of the in-plane magnetoresistance in high mobility (100) Si-MOS structures*", Phys. Rev. Lett., in print.
36. C. Skierbiszewski, P. Perlin, P. Wisniewski, T. Suski, J. Geisz, K. Hingerl, W. Jantsch, D. Mars, W. Walukiewicz: "*Band structure and optical properties of* $In_xGa_{1-x}As_{1-y}N_y$", Phys. Rev. B
37. W. Jantsch, Z. Wilamowski, N. Sandersfeld, M. Mühlberger, F. Schäffler: "*Spin lifetimes and g-factor tuning in Si/SiGe quantum wells*", Physica E
38. C. Skierbiszewski, S. P. Sepkowski, P. Perlin, T. Suski, W. Jantsch, J. Geisz: "*The effective mass and conduction band states of GaAsN/GaAs quantum wells*", Physica E
39. G. Kocher, H. Przybylinska, M. Stepikhova, L. Palmetshofer, W. Jantsch: "*Erbium in* SiO_x *environment: ways to improve the 1.54 μm emission*", Physica B
40. Kozanecki, H. Przybylinska, D. Kuritsyn, W. Jantsch: "*Site selective excitation of* Er^{3+} *ions in oxygen-rich Silicon*", Proc. ICDS-21, Gießen 2001, Physica B
41. W. Heiss, T. Schwarzl, J. Roither, G. Springholz, M. Aigle, H. Pascher, K. Biermann, K. Reimann: "*Epitaxial bragg mirrors for the mid-infrared and their applications*", Progress in Quantum Electronics
42. T. Schwarzl, W. Heiss, G. Springholz, K. Biermann, K. Reimann: "*Above-room-temperature operation of IV-VI microcavity lasers*", Physica E

Presentations

Invited Talks:

1. T. Schwarzl, W. Heiss, G. Springholz, M. Aigle and H. Pascher, (invited): "*Lead salt vertical cavity surface emitting lasers for the 3 - 6 μm wavlength range*", Photonics West, 22.1.-28.1.2001, San Francisco, USA
2. G. Brunthaler: "*Exclusion of quantum coherence as the origin of the 2D Metallic State in Si-MOS*", Invited talk at the Minerva Workshop, Dead Sea resort, Israel, March 26th - 28th, 2001
3. G. Springholz: "*Self-organized MBE growth of narrow gap PbSe quantum dots*", 10th International Conference on Narrow Gap Semiconductors and Related Small Energy Phenomena, Physics and Applications, 27.5.-31-5-2001, Ishikawa, Japan

4. J. Stangl, V. Holy, G. Bauer, I. Kegel, T.H. Metzger: "*Semiconductor Nanostructures: shape, strain and composition*", E-MRS 2001 Spring Meeting, Strasbourg, France, June 5-8, 2001.
5. G. Springholz: "*Vertical and lateral ordering in self-organized quantum dot superlattices*", E-MRS 2001 Spring Meeting, Strasbourg, France, June 5-8, 2001.
6. G. Springholz: "*Quantum dots in IV-VI diluted magnetic semiconductors*", 1st CELDIS Workshop on Low Dimensional and Hybrid Diluted Magnetic Semiconductor Structures, 22.6. - 23.6.2001, Obory, Poland.
7. G. Springholz: "*Selbst-Organisierte Quantenpunkte in IV-VI Halbleitern*", Physik Kolloquium der Universität Bayreuth, 3.7.2001, Bayreuth, Germany
8. G. Springholz: "*Selbst-Organisierte Halbleiter-Quantenpunkte - Ordnungsphänomene und praktische Anwendungen*", Seminar am Institut für Physik der kondensierten Materie, Heinrich Heine Universität Düsseldorf, 4.7.2001, Düsseldorf, Germany.
9. J. Stangl, G. Bauer, V. Holy: "*Determination of strain and composition of self-organized islands using x-ray diffraction techniques*", 4th International Workshop "Modelling, Growth, Properties and Devices of Epitaxial Semiconductors on Novel Index Surfaces" (NIS'01), Aspet, France, September 16-20, 2001.
10. G. Springholz: "*Self-organized Growth of Semiconductor Nanostructures*", Combined 15th International Vacuum Congress and 11th International Conference on Solid Surfaces and 48th International Symposium of the American Vacuum Society, San Francisco, 28.10.-2.11.2001.
11. G. Bauer: "*Characterization of quantum dots by x-ray diffraction*", International Symposia "Röntgen's Heritage, Quantum Hall Effect and Heterostructures", University of Würzburg, Germany, December 11-15, 2001.
12. W. Jantsch, Z. Wilamowski, N. Sandersfeld, and F. Schäffler: "*Spin resonance of the two-dimensional electron gas - a new method to investigate potential fluctuations*", Workshop "Science and Technology in Nanostructures and Low Dimensional Materials" (STNLD '01), Granada, 28 February – 3 March, 2001
13. W. Heiss: "*PbTe/EuTe-Vielschichtstrukturen: Vom exotischen Halbleiter zum optischen Bauelement*", Walter-Schottky-Seminar, TU München, June 2001
14. T. Schwarzl, W. Heiss, G. Springholz, K. Biermann, K. Reimann, M. Aigle, H. Pascher: "*Midinfrared surface-emitting quantum well and quantum dot lasers based on IV-VI semiconductors*", Mini-Symposium on Application of Free Electron Lasers, Cumbria, U.K., Sept. 2001
15. T. Schwarzl, W. Heiss, G. Springholz, M. Aigle, H. Pascher, K. Biermann, K. Reimann: "*Lead-salt-based vertical-cavity surface-emitting lasers for the 3 – 6 micron range*", Mid-Infrared Network Meeting, Guildford, U.K., July 2001
16. G. Springholz, M. Pinczolits, P. Mayer, A. Raab, R. Lechner, V. Holy, G. Bauer, T. Schwarzl, W. Heiss, M. Aigle, H. Pascher, H.H. Kang, L. Salamanca-Riba: "*Self-assembled PbSe quantum dot superlattices: Ordering and device applications*", 10th Int. Conf. Narrow Gap Semiconductors, Ishikawa, Japan, May 2001

17. W. Heiss, T. Schwarzl, G. Springholz, M. Aigle, H. Pascher, K. Biermann, K. Reimann: "*Spectroscopy on vertical microcavities for the mid-infrared*", Int. Workshop on Microcavity Light Sources, Paderborn, Germany, April 2001
18. W. Heiss, T. Schwarzl, G. Springholz: "*Bleisalz-Mikroresonatoren für das mittlere Infrarot*", GMe-Forum 2001, Wien, April 2001
19. T. Schwarzl, W. Heiss, G. Springholz, M. Aigle, H. Pascher, K. Biermann, K. Reimann: "*Lead salt based VCSELs for the 3 – 6 micron range*", Photonic West – Optoelectronics 2001, St. Jose, USA, Jan. 2001
20. H. Sitter, A. Bonanni, D. Stifter, K. Hingerl: "*MOCVD growth of GaN*", Review Seminar on Scientific Cooperation between Austria and Poland, May 2001
21. H. Sitter: "*Herstellung epitaktischer Schichten*", Physikkolloquium TU Graz, May 2001
22. H. Sitter: "*Epitaxial growth – close and far away from thermodynamic equilibrium*", Pre-Conference School, Jaszoviec, Poland, June 2001
23. H. Sitter: "*Molecular-beam epitaxy – fundamentals and application*", Iberomerican School on Epitaxial Growth of Semiconductor Nanostructures, Univ. Sao Paulo, Nov. 2001
24. H. Sitter: "*In-situ characterization in MBE systems*", Iberomerican School on Epitaxial Growth of Semiconductor Nanostructures, Univ. Sao Paulo, Brasilien, Nov. 2001
25. H. Sitter: "*Organic epilayers grown by hot-wall epitaxy*", Instituto de Pesquisas Espaciais, San Jose dos Campos, Brasilien, Nov. 2001
26. A. Bonanni: "*Optical polarization probes on semiconductor and metal surfaces*", Physikkolloquium Univ. Graz, June 2001

Conference presentations (talks and posters):

1. A. Raab, R. Lechner, and G. Springholz: "*Self-Organized Lateral Ordering in Vertically Aligned PbSe Quantum Dot Superlattices*", Fall Meeting of the Materials Research Society, Boston 26.-30.1.2001
2. C. Schelling, M. Mühlberger, G. Springholz, F. Schäffler: "*The surface morphology of single Si1-xGex layers grown on vicinal Si (001): step bunching and strain-effects*", 10th International Conference on Modulated Semiconductor Structures (MSS10), Linz, Austria, July 23-27, 2001.
3. C.Schelling, M.Mühlberger, G.Springholz, F.Schäffler: "*The surface morphology of single SiGe layers grown on vicinal Si (001)*", Euro-MBE, Hinterzarten (Germany), 05.-07.02.01
4. D. Gruber, M. Mühlberger, F. Schäffler: "*Characterization of Si/$Si_{1-x-y}Ge_xC_y$ heterostructures for device applications*", Seminar "GMe Forum 2001", Gesellschaft für Mikroelektronik, Vienna, April 5-6, 2001.
5. D. Gruber, M. Mühlberger, T. Fromherz, F. Schäffler, M. Schatzmayr: "*Fourier Transform Infrared Investigations of SiC Structures for HBT Applications*", 2nd Int. Conf. Si MBE and Heterostructures, Straßburg (France) 05. - 08.05.01.

6. D. Gruber, T. Fromherz, M. Mühlberger, C. Schelling, L. Palmetshofer, F. Schäffler: "*Characterization of Si/SiGeC heterostructures for device applications*", Seminar "GMe Forum 2001", Gesellschaft für Mikroelektronik, Vienna, April 5-6, 2001.
7. D.Gruber, M.Mühlberger, T.Fromherz, F.Schäffler: "*Fourier-Transform Infrared Investigations of SiC Structures for HBT Applications*", MRS Fall Meeting, Boston (USA) 26. - 30.11.2001
8. G. Grabecki, J. Wrobel, T. Dietl, E. Papis, E. Kaminska, A. Piotrowska, G. Springholz, G. Bauer: "*Spin alignment of electrons in PbTe/(Pb,Eu)Te nanostructures*", 10th International Conference on Modulated Semiconductor Structures (MSS10), Linz, Austria, July 23-27, 2001.
9. G. Springholz, M. Pinczolits, P. Mayer, A. Raab, R. Lechner, V. Holy, G. Bauer, T. Schwarzl, W. Heiß, M. Aigle, H. Pascher, H. Kang, L. Salamanca-Riba: "*Self-assembled PbSe quantum dot superlattices: ordering and device applications*", 10th International Conference on Narrow Gap Semiconductors, May 27-31, 2001, Ishikawa, Japan.
10. G. Springholz, R. T. Lechner, M. Pinczolits, P. Mayer, V. Holy, G. Bauer: "*Tuning of vertical and lateral correlations in self-organized quantum dot superlattices*", 4th International Workshop "Modelling, Growth, Properties and Devices of Epitaxial Semiconductors on Novel Index Surfaces" (NIS'01), Aspet, France, September 16-20, 2001.
11. G. Springholz, T. Schwarzl, W. Heiss, M. Aigle, H. Pascher, K. Biermann, K. Reimann: "*Fabrication of mid-infrared vertical cavity surface emitting PbTe quantum well lasers for the 3-5 μm spectral region*", 10th International Conference on Narrow Gap Semiconductors, May 27-31, 2001, Ishikawa, Japan.
12. G. Springholz, T. Schwarzl, W. Heiss, M. Aigle, H. Pascher, T. Fromherz, G. Bauer: "*Mid-infrared surface-emitting PbSe/PbEuTe quantum dot lasers*", 10th International Conference on Modulated Semiconductor Structures (MSS10), Linz, Austria, July 23-27, 2001.
13. G. Springholz and K. Wiesauer: "*Dislocation pattering in PbTe on PbSe (100) lattice-mismatched heteroepitaxy studied by scanning tunneling microscopy*", 10th International Conference on Narrow Gap Semiconductors and Related Small Energy Phenomena, Physics and Applications, 27.5.-31-5-2001, Ishikawa, Japan
14. G. Springholz and K. Wiesauer: "*Strain relaxation and misfit dislocation formation in PbTe/PbSe (001) hetereoepitaxy*", European Materials Research Society Spring Meeting, 5.6.-8.6.2001, Strasbourg, France.
15. J. Myslivecek, C. Schelling, G.Springholz, F. Schäffler, B. Voigtländer, P. Šmilauer: "*On the Microscopic Origin of Kinetic Growth Instabilities in Si(001) Homoepitaxy*", MRS Fall Meeting, Boston (USA) 26. - 30.11.2001
16. J. Stangl, G. Bauer, A. Hesse, T. Roch, V. Holy, M. Pinczolits, G. Springholz: "*X-Ray scattering from Semiconductor Nanostructures*", NESY Ferienschule "Forschung mit Röntgen- und Neutronenstreuung an Europäischen Großforschungsanlagen", Planneralm 2001, March 11-17, 2001.

17. J. Myslivecek, C. Schelling, G. Springholz, F. Schäffler, B.Voigtländer, P. Šmilauer: "*On the origin of the kinetic growth instability of homoepitaxy on Si (001)*", 2nd Int. Conf. Si MBE and Heterostructures, Straßburg (France) 05. - 08.05.01.
18. K. Wiesauer, G. Springholz: "*Observation of misfit dislocation formation in PbTe/PbSe (001) lattice-mismatched heteroepitaxy by in situ RHEED and scanning tunneling microscopy*", 10th International Conference on Narrow Gap Semiconductors, May 27-31, 2001, Ishikawa, Japan.
19. K. Wiesauer, G. Springholz: "*Nano-scale dislocation pattering in PbTe on PbSe (100) heteroepitaxy studied by UHV scanning tunneling microscopy*", 10th International Conference on Modulated Semiconductor Structures (MSS10), Linz, Austria, July 23-27, 2001.
20. K. Wiesauer, G. Springholz: "*Nano-scale dislocation patterning in PbTe on PbSe (100) heteroepitaxy studied by Scanning Tunneling Microscopy*", Seminar "GMe Forum 2001", Gesellschaft für Mikroelektronik, Vienna, April 5-6, 2001.
21. K. Wiesauer, G.Springholz: "*Growth spirals far from thermodynamic equilibrium in PbTe molecular beam epitaxy on BaF_2 (111)*", European Conference on Molecular Beam Epitaxy, 2.1.-8.2.2001, Hinterzarten, Germany.
22. K. Wiesauer,G. Springholz: "*Strain relaxation mechanisms and dislocation patterning in PbTe on PbSe (100) heteroepitaxy*", European Conference on Molecular Beam Epitaxy, 2.1.-8.2.2001, Hinterzarten, Germany
23. M. Mühlberger, C.Schelling, G. Springholz, F. Schäffler: "*Step bunching and strain-effects in $Si_{1-x}Ge_x$ layers and Superlattices grown on vicinal Si(001)*", 2nd Int. Conf. Si MBE and Heterostructures, Straßburg (France) 05. - 08.05.01.
24. M. Mühlberger, C.Schelling, G. Springholz, F. Schäffler: "*Step bunching and strain-effects in $Si_{1-x}Ge_x$ layers and Superlattices grown on vicinal Si(001)*", 10th International Conference on Modulated Semiconductor Structures (MSS10), Linz, Austria, July 23-27, 2001
25. R. T. Lechner, A. Raab, G. Springholz, M. Pinczolits, V. Holy, P. Mayer, G. Bauer, H. Kang, L. Salamanca-Riba: "*Finite size effects in the vertical and lateral ordering of self-organized PbSe quantum dor superlattices*", 10th International Conference on Modulated Semiconductor Structures (MSS10), Linz, Austria, July 23-27, 2001.
26. R.T. Lechner, A. Raab, G. Springholz, M. Pinczolits, V. Holy, P. Mayer, G. Bauer, H.H. Kang, L. Salamanca-Riba: "*Molecular beam epitaxy of self-organized PbSe quantum dot superlattices*", Seminar "GMe Forum 2001", Gesellschaft für Mikroelektronik, Vienna, April 5-6, 2001.
27. R. T. Lechner, A. Raab, G. Springholz, M. Pinczolits, V. Holy, P. Mayer, G. Bauer, H. Kang, and L. Salamanca-Riba: "*The dot size dependence of vertical and lateral and vertical ordering in self-organized PbSe quantum dot superlattices*", European Conference on Molecular Beam Epitaxy, 2.1.-8.2.2001, Hinterzarten, Germany
28. T. Berer, G. Pillwein, G. Brunthaler, G. Strasser: "*Fabrication of AlGaAs nanostructures*", Seminar "GMe Forum 2001", Gesellschaft für Mikroelektronik, Vienna, April 5-6, 2001.
29. T. Ikaida, N. Miura, S. Tsujino, P. Xomalin, S.J. Allen, G. Springholz, M. Pinczolits, G. Bauer: "*Study of electronic states in PbSe/PbEuTe quantum dot*

crystals by cyclotron resonance at very high magnetic fields", 10th International Conference on Narrow Gap Semiconductors, May 27-31, 2001, Ishikawa, Japan.

30. T. Schwarzl, W. Heiss, G. Springholz, K. Biermann, K. Reimann: "*Above-room temperature operation of IV-VI microcavity lasers*", 10th International Conference on Modulated Semiconductor Structures (MSS10), Linz, Austria, July 23-27, 2001.
31. T. Schwarzl, W. Heiss, G. Springholz, S. Gianordoli, G. Strasser, M. Aigle, H. Pascher: "*Mode Splitting and Lasing in detuned lead salt microcavity and microdisk resonances*", Seminar "GMe Forum 2001", Gesellschaft für Mikroelektronik, Vienna, April 5-6, 2001.
32. T. Schwarzl, W. Heiß, G. Springholz, K. Biermann, K. Reimann, M. Aigle, H. Pascher: "*Advances in IV-VI vertical emitting lasers: Above-room-temperature operation and quantum dots as active material*", IVth International Conference on Mid-Infrared Optoelectronics - Materials and Devices MIOMD, 2.-3.4.2001, Montpellier, France.
33. W. Heiss, T. Schwarzl, G. Springholz, T. Fromherz, G. Bauer, M. Aigle, H. Pascher, K. Biermann, K. Reimann: "*Lead-salt microcavities for the mid-infrared*", Seminar "GMe Forum 2001", Gesellschaft für Mikroelektronik, Vienna, April 5-6, 2001.
34. W. Heiss, T. Schwarzl, G. Springholz, M. Aigle, H. Pascher, K. Biermann, K. Reimann: "*Spectroscopy on vertical microcavities for the mid-infrared*", Workshop on Microcavity Light Sources, 6.-7.4.2001, Paderborn, Germany
35. W. Mac, T. Fromherz, C. Miesner, K. Brunner, G. Bauer, G. Abstreiter: "*Intersubband transitions in boron doped self-assembled Ge quantum dots*", 10th International Conference on Modulated Semiconductor Structures (MSS10), Linz, Austria, July 23-27, 2001.
36. N. Sandersfeld, M. Mühlberger, W. Jantsch, Z. Wilamowski, F. Schäffler: "*Spin life times and g-factor tuning in Si/Ge quantum wells*", 10th International Conference on Modulated Semiconductor Structures (MSS10), Linz, 23-27 July 2001
37. Z. Wilamowski, W. Jantsch: "*Determination of the Rashba field in modulation doped Si/SiGe quantum wells from conduction electron spin resonance*", 10th International Conference on Modulated Semiconductor Structures (MSS10), Linz, 23-27 July 2001
38. C. Skierbiczewski, S. P. Lepkowski, P. Perlin, T. Suski, W. Jantsch: "*The effective mass and conduction band states of GaAsN/GaAs quantum wells*", 10th International Conference on Modulated Semiconductor Structures (MSS10), Linz, 23-27 July 2001
39. Z. Wilamowski and W. Jantsch: "*ESR studies of the Bychkov-Rashba field in modulation doped Si/SiGe quantum wells*", 14th Int. Conf. Electronic Props. of Two-Dimensional Systems, EP2DS-14, Prague 2001
40. G. Kocher, H. Przybylinska, M. Stepikhova, L. Palmetshofer and W. Jantsch: "*Erbium in SiO_x environment: Ways to improve the 1.54 μm emission*", 21st International Conference on Defects in Semiconductors, ICDS-21, Gießen, 16-20 July 2001

41. G. Kocher, W. Jantsch, N. Abrosimov, S. Egorov, A. Zabrodskii, B. Andreev, H.G. Grimmeiss: "*Alloy fluctuations in $Si_{1-x}Ge_x$ crystals*", 21st International Conference on Defects in Semiconductors, ICDS-21, Gießen, 16-20 July 2001

42. H. Przybylinska, W. Jantsch, A. Kozanecki, D.J. As, K. Lischka: "*Photoluminescence properties of Er-doped GaN*", 21st International Conference on Defects in Semiconductors, ICDS-21, Gießen, 16-20 July 2001

43. A. Kozanecki, H. Przybylinska, D. Kuritsyn, W. Jantsch: "*Site selective excitation of Er^{3+} ions in oxygen-rich Silicon*", 21st International Conference on Defects in Semiconductors, ICDS-21, Gießen, 16-20 July 2001

44. T. Schwarzl, W. Heiss, G. Springholz, K. Biermann, K. Reimann: "*Above-room-temperature operation of IV-VI microcavity lasers*", 10th Int. Conf. On II-VI Compounds , Bremen, Germany, Sept. 2001

45. T. Schwarzl, W. Heiss, G. Springholz, T. Fromherz, A. Raab, I. Vavra: "*Mid-infrared absorption of PbSe/PbEuTe quantum dot superlattices in IV-VI microcavities*", 7th Int. Conf. On Optics and Excitons in Confined Systems, Montpellier, France, Sept. 2001

46. M. Böberl, W. Heiss, T. Schwarzl, G. Springholz: "*IV-VI resonant-cavity photodetectors for the mid-infrared*", Int. Workshop on Microcavity Light Sources, Paderborn, Germany, April 2001

47. T. Schwarzl, W. Heiss, G. Springholz, S. Gianordoli, G. Strasser, M. Aigle, H. Pascher: "*Stark verstimmte Resonanzen in IV-VI Mikroresonatoren und Mikrodisks: Modenaufspaltung und Lasertätigkeit*", GMe-Forum 2001, Wien, April 2001

48. T. Schwarzl, W. Heiss, G. Springholz, K. Biermann, K. Reimann, M. Aigle, H. Pascher: "*Advances in IV-VI vertical emitting lasers: Above-room-temperature operation and quantum dots as active material*", IV. Int. Conf. on Mid-Infrared Optoelectronics Materials and Devices, Montpellier, France, April 2001

49. R.E. Balderas-Navarro, A. Bonanni, D. Stifter, H. Sitter, K. Hingerl: "*Reflectance difference spectroscopy during CdTe/ZnSe interface formation*", 8th Int. Conf. On the Formation of Semiconductor Interfaces (ICFSI-8), Sapporo, Japan, June 2001

50. R.E. Balderas-Navarro, A. Bonanni, D. Stifter, A. Montaigne-Ramil, H. Sitter, K. Hingerl: "*Collective dimer stress induced dichroism in II-VI semiconductors*", 10th Int. Conf. On II-VI Compounds, Bremen, Germany, Sept. 2001

51. K. Himmelbauer, H. Sitter, H. Krenn: "*Magnetic properties of thin iron films*", GMe-Forum 2001, Wien, April 2001

52. H. Sitter, A. Andreev: "*Kristalline dünne Filme aus Para-Hexaphenyl hergestellt mit Hot-Wall-Epitaxie*", GMe-Forum 2001, Wien, April 2001

53. H. Plank, R. Resel, J. Keckes, A. Andreev, H. Sitter, S. Purger, A. Thierry, B. Lotz: "*Epitaxial growth of para-sexiphenyl films on mica characterized with x-ray diffraction pole figure technique*", 10th Int. Conf. On Modulated Semiconductor Structures (MSS10), Linz, Austria, July 2001

54. A. Andreev, C.J. Brabec, N.S. Sariciftci, P. Hinterdorfer, H. Sitter, G. Springholz, H. Plank, R. Resel: "*Investigation of highly ordered para-sexiphenyl structures by*

atomic force microscopy", European Material Research Society Meeting, Symposium P, Strassbourg, July 2001

55. H. Sitter: "*Hot-wall epitaxy – the method of choice for the growth of highly ordered organic epilayers*", Material Research Society Meeting, San Francisco, Symposium C, April 2001

56. A. Andreev, C.J. Brabec, N.S. Sariciftci, H. Sitter, G. Springholz, P. Hinterdorfer: "*Self-assembled growth of highly oriented para-sexiphenyl thin films controlled by elastic strain*", Material Research Society Meeting, San Francisco, Symposium C, April 2001

57. A. Andreev, H. Sitter, C.J. Brabec, R. Resel, H. Plank, N.S. Sariciftci: "*Morphology and growth of highly ordered para-sexiphenyl structures deposited by HWE*", Verhandlungen der Deutschen Physikalischen Gesellschaft, Symposium Organische Festkörper, Hamburg, March 2001

Doctor's Theses

Finished in 2001:

1. Dipl. Phys. Nils Sandersfeld: "*Modulationsdotierte Si/SiGe and Si/SiGeC Feldeffekttransistoren*"
2. Dipl.-Ing. Erik Thor: "*Untersuchung tiefer Störstellen in Si und SiGeC*"

Current works:

1. Dipl. Phys. Anke Hesse: "*Strukturelle Untersuchungen an Halbleiternanostrukturen*"
2. Dipl. Phys. Tobias Schülli: "*Magnetic Nanostructures: GID and XMCD investigations*"
3. Dipl. Ing. Michael Mühlberger: "*Epitaktisches Wachstum von modulationsdotierten Si/SiGe Si/SiGeC Heterostrukturen*"
4. Dipl. Ing. Adrian Prinz: "*Untersuchung von Lokalisierungseffekten in Halbleiterstrukturen mittels Magnetotransport*"
5. M.Sc. Tomas Roch: "*Characterization of semiconductor nanostructers*"
6. Dipl. Ing. Karin Wiesauer: "*Scanning tunneling microscopy studies of dislocation structures in IV-VI heterostructures*"
7. Dipl. Ing. Anneliese Raab: "*Molecular beam epitaxy of self-assembled IV-VI quantum dots*"
8. Mag. Rainer T. Lechner: "*Herstellung und Charakterisierung von EuSe-Nanostrukturen*"
9. Dipl.-Ing. Gernot Fattinger: "*Methoden zur statistischen und dynamischen Charakterisierung von Mikrostrukturen*"
10. Dipl.-Ing. Gudrun Kocher-Oberlehner: "*Er-dotiertes Si und SiGe für optoelektronische Anwendungen im Bereich von 1,54 μm*"

11. M.Sc. Alberto Montaigne-Ramil: "*Fabrication and ex-situ characterization of wide band gap semiconductor materials*"
12. Dipl.-Ing. Klaus Schmidegg: "*Growth and optical characterization of GaAlN and GaInN*"
13. Dipl.-Ing. Thomas Schwarzl: "*Vertikal emittierende Bleisalzlaser*"

Diploma Theses

Finished in 2001:

1. Georg Pillwein: "*Elektronische Eigenschaften von Halbleiterstrukturen bei tiefen Temperaturen*"
2. Thomas Berer: "*Herstellung und Untersuchung von Halbleiternanostrukturen*"
3. Daniel Gruber: "*Substitutioneller Kohlenstoff in dotierten Si/SiGeC Heterostrukturen*"
4. Eva Breuer: "*Untersuchungen an Halbleiternanostrukturen mittels Röntgenbeugung und -reflexion*"

Current works:

1. Wolfgang Schwinger: "*Transmissionselektronenmikroskopie an Halbleiternanostrukturen*"
2. Herbert Lichtenberger: "*Überwachsen und Charakterisierung strukturierter Si-Substrate*"
3. Mathias Simma: "*Photoleitungsuntersuchungen an Quantenpunkten*"
4. Stefan Griesser: "*Leitfähigkeitsmessungen an zweidimensionalem Elektronengas*"
5. Böberl Michaela: "*Bauelemente mit vertikalen Resonatoren basierend auf Blei-Salz-Metallstrukturen*"
6. Roither Jürgen: "*Mikroresonatoren aus dielektrischen Bragg-Spiegeln für lichtemittierende II-VI-Halbleiterbauelemente*"

Cooperations

1. Academy of Sciences, Bratislava, Slovakia
2. Aixtron, Aachen
3. Akademie der Wissenschaften, Troits, Moskau
4. Akademie der Wissenschaften, Warschau, Polen
5. AMS Unterpremstätten
6. Bosch (Stefan Holl), Linz
7. CENG Grenoble
8. CNRSM-PASTIS, Brindisi
9. Daimler Benz Reserach Laboratories Ulm, Dr. Presting, Dr. König

10. DESY, Hasylab, Hamburg
11. E+E Electronic GmbH, Engerwitzdorf
12. ELETTRA, Triest
13. ENEA, Roma
14. ESRF Grenoble
15. ETH, Zürich
16. FOM Institute Rijnhuizen, Niederlande
17. Fraunhofer-Institut (IAF) Freiburg (Chiptechnologie)
18. Heriot Watt University, Edinburgh, Scotland
19. High Magnetic Field Lab., Grenoble
20. High Pressure Research Center, Warschau, Polen
21. IAF Freiburg
22. IBM Research Center, Yorktown Heights
23. INFINEON Villach,
24. INSA, Lyon
25. Inst. f. Experimentalphysik I, Universität Bayreuth
26. Institut für Festkörperelektronik, TU Wien
27. Institut für Halbleiterphysik, Frankfurt/Oder
28. KEBA, Linz, Ing.G.Krippner
29. MIT, Cambridge, MA, USA
30. Nanoelectronics Research Center, University of Glasgow, Scotland
31. NIST, Gaithersburg, MD, USA
32. North Carolina State University, NC, USA
33. Philips Almelo, Niederlande
34. Philips Analytics, Almelo
35. Physics Department, Cornell University
36. Profactor, Steyr, Upper Austria
37. Purdue University, Lafayette, IN, USA
38. Sektion Physik, Ludwig-Maximilians Universität München
39. Sentech, Berlin
40. Siemens München, Dr.Heide
41. Siemens München, Zentrale Technik, Bereich Halbleiter
42. TASC Triest
43. Thomson, Paris
44. TU Berlin, Institut für Festkörperphysik

45. TU-München (Mikrowellentechnik)
46. Universität Bremen
47. Universität Graz, Institut für Experimentalphysik
48. Universität Paderborn
49. Universität Würzburg
50. Université de Montpellier
51. Universiteit Instelling, Antwerpen, Niederlande
52. University of Southampton, England
53. University of Warwick, Coventry, England
54. VOEST ALPINE, Linz, Dr.Angerer,
55. Walter Schottky Institut, TU München

Fourier Transform Infrared Spectroscopy of β-SiC Precipitation in SiGeC Epilayers

D. Gruber, T. Fromherz, M. Mühlberger, F. Schäffler

Institut für Halbleiter- und Festkörperphysik, Johannes-Kepler-Universität Linz, A-4040 Linz

1. Introduction

The ternary $Si_{1-x-y}Ge_xC_y$ alloy was considered a promising material for band structure engineering of Si-based heterostructures. However, in contrast to the binary $Si_{1-x}Ge_x$ alloys, which are completely miscible, C has a negligible solid solubility in both Si and Ge, and only one stable phase, that of SiC. This makes metastable $Si_{1-x-y}Ge_xC_y$ alloys with useful C concentrations of a few tenths of a percent unstable against the formation of β-SiC precipitates. A typical example is shown in Fig. 1: The high-resolution cross sectional transmission electron micrograph (XTEM) shows incoherent β-SiC precipitates in a single crystalline Si matrix. Since Si and β-SiC differ in their respective lattice constants by about 20%, a Moiré pattern becomes observable at places where relaxed β-SiC precipitates are surrounded by undisturbed Si. The spacing of the Moiré pattern depends on the difference of the two lattice constants, and thus allows an unambiguous identification of β-SiC.

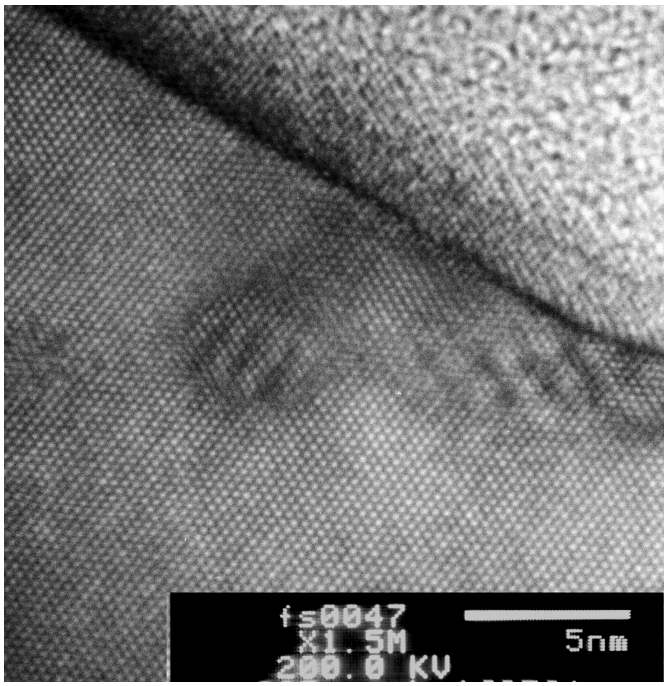

Fig. 1: XTEM micrograph of β-SiC precipitates in a Si matrix. Individual Si [111} lattice planes with a spacing of 3Å are resolved. The β-SiC precipitates lead to a Moiré pattern because of their 20% smaller lattice constant.

β-SiC precipitation restricts the potential use of $Si_{1-x-y}Ge_xC_y$ alloys to applications that can either be kept far from thermal equilibrium or require very small amounts of carbon. The most interesting of these applications is the exploitation of substitutional carbon (C_S) for the suppression of transient enhanced diffusion (TED) of Boron in Si/SiGe:C heterobipolar transistors. But even though the required C concentrations are reasonably low (0.2 at.%), high temperature annealing steps are unavoidable during standard Si technology. It is therefore necessary to optimize the layer parameters and thermal budgets.

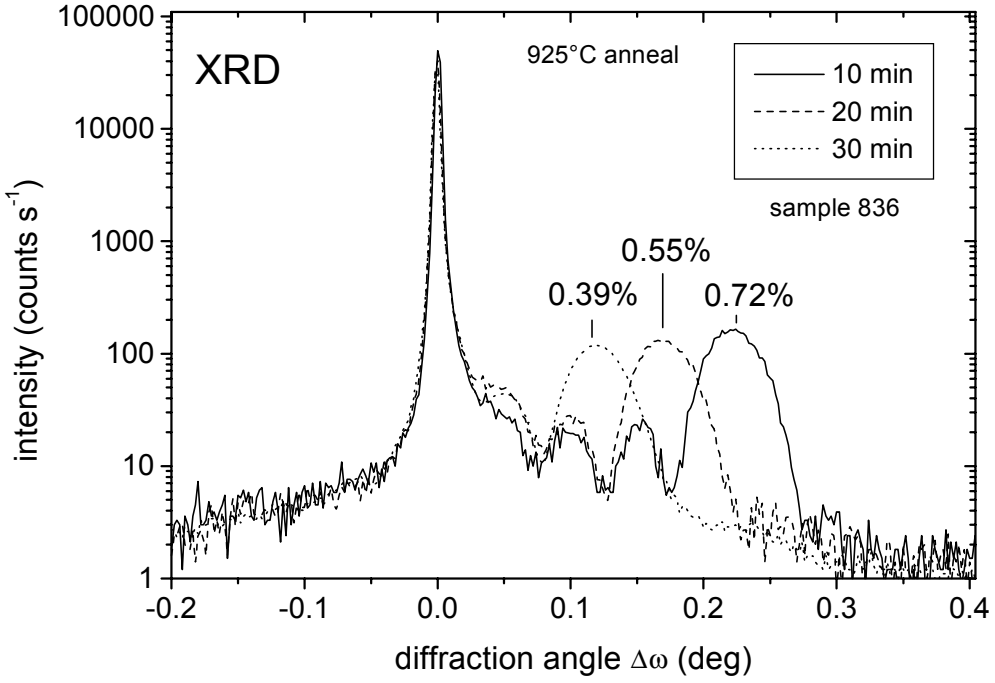

Fig. 2: X-ray rocking curves of $Si_{1-y}C_y$ films that underwent annealing at 925 °C for increasing periods of time. The (smaller) $Si_{1-y}C_y$ peak moves toward the (dominant) substrate peak with prolonged annealing time, indicating gradual relaxation of the film stress. The curves are labeled with their remaining substitutional carbon concentration y_{eff} that has to be compared to y = 1% of the as-grown sample.

2. Experimental

Based on the standard AIST procedure for the characterization of C_S in bulk Si, we exploit the local vibration modes of C to identify the local chemical environment [1]. This gives access not only to the concentration of C_S, but also to pseudomorphic and incoherent β-SiC precipitates. Problems are the small absolute concentrations of either type of C bonds in the thin epilayers under study, and the presence of a Si phonon mode that overlaps the relevant frequency range of the local modes. It is therefore essential to achieve high sensitivity and accurate subtraction of the bulk signal. These aims were achieved by employing Fourier Transform Infrared Spectroscopy (FTIR), and thickness corrections for the reference bulk sample with an accuracy of a few μm. The latter was achieved by a first FTIR reference measurement with high resolution (cm^{-1}), which

gives access to the sample thickness via the thickness interference fringes of the plan-parallel, one-sided polished substrates. For the subsequent measurement of the local carbon vibration modes the resolution was then lowered to 4 cm^{-1} to suppress the thickness fringes.

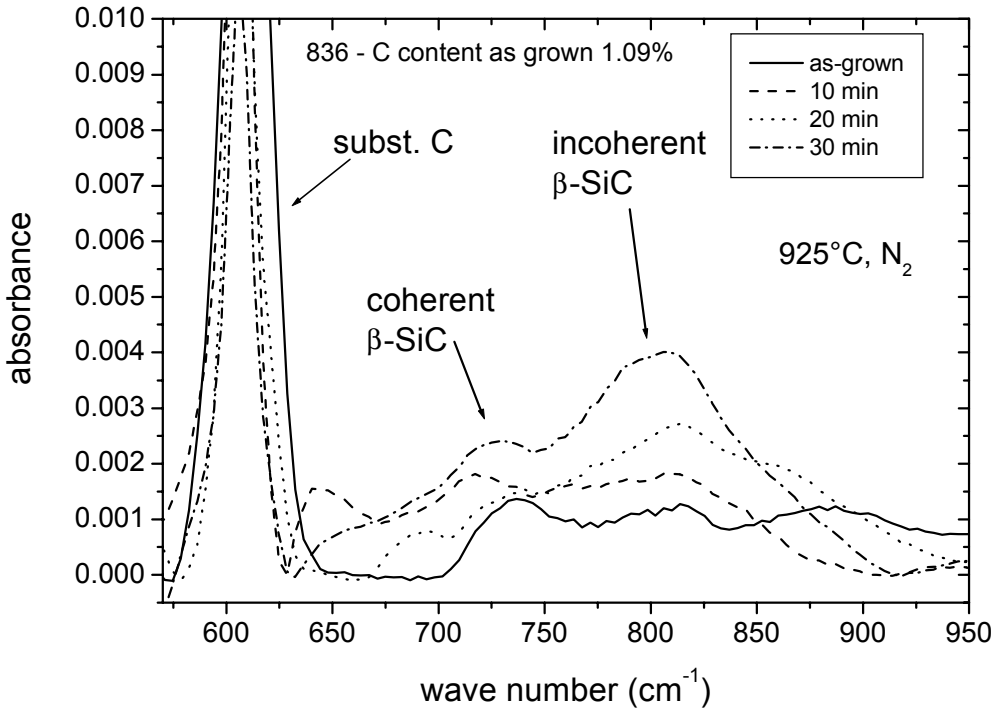

Fig. 3: FTIR spectra of the sample in Fig. 2 in the frequency range of the carbon-related local vibration modes. With increasing annealing time more and more carbon moves from substitutional into SiC sites.

3. Results

Figures 2 and 3 show typical results of 100 nm thick $Si_{0.99}C_{0.01}$ films annealed at process temperatures of 925 °C for various times. The x-ray rocking curves in Fig. 2 reveal a substantial amount of film relaxation, with <40% of the originally present C remaining at substitutional sites. This can directly been followed in the attenuation of the local C_s mode at 608 cm^{-1} in the FTIR spectra of Fig. 3. Simultaneously, the signals at 750 and 820 cm^{-1} gain intensity, indicating that coherent, and incoherent β-SiC, respectively, have formed, which are the main sources of strain relaxation in these films.

To study the time scale for complete film relaxation, similar films were annealed at 1000 °C for extended periods of time. Under these conditions we found that after 240 min the films were completely relaxed: The local mode of substitutional C has then vanished, and most of the C has formed incoherent β-SiC precipitates (Fig. 4). Correspondingly, no $Si_{1-y}C_y$-related signal can be observed in the x-ray rocking curves.

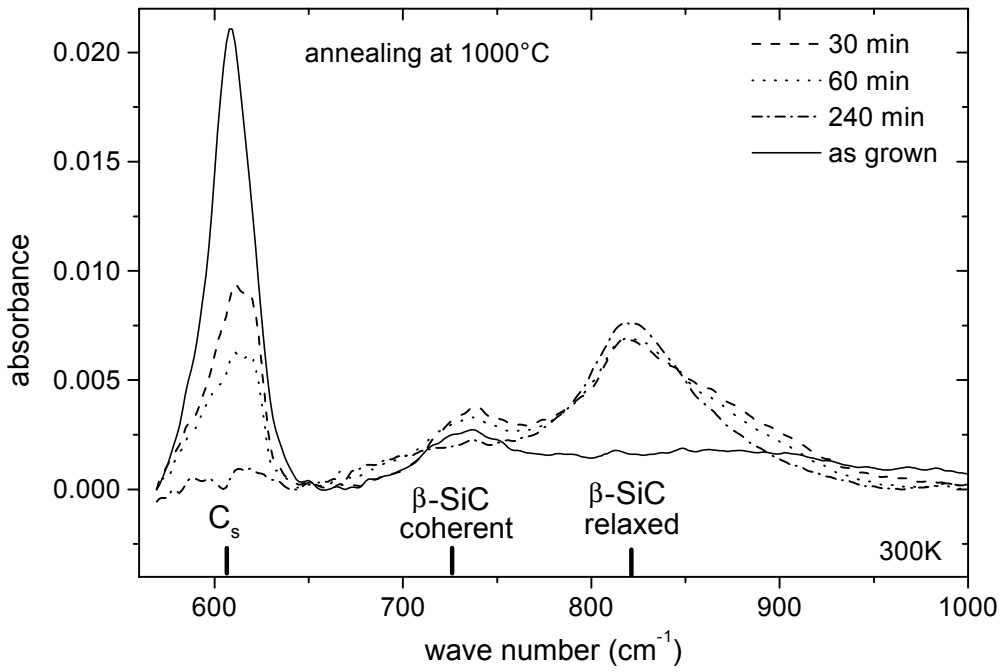

Fig. 4: Same as Fig. 3 but annealing at 1000 °C for extended periods of time. Note that substitutional carbon has completely disappeared after 240 min at 1000 °C.

4. Conclusion

The results have important implications for the application of $Si_{1-x-y}Ge_xC_y$ films. Typical processing temperatures during standard Si technology are comparable to our experimental range, with 925 °C being a rather low limit for the activation of implanted contact regions. However, processing times are significantly shorter than in our oven anneals, typically on the order of 1 min (rapid thermal processing [RTA]). Our experiments show that the formation of β-SiC precipitates is a rather slow process, provided the C concentrations are kept at low enough levels. Hence, even 1000 °C RTA steps may be acceptable, if processing steps are kept low enough. However, generally both the C concentration and the thermal budget of the process should be kept as low as possible. In any case, monitoring of the complete device processing with respect to β-SiC precipitation is important. FTIR is the technique of choice with respect to sensitivity and selectivity of different carbon environments. Of course, electrical measurements of e.g. the generation/recombination behavior are required in addition.

References

[1] D.Gruber et al., *Mat. Sci. Eng*. **B89**, 97 (2001)

Growth Phenomena of Si/$Si_{1-x-y}Ge_xC_y$ Epilayers and Superlattices

H. Lichtenberger, W. Schwinger, A. Halilovic, M. Teuchtmann, F. Schäffler

Institut für Halbleiter- und Festkörperphysik, Johannes-Kepler-Universität Linz, A-4040 Linz

Heteroepitaxial growth allows the reduction of the dimensionality of a carrier system along the growth direction by exploiting carrier confinement at heterointerfaces. A further reduction to 1D and 0D systems requires in addition either lateral structuring or a self-organized growth scheme. We investigate both approaches in the $Si_{1-x-y}Ge_xC_y$ heterosystem by using epitaxial growth on pre-patterned substrates and a novel route to quantum dots with mono-modal size distribution.

1. Introduction

The investigation of low-dimensional structures becomes increasingly relevant as critical dimensions of commercial devices reach the nanometer range. Presently, devices with gate lengths of 65 nm are in large scale production (130 nm technology node), and the SIA roadmaps predict critical dimensions of 9 nm for 2016. This top-down-approach by down-scaling of existing technologies has in recent years been supplemented by attempts to use self-assembling growth phenomena for the fabrication of 1D and 0D quantum systems. Here we report on two such attempts in the $Si_{1-x-y}Ge_xC_y$ material system, namely the epitaxial overgrowth of pre-patterned substrates, and the growth of SiC quantum dots. This material system is of special interest because of its compatibility with standard Si technologies.

2. Morphological Development of Si Wire Templates During Annealing and Overgrowth

The exploitation of structured substrate templates is an attractive option both in connection with self-organization growth modes, and for improved defect control of relaxed SiGe buffer layers. On Si(001) substrates we prepared wire structures with periods down to 300 nm by holographic lithography and reactive ion etching. The photoresist and RIE residues were removed wet-chemically, and just before MBE growth a thermal cleaning step was performed *in situ* at 900 – 950 °C. We found an unexpectedly large surface mass transport even at these temperatures, which are significantly below the melting point of Si (1330 °C). Wires of square or a slight trapezoidal cross section develop pronounced {311} facets, concomitant with a significant loss of height. Overgrowth with SiGe superlattices partly reestablish the (001) top facet, which becomes wider with increasing epilayer thickness (Figs. 1, 2). These results have important implications for the shape preservation of structured substrates during annealing and overgrowth.

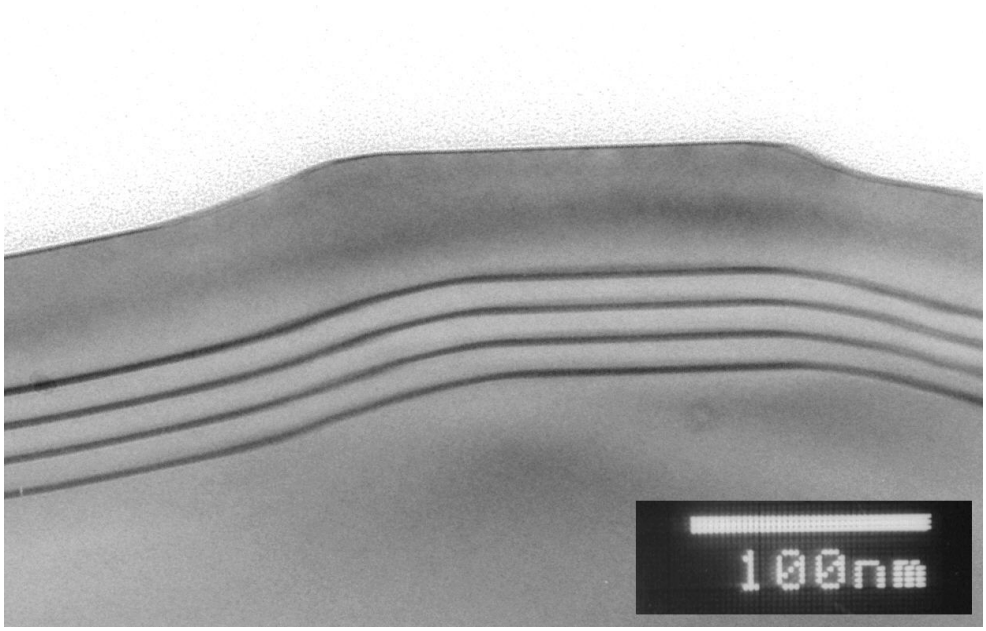

Fig. 1: XTEM image of a Si wire structure overgrown by a Si/SiGe superlattice. Thermal annealing led to substantial mass transport on the Si template that transformed the slightly trapezoidal wire cross sections into flat wires with [311} side facets.

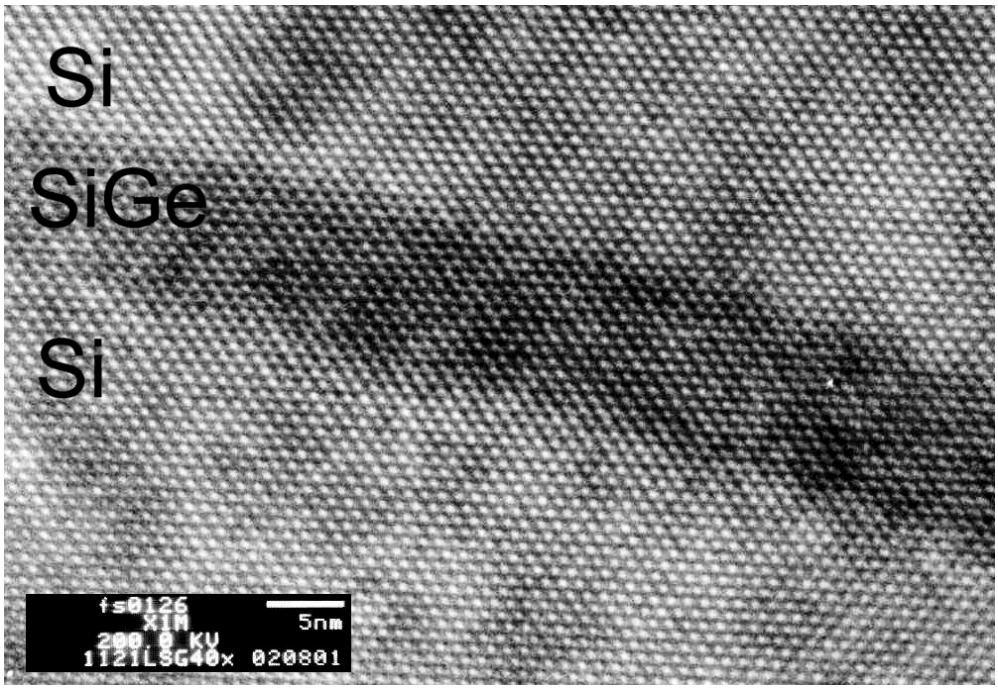

Fig. 2: High resolution XTEM of the superlattice in Fig. 1. The image was taken in a region where the (001) top facet is gradually transformed into a {311} facet that was created by thermal cleaning of the wire-structured substrate.

3. β-SiC Formation

Carbon concentrations exceeding the solid solubility limit of about 10^{17} cm^{-3} lead to β-SiC precipitation near thermal equilibrium. This can be a detrimental effect if it happens, e.g., during processing of high-speed SiGeC heterobipolar transistors (see separate report on FTIR spectroscopy of C-complexes in Si). On the other hand, such β-SiC precipitates may be useful for the creation of quantum dots in Si. For that purpose carbon clusters of well-defined size are incorporated into a Si matrix and subsequently converted into β-SiC by high temperature annealing. Especially attractive appear the use of Fullerens (C_{60}), or of defined fractions of these molecules which became available recently, because they would allow a mono-modal size distribution of the β-SiC clusters. Because of the larger band gap of β-SiC the clusters are not quantum dots themselves, but they can be used as stressors to induce carrier confinement in the surrounding Si matrix or in a near-by SiGe layer.

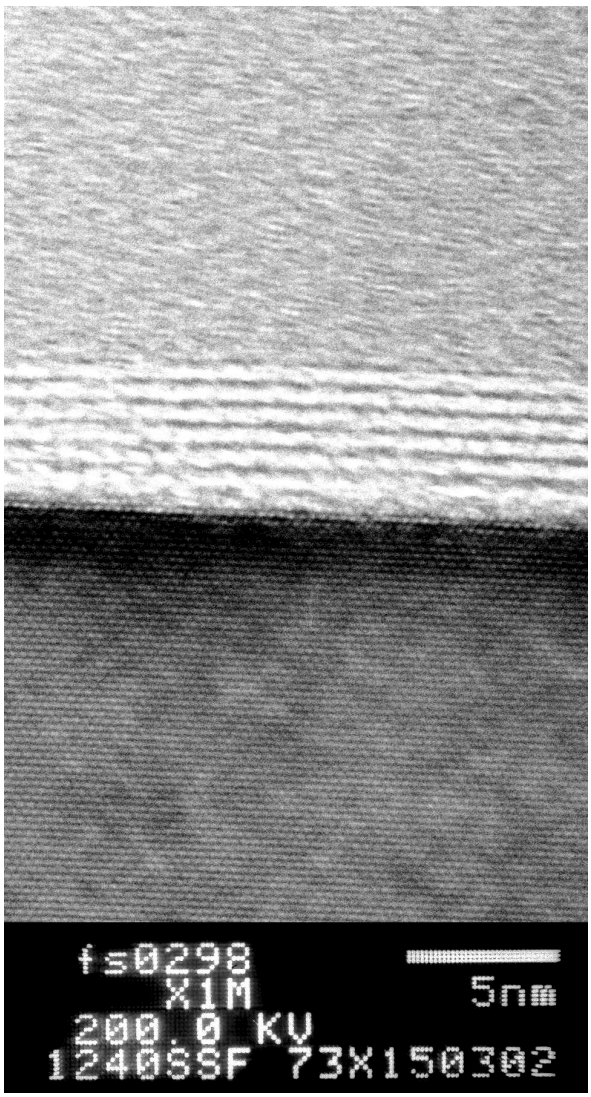

Fig. 3: Layer sequence for the calibration of the C_{60} source. In the XTEM micrograph 7 monolayers of Fullerens can be seen. The lower layer is crystalline Si(001) (point resolution is 0.32 nm), above the Fulleren layer an amorphous Si cap layer has been deposited.

The experiments are performed in a newly commissioned growth chamber for the deposition of Fullerens, which is attached to the our Siva 45 Si-MBE machine. To calibrate the flux of the Fulleren source, relatively thick layers were deposited on a Si substrate at room temperature and subsequently capped by amorphous Si. Figure 3 shows a high resolution XTEM image of such a layer sequence. Seven monolayers of C_{60} on the crystalline Si substrate can be distinguished. Because of the low deposition temperature, the C_{60} layer is polycrystalline. With flux calibration from Fig. 3, submonolayer C_{60} coverages were deposited at 300 K, capped by 5 nm of amorphous Si, annealed at 1200 °C, and finally overgrown by 15 nm of crystalline Si. Figure 4 shows an example of such a layer sequence. SiC clusters are clearly distinguishable through a Moiré pattern that develops when crystalline materials with different lattice constants are contained within the thickness of the TEM specimen. In addition, defective solid phase overgrowth can be seen above one of the SiC particles. The size of the SiC inclusions is on the order of 5 nm, i.e. much larger than expected from the reaction of an individual C_{60} molecule. Obviously, even at the low deposition temperatures employed, clustering of Fullerens must have taken place. Further experiments are required to demonstrate the feasibility of SiC particles created from isolated C_{60} molecules. The aim is to optimize the growth parameters until pseudomorphic β-SiC clusters of identical size and strain fields can be produced.

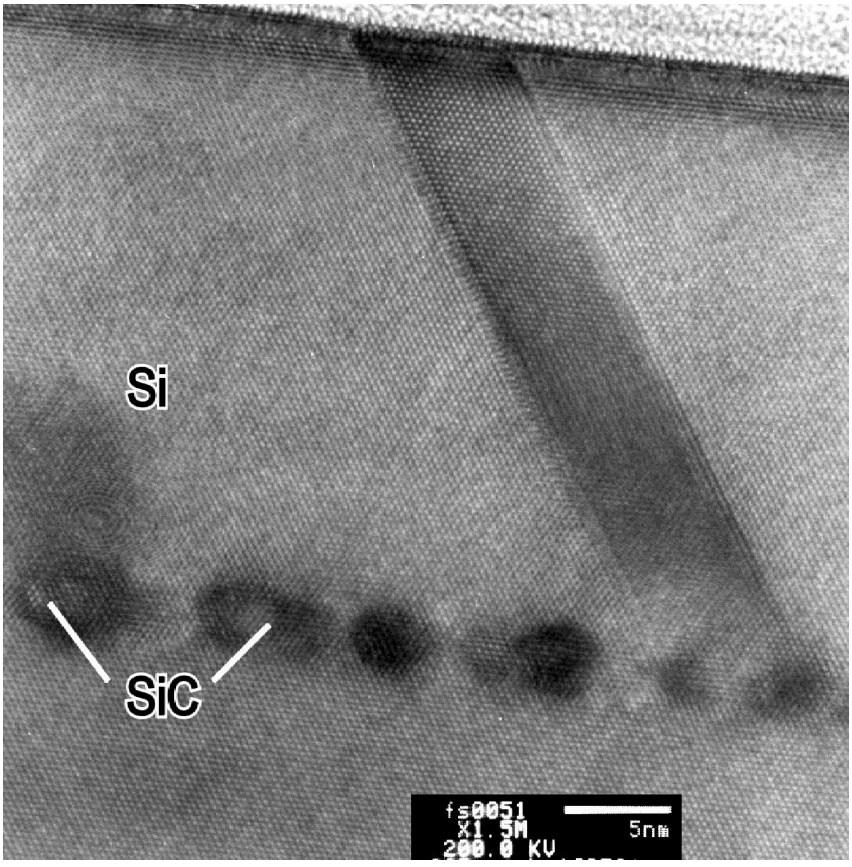

Fig. 4: β-SiC nanocrystals generated by high-temperature annealing of Fulleren clusters that were capped by amorphous Si. The contrast results from lattice distortions and partial dislocations that have formed around the incoherent β-SiC nanocrystals.

4. Conclusions

Two approaches are followed to produce 1D and 0D structures in the $Si_{1-x-y}Ge_xC_y$ heterosystem. In both cases unexpected growth phenomena were encountered, which require further optimization of the growth parameters. The use of Fullerens for the implementation of mono-modal quantum dots appears promising, but requires addition experiments to suppress clustering of the weakly bound C_{60} molecules.

Acknowledgements

This work was financially supported by OeNB, Land Oberösterreich, and GMe.

Results on a HEIFET Including The Gunn Effect

E. Kolmhofer, K. Luebke, H. Thim
Microelectronics Institute, University of Linz, Austria

A modified version of our 'Hot Electron Injection Field Effect Transistor', utilizing the Gunn effect to enhance microwave performance, is presented. The necessary changes to the device structure and measurement results are given.

1. Introduction

The purpose of the work reported is to present the recent modifications which we applied to our **H**ot **E**lectron **I**njection **F**ield **E**ffect **T**ransistor (HEIFET). In our modified structure the ohmic source and drain contacts of a MESFET are both replaced by a combination of an ohmic contact and a Schottky contact. In addition we tried to enhance the function of our device by utilization of the Gunn effect.

2. Layout Modifications

In our opinion in the HEIFET structure reported in [1] the most critical geometrical parameter is the separation between the MESFET gate and the overlapping gate. Due to improvements in our electron beam lithography system we have been able to reduce the length of the MESFET gate to values around 0.4 µm and the separation to values around 0.3 µm. Unfortunately these and other modifications indicated in [1] failed to raise our transistor's frequency limits significantly. Particularly the transit frequency of the unilateral power gain f_{max} (maximum frequency of oscillation) remained below our expectations. In order to improve the microwave behavior of our devices we decided to utilize the Gunn effect.

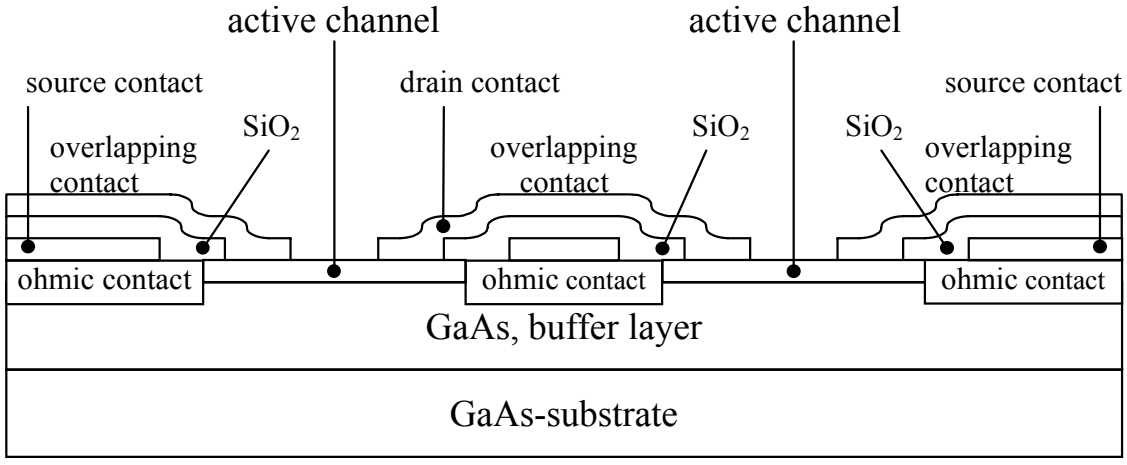

Fig. 1: Cross sectional view of the modified HEIFET.

In GaAs the Gunn effect weakens with increasing doping density and almost completely disappears at the value of $N_D = 2 \cdot 10^{17}$ cm^{-3} which we used. Therefore a reduction to $N_D = 4 \cdot 10^{16}$ cm^{-3} was necessary. The reduction of drain saturation current coming along with a lower N_D has been remedied by increasing the channel's width and thickness. The second significant modification was replacing the MESFET gate with a gate overlapping the ohmic drain contact. Figure 1 shows a cross sectional view of the modified HEIFET structure.

3. Measurement Circuit

The microwave probing of the devices, manufactured in the cleanroom of the Microelectronics Institute, has been carried out on a Cascade Microtech waverprober using a HP 8510C vector network analyzer. Since our waverprober is equipped with ground-signal-ground coplanar probes the transistors have been built symmetrically resulting in the layout shown in Fig. 2.

Fig. 2: Symmetric layout of the measurement circuit.

The symmetric layout of the transistor and the circuit help in avoiding measurement errors which arise from unsymmetrical modes in the GSG waverprobing setup. Furthermore the use of two channel regions helps in achieving the necessary width of the device. For biasing the ohmic and the Schottky drain contact the bias-tees built into the HP 8510C can be used.

4. Results

Using the setup described above the modified HEIFETs have been measured in a frequency range from 45 MHz to 50 GHz. Figure 3 shows typical deembedded S-parameters of one of our devices while Fig. 4 shows the unilateral power gain U calculated from these S-parameters. From Fig. 3 and Fig. 4 it is obvious that the device operates up to a frequency of 45 GHz. The unilateral power gain determines the maximum frequency of oscillation reachable with a device which is therefrom found to be 45 GHz.

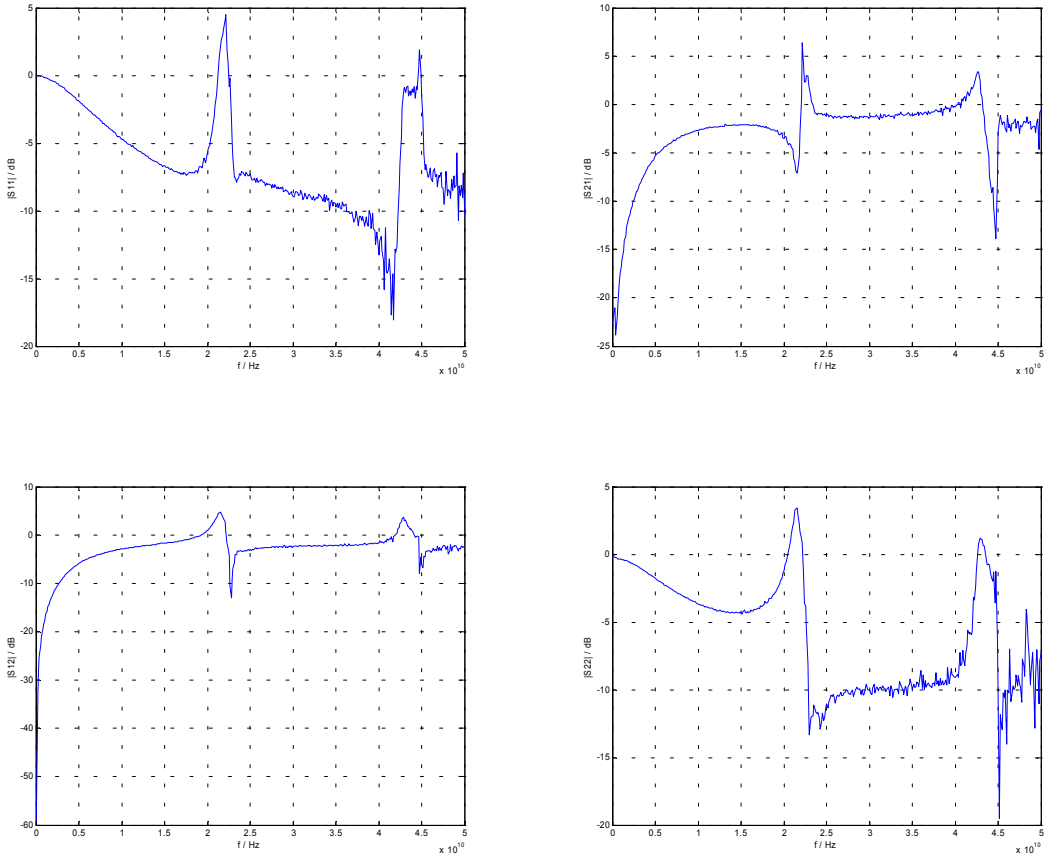

Fig. 3: Deembedded S-parameters of a modified HEIFET.

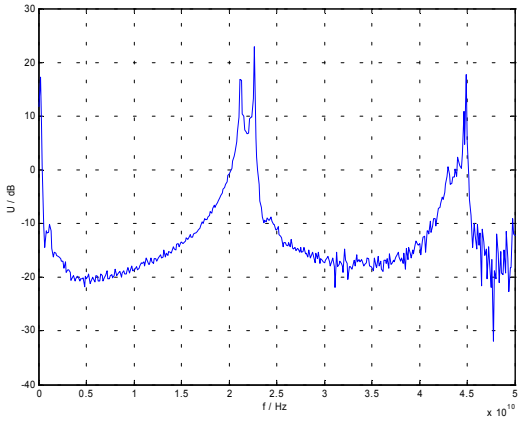

Fig. 4: Deembedded unilateral power gain of a modified HEIFET.

5. Conclusion

The modifications applied to the HEIFET helped to raise the upper limiting frequency of the HEIFET to at least 45 GHz which can largely be attributed to the utilization of the Gunn effect. Operation of our actual HEIFETs could be possible at even higher frequencies which currently lie beyond our measurement capabilities. Further experimental work will include the design of HEIFET based oscillator circuits.

Acknowledgements

The authors would like to thank M. Hinterreiter and J. Katzenmayer for fabricating the devices. This work is supported by the Austrian Science Foundation (FWF) under contract No. P12702 TEC.

References

[1] E. Kolmhofer, K. Luebke, H. Thim, “Hot Electron Injection Field Effect Transistor”, *Annual Report 2000*, Society for Microelectronics.

Electrical Investigations on Quantum Point Contacts

T. Berer[1], G. Pillwein[1], G. Brunthaler[1], G. Strasser[2]

[1]Institute for Semiconductor Physics, Univ. Linz, Austria

[2]Institute for Solid State Electronics, TU Vienna, Austria

Quantum point contacts were fabricated from a two-dimensional AlGaAs structure by electron beam lithography in different techniques. Best electrical characteristics were achieved in split gate geometry. The resistance steps due to lateral quantization of the electron gas were observed. In addition conductance peaks in the high ohmic region due to Coulomb blockade of a random quantum dot appeared in the same samples. The diameter of the random quantum dot was estimated to be about 80 nm.

1. Introduction

In order to raise the skills in fabrication and investigation of quantum nanostructures, two diploma works were performed at the Institute for Semiconductor Physics in Linz. The main subject of the first work was the preparation of the structures, whereas the goal of the second work was its electrical characterization at low temperatures. The final goal of the project is to contribute to the upcoming quantum information technology.

2. Experimental

Quantum point contacts were prepared on high-mobility GaAs/AlGaAs Hall bars grown by MBE. The Hall bars were defined by conventional optical lithography and prepared by wet chemical etching [1]. For the point contacts different techniques were compared. Point contacts with deep etched sidewalls are sometimes not conducting due to the depletion layer along the damaged surfaces. Quantum point contacts which were defined by split gates on top of the Hall bars showed a better controllability and reproducibility. Images of such structures are shown in Fig. 1. The lateral opening of the point contacts is about 300 nm.

The structures were investigated at low temperatures of 1.4 K (^{4}He cryostat) and of 300 mK (^{3}He cryostat) with and without magnetic fields. When a negative gate voltage V_g is applied to the split gate fingers, the two-dimensional (2D) electron gas layer is depleted just below. This can be seen for sample BT-482 in Fig. 2 (a), where the resistance increases from region “a” to region “b”. The current which flows along the Hall bar then can pass the gated region only through the narrow constriction in the 2D layer. Inside the quantum point contact, the electron wave is quantized in lateral modes. When the negative gate voltage is further increased, the lateral opening of the point contact is reduced and the number of occupied modes below the Fermi energy decreases. This is visible in a stepwise increase of the resistance of the quantum point contact in region “c” of Fig. 2 (a).

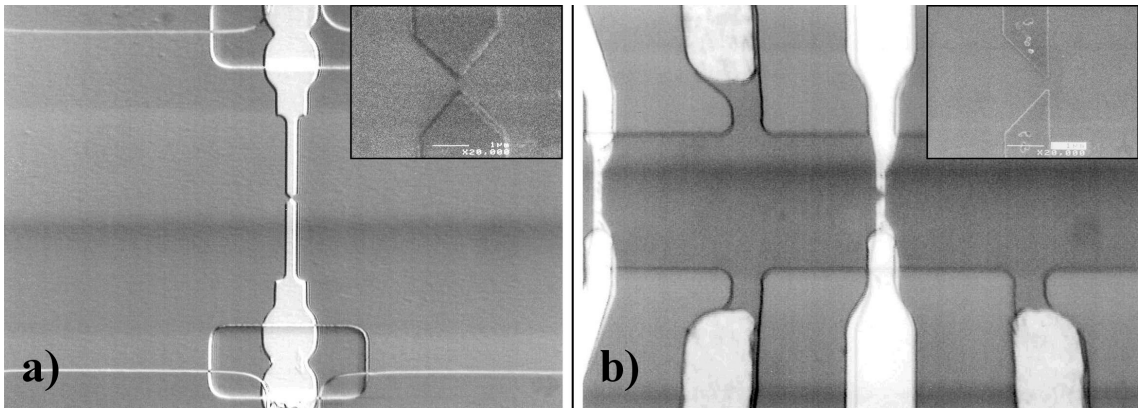

Fig. 1: Optical microscope pictures of split gate point contacts for samples a) BT-482 and b) BT-489. Details of the point contacts are shown in SEM-images as insets at the upper right corners.

In sample BT-489, in addition to the steps also peaks in the resistance are visible (see Fig. 2 (b)). These peaks in the resistance correspond to minimums in the conductance. It will be shown in the following that the conductance minimums correspond to the Coulomb-blockade regime of a random quantum dot inside the point contact [2]. Such a quantum dot can easily be formed by the potential fluctuations due to the remote doping centers and is illustrated in an inset in Fig. 2 (b).

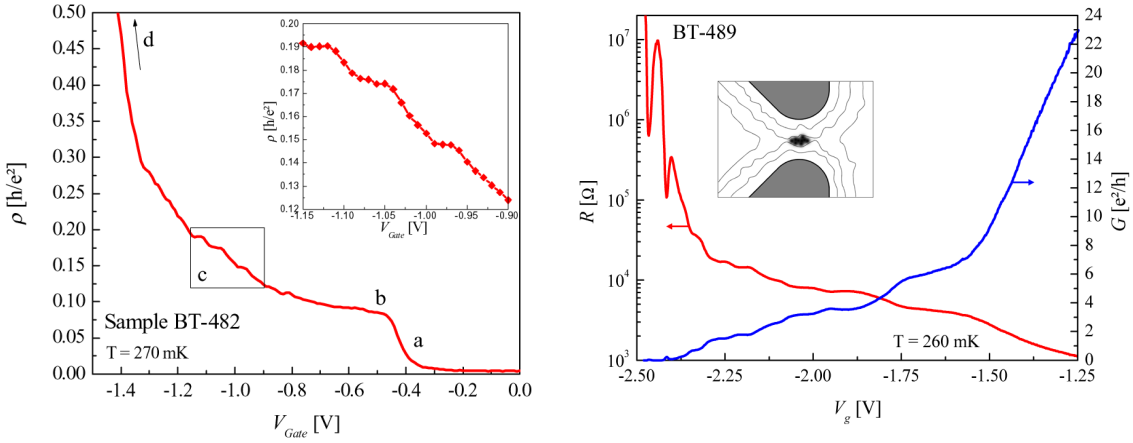

(a) (b)

Fig. 2: (a) Resistance of sample BT-482 versus split gate voltage. Different regions of the 2D electron gas depletion and channel narrowing are visible. (b) Peaks in the resistance of sample BT-489 due to Coulomb blockade in a random quantum dot. The inset shows schematically how such a random dot could appear.

It is well known that due to the small size of a quantum dot, an additional single electron increases the potential of the dot so strongly that no further electron can enter. This is the Coulomb blockade regime. In order to test this behavior, a large source-drain voltage V_{sd} across the quantum dot can be applied. If the voltage is large enough that it shifts the next electronic level below the Fermi energy at one side, an additional electron can enter the dot and leave at the lower Fermi energy side. Thus the conductivity increases.

Fig. 3 (a) shows the differential conductance versus V_{sd} for the case that the Fermi energy is about in the center of the Coulomb gap. In comparison, Fig. 3 (b) shows the situation where the total energy of the n and the n+1 electron states are equal and the Coulomb gap is not effective. The conductance is than high at zero source-drain voltage.

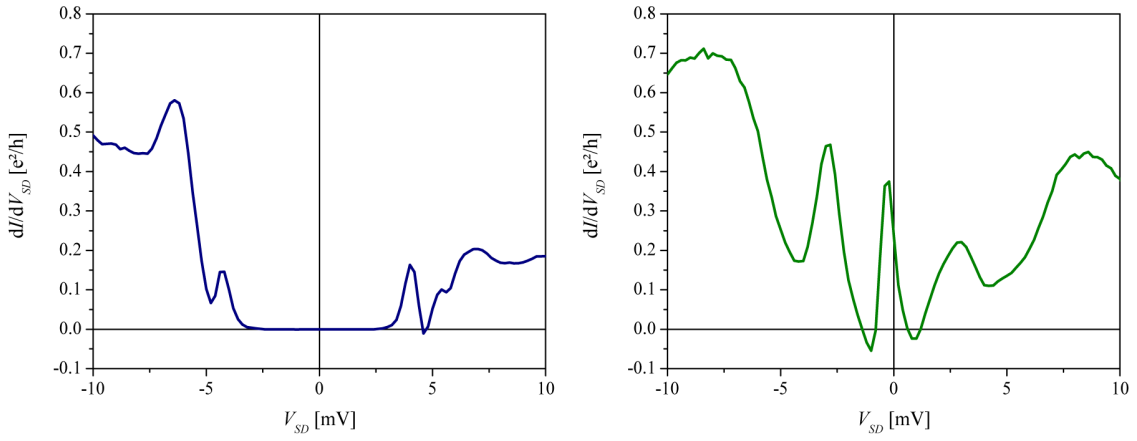

(a) (b)

Fig. 3: Differential conductance as a function of the source-drain voltage (a) in the Coulomb blockade regime and (b) in the conducting regime of a random quantum dot inside the point contacts of sample BT-489.

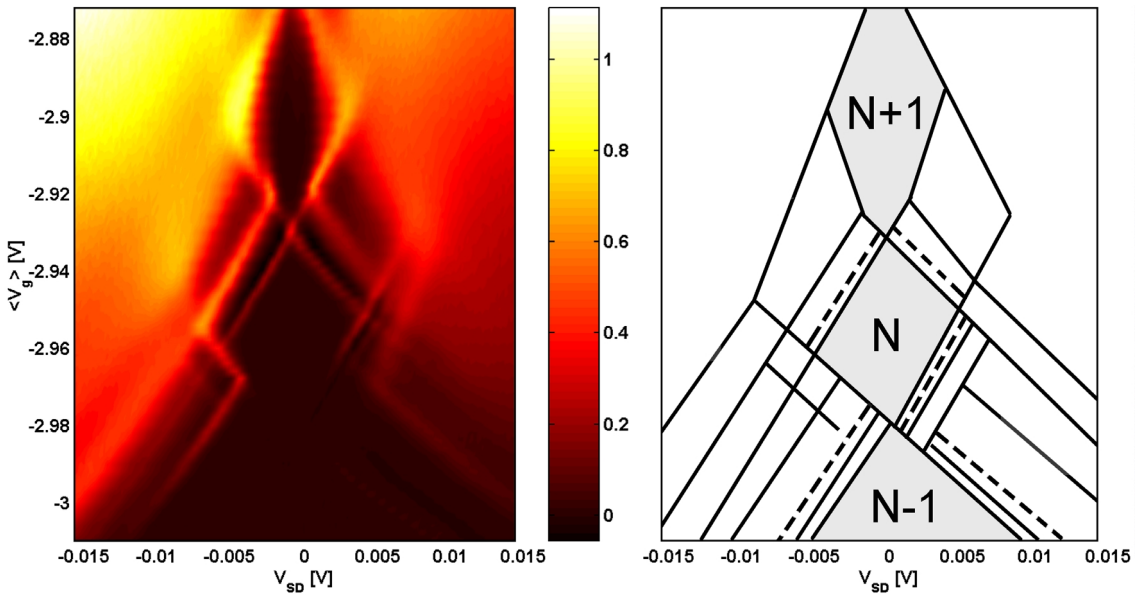

(a) (b)

Fig. 4: Conductance spectrum of the quantum dot in sample BT-489. (a) Two-dimensional grayscale plot of the differential conductance $G = dI/dV_{SD}$ measured versus source-drain voltage V_{SD} and gate voltage V_g. (b) Schematic diagram of the same data showing only the main features.

Figure 4 (a) shows the grayscale plot of the differential conductance. The horizontal axis corresponds to the source-drain voltage, the vertical axis to the split gate potential. The

lighter areas correspond to higher conductance values. The same information is shown in Fig. 4 (b) in a schematic diagram. In Fig. 4 (b) one can see that the Coulomb blockade regimes form diamond-like shapes. At certain gate voltages, the necessary source-drain voltage in order to get conductivity through the quantum dot vanishes whereas at other source-drain voltages it is quite large. The solid lines in Fig. 4 (b) correspond to maximums in the differential conductance whereas the dashed lines mark regions of negative differential conductance. Such a decrease in the conductance with increasing source-drain voltage appears when an additional excited states opens up which has a slow transfer rate and thus blocks the quantum dot partly.

A detailed analysis of the different voltages reveals the most important dot parameters. From the vertical separation ΔV_g = 48 meV of the conductance peaks in Fig. 4, a gate capacitance of 3.3×10^{-18} F can be estimated. The slopes of the conductance peaks lead to a total capacitance of 32×10^{-18} F, which determines an absolute energy scale of the quantum dot. The Coulomb gap thus corresponds to a relative large energy of E_C = 5 meV. The additional lines parallel to the Coulomb diamonds in Fig. 4 correspond to conduction through excited states of the quantum dot. From the energetic separation of the excited states in the energy spectrum the density of states can be estimated which gives a rough hint about the size of a small two-dimensional object. According to that, the dot has a diameter of about 80 nm, which is quite small.

3. Conclusion

Quantum point contacts were fabricated in 2D-AlGaAs heterostructures by electron beam lithography. The point contact structures showed the expected quantization steps in the resistance. In addition, a random quantum dot inside a quantum point contact could be characterized as well. With the acquired know-how in the fabrication of nanostructures it is planned to continue the work on quantum dots and to prepare especially coupled dot structures in order to investigate the elementary processes for quantum information.

References

[1] T. Berer, G. Pillwein, G. Brunthaler, and G. Strasser: “Fabrication of AlGaAs quantum wires”, in *Proceedings of GME Forum*, Vienna 2001, p. 159.

[2] U. Meirav and E.B. Foxman: “Single-electron phenomena in semiconductors”, *Semicond. Sci. Technol.* **10**, 255 (1995).

Erbium in Silicon: Design Concepts and Luminescence Enhancement by Hydrogenation

G. Kocher[1], W. Jantsch[1], L. Palmetshofer[1], A. Ulyashin[2], Margarita Stepikhova[3]

[1]Univ. of Linz, Altenbergerstr. 69, A-4040 Linz, Austria
[2]Univ. of Hagen, Haldener Str. 182, PO Box 940, D-58084 Hagen, Germany
[3]Russ. Academy of Science, Nishny Novgorod, Russia

Si:(Er,O) based light emitting diodes were developed and fabricated, emitting at room temperature in the breakdown regime at a wavelength of 1.54 µm. By adjusting the diode design we were able to increase the electroluminescence (EL) intensity by one order of magnitude. We also investigated codoping with hydrogen in order to increase the luminescence. With this we achieved an increase of the luminescence intensity at temperatures below 150 K by a factor of five.

1. Introduction

Ever since the first report on the observation of 1.5 µm photoluminescence (PL) due to Er in Si by Ennen and Schneider [1], [2] erbium doped semiconductors have attracted a lot of attention as it seemed to indicate a way to obtain temperature stable emission at a well defined wavelength [3]. Room temperature electroluminescence at 1.54 µm in Si diodes due to intra-atomic transitions of erbium is achieved via excitation of SiO_2:Er clusters by hot electrons injected in a reverse biased diode. Impact excitation of erbium and thus electroluminescence can be achieved in tunneling diodes, although at very small excitation volume, which would cover only a small fraction of a wave guide. Making use of an avalanche process allows to increase the excitation volume considerably [4]. This requires accurate control of doping gradients and thus knowledge of the electrical activity and the distribution of the implanted dopants. With data from SIMS and Hall effect investigations, which demonstrate significant deviations from TRIM simulations of the implantation profiles and the hitherto assumed electrical activity of Er in such environment, we were able to optimize the parameters for the design of our diodes and to increase the intensity of the room temperature EL by an order of magnitude.

In order to further increase the intensity of the luminescence, we used additional codoping of hydrogen in our samples. Hydrogen plasma treatment is widely used in semiconductor technology as a technological step in production. Hydrogen is known to enhance O_i diffusion and O_i precipitation in silicon [5]. Both characteristics should have a positive influence on Er-related luminescence in c-Si. Studies of the excitation dependence on power indicate a higher concentration of optically active Er in the hydrogenated samples. All samples showed a large enhancement of the luminescence by at least a factor of 5. The most prominent change appeared at annealing temperatures > 600 °C, with the appearance of the so-called “cubic center” which was previously observed only in samples with a low dose of Er and O [6].

2. Design Parameters for Diodes

An important property entering design considerations is of course the electrical activity of the Er centers. We investigated our SiO_x:Er precipitates by means of Hall effect measurements. The measurements were performed on samples prepared by implanting Er and O into high resistivity Si substrates. Whereas for isolated centers a large portion can be electrically active, for our sample we found that the sheet concentration of the free carriers is only a few percent of that of the incorporated Er ions after annealing.

In order to gain information on the actual structure of our diodes we applied SIMS for two different structures at various annealing temperatures. It turned out that the experimental values for the mean projected range Rp are about 20% larger than values obtained by simulation [7]. The experimental values for the range straggling, Rp, are almost twice as large as TRIM table values. The same discrepancy was found for Er implanted into amorphous SiO_2, so channeling effects appear unlikely as an explanation.

Due to the low electrical activity of Er under the preparation conditions used, this difference would not significantly change the electronic properties of a diode but it may crucially impair the optimal spatial overlap of the Er profile with the avalanche excitation volume.

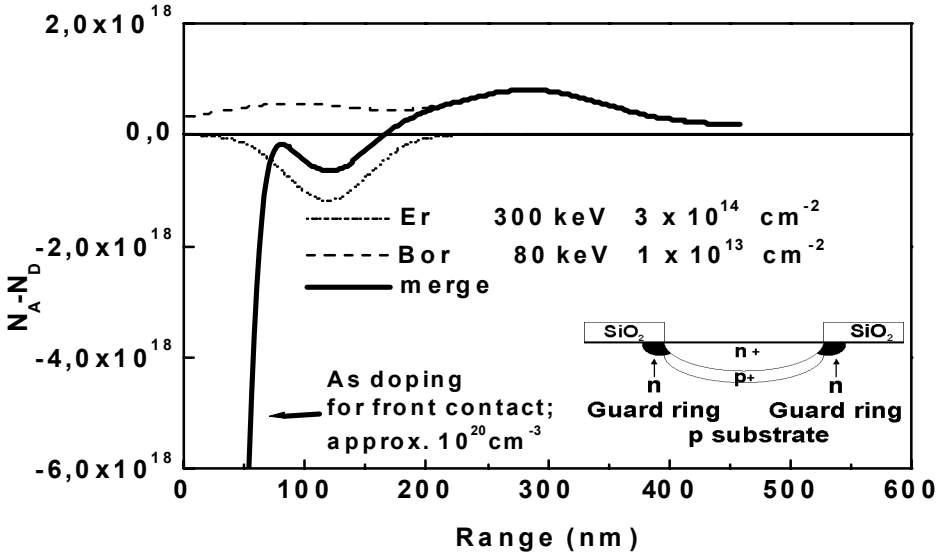

Fig. 1: Simulated doping profiles according to SIMS results. The insert shows a typical structure for an avalanche diode.

To adjust the doping gradient according to these results, we fitted the SIMS data with a Gaussian function containing exponential correction terms. A schematic diagram for our diode structure is shown as insert in Fig 1. Although the implantation energies stayed the same, the implantation doses and annealing procedure had to be changed according to the SIMS results. In order to avoid excessive diffusion of shallow dopants, a two step implantation and annealing procedure was adopted. After implanting Er and O and subsequent annealing at 1000 °C for 30 min, additional lithography and annealing steps were inserted for arsenic and boron, which provide the contact- and background doping respectively. To keep the diffusion low, the annealing temperature was lowered to 400 °C.

With the structure shown in Fig. 1 we were able to get room temperature luminescence of Er for excitation in reverse bias. The intensity of the luminescence increased at least one order of magnitude compared to a similar diode structure designed using TRIM code simulations only.

3. Hydrogenation

After implanting Er and O in c-Si ($1x10^{14}$ cm^{-2} / $1x10^{15}$ cm^{-2}, respectively) two sets of samples – one annealed at 600 °C/15 min. in N_2 atmosphere, the other "as implanted" – were hydrogenated using a plasma treatment for 1 hour at 260 °C. The samples were then annealed at various temperatures in the range of 450 °C to 1000 °C.

All samples showed large enhancement of the photoluminescence by at least a factor of 5. Comparing the intensity with non-hydrogenated samples, the hydrogenated samples show higher intensities at low annealing temperatures (400 – 450°C), then the intensity decreases, reaches a minimum at 600 °C and starts to rise again. It is much higher than in the non-hydrogenated samples at 800 and 900 °C. At annealing temperatures higher than 700 °C the so called "cubic center", which was previously observed only in samples with low concentration of Er and O, started to become more and more visible. It was most dominant in samples annealed at 900 °C, whereas the previously observed center for high Er concentrations and similar annealing conditions due to Er-O complexes [6] was completely missing.

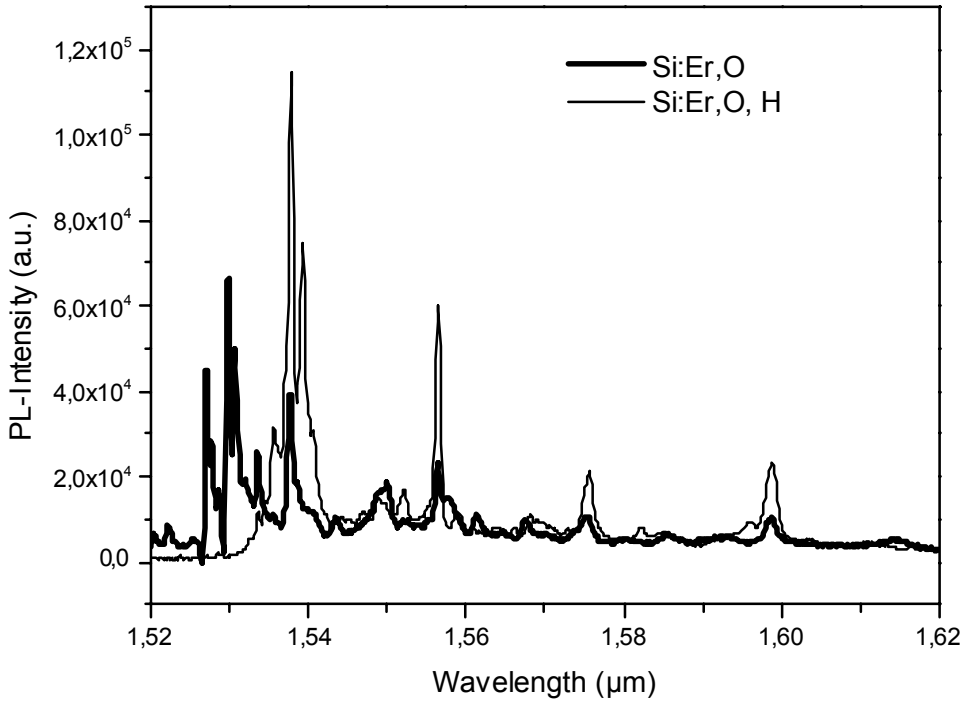

Fig. 2: Comparison of PL-spectra of Si:Er,O with (thin line) and without (thick line) hydrogenation. Both samples were implanted with the same doses of Er and oxygen treated with the same annealing procedure. The intensity is more than 5 times bigger in samples additionally doped with hydrogen.

4. Conclusion

Accurate control of doping gradients and thus knowledge of the electrical activity and the distribution of the implanted dopants are essential for the location and impurity gradient of the pn-junction. Careful consideration has thus to be put into diode design in order to achieve avalanche rather than tunneling breakdown in a diode. TRIM simulations turn out to be insufficient. After adjusting the diode design according to SIMS results the intensity of the electroluminescence at room temperature increased by at least one order of magnitude.

Hydrogenation of Si:Er, O leads to an increase in luminescence yield. We found that hydrogen enhances the solubility of Er in silicon and also suppresses the formation of other Er-O complexes as well as that of other, non-radiative Er centers, leading to an increase of luminescence yield at temperatures below 150 K. This is supported by power dependence studies which also indicate a higher concentration of optically active Er in the hydrogenated samples.

Acknowledgements

FWF, BMWV

References

[1] H. Ennen, J. Schneider, G. Pomrenke, A. Axmann, *Appl. Phys. Lett.* 43 (1983) 943

[2] H. Ennen, G. Pomrenke, A. Axmann, K. Eisele, W. Haydl, J. Schneider, *Appl. Phys. Lett.* 46 (1985) 381

[3] S. Coffa, G. Franzo, F. Priolo, *MRS Bulletin 23* (1998) 25

[4] "Erbium in SiOx Environment: Ways to Improve the 1.54 μm Emission", G. Kocher, H. Przybylinska, M. Stepikhova, L. Palmetshofer and W. Jantsch*, Physica B*, in print

[5] R. Job, A. G. Ulyashin, W. R. Fahnrer, A. I. Ivanov, L. Palmetshofer, *Appl.Phys. A* 72 (2001) 325

[6] H. Przbylinska, et.al. *Phys.Rev.B* 54 (4) (1996) 2532

[7] L. Palmetshofer, M. Gritsch, G. Hobler, , *Mat. Sci. Eng.*B B81 83 (2001) 83

Self-Organized Lateral Ordering in Vertically Aligned PbSe Quantum Dot Superlattices

G. Springholz, A. Raab, R.T. Lechner
Institut für Halbleiter- und Festkörperphysik,
Johannes Kepler Universität, A-4040 Linz, Austria

Self-organized lateral ordering is studied for vertically aligned self-assembled PbSe/ $Pb_{1-x}Eu_xTe$ quantum dot superlattices. It is found that a pronounced hexagonal lateral ordering tendency exists for $Pb_{1-x}Eu_xTe$ spacer thicknesses around 160 Å with a resulting narrowing of the size distribution. In addition, the in-plane dot separations and the dot density are tunable by changes in the spacer thickness with an almost two-fold density increase for spacer thicknesses from 100 to 275 Å. Similar marked changes are also found for PbSe dot shapes as well as the dot sizes. This provides additional means for the tuning of the optical and electronic properties of the dots.

1. Introduction

Self-organization during strained-layer heteroepitaxy of self-assembled quantum dot superlattices has recently been shown to result in the formation of vertically and laterally ordered dot superstructures [1] – [3]. This is based on the elastic interaction between the dots on the surface and the buried dots during superlattice growth [1], [2]. Experimentally, different types of dot arrangements have been observed for different materials systems [1], [2]. This is due to the strong influence of the elastic anisotropy and the growth orientation on these interactions [3]. The PbSe/$Pb_{1-x}Eu_xTe$ system is unique in this respect because different vertical and lateral correlations can be obtained in the superlattices just by changes in the spacer thickness [4]. In particular, either an *fcc*-like stacking or a vertical dot alignment is obtained for spacer thicknesses either larger or smaller than about 380 Å. For the *fcc*-stacked superlattices, a highly efficient lateral ordering mechanism was found in our previous work [2] which results in significant dot size homogenization [5]. Based on such structures we have recently fabricated mid-infrared vertical cavity surface emitting PbSe quantum dot lasers [6]. In the present work, it is demonstrated that also for the vertically aligned PbSe dot superlattices a pronounced hexagonal lateral ordering tendency exists. This ordering process strongly depends on the $Pb_{1-x}Eu_xTe$ spacer thickness, and is most pronounced for spacer thicknesses around 150 Å, leading to a narrowing of the size distribution. Marked changes are also found for the PbSe dot shapes as well as the dots size. This provides additional means for the tuning of the optical and electronic properties of the dots for device applications.

2. Experimental

The samples were grown by molecular beam epitaxy onto 1.5 μm PbTe buffer layers predeposited on (111) BaF_2 substrates. Each superlattice (SL) consists of 50 periods of 5 monolayers (ML) PbSe alternating with $Pb_{1-x}Eu_xTe$ spacer layers with varying thickness but constant Eu concentration of 8%. Due to the corresponding -5.4% PbSe/ $Pb_{1-x}Eu_xTe$ lattice-mismatch, strain-induced coherent 3D islands are formed in each PbSe layer

when the thickness exceeds 1.5 monolayers (ML). For all samples a substrate temperature of 360°C and growth rates of 0.12 and 1 ML/sec for PbSe and $Pb_{1-x}Eu_xTe$ were used, respectively. For the investigation of the lateral ordering process a series of superlattice samples was prepared with $Pb_{1-x}Eu_xTe$ spacer layers varying from 80 to 330 Å. This is the range of spacer thicknesses where the PbSe dots are aligned vertically along the growth direction. After growth, all samples were analyzed by high resolution x-ray diffraction and by contact-mode atomic force microscopy. Statistical information on the dot size distributions and the lateral ordering tendency was obtained by means of a special image processing software.

3. Results

For superlattices with spacer thicknesses of 105 to 330 Å, representative AFM images are shown in Fig. 1 a) to e). As compared to the completely disordered dot arrangement of the single dot reference layer (see Fig. 1 f)), in the superlattices there is a clear tendency for a lateral alignment of the dots along the in-plane <-110> surface directions. As a result, a 2D hexagonally ordered dot arrangement is formed, which is directly evidenced by the appearance of six-fold symmetric satellite peaks in the Fourier transform (FFT) power spectra of the AFM images shown as inserts in Fig. 1. In addition, the dot sizes and spacings in the superlattices are much larger as those of the single dot reference layer, and the spacing and size continuously increase with increasing spacer thickness. In the FFT power spectra of Fig. 1, this is reflected by the corresponding decrease in the FFT satellite peak separations.

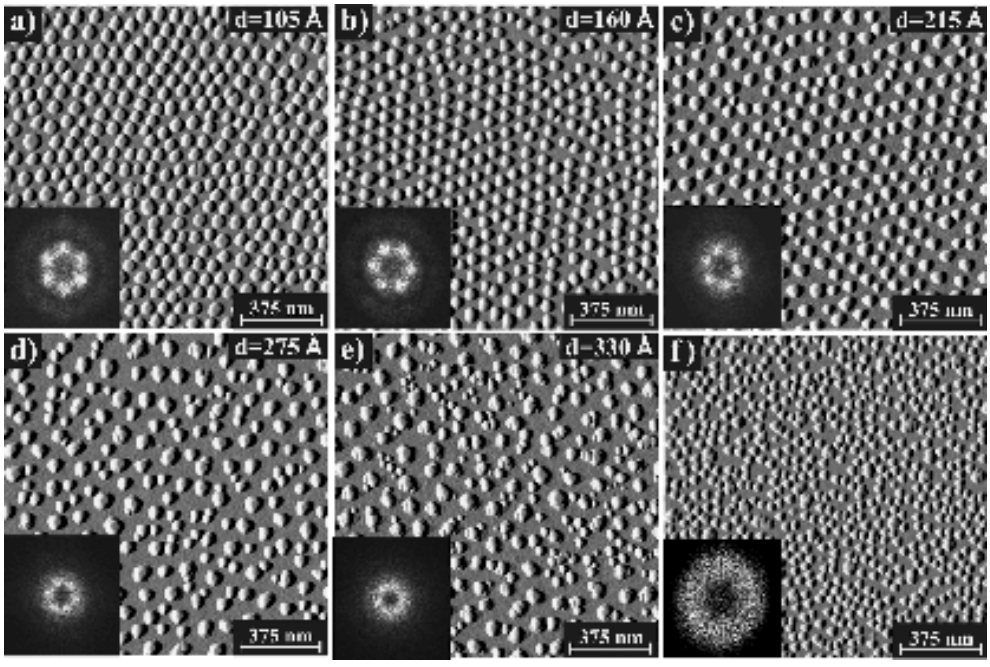

Fig. 1: AFM surface images of PbSe/$Pb_{1-x}Eu_xTe$ quantum dot superlattices (50 periods) with varying $Pb_{1-x}Eu_xTe$ spacer thicknesses of 105, 160, 215, 275 and 330 Å, from a) to e), respectively. (f) AFM image of a 5 ML single PbSe dot reference layer. Inserts: 2D FFT power spectra of the AFM images.

Even more striking is the fact that the best lateral dot order is formed for the superlattices with spacer thicknesses in the range of 100 – 220 Å. In this case, the FFT satellite peaks are most pronounced and narrow in width, and even a weaker ring of second order satellite peaks becomes visible in the FFT spectra (see inserts of Fig. 1a) – c)). On the other hand, for spacer thicknesses larger than 220 Å, the FFT satellites become increasingly smeared out, and they almost disappear for the superlattice with 330 Å spacers. This indicates an increasing disorder in the dot arrangement. In addition, the corresponding AFM image in Fig. 1f) shows that a second type of smaller PbSe dots appears on the surface in between the widely spaced larger dots. These small dots tend to nucleate in a triangularly ordered manner; and because the 330 Å spacer thickness is already close to the transition to the *fcc*-like dot stacking at 380 Å [4], these interstitial dots obviously represent precursor regions for the *fcc*-like dot stacking in which the lateral dot distances are much smaller than those for the vertically aligned superlattices.

For a more quantitative analysis of the lateral ordering process we have determined the preferred lateral dot spacing L from the separation of the FFT satellite peaks. For the hexagonally ordered samples L can be also calculated from the dot density n using $L = (n \sin 60°)^{-1/2}$. The results are plotted in Fig. 2 as a function of spacer thickness. Clearly, the preferred lateral dot spacing increases strongly with increasing spacer thickness, but it obviously does not follow a strict linear dependence as observed in the case the *fcc*-stacked dot superlattices [2]. With respect to the width of the FFT satellite peaks, there is a clear minimum at a spacer thickness of 160 Å, where the most pronounced lateral dot ordering occurs (Fig. 1 b)). For thinner, as well as thicker, $Pb_{1-x}Eu_xTe$ layers, the FWHM gradually increases from ±16% at d_s = 160Å to about ±21% for d_s = 80Å and 300 Å. Thus, the best hexagonal dot ordering occurs for spacer thicknesses around 160 Å.

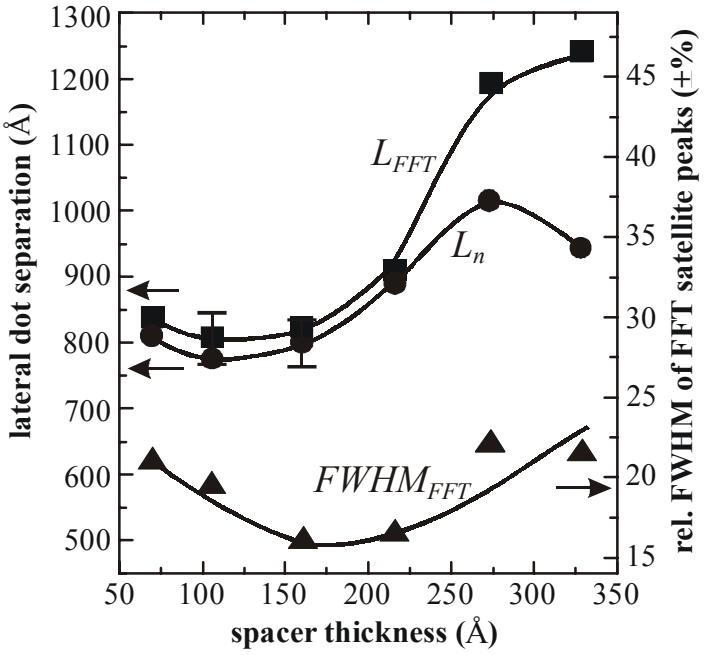

Fig. 2: Lateral dot spacing obtained from the FFT satellite spacings (squares) and the PbSe dot density (circles) plotted as a function of $Pb_{1-x}Eu_xTe$ spacer thickness d_s. Also plotted is the variation of the FWHM (triangles) of the FFT satellite peaks with d_s.

For the well-ordered samples, the average dot separations obtained from the dot densities agree very well with those deduced from the FFT spectra. For spacer thicknesses exceeding 250 Å, however, L_{FFT} becomes significantly larger than the L_n value. This is due to the appearance of the smaller dots in the AFM images. This increases the dot density but does not affect much the preferred separation of the larger dots.

To characterize the dependence of the dot sizes and shapes as a function of SL spacer thickness, we have determined the dot size distributions for all samples. Figure 3 shows representative dot height histograms of the superlattice samples with spacer thicknesses of 160 and 275 Å, as well as that of the single PbSe dot reference layer. The height distribution at d = 160 Å is remarkably narrow (±8%). At a spacer thickness of 275 Å the histogram is strongly shifted to larger height values and a small left hand shoulder (A) starts to emerge at smaller dot heights. This effect is due to the appearance of the additional smaller dots in the AFM images in between the larger dots.

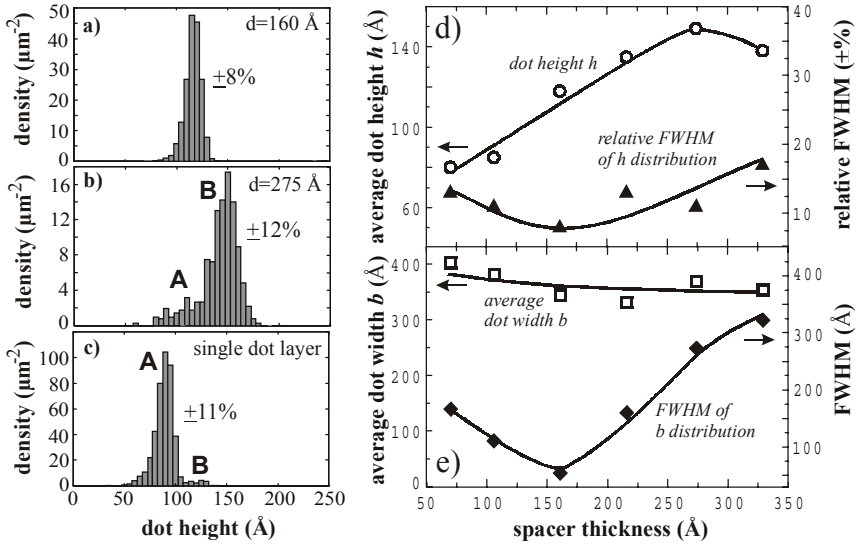

Fig. 3: Left hand side: normalized dot height histograms obtained from the AFM images of Fig. 1 for superlattices with a) 160 and b) 275 Å spacers. The histogram for the 5 ML PbSe single layer reference sample is shown in c). Note the different ordinate scales in the histograms. Right hand side: Average PbSe dot height (d) and width (e) and corresponding FWHM of the size distributions plotted as a function of $Pb_{1-x}Eu_xTe$ spacer thickness.

Figures 3 (d) and (e) summarize the dependence of the average dot height $\bar{h}$ and the dot width b as a function of spacer thickness. The average dot height $\bar{h}$ obtained from the histograms is plotted as a function of spacer thickness. Clearly, up to a spacer thicknesses of 275 Å the height increases essentially linearly with increasing spacer thickness starting from a value of $\bar{h}$ = 80 Å for d = 80 Å to $\bar{h}$ = 149 Å for d = 275 Å, respectively. On the contrary, the dot base width is essentially constant in this range at around 320 Å. Thus, the changes in the dot density induced by the changes in spacer thickness mainly translate into a different vertical dot growth while not affecting much the lateral dot size. From zoomed-in AFM images recorded with selected ultra-sharp AFM tips, it turns out that the dot shapes in the superlattices basically correspond to truncated pyramids with triangular base and {100} side facets. For the very thin spacer layers, the

PbSe dots are rather flat with an aspect ratio of only about 1:5, whereas for the thicker spacers the aspect ratio increases to values around 1:3. This is still significantly smaller than the 1:2.2 aspect ratio of the pyramidal dots of the single PbSe dot layers [2], which do not show any flattening of the island tips. Therefore, the modification in the dot shape in the superlattices must be induced by the elastic strain fields of the buried dots. These are strongest for the thinnest spacers and rapidly decay as its thickness increases.

Perhaps the most interesting feature of our samples is the pronounced narrowing of the size distribution for the ordered superlattice samples. This follows from the dependence of the width of the size distributions also plotted in Figs. 3 (d) and (e) as a function of spacer thickness (full symbols). With respect to the height distributions (Fig. 3 (d)), the statistical variation decreases from ±13% to ±8% for d_s increasing from 80 to 160 Å, after which it increases again to above ±15% for the d_s = 330 Å superlattice. A similar but even more pronounced trend is observed for the statistical variation of the lateral dot widths (Fig. 3 (e)), which again shows a pronounced minimum at a spacer thickness of 160 Å with a rapid increase for thinner as well as thicker spacers. Clearly, this narrowing is most pronounced for the sample with the sharpest FFT satellite peaks, *i.e.*, with the best developed hexagonal order in the dot arrangement. Thus, the size homogenization is a direct consequence of the lateral ordering caused by the elastic interactions during superlattice growth. In addition, it is emphasized that the uniformity of the dots in the d_s = 160 Å superlattice is not only much better than that of the PbSe single dot reference layer (FWHM of the height distribution of ±11%), but it is also as high as the uniformity obtained for trigonally ordered *fcc*-stacked dot superlattices.

4. Conclusions

To conclude, we have demonstrated an efficient lateral ordering of self-assembled vertically aligned PbSe quantum dots superlattices leading to a pronounced narrowing of the size distribution. Furthermore, the adjustment of the superlattice spacer thicknesses provides an effective means for tuning of the lateral dot spacings, the overall dot densities as well as the dot heights, where the latter even show a linear dependence on spacer thickness. This shows that multi-layering is an efficient method for controlling the dimensions and arrangements of self-assembled quantum dots.

This work was supported by the Fonds zur Förderung der wissenschaftlichen Forschung, the Academy of Sciences (APART) and the GME of Austria.

References

[1] J. Tersoff, C. Teichert, and M.G. Lagally, Phys. Rev. Lett. 76, 1675 (1996).

[2] G. Springholz, Holy, M. Pinczolits, and G. Bauer, "Self-Organized Growth of 3D Quantum Dot Superlattice with fcc-like Vertical Stacking and Tunable Lattice Constant", Science 282, 734 (1998).

[3] V. Holy, G. Springholz, M. Pinczolits, G. Bauer, "Strain Induced Vertical and Lateral Correlations in Quantum Dot Superlattices", Phys. Rev. Lett. 83, 356 (1999).

[4] G. Springholz, M. Pinczolits, P. Mayer, V. Holy, G. Bauer, H. Kang, and L. Salmanca-Riba, "Tuning of lateral and vertical correlations in self-organized PbSe/PbEuTe quantum dot superlattices", Phys. Rev. Lett. 84, 4669 (2000).

[5] M. Pinczolits, G. Springholz, and G. Bauer, “Evolution of hexagonal lateral ordering in strain-symmetrized PbSe/PbEuTe quantum dot superlattices”, Phys. Rev. B 60, 11524 (1999).

[6] G. Springholz, T. Schwarzl, W. Heiss, G. Bauer, M. Aigle, and H. Pascher, “Mid infrared surface emitting PbSe/PbEuTe quantum dot lasers”, Appl. Phys. Lett. 79, 1225 (2001).

[7] A. Raab, R. Lechner, G. Springholz “Self-organized lateral ordering for vertically aligned PbSe/PbEuTe quantum dot superlattices”Appl.Phys.Lett. **80**, 1273 (2002).

Stimulated Emission and Absorption of Highly Ordered Self-Organized PbSe Quantum Dots in Vertical Cavities

W. Heiss[1], T. Schwarzl[1], M. Böberl[1], G. Springholz[1], T. Fromherz[1], A. Raab[1], J. Fürst[2], H. Pascher[2]

[1]Institut für Halbleiter und Festkörperphysik, Universität Linz, Altenbergerstraße 69, A-4040 Linz, Austria

[2]Experimentalphysik I, Universität Bayreuth, 95447 Bayreuth, Germany

Vertical cavities containing PbSe/PbEuTe superlattices with self-organized PbSe quantum dots, ordered in lateral as well as in vertical direction, are investigated by optical spectroscopy. Stimulated emission from the quantum dots, optically excited with 10 ns long pulses, is observed up to 140 K. The absorption spectrum of the superlattice is deduced from the width of the resonator modes, obtained by a transmission experiment. The quantum dot absorption can clearly be distinguished from the wetting layer signal.

1. Introduction

For III-V diode lasers, the introduction of quantum dots into the active zone of the laser allows to reduce the threshold current density [1], to increase the modulation band width, and to improve the temperature stability. This is the motivation for us to test quantum dot superlattices based on lead-salts as active material in vertical-cavity surface-emitting lasers for the mid-infrared. In self-assembled quantum dot superlattices, the elastic interactions between the growing dots on the surface and those buried within the previous layers often lead to the formation of long range correlations within the dot ensembles [2]. In lead-salt quantum dot superlattices, in particular, dot correlations inclined to the growth direction are observed, dependent on the superlattice period. This leads to a unique fcc-like ABCABC... vertical dot stacking sequence and a nearly perfect lateral ordering within the growth plane, corresponding to the formation of self-organized trigonal 3D lattices of dots [3].

While the ordering mechanism and the topography of the correlated PbSe quantum dot superlattices have been clarified [2], [3], there are almost no *optical* studies on PbSe quantum dots reported. Up to now, absorption measurements did not give conclusive results, due to the small optical density of the dots, and due to fact that absorption spectra of lead salt films are dominated by strong interference fringes. In this work, we study both the stimulated emission as well as the absorption of a lead salt quantum dot superlattice which is embedded between two dielectric bragg mirrors within a vertical cavity.

2. Sample Details

The high-finesse lead-salt microcavity samples filled with the PbSe quantum dot superlattice were grown by molecular beam epitaxy (MBE) onto (111) oriented BaF_2 sub-

strates. The pyramidal shaped self-organized PbSe quantum dots were formed during Stranski-Krastanow heteroepitaxial growth of PbSe on PbEuTe due to the 5.4 % lattice mismatch [3]. The dot superlattices were grown at 360 °C deposition temperature by alternating 5 monolayers (MLs) of PbSe with 480 Å PbEuTe spacer layers on a PbEuTe buffer layer. Under these conditions, the dots in the superlattice are aligned in directions inclined by about 39° to the growth direction. An areal dot density of about 250 μm^{-2} (lateral separation 680 Å), an average dot height of 120 Å, and a base width of 300 Å with a relative full width at half maximum of the dot size distribution of about ±10 % is observed for superlattices with more than 60 bilayers [3]. The strong increase of the band gap energy of PbEuTe with increasing Eu content and the larger band gap of PbTe as compared to PbSe lead to a significant quantum confinement of the free carriers in the PbSe dots. In bulk material, the energy gaps at 4 K amount to 422 meV and 146 meV for $Pb_{0.95}Eu_{0.05}Te$ and PbSe, respectively.

The dot superlattices are sandwiched between two high-reflectivity Bragg mirrors. For sample 1 each mirror consists of 3 periods of quarter wavelength EuTe/$Pb_{0.94}Eu_{0.06}Te$ bilayers. For sample 2 the bottom mirror consists of 4 bilayers EuTe/$Pb_{0.94}Eu_{0.06}Te$ whereas the top mirror is grown with a higher Eu content of 20 %, to make it transparent for the pump laser wavelength of 1.9 μm. To achieve a reflectivity higher than 99% for this mirror 5 layer pairs are used. For sample 1 (2) we used a superlattice with 140 (236) periods grown on a 3 μm (1.8 μm) thick buffer layer and the designed center wavelength of the Bragg mirror is 4.3 μm (3.3 μm). The vertical cavity of sample 1 is 10 μm long whereas the length of the sample 2 cavity amounts 14 μm.

3. Stimulated Emission

For optical pumping of the vertical cavity structure, the first Stokes shifted line of a Q-switched Nd:YAG laser, produced in a hydrogen Raman cell, was used, resulting in a wavelength of 1.907 μm. The pulse length was about 10 ns and the repetition rate 50 Hz. The laser beam was focused on the sample to a spot size of 320 μm and the emission was recorded by an InSb detector using a box-car technique. For sample 1 we observe stimulated emission at energies around 300 meV (4.1 μm). With increasing temperature the emission shifts to higher energies due to the temperature dependence of the PbSe band gap. Finally, the stimulated emission disappears at a temperature of 100 K, because the laser gain spectrum shifts away from the energy range where the Bragg interference mirror exhibits a sufficiently high reflectivity.

For sample 2 much higher operation temperatures should be accessible, since the center of the Bragg mirror stop band agrees with the expected emission wavelength of the PbSe quantum dots at room temperature. As shown in Fig. 1, the emission spectrum consists of up to five lasing modes, where the envelope of the laser lines corresponds to the laser gain spectrum. The gain spectrum again shifts to higher energies with increasing temperature. When the temperature increases from 10 K to 100 K the emission intensity increases by an order of magnitude. For higher temperatures the intensity drops again and at about 150 K no emission is observed any more. For sample 2, the quenching of the stimulated emission is not due to a detuning of the emission energy in respect to the Bragg mirror stop band center. Therefore, it must be concluded that some intrinsic processes are responsible for the disappearance of the laser emission at 150 K. To prove this we have investigated the stimulated emission of a reference sample with a bulk like PbTe layer as laser active medium, again designed for operation at room temperature.

For this sample we obtain much better results than with the quantum dots samples. By optically pumping laser emission is observed up to 45 °C and the minimum threshold is about 200 times smaller than for the quantum dot cavities [4]. This result shows that the PbSe quantum dots are not at all advantageous for laser emission compared to bulk PbTe, which might be an indication that the band alignment between PbSe and PbEuTe is not of type I, or that the luminescence efficiency of the PbSe dots is reduced due to Eu intermixing from the PbEuTe barriers. To decide this, further experimental results on the quantum dot superlattices are needed.

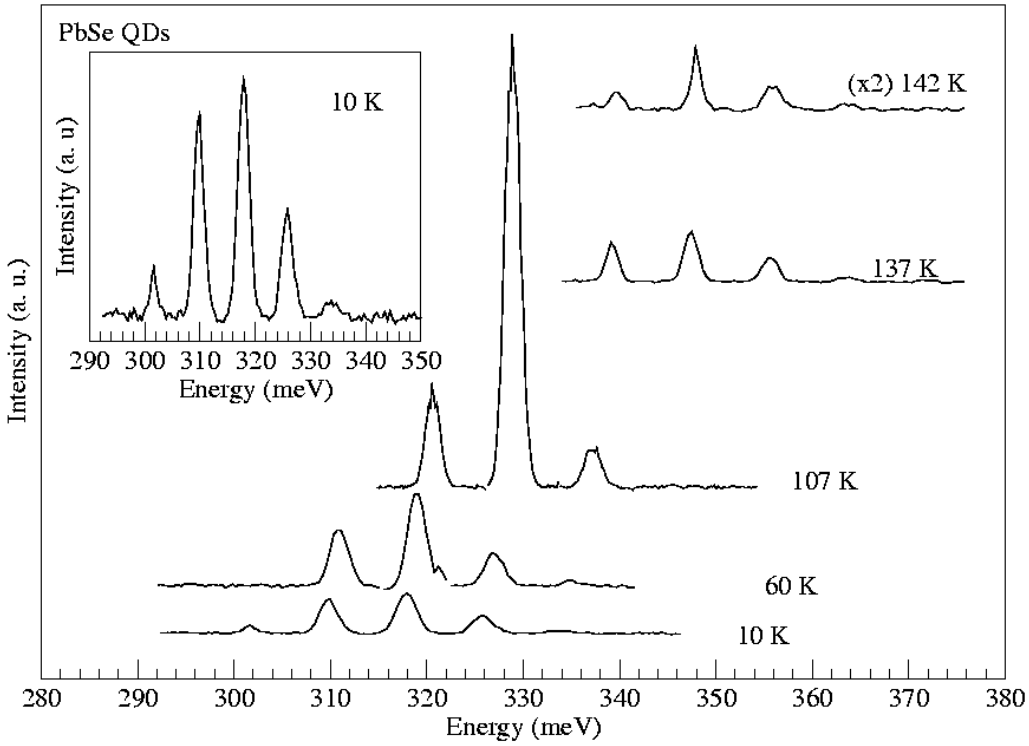

Fig. 1: Emission spectrum of sample 2 for various temperatures. The inset shows the 10 K spectrum with enhanced sensitivity to demonstrate the 5 laser modes observed at low temperatures.

4. Q-dot Absorption

To deduce the absorption of the quantum dots from a conventional PbSe/PbEuTe quantum dot superlattice by a transmission experiment is not possible, due to the small optical density of the quantum dots. Furthermore, the transmission spectrum of a single lead-salt layer predominantly shows strong interference fringes due to multiple reflections on the sample surface and the layer to substrate interface. When the superlattice is placed in a vertical cavity, however, the absorption is strongly enhanced and thus can be detected. In particular, the absorption causes a damping and a broadening of the cavity resonances. The extinction coefficient is directly proportional to the difference between the width of the damped resonance w and that of the resonance without damping w_0, normalized to the energy of the resonance ν [5]. So the extinction coefficient κ can be

determined from a transmission experiment at the resonance energies. The proportionality factor between $(w_0 - w)/\nu$ can be obtained from a simulation of the transmission spectrum by the use of the transfer matrix method [5].

The results shown in Fig. 2 are obtained for sample 1. The transmission spectrum of this sample exhibits 17 cavity resonances within the stop band of the Bragg mirror. From the transmission experiment at low temperatures the width of the damped resonances is determined, while that of the undamped resonances is obtained from a measurement at room temperature. This can be done because at room temperature the PbSe quantum dot absorption is shifted to higher energies, out of the Bragg mirror stop band. The extinction coefficient in Fig. 2 shows a small peak around 240 meV due to quantum dot absorption of the longitudinal valley, whereas at 310 meV a stronger absorption peak is observed due to a transition within the oblique valleys. At 330 meV a step-like onset of κ is observed caused by absorption of the wetting layers. Most interestingly, the peak absorption of the quantum dots is slightly weaker than that of the two-dimensional wetting layer, in contrast as it would be expected from the peak-like density of states of the quantum dots. This might be an additional reason why the performance of the quantum dot laser is worse than that of the reference laser sample with a bulk-like active zone.

The stimulated emission of sample 1 at 10 K is shown in the inset of Fig. 2. The spectrum shows two laser modes with the orders m = 28 and m = 29. Fore these modes indeed the peak of the quantum dot absorption is deduced, confirming that lasing in the vertical-cavity sample 1 is caused by the quantum dots and not by the wetting layer.

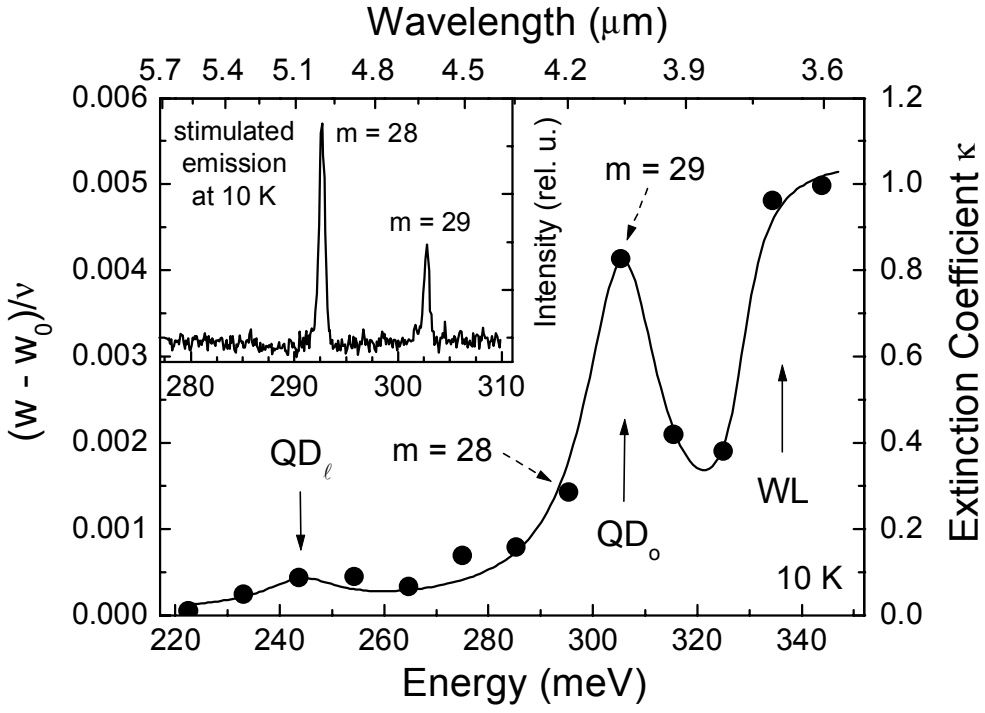

Fig. 2: Absorption spectrum from a PbSe quantum dot superlattice deduced from the width of the cavity resonances of a vertical cavity (sample 1). The dot absorption can be clearly distinguished from the wetting layer. The stimulated emission observed for this sample is shown in the inset. The emitting modes m = 28 and m = 29 agree with the absorption peak caused by the quantum dots.

3. Summary

We investigated the stimulated emission and absorption of vertical cavities containing PbSe/PbEuTe superlattices with self-organized PbSe quantum dots which are ordered in lateral as well as in vertical direction. Under optical excitation with 10 ns long pulses, stimulated emission in the mid-infrared spectral range is obtained from the quantum dot superlattice up to a temperature of 140 K. The absorption spectrum of the superlattice is deduced from the width of the resonator modes, as measured by transmission experiments. The quantum dot absorption can clearly be distinguished from the wetting layer signal, despite their small optical density. Therefore, the measurement procedure demonstrated here for PbSe quantum dots might be applied also for other systems with small optical densities in the near future.

References

[1] D.L. Huffaker, G. Park, Z. Zhou, O.B. Shchekin, D.G. Deppe, 1.3 mu m room-temperature GaAs-based quantum-dot laser, *Appl. Phys. Lett.* **73**, 2564 (1998)

[2] V. Holy, G. Springholz, M. Pinczolits, G. Bauer, Strain induced vertical and lateral correlations in quantum dot superlattices, *Phys. Rev. Lett.* **83**, 356 (1999)

[3] G. Springholz, V. Holy, M. Pinczolits, G. Bauer, Self-organized growth of three-dimensional quantum-dot crystals with fcc-like stacking and a tunable lattice constant, *Science* **282**, 784 (1998)

[4] J. Fürst, H. Pascher, T. Schwarzl, M. Böberl, W. Heiss, G. Springholz, G. Bauer, Mid-infrared IV-VI vertical-cavity surface-emitting lasers with 0-. 2- and 3-dimensional systems in the active regions, submitted to *Appl. Phys. Lett.*

[5] T. Schwarzl, W. Heiss, G. Springholz, H. Krenn, T. Fromherz, A. Raab, I. Vavra, Mid-infrared absorption of PbSe/PbEuTe quantum dot superlattices in high-finesse IV-VI microcavities, submitted to *Phys. Rev. B*

In-situ Control of MOCVD Nitrides Deposition via Spectroscopic Ellipsometry

A. Bonanni, D. Stifter, A. Montaigne, K. Schmidegg, H. Sitter

Institut für Halbleiter- und Festkörperphysik
Johannes Kepler Universität, A-4040 Linz, Austria

Within the frame of an EU project we had the possibility to install a MOCVD system for the growth of GaN and its ternary alloys containing In and Al. As dopand sources we installed Si for n-type and Mg for p-type. The main purpose of the project was the installation of an *in situ* monitoring of the layer thickness and composition during growth. This could be managed by spectroscopic ellipsometry.

1. Introduction

In February and March of this year we had a very busy time with the transport, setup and installation of the MOCVD machine. The machine was shipped to our lab, where we had to overcome the limits of our building, which allowed only a transport through the windows, due to the size of the components.

At the end of April of this year we had the start-up procedure of the MOCVD equipment, where we could grow the first layers of GaN and GaInN together with p- and n-doping. Although we had a delay of 4 months at the time of setup of the MOCVD equipment in comparison to the work plan of the project, we managed to catch up the time schedule within one month.

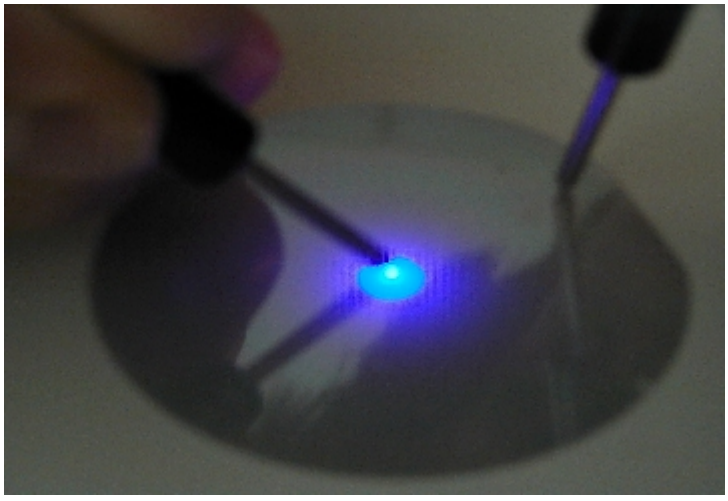

Fig. 1: Blue light emission from the first LED structure grown in our MOCVD reactor after thirteen growth runs.

2. Startup of the MOCVD System

To get some experience with ternary compounds the startup engineer from Aixtron introduced us to the growth of GaInN, since the Al source was not available at this time. So all components for the growth of an LED with a small GaInN quantum well were tested. Finally in the 13th growth run a simple LED structure was grown. The obtained result can be seen in Fig. 1.

The mounting of the optical components for ellipsometry measurements needed the construction of a special holder structure. The fixing turned out to be quite tricky because of the limited space in the reactor cabinet. Even more sophisticated was the exact alignment of the ellipsometer, which needed the help of a specialist from the ellipsometer supplier to optimize the output of the optical signal.

In all our experiments, whole 2 inch (0001)-oriented Al_2O_3 substrates are employed, and the growth stages are constantly monitored with the final goal of developing a closed loop control of the nucleation process. Special effort has been devoted to the monitoring of the initial stages of GaN growth (e.g. a low temperature GaN nucleation layer deposited onto the substrate in order to promote the transition between substrate and GaN device layers) and to the interface formation (nucleation layer/GaN, GaN/ternaries). The growth parameters have been optimised and at present we can fabricate state-of-the-art pure hexagonal GaN (FWHM of XRD rocking curve of 250”), p- and n-type doped GaN and ternary compounds (AlGaN, InGaN). The ‘yellow luminescence’, characteristic of nitride materials and detrimental for device performance, has been dramatically reduced compared with the first deposition runs and we are able to routinely produce blue LEDs (one example is shown in Fig. 1).

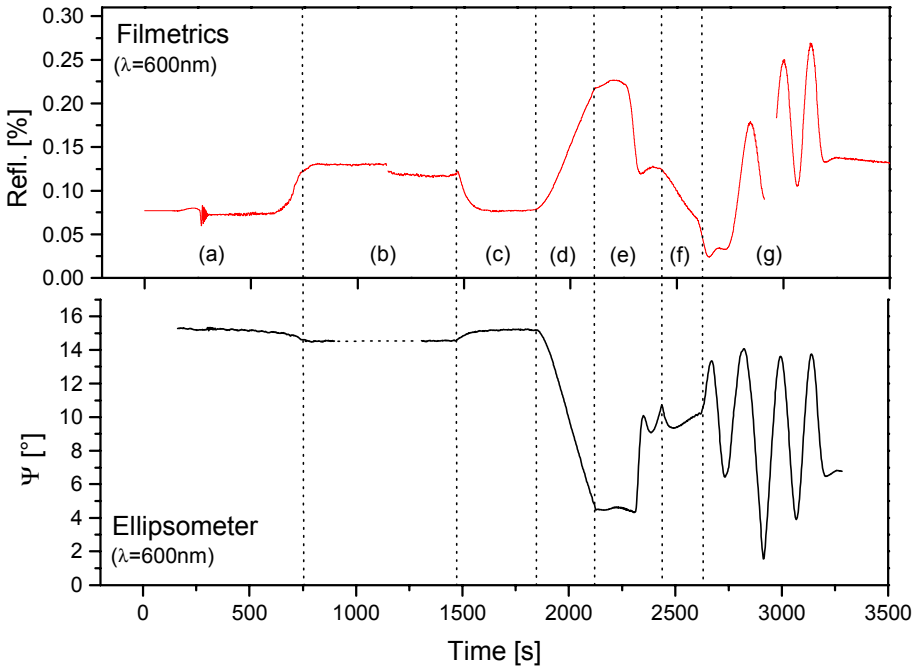

Fig. 2: Comparison between reflectivity (up) and kinetic SE acquired during the fabrication of GaN on sapphire.

3. In Situ Monitoring of the Growth

Concerning the in-situ monitoring of the growth process, special attention has been devoted to the comparison between SE and reflectometry measurements performed in parallel during deposition. Figure 2 gives an example of the two sets of data acquired during the fabrication of a standard GaN layer on Al_2O_3. All the information obtainable from reflectivity is also contained in the SE optical response. In addition, since reflectivity is intensity dependent, the signal is crucially influenced by wobbling of the sample (unavoidable in the reactor) and by light emission during the heating stages. On the contrary, SE is polarisation dependent and therefore much less sensitive to light interference and wobbling, so a far better signal-to-noise ration can be obtained (at the same wavelength). By *in situ* monitoring of GaN and ternaries deposition, we can obtain reproducible data on device quality material.

One of the goals of the in-situ monitoring is to have the possibility to determine in real time during growth the actual composition of the depositing layers.

In this perspective, series of AlGaN (and InGaN) layers with different concentrations have been grown. Kinetic SE measurements (ellipsometric angles/dielectric function vs. time) have been taken above the energy gap during the whole growth procedure, and an example of the results is reported in Fig. 3, where the imaginary part (ε_i) of the dielectric function is given as a function of the real part (ε_r). The obtained exponential spirals are typical of an interface which is continuously overgrown, and their radius is determined by the amplitude of the growth oscillations. The spirals convergence points give, in the complex plane, the values of the dielectric function of the deposited material and, therefore, the actual alloy composition.

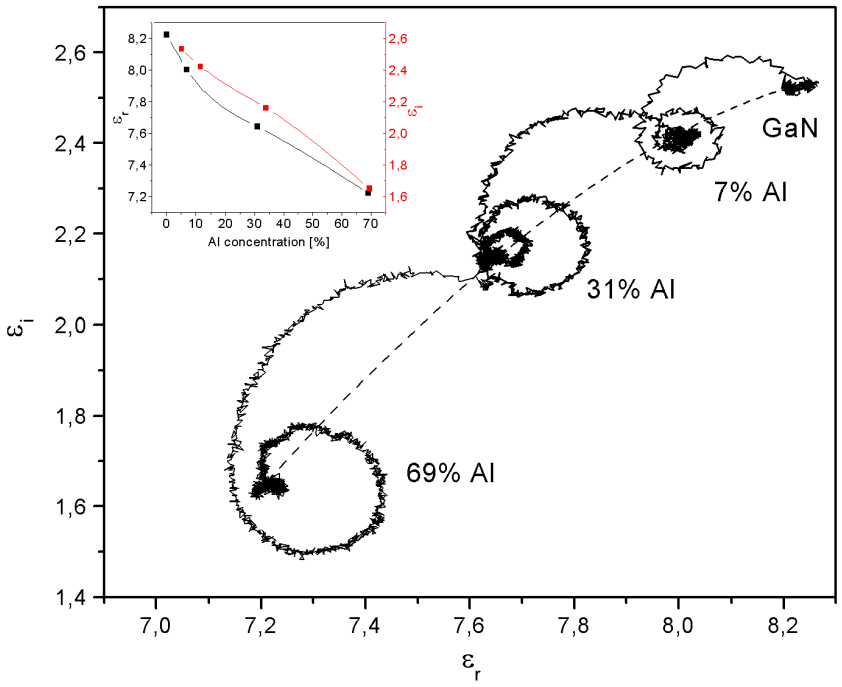

Fig. 3: Imaginary (ε_i) vs. real (ε_r) part of the dielectric function for layers with different Al content. The inset shows ε_i and ε_r respectively, as a function of the Al concentration.

Furthermore, we recently developed an algorithm for the real time determination of the compound concentration of ternary GaN (AlGaN, InGaN) during growth using the virtual interface (VI) model proposed by D. Aspnes for optical absorbing semiconductor crystal layers.

The last development regards the growth of pure cubic GaN we carried out on MBE-grown templates on GaAs (001). To our knowledge the first cubic MOCVD GaN in Europe.

Structural Investigation of Si/SiGe Quantum Cascade Structures

T. Roch, J. Stangl, R.T. Lechner, G. Bauer

Institut für Halbleiter- und Festkörperphysik
Johannes Kepler Universität Linz, Altenbergerstr. 69, A-4040 Linz, Austria

S. Mentese, D. Grützmacher

Laboratory for Micro- and Nanotechnology,
Paul Scherrer Institut, CH-5232 Villigen, Switzerland

We have investigated the structural properties of Si/SiGe electroluminescent quantum-cascade structures, by means of x-ray reflectivity and diffraction. The cascade structures were grown at a comparatively low temperature of T = 350 °C to avoid misfit dislocation formation. Despite an overall thickness of the cascade structures of about 9000 Å and Ge contents of up to more than 40% in some of the SiGe wells, the as grown stack of layers is indeed pseudomorphic with respect to the Si substrate. The analysis of x-ray reflectivity data yields a rather small r.m.s. interface roughness below 3 Å throughout the cascade structures. An annealing study of the structures was performed in order to determine the allowable thermal budget during processing. It was found that the structures are highly metastable, and annealing at 600 °C for 10 minutes leads already to partial plastic relaxation.

1. Introduction

Recently it has been shown that the concept of quantum cascade structures (QC), which has first been demonstrated for InGaAs/InAlAs [1], can be extended to the Si/SiGe system [2]. In QC structures, the optically active transitions occur within one band, between subbands formed in a sequence of quantum wells, under applied bias. In strained Si/SiGe heterostructures grown pseudomorphically on Si, considerable band offsets exist only in the valence bands of light and heavy holes. Recently, Si/SiGe based QC emission structures exhibiting well-resolved electroluminescence in the 10 μm wavelength range and linewidths down to 22 meV have been demonstrated [2].

To achieve a high emission efficiency of such QC emission structures, all design parameters (quantum well thicknesses and Ge contents) have to be met very accurately and with rather precise layer to layer reproducibility. In QC emission devices, an active unit consists of an injector, the active quantum well, and a collector. These units are repeated several times, thus making up rather complex many-layer heterostructures.

Despite the lattice mismatch of 4.17% between Ge and Si and the large overall thickness of QC structures, plastic strain relaxation has to be avoided, because dislocations represent nonradiative recombination sites. Furthermore, any change of the strain state alters the band alignment, which is crucial for QC devices. To avoid dislocation formation, the growth temperature has to be kept rather low. The resulting structures are highly metastable, and thermal treatment, e.g., during subsequent processing steps, may lead to

plastic relaxation as well. Hence the thermal budget allowable without degradation of the structures is an important parameter.

2. Experimental

The cascade structures were grown using molecular beam epitaxy at a substrate temperature of 350 °C on high resistivity Si (001) substrates with a very small miscut of about 0.1° and with a miscut azimuthal direction of 3° off the [100] direction. Details on growth and the electroluminescence can be found in Ref. [2].

The interface roughness in these sample has been investigated from reciprocal space maps in x-ray reflectivity (XRR) geometry (Fig. 1, left panel). The intensity is peaked into so-called resonant diffuse scattering (RDS) sheets. Their width along q_z is inversely proportional to the vertical correlation length, giving a measure of how far the interface morphology in the multi layer stack is replicated. Obviously, the width of these sheets depends on q_x. The right panel of Fig. 1 shows this dependence for several scans taken from the maps in the indicated position. The width follows very well a quadratic increase as a function of q_x [3]. From this analysis, we find that in the roughness spectrum, higher spatial frequencies are replicated to a lower extent than those with low spatial frequencies [4]. With interface roughnesses below 3 Å throughout the whole stack [4], the structural quality of the investigated sample is very high.

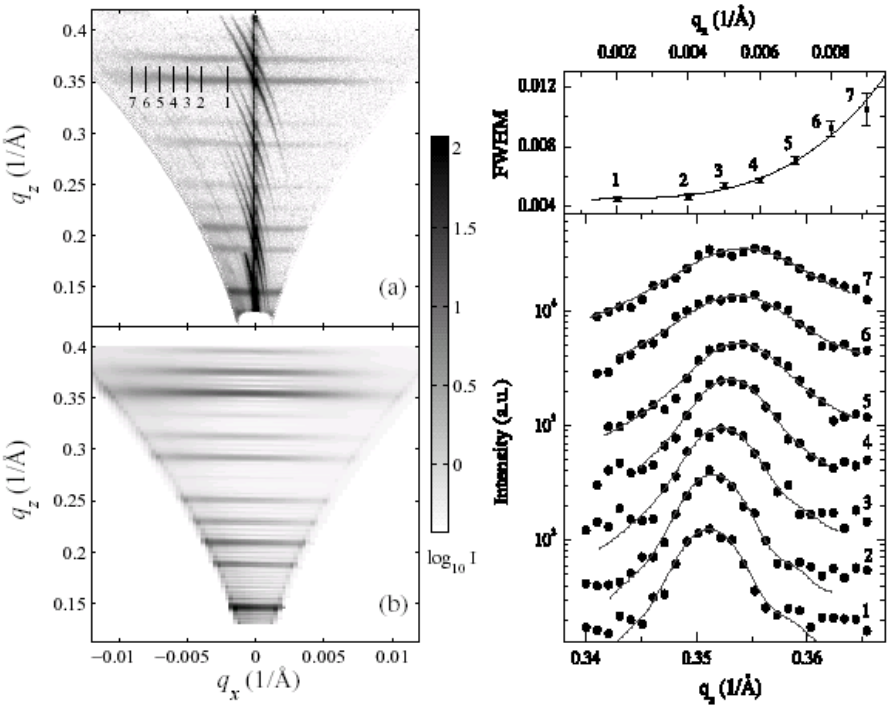

Fig. 1: Left panel: reciprocal space map in XRR geometry of the as grown cascade structure (a), and simulated diffuse intensity distribution (b). The correlated interface roughness leads to intensity sheets along q_x. Their width along q_z as a function of q_x is shown in the right panel for the selected positions as indicated. The increase indicates a decrease of correlation for decreasing roughness wavelengths.

In order to prove the pseudomorphic growth, high resolution x-ray diffraction (XRD) reciprocal space maps were recorded. We have used reciprocal space mapping around the symmetric (004) and asymmetric (224) reflection, shown in Fig. 2, left panel. The diffraction pattern due to the superlattice appears at the same q_x position as the Si substrate peak, and the width of the intensity distribution along q_x is rather small, i.e., with a similar FWHM as that of the Si substrate. These two facts indicate that the entire cascade structure is grown coherently with the in-plane lattice parameter being the same in all layers of the sample.

However, due to the large number of SiGe layers, the total strain is rather large, and the structure is highly metastable. Therefore we performed an annealing study, in order to determine the thermal budget allowable for such cascade samples during subsequent processing steps. We have annealed the sample in high vacuum conditions for 10 minutes at temperatures of 500 °C and 600 °C, respectively. In order to monitor a possible relaxation, we recorded reciprocal space maps around the (224) reflection in coplanar geometry (Fig. 2). The left panel shows the pseudomorphic as-grown structure. The center panel for the piece annealed at 500 °C already shows an increase in the diffuse scattering, but no significant shift of the superlattice peaks with respect to the Si substrate peak. In the right panel, plastic relaxation is clearly visible for the piece annealed at 600 °C: the superlattice peaks are broadened, and the whole pattern is shifted towards higher q_x (lower absolute value), indicating an increase in the in-plane lattice parameter in the multi layer stack. Hence for these cascade structures, annealing at 500 °C for several minutes is the limit of thermal budget in order to keep a pseudomorphic layer structure and avoid dislocation formation, which would be detrimental for the optoelectronic performance.

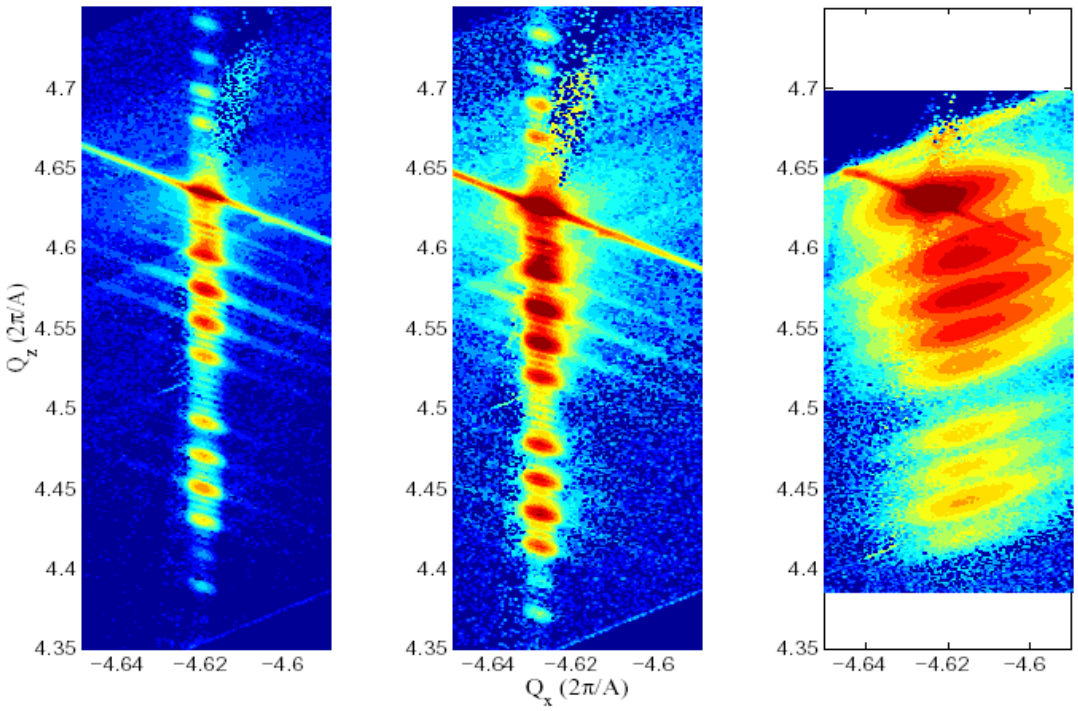

Fig. 2: Reciprocal space maps around the (224) reflection for the as-grown cascade structure (left), and after annealing for 10 minutes at 500 °C (center) and 600 °C (right).

3. Conclusion

The x-ray diffraction and reflectivity data investigations demonstrate a high degree of structural perfection of the Si/SiGe quantum cascade structures. The whole multilayer stack with a total thickness of more than 900 nm and an average Ge content of about 10% grows pseudomorphically on the (001) Si substrate. The Si/SiGe interfaces are rather smooth, with r.m.s. roughness values of about 2.5 Å. The vertical correlation length of the interface roughnesses is of the order of the thickness of two cascades (about 600 Å) for long range interface fluctuations (> 1500 Å) but corresponds only to one cascade, i.e., to 300 Å for short range lateral fluctuations (< 900 Å). Very smooth interfaces have been achieved despite a growth temperature of the Si/SiGe multilayers as low as 350 °C, and consequently the structures are well suited for observing intersubband cascade emission. However, the structures are highly metastable against thermal treatment. An annealing study showed that a thermal budget in device processing up to about 10 min. at 500 °C is tolerable, before plastic relaxation leads to a degradation of the structures.

Acknowledgements

This work was supported by the IHP-Contract HPRI-CT-1999-00040 of the European Commission.

References

[1] J. Faist, F. Capasso, D. Sivco, C. Sirtori, A.L. Hutchinson, A.Y. Cho, *Science*, vol. 264, p. 553, 1994.

[2] G. Dehlinger, L.Diehl, U. Gennser, H. Sigg J. Faist, K. Ensslin, D. Grützmacher, and E. Müller, *Science*, vol. 290, p. 2277, 2001.

[3] M. Kardar, G. Parisi, Y.C. Zhang*, Phys. Rev. Lett*., vol. 56, p. 889, 1986.

[4] T. Roch, M. Meduna, J. Stangl, A. Hesse, R.T. Lechner, G. Bauer, G. Dehlinger, L. Diehl, U. Gennser, E. Müller, D. Grützmacher, *J. Appl. Phys*., in print, 2002.

Optical Characterization of Self-Assembled Si/SiGe Nano-Structures

T. Fromherz, W. Mac, G. Bauer

Institut für Festkörper- u. Halbleiterphysik, Johannes Kepler Universität Linz, Altenbergerstraße 69 , A- 4040 Linz, Austria

C. Miesner, J. Zhu, K. Brunner, G. Abstreiter

Walter Schottky Institut, TU München, Am Coulombwall, D-85748 Garching, Germany

Self-assembled SiGe nano-structures buried under a Si cap layer have been investigated by infra-red absorption and photoluminescence spectroscopy. Together with results of x-ray diffraction and reflection experiments, from these experiments detailed information about the alloy concentration in and the size of the nano-structures is obtained.

1. Introduction

The optical properties of low dimensional structures in the Si/SiGe system are of special interest since by integrating such structures in standard Si technology it is possible to add optoelectronic performance to mainstream material for integrated circuits. The self-organized growth of nano-structures (i.e. Stransky-Krastanow growth mode for quantum dots, step bunching along the terraces of a vicinal substrate for quantum wires) appears to be very appealing, since by these methods rather uniform nano-structures with high density can be achieved without structuring the samples for example by photo- or electron-lithography. However, since the self-assembling is a statistical process, the size and the alloy concentration of the nanostructures are statistically distributed. Therefore, a sensitive characterization of the structural parameters of the nano-structures is essential. For possible future applications, the nanostructures have to be overgrown, and surface scanning methods are not applicable for the characterization of these structures. We show that in addition to x-ray diffraction, absorption, and photoluminescence experiments are valuable tools for the non-destructive characterization of overgrown nano-structures.

2. Experimental

In this work we have performed infrared transmission (TR) experiments for the structural characterization of SiGe quantum dots (QD) formed by the Stranski-Krastanow mode on a SiGe wetting layer and photoluminescence (PL) experiments for the characterization of SiGe quantum wires (QWR) grown by step bunching along terraces of a vicinal Si substrate.

The SiGe QDs were grown by solid-source molecular beam epitaxy on an insulating Si substrate at a substrate temperature of T = 525 °C and a Ge deposition of 8 monolayers. The samples consist of 30 QD layers separated by 50 nm Si barriers. The nominal dot

height (3 nm), diameter (35 nm) and density (6 x 10^{10} cm^{-2}) were determined by atomic force microscopy on reference samples without a Si cap. The samples are p-type (Boron) modulation doped to a level of approximately 4 holes per dot.

Transmission experiments were performed in waveguide geometry with the sample facets wedged at 30° (see inset of Fig. 1) and gold evaporated on the sample surface. In Fig. 1, the ratio of TR measured in TM and TE polarization is shown. The spectra were measured at the temperatures indicated in the plot and normalized to the respective ratio of spectra measured at room temperature in order to remove a wavelength dependent background. For clarity, the curves are vertically shifted by -0.005 for each measurement at lower temperature. An absorption line centered around 260 meV is clearly observed. Model calculations described in Ref. [1] show that the absorption is due to hole transitions between the heavy hole (HH) ground state and the first excited HH state resulting from the confinement in growth direction.

In lateral photocurrent (PC) experiments performed on the same samples, transitions to delocalized continuum states are observed, resulting in an onset of the photo signal at a higher energy than the onset of the absorption observed in the TR experiment (transitions to bound states) [1]. By comparing the measured transition energies to both the confined and continuum states to the model calculations described in [1] it is possible to estimate both the average Ge content (65% – 75%) and the dot height (27 Å). These results show that even at the moderate growth temperatures used for the samples investigated in this work, significant alloying occurs during the overgrowth of the dot layers.

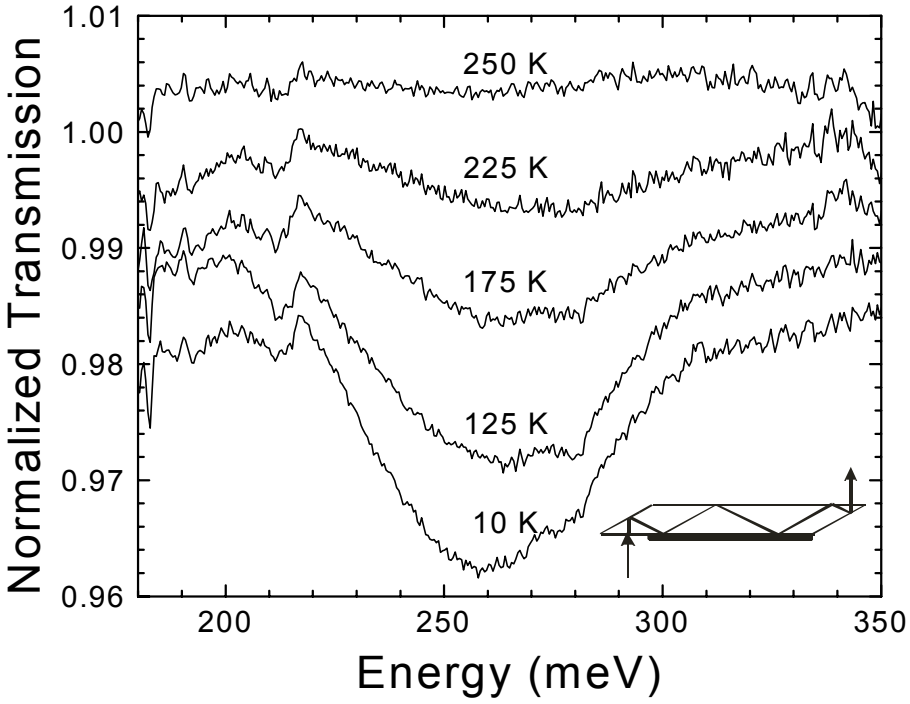

Fig. 1: TR spectra of the SiGe QD sample measured in waveguide geometry at the temperatures indicated in the plot. On the ordinate axis, the ratio of TR measured in TM and TE polarization normalized to the respective ratio measured at room temperature is plotted. For clarity, the spectra are vertically displaced by -0.005 for each temperature step.

The structural properties of a series of SiGe quantum wires (QWR) grown on vicinal (001) Si substrates have been investigated by x-ray diffraction and PL measurements [2]. The samples consist of 20 periods of nominally 25 Å thick $Si_{1-x}Ge_x$ layers separated by 100 Å Si layers. The nominal Ge content of the alloy layers is 0.35, 0.40, 0.45 for samples A, B and C, respectively. In order to initiate step bunching, and the wire growth, a vicinal (001) Si substrate with a rather large miscut angle of 3.5° towards [100] direction was chosen. All samples were capped with a 100 Å Si layer. The details on the MBE growth are given in Ref. [3]. The results of the x-ray experiments [2] clearly indicate that the wires have a triangular cross section with a base length of about 350 Å and a facet angle of 6°. The wires have assembled on top of a SiGe wetting layer (WL) with a thickness of approximately 25 Å and a Ge concentration 0.33.

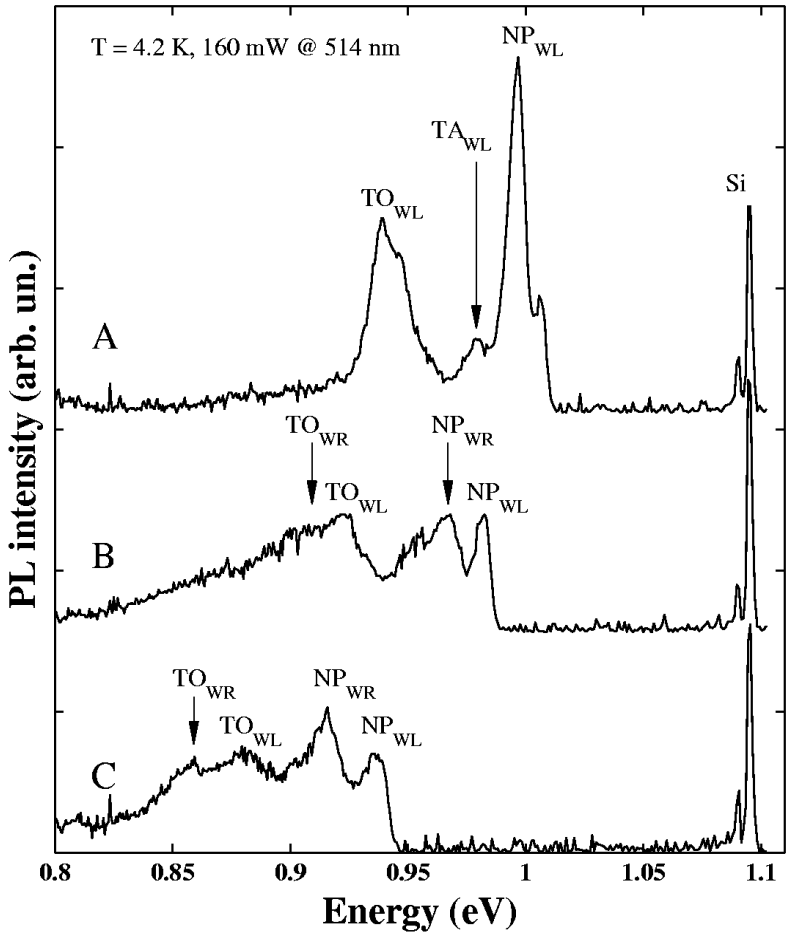

Fig. 2: Photoluminescence spectra of samples A,B, and C. The PL peaks are labeled according to the type of phonons involved in the exciton recombination (NP: no phonon, TO: transverse optic, TA: transverse acoustic) with a subscript indicating where the recombination occurs. (WL: wetting layer, WR: quantum wire).

Low temperature (T = 4.2 K) PL spectra of samples A,B, and C are shown in Fig. 2. The PL was excited by the 514 nm line of an Ar^+ laser with an intensity of 0.8 W/cm^2. The spectrum of the sample with the lowest Ge content (A) is typical for a 2 dimensional

SiGe quantum well layer. The lines at 0.997 eV, 0.979 eV and 0.940 eV (labeled NP_{WL} TA_{WL} and TO_{WL} in Fig. 2) are commonly attributed to the no-photon luminescence of a SiGe quantum well exciton and its transverse-acoustic and transverse-optical phonon replica. No indication of PL from quantum wires is observed in the spectrum of sample A. Therefore, we conclude that in this sample no quantum wires have formed and the observed PL is due to recombination of excitons confined to the WL only. Also in the x-ray experiments, no diffraction pattern characteristic for QWR is observed for this sample. The PL spectra of the samples with the higher Ge content (B, C) significantly differ from the spectrum of sample A: In addition to the strongly quenched NP_{WL} line and its phonon replica, new PL peaks appear in the spectra: a broad PL line (labeled NP_{WR}) is observed approx. 20 meV below the NP_{WL} line. This peak dominates any contribution of the TA_{WL} line possibly present in the spectra of samples B and C. We assign the NP_{WR} peak to PL from excitons confined to the self-organized quantum wires. For the sample with the highest Ge content investigated in this work (C), the NP_{WR} becomes the strongest signal in the PL spectrum. In addition to the NP_{WR} peak, a line labeled TO_{WR} is clearly resolved in the spectrum of sample C. Since this line is shifted to lower energies by the energy of a Si-Si TO phonon (58 meV) with respect to the NP_{WR} peak position, we assign it to a TO phonon replica of the NP_{WR} line. For sample B, the TO_{WR} signal is less pronounced and appears as a shoulder in the PL spectrum. Using the energy difference between the NP_{WL} and NP_{WR} lines observed in the luminescence spectra of sample B and C (20 meV), we have estimated the Ge concentration in the SiGe QWRs by calculating the confinement energies in the WL and in the QWR. Since the extension of the wires in lateral direction is approx. 10 times larger than in vertical direction, in the calculations we neglect the lateral confinement and model the quantum wire structure consisting of the WL and the self-assembled wire part by a two dimensional step quantum well. In Ref. [2] it is shown that within this model the small energy difference of 20 meV can be explained if Ge concentration in the range between 20% – 30% is assumed in the QWR, i.e. a *smaller* Ge concentration than determined for the WL by x-ray diffraction (33%). This unexpected finding is in excellent agreement with the results of x-ray measurements, which indicate 20 ± 10% Ge concentration in the QWR [2].

3. Conclusion

By carefully analyzing TR, PC and PL spectra we have shown that significant alloying occurs during the overgrowth of self-assembled SiGe quantum dots even at moderate growth temperatures around 525 °C. In addition we have shown that unlike in SiGe QDs, where the Ge content is usually higher in the self-assembled dots than in the WL, in the QWRs investigated in this work the WL contains a higher Ge fraction than the self-assembled wires.

Acknowledgements

Part of the work was supported by the FWF under *Lise-Meitner Programm*, Proj. Nr. M561 – TPH

References

[1] T. Fromherz, W. Mac. A. Hesse, G. Bauer C. Miesner, K. Brunner, G. Abstreiter: "Intraband absorption and photocurrent spectroscopy of self-assembled p-type Si/SiGe quantum dots", *Appl. Phys. Lett.*, Vol. 80, 2002, pp. 2093 – 2095.

[2] T.Roch, V. Holý, A. Hesse, J. Stangl, T. Fromherz, G. Bauer, T. H. Metzger, S. Ferrer: "Strain in buried self-assembled SiGe wires studied by grazing –incidence x-ray diffraction", *Phys. Rev. B*, accepted for publication.

[3] K. Brunner, J. Zhu, C. Miesner, G. Abstreiter, O. Kienzle, F. Ernst:"Self-organized periodic arrays of SiGe wires anGe islands on vicinal Si substrates", *Physica E.*, Vol. 7, 2000, pp 881- 886.

Spin Relaxation and g-Factor of 2-Dimensional Electrons in Si/SiGe Quantum Wells

W. Jantsch, N. Sandersfeld, M. Mühlberger, F. Schäffler

Institut für Halbleiter- und Festkörperphysik, Johannes-Kepler-Universität Linz, A-4040 Linz, Austria

Z. Wilamowski

Institute of Physics, Polish Academy of Sciences, Al Lotnikow 32/64, PL-0668 Warsaw, Poland

We investigate spin relaxation and the g-factor of conduction electrons in modulation doped Si/SiGe quantum wells by means of electron spin resonance. We find that both the transverse and the longitudinal relaxation times are of the order of microseconds, much longer than in III-V compounds. For high mobility, at carrier densities sufficiently far away from the metal-to-insulator transition, both quantities can be explained consistently in terms of the Bychkov-Rashba field, together with the g-factor anisotropy and its dependence on the carrier density. The properties found make Si/SiGe quantum structures interesting candidates for quantum computing.

1. Introduction

One essential prerequisite for spintronics is the ability to manipulate individual spins. Spin manipulation requires that both the longitudinal [1] (spin-lattice) relaxation time, T_1, and the transverse spin (dephasing) time [1], T_2, are longer than the time required to flip a spin, T_π. It is generally accepted that in many spin relaxation processes spin orbit interaction, SOI, enters [2]. Therefore materials with small SOI should be better suited for spintronic applications, and in some concepts for quantum computing silicon is chosen accordingly [3]. Nevertheless, most experimental [4], [5], [6] and many theoretical papers [2], [7], [8] are dealing with spin relaxation in III-V and II-VI compounds with much faster spin relaxation. Therefore spin relaxation in low-dimensional Si structures deserves attention [2]. There are of course also other requirements for spintronic devices, like the effective injection of spin-polarized electrons into the active material. Here again III-V and II-VI compounds have been investigated since they have well-known semimagnetic or even ferromagnetic variants. Now, most recently, ferromagnetism was reported also for an epitaxially grown group IV material [9], $Ge_{1-x}Mn_x$, which may be taken as indication that eventually spin injection may work also in the Si-Ge system.

In this work, we investigate spin relaxation and spin manipulation of two-dimensional (2D) electrons in Si and SiGe quantum wells. We make use of the electron spin resonance of conduction electrons, CESR, which, because of the outstandingly long relaxation times can be easily observed on single quantum wells in a conventional ESR spectrometer. We determine T_2 from the line width, and T_1 from the saturation behavior seen both in the power dependencies of the ESR amplitude and the line width. We show that

T_1 and T_2 are of the order of microseconds for conduction electrons in Si quantum wells embedded between $Si_{1-x}Ge_x$ barriers. On the other hand, for the power available in a standard pulsed-ESR spectrometer and the parameters of Si, the time required to invert the spin polarization is of the order of $T_\pi \sim 10$ ns and can be shorter for higher power.

We show also that the g-factor can be easily adjusted by either changing the Fermi energy or by shifting the electron to a SiGe layer, and the g-shift is sufficient to change the ESR resonance field to an extent that exceeds the line width. This observation demonstrates that it is possible to select individual spins, *e.g.*, by a voltage on some gate structure, and to manipulate it by a resonant microwave field on a time scale that is short in comparison to the spin life times. This possibility proves that Si is attractive candidate for quantum computing devices.

2. Experimental

CESR in modulation doped Si quantum wells has been observed in conventional microwave absorption experiments [10], [11] and also by electrically detected magnetic resonance [12], EDMR. The latter originates from the spin-dependent conductivity, $\sigma(\Pi)$, of the 2DES, where the spin polarization Π is changed at resonance. In conventional CESR experiments, this effect causes unusual signal shapes (see Fig. 1): apart from the microwave absorption signal observed in the reflectivity of a critically tuned cavity (the absorption is proportional to the imaginary part of the magnetic susceptibility, χ"), there is also a contribution of the EDMR effect – an indirect "polarization" signal that is proportional to $d\sigma/d$Þ and thus it may even differ in sign [13]. (Both signals are detected as derivatives with respect to the static magnetic field since the latter is modulated in order to improve the signal to noise ratio).

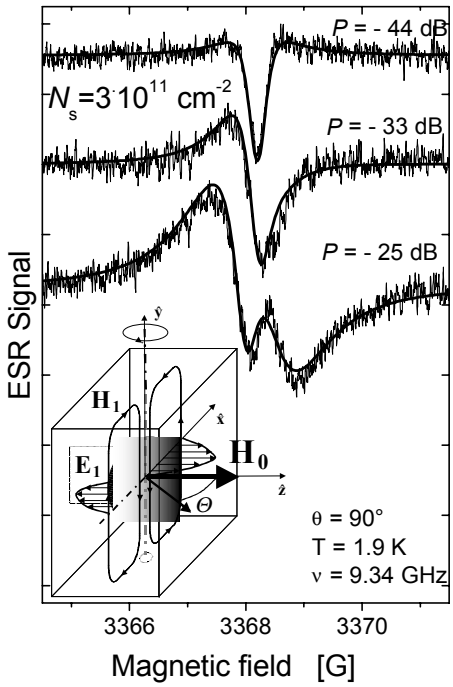

Fig. 1: ESR spectra at different microwave power. The inset schematically shows the mode used in the rectangular cavity.

Parts of the sample experience an in-plane component of microwave electrical field. Therefore we have to deconvolve the signal into its components. This is possible because of their different dependencies on the microwave power P – the polarization signal is proportional to $P^{3/2}$ in contrast to the absorption which varies like $P^{1/2}$. There is still another type of signal that appears because of the automatic frequency control of standard ESR equipment. This unit is used in ESR in order to keep the microwave frequency at the minimum reflection of the cavity and thus it eliminates contributions due to the dispersive part of the magnetic susceptibility, χ'. Here a dispersive signal appears again because of the frequency dependence of the conductivity. This dispersion signal is proportional to $d\sigma/d\omega$, it has even parity in its derivative in contrast to the absorption and polarization signals and it varies as $P^{1/2}$.

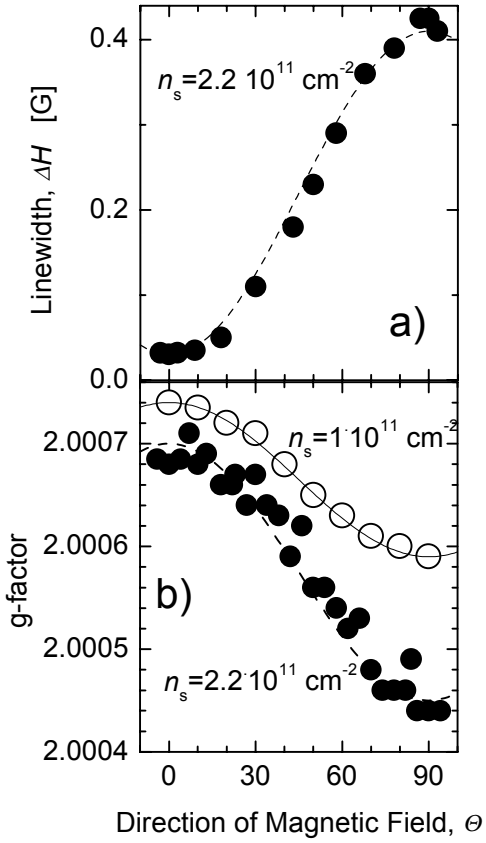

Fig. 2: (a) ESR line width and (b) g-factor as a function of the tilt angle, θ, of the sample relative to the surface normal.

The effective transverse spin relaxation rate is obtained from the CESR line width in the low power limit where the polarization signal amplitude and saturation broadening are negligible. Results are given in Fig. 2 (a) as a function of the tilt angle θ of the static magnetic field. The line width and thus T_2 show a strong anisotropy which depends also on the carrier density. Both dependencies can be explained consistently in terms of the Bychkov-Rashba field, H_{BR} [14]. For perpendicular field (θ = 0), where the longitudinal component of H_{BR} (parallel to H_0) vanishes, the line width turns out to be life time limited. From the linewidth we obtain then a T_2 value of 1..2 μs.

Another quantity that can be determined from the CESR spectra right away is the g-factor. Owing to the narrow line width of the CESR the g-factor can be determined with great accuracy. Results are given in Fig. 2 (b) as a function of θ for two different n_s values. A strong n_s-dependent anisotropy is visible, consistent again with the Rashba field [14].

The evaluation of the longitudinal relaxation rate, T_1^{-1}, is somewhat more complex. In cw CESR measurements it relies on investigations of the saturation behavior of the absorption. This is a standard procedure in the investigation of localized paramagnetic defect states in semiconductors and insulators. Usually T_1 is evaluated from the ESR amplitude measured as a function of power. Here, since the amplitude is a relatively complicated function of power already due to its different contributions, we preferred to use the power dependence of the line width which also shows saturation effects. Results for T_1 are given in Fig. 3.

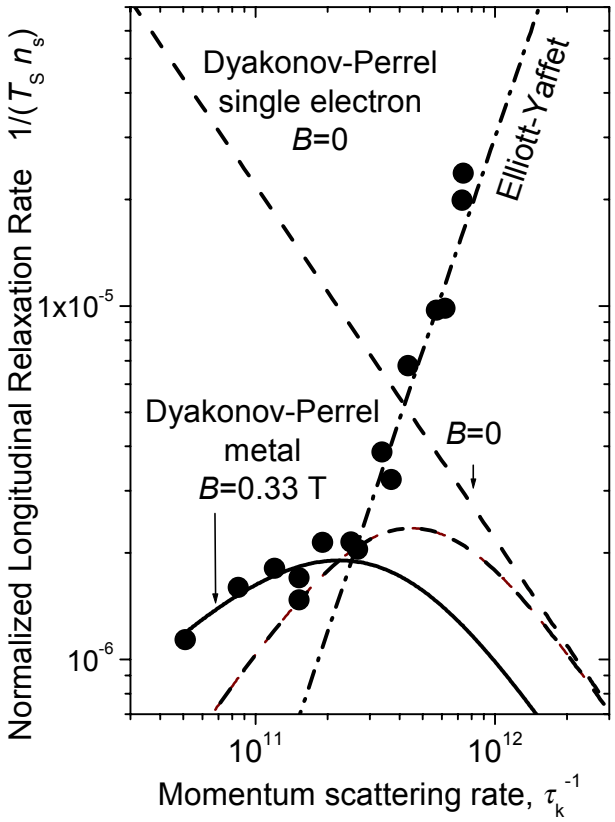

Fig. 3: Longitudinal spin relaxation rate, normalized with respect to the density of a 2D electron system in a Si quantum well at 1.9 K as a function of the electron scattering rate. The former is obtained from the power dependent line width, the latter from the cyclotron resonance width. The straight dash-dotted line is calculated for the Elliott-Yafet mechanism, the straight dashed line for the D'yakonov-Perel' mechanism for non-interacting electrons, the dash-dotted line taking Fermi statistics into account for B=0, and the full curve for B≠0.

3. Conclusion

In order to manipulate a spin in a specific quantum dot that might be defined by a gate structure, a change in the gate voltage may be used in the following way. Let us assume the whole structure (containing many quantum dots) is exposed to a cw microwave field and a static magnetic field, slightly off-resonance. A slight modification of the g-factor (we have very narrow lines) will be sufficient to bring individual electrons into resonance. This g-factor tuning can be achieved either by moving the wavefunction of the electron into a region with different g-factor due to (i) some admixture of Ge, or (ii) by changing the localization of the electron. Replacing (i) the Si well material by a $Si_{1-x}Ge_x$ alloy has been shown to change the resonance field by more than the linewidth for a Ge content of 5% already. The dependence of the g-factor on the Fermi energy in a 2DES indicates that the g-factor will be sensitive also to localization, and the latter can be also changed in a split-gate structure by the gate voltages. In both cases, a voltage pulse of appropriate duration can be used to bring a specific electron into resonance and to flip its spin.

In summary, we have shown that SiGe-based structures have a few properties that appear attractive and promising for spintronic applications: spin control and spin memory appear favorable under realistic conditions.

Acknowledgements

Work supported by FWF and ÖAD.

References

[1] We use throughout this paper the definitions for T_1 and T_2 as introduced for the Bloch equations as given *e.g.* in C.P. Slichter: "Principles of magnetic Resonance", Springer Series in Solid State Physics (2.ed., Springer, Berlin 1978)

[2] J. Fabian and S. Das Sarma, J. Vac. Sci Technol. **B17**, 1708 (1999) and cond-mat/0002256v1 (16 Feb 2000) and ibid /9912040v3 (17 Mar 2000)

[3] B.E Kane, Nature **393,** 133 (1998) and R. Vrijen *et al*., Phys. Rev. **A62**, 012306 (2000)

[4] Y. Ohno, R. Terauchi, T. Adachi, F. Matsukura and H. Ohno, Phys. Rev. Lett. **83**, 4196 (1999)

[5] A. Malinowski, R. S. Britton, T. Grevatt, and R. T. Harley, D. A. Ritchie and M. Y. Simmons., Phys. Rev. **B62**, 13034 (2000)

[6] G. Salis, Y. Kato, K. Ensslin, D.C. Driscoll, A. C. Gossard, and D.D. Awschalom, Nature **414**, 619 (2001)

[7] P.H. Song and K.W. Kim, cond-mat/0111076v3 (25 Nov 2001)

[8] N.S. Averkiev and L.E. Golub, Phys. Rev. **B60**, 15582 (1999)

[9] Y.D. Park, H.D. Hanbicki, S.C. Erwin, C.S. Hellberg, J.M. Sullivan, J.E. Mattson, T.F. Ambrose, A. Wilson, G. Spanos, and B.T. Jonker, Science **295**, 651, (2002).

[10] W. Jantsch, Z. Wilamowski, N. Sandersfeld and F. Schäffler, Phys. stat. sol. (b) **210**, 643 (1998)

[11] N. Nestle, G. Denninger, M. Vidal, and C. Weinzierl, Phys. Rev. **B56**, R4359 (1997) and private communication

[12] C.F.O. Graeff, M.S. Brandt, M. Stutzmann, M. Holzmann, G. Abstreiter, F. Schäffler, Phys. Rev. **B59**, 13242 (1999)

[13] Z. Wilamowski and W. Jantsch, Physica E **10**, 17-21 (2001)

[14] Z. Wilamowski, W. Jantsch, N. Sandersfeld, M. Mühlberger, F. Schäffler and S. Lyon: Physica E, in print.

Appendix

The Society's Managing Committee and Address

President:

Univ.Prof. Dr. Günther BAUER (up to December 31st, 2001)
Universität Linz, Institut für Halbleiter- und Festkörperphysik

Univ.Prof. Dr. Erich GORNIK (from January 1st, 2002)
TU Wien, Institut für Festkörperelektronik

First Vice-President:

Dipl.-Ing. Gerhard KRAINZ (up to December 31st, 2001)
Wirtschaftskammer Österreich

Mag. Miron PASSWEG (from January 1st, 2002)
Bundesarbeitskammer

Second Vice-President:

Univ.Prof. Dr. Günther BAUER (from January 1st, 2002)
Universität Linz, Institut für Halbleiterphysik

Univ.Prof. Dr. Erich GORNIK (up to December 31st, 2001)
TU Wien, Institut für Festkörperelektronik

Board:

Univ.-Prof. Dr. Emmerich BERTAGNOLLI
TU Wien, Institut für Festkörperelektronik

Univ.Prof. Dr. Wolfgang FALLMANN
TU Wien, Institut für Industrielle Elektronik und Materialwissenschaften

Dr. Ernst HAMMEL (from January 1st, 2002)
Electrovac GmbH, 3400 Klosterneuburg

Univ.Prof. Dr. Helmut HEINRICH
Universität Linz, Institut für Halbleiter- und Festkörperphysik

Dr. Heinz LASEK (from January 1st, 2002)
Wirtschaftsförderungsinstitut der Wirtschaftskammer Österreich

Univ.Prof. Dr. Hans LEOPOLD
TU Graz, Institut für Elektronik

Dr. Humbert NOLL (from January 1st, 2002)
AMS Austria Mikrosystems AG, 8141 Unterpremstätten

Univ.Prof. Dr. Fritz PASCHKE
TU Wien, Institut für Industrielle Elektronik und Materialwissenschaften

Mag. Miron PASSWEG (up to December 31st, 2001)
Bundesarbeitskammer

Dr. Robert SCHAWARZ
TU Wien, Institut für Industrielle Elektronik und Materialwissenschaften

Univ.Prof. Dr. Arnold SCHMIDT (up to December 31st, 2001)
TU Wien, Institut für Photonik

Univ.Prof. Dr. Siegfried SELBERHERR
TU Wien, Institut für Mikroelektronik

Rainer URANSCHEK (up to December 31st, 2001)
Forschungs- und Prüfzentrum Arsenal GmbH

Secretary-General:

A.o. Univ.Prof. Dr. Karl RIEDLING
TU Wien, Institut für Industrielle Elektronik und Materialwissenschaften

Administration:

Claudia BENEDELA

Address:

Gesellschaft für Mikroelektronik
c/o Technische Universität Wien
Institut für Industrielle Elektronik und Materialwissenschaften
Gußhausstraße 27-29/366, A-1040 Wien

Phone: +43-1-588 01-36657

Fax: +43-1-588 01-36699

Mail: gme@iemw.tuwien.ac.at

WWW: http://gme.tuwien.ac.at/